Insights into Polymer Biodegradation

Investigations on oxidative, hydrolytic and enzymatic Pathways

Dissertation

zur Erlangung des naturwissenschaftlichen Doktorgrades der Julius-Maximilians-Universität Würzburg

vorgelegt von

M.Sc. Juliane Ulbricht

aus Großenhain

Würzburg 2017

Eingereicht bei der Fakultät für Chemie und Pharmazie am

_____

Gutachter der schriftlichen Arbeit

1. Gutachter: _____
2. Gutachter: _____

Prüfer des öffentlichen Promotionskolloquiums

1. Prüfer: _____
2. Prüfer: _____
3. Prüfer: _____

Datum des öffentlichen Promotionskolloquiums

01. März 2018

Doktorurkunde ausgehändigt am

_____

Erratum

S. 34 Figure 2.20 oxidativer Abbau von Polysarkosin

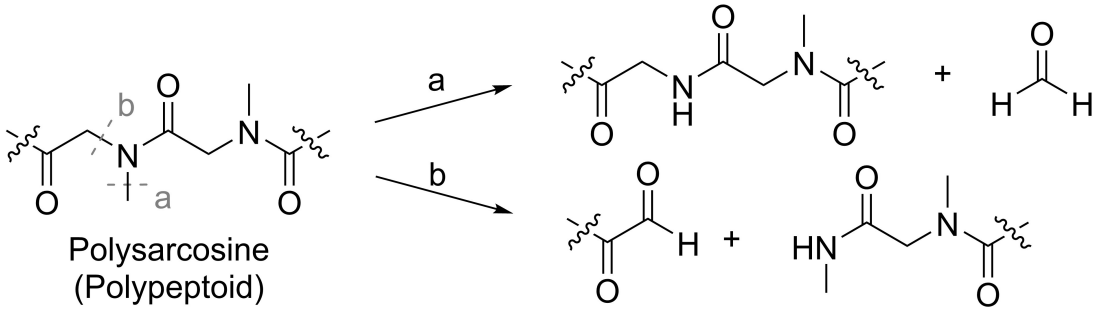

S. 115 Z. 29 secondary/tertiary

In contrast to PEG, PMeOx comprises **tertiary** amide bonds as an integral part of the side chain.

S. 131 Z. 2 secondary/tertiary

Catalyzing the hydrolysis of β-1,4-glycosidic linkages between *N*-acetylmuramic acid and *N*-acetyl-D-glucosamine residues in peptidoglycan and between *N*-acetyl-D-glucosamine residues in chitodextrins, they are not considered to cleave **tertiary** amide bonds as found in PSar.

S. 131 Z. 9 secondary/tertiary

Nevertheless, with respect to the number and diversity of proteins in egg white, the presence of enzymes capable of hydrolyzing **tertiary** amide bonds cannot be excluded.

S. 131 Z. 20: fehlender Satzanfang

However, under these conditions not only potentially polymer digesting enzymes are heat inactivated, but also lysozyme protecting the egg from bacterial infestation.[406]

für Ella

If you hear a voice within you say 'you cannot paint,' then by all means paint, and that voice will be silenced.

Vincent Van Gogh

Die vorliegende Arbeit wurde in der Zeit von Januar 2014 bis Dezember 2016 am Lehrstuhl für Chemische Technologie der Materialsynthese der Universität Würzburg unter Betreuung von Herrn Prof. Dr. Robert Luxenhofer angefertigt.

Danksagung

An dieser Stelle möchte ich mich bei all denjenigen bedanken, die mich während meiner Promotionszeit unterstützt, motiviert und in den richtigen Momenten abgelenkt haben.

Mein außerordentlicher Dank gilt meinem Doktorvater Prof. Dr. Robert Luxenhofer für die Überlassung dieses interessanten Projekts und die wissenschaftliche Betreuung während der letzten sieben Jahre meines Studiums, den unkomplizierten Umgang und seine jederzeit offene Tür. Die vielen wertvollen Anregungen und Ideen sowie das kritische Hinterfragen meiner Arbeit haben mich immer wieder motiviert und voran gebracht. Dankbar bin ich auch für die Möglichkeit der Teilnahme an zahlreichen Konferenzen in Valencia, San Francisco, Waterville Valley, Dresden und Philadelphia.

Allen Mitarbeitern des Lehrstuhls für Chemische Technologie der Materialsynthese und ganz besonders des AK Luxenhofers (& Markus) danke ich für die angenehme und entspannte Arbeitsatmosphäre, unzählige unterhaltsame fachliche und weniger fachliche Diskussionen und die moralische Unterstützung. Ganz besonders bedanken möchte ich mich bei Thomas, Fabian, Michael, Corinna und Miya, die meine Zeit am Lehrstuhl unvergesslich gemacht haben.

Meinen Bachelor- und Masteranden Annemarie Ringhand, Fabian Wieghardt, Johanna Eisenreich, Maria Krebs und Sandra Stets danke ich für die gute Zusammenarbeit. Ich hoffe ihr konntet von mir genauso viel lernen wie ich von euch.

Christian May danke ich für die schnelle Hilfe und Unterstützung bei Laborproblemen jeder Art und seinen unermüdlichen Einsatz bei der Erledigung alltäglicher Laborarbeiten. Bei Guntram Schwarz möchte ich mich für seine Hilfsbereitschaft und die schnelle Lösung aller meiner PC-Probleme bedanken.

Dr. Oliver Tröppner und Carina Süßmeier vom Süddeutschen Kunststoffzentrum danke ich für die Durchführung meiner GC/MS-Messungen.
Der Gesellschaft Deutscher Chemiker, dem Fonds der chemischen Industrie, dem Deutschen Akademischen Austauschdienst sowie dem Freitstaat Bayern danke ich für die Finanzierung meiner Forschung und Konferenzreisen.
Ein großer Dank gilt meiner Mutter Korina Ulbricht für ihre Unterstützung und ihr vorbehaltloses Vertrauen in mich.
Nicht zuletzt gilt mein größter Dank meinem Mann Martin, der nicht nur unermüdlich und akribisch Kapitel für Kapitel Korrektur gelesen, sondern mir auch den Rücken frei gehalten und mich wann immer nötig wieder auf die Beine gestellt hat. Du hattest Verständnis, wenn ich mit dem Kopf im Labor geblieben bin, hast mich wo immer möglich unterstützt, bis zum letzten Moment motiviert und immer an mich geglaubt - Danke!

Publikationsliste

»Degradation of high molar Mass Poly(ethylene glycol), Poly(2-ethyl-2-oxazoline) and Poly(vinyl pyrrolidone) by reactive Oxygen Species«
J. Ulbricht, M. Faust, R. Luxenhofer
Macromol. Biosci., submitted

»Peptoids and Polypeptoids at the Frontier of Supra-and Macromolecular Engineering«
N. Gangloff, J. Ulbricht, T. Lorson, H. Schlaad, R. Luxenhofer
Chem. Rev **116**, 1753-1802 (2016)

»Self-Assembly of amphiphilic Block Copolypeptoids with C2-C5 Side Chains in aqueous Solution«
C. Fetsch, S. Flecks, D. Gieseler, C. Marschelke, J. Ulbricht, K.-H. van Pée, R. Luxenhofer
Macromol. Chem. Phys **216**, 547-560 (2015)

»On the Biodegradability of Polyethylene Glycol, Polypeptoids and Poly(2-oxazoline)s«
J. Ulbricht, R. Jordan, R. Luxenhofer
Biomaterials **35**, 4848-4861 (2014)

Contents

Abbreviations and Symbols

ACN	acetonitrile
APP	aminopeptidase P
ADP	adenosine diphosphate
ATP	adenosine triphosphate
ATR	attenuated total reflection
BHT	butylhydroxytoluene
BHMT	betaine-homocysteine S-methyltransferase
CGD	chronic granulomatous disease
COQ	coenzyme Q
CYP	Cytochrome P450
DFP	diisopropyl fluorophosphate
Đ	dispersity
DMAP	4-dimethylaminopyridine
DMF	*N*,*N*-dimethylformamide
DMGDH	dimethylglycine dehydrogenase
DNA	deoxyribonucleic acid

DP	degree of polymerization
DPP II	dipeptidyl peptidase II
DPP IV	dipeptidyl peptidase IV
DTGS	deuterated triglycine sulfate
DUOX	dual oxidase
EMA	European Medicines Agency
E. coli	*Escherichia coli*
EtOx	2-ethyl-2-oxazoline
FDA	U.S. Food and Drug Administration
FITC	fluorescein isothiocyanate
FRAT	*Free Radical Theory of Aging*
GC/MS	gas chromatography–mass spectrometry
GNMT	glycine *N*-methyltransferase
GPC	gel permeation chromatography
GSH	glutathione
GSSG	glutathione dimer
HFIP	hexafluoroisopropanol
HIV/AIDS	human immunodeficiency virus infection and acquired immune deficiency syndrome
HX	hypoxanthine
IR	infrared
LCST	lower critical solution temperature
MALDI-ToF	matrix-assisted laser desorption/ionization time of flight

MeOTf	methyl trifluoromethanesulfonate
MeOx	2-methyl-2-oxazoline
M_n	number average molar mass
MnSOD	manganese SOD
M_p	peak molecular weight
MPO	myeloperoxidase
M_w	mass average molar mass
m/z	mass-to-charge
NADH	nicotinamide adenine dinucleotide-hydrogen
NADPH	nicotinamide adenine dinucleotide phosphate-hydrogen
NCA	α-amino acid *N*-carboxyanhydride
n.d.	not determined
NHC	*N*-heterocyclic carbene
NMP	*N*-methyl-2-pyrrolidone
NNCA	*N*-substituted α-amino acid *N*-carboxyanhydride
NOESY	Nuclear Overhauser Effect Spectroscopy
NOS	nitric oxide synthase
NOX	NADPH oxidase
NMR	nuclear magnetic resonance spectroscopy
NPA	neopentylamine
NTA	*N*-thiocarboxyanhydride
PBS	phosphate buffered saline

PBuOx	poly(2-butyl-2-oxazoline)
PEG	poly(ethylene glycol)
PEI	polyethylenimine
PEO	poly(ethylene oxid)
PEP	proline endopeptidase
PEtGly	poly(*N*-ethylglycine)
PEtOx	poly(2-ethyl-2-oxazoline)
P^{i}PrOx	poly(2-isopropyl-2-oxazoline)
PLLA	poly(lactic acid)
PMeOx	poly(2-methyl-2-oxazoline)
PLD-D	prolidase deficiency
POE	poly(oxyethylene)
POx	poly(2-alkyl-2-oxazoline)
PPro	polyproline
PPrOx	poly(2-propyl-2-oxazoline)
PSar	polysarcosine
PVP	poly(*N*-vinylpyrrolidone)
RT	room temperature
RNA	ribonucleic acid
RNS	reactive nitrogen species
ROS	reactive oxygen species
SAH	S-adenosylhomocysteine

SAM	S-adenosylmethionine
SARDH	sarcosine dehydrogenase
SAROx	sarcosine oxidase
Sar-NCA	sarcosine *N*-carboxyanhydride
SD	standard deviation
SEM	standard error of the mean
SGF	simulated gastric fluid
SHMT	serine hydroxymethyltransferase
SIF	simulated intestinal fluid
SOD	superoxide dismutase
SPSS	solid-phase submonomer synthesis
SulfoPBI	sulfo perylene bisimide
TEA	triethylamine
ThOX	thyroid oxidase
TMSP	trimethylsilylpropanoic acid
XO	xanthine oxidase
UV/Vis	ultraviolet-visible

1 Introduction

If you think the price of organic food is expensive, have you priced cancer lately?

Joel Salatin, Owner of Polyface Farm

During the second half of the 20th century, a rapidly increasing demand for cheap and easily accessible food changed the culinary culture worldwide. The concepts of ready-cooked meals and take-away fast food restaurants provided the foundation for rising and profitable businesses.

However, lately, a growing awareness for healthy food and lifestyle emerges. With deficient nutrition being associated with diseases and pathological conditions, increasing demand for food free of artificial additives, hormones, antibiotics, genetically modified organisms as well as trans-fats and fast food branches experiencing declining sales and store closures, it appears that the golden era of fast food is ending, thus paving the way for a new era of health consciousness.

The *Slow Food* philosophy asks for food that is good ("a fresh and flavorsome seasonal diet that satisfies the senses and is part of our local culture"), clean ("food production and consumption that does not harm the environment, animal welfare or our health") and fair ("accessible prices for consumers and fair conditions and pay for small-scale producers").[1] Similar trends are emerging in the fields of cosmetics and healthcare, with increasing emphasis on natural ingredients and eco-friendly production.

Overall, society's growing awareness for health and well-being is reflected by a high interest in substances entering the human body. Especially in the area of healthcare, medicine and pharmaceuticals, polymers are esteemed for their versatile and tailorable properties and gain in importance. Quite often, polymers are brought into direct contact with food, e.g. as packaging material or during processing. Furthermore, polymeric emulsifiers are essential components in personal care products like, for instance, lotions, creams, shampoos and toothpastes. In the field of medicine and pharmaceuticals, polymers are indispensable materials for consumables, sutures and implants (e.g. for dental or orthopedic purposes). Recently, polymeric therapeutics such as polymer-protein conjugates, polymer-drug conjugates and supramolecular drug delivery systems are subject of intensive research. Attaching poly(ethylene glycol) (PEG) to proteins, drugs or antibodies, referred to as PEGylation, may reduce immunogenicity and antigenicity (*stealth* behavior), prolong circulation time by increasing the hydrodynamic radius and therefore reducing renal clearance and increase

solubility of hydrophobic components. However, the role of PEG as the 'gold standard' of polymers used for bioconjugation is heavily criticized. Investigations on the *in vivo* cellular distribution of high molecular weight PEG provide evidence for an immunoreactivity of PEG (10-40 kDa) itself as well as renal cellular vacuolation (40 kDa PEG, Figure 1.1).[2] Whether or not accumulation of PEG provokes toxicological implications has not been fully elucidated yet, however, in view of the a large range of naturally occurring polymers such as cellulose, starch, natural rubber, asphalt and proteins, orientation towards polymers more similar to endogenous macromolecules is a highly promising approach to replacing PEG with biocompatible and biodegradable alternatives.

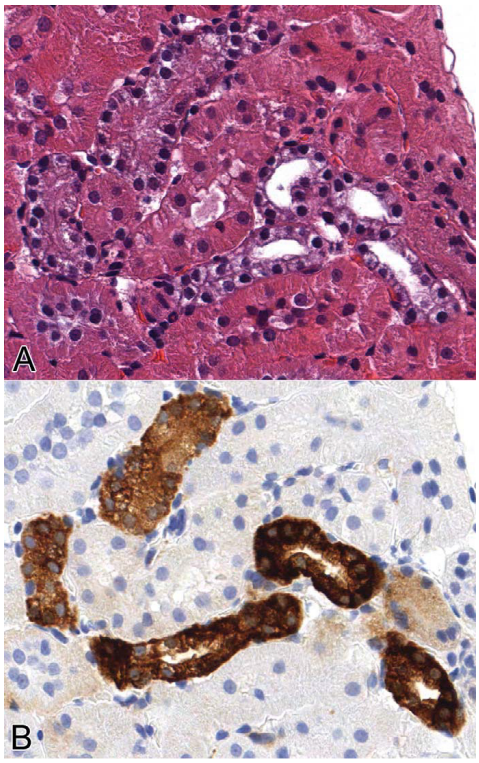

Figure 1.1: (A) Renal tubular degeneration and vacuolation (B) associated with PEG immunoreactivity and accumulation after treatment of a rat with 100 mg/kg PEG (40 kDa). Magnification = 250x. Reprinted with permission from ref [2]. Copyright 2013 Society of Toxicologic Pathology.

High similarity to peptides, good solubility in water as well as most organic solvents and excellent synthetic versatility focused attention on poly(2-alkyl-2-oxazoline)s (POx) and polypeptoids, two polymers possessing peptide bonds within the side chain or backbone, respectively. Cell culture studies indicate good biological acceptance of both polymers, nevertheless, prevention of accumulation as observed in case of PEG is a key factor for the design of biomaterials. Therefore, biodegradability within a reasonable timescale is a highly desirable aspect.

Previous studies investigated the degradation of poly(2-alkyl-2-oxazoline) (POx) and polypeptoids under biologically relevant oxidative conditions. With the intention of giving more insights into polymer biodegradation, the present thesis is concerned with the oxidative, enzymatic and hydrolytic degradation of polymers considered for or already used in biomedical applications.

2 State of Knowledge

2.1 Polymers in biomedical Applications: Opportunities and Obstacles

Polymers are an indispensable part of modern life. Since the early days of earth, nature evolved biopolymers like polysaccharides, cellulose, starch and DNA. Centuries before synthetic polymers appeared on the scene, humans applied cotton, rubber and various other natural occurring polymers to make life more comfortable, convenient and enjoyable. During the last decades, a great variety of polymers gained interest as biomaterials for biomedical applications, *inter alia* applied in implants and devices[3], tissue engineering[4] as well as drug solubilization and delivery[5]. However, well-defined polymeric materials displaying a designated degree of polymerization (DP) and narrow dispersity are clearly underrepresented due to the high demands placed on their large-scale preparation and little to no knowledge on structure-property relationships.

In recent years, poly(ethylene glycol) (PEG) represented the 'gold standard' of well-defined, water soluble polymeric biomaterials, a status crumbling more and more these days. As concerns regarding the biocompatibility of PEG are raised, interesting alternatives like poly(2-alkyl-2-oxazoline)s (POx), polypeptoids (Figure 2.1), polypeptides, polypeptide hybrids, polyglycerols, poly(*N*-vinylpyrrolidone)s and polyacrylates move into the focus of attention. The following sections are intended to provide a short and concise overview on PEG, POx and polypeptoids, the biopolymers of relevance in context of the present thesis.

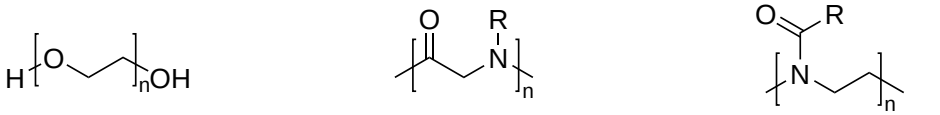

Figure 2.1: Chemical structures of PEG, polypeptoids and POx (R ≠ H).

2.1.1 Poly(ethylene glycol)

Poly(ethylene glycol) (PEG), often also referred to as poly(ethylene oxid) (PEO) or poly(oxyethylene) (POE), is a synthetic polyether available with reasonable definition in a wide range of molecular weights from ≈ 200 g/mol to ≈ 500 kg/mol. Industrial scale production of PEG is easily implemented via cationic or anionic polymerization

of ethylene oxide or ethylene glycol in aqueous solution. Furthermore, application of PEG takes advantage of excellent solubility in water and many organic solvents over the whole range of molecular weights, availability of both linear and branched structures and access to a variety of functionalities replacing the hydroxyl chain ends, e.g. amine, thiol, methoxy, carboxyl, acrylate, azide, vinyl sulfone, azide and acetylene groups.[6, 7] In the biomedical context, PEG convinces with biocompatibility, non-immunogenicity and resistance to protein adsorption conferring the so called *stealth* effect.[8, 9] PEGylation, the covalent or non-covalent attachment of PEG to proteins or drugs, is intended to improve the pharmacokinetics and pharmacodynamics of certain agents by increasing their solubility and blood circulation time and providing a mask protecting the therapeutic from proteolytic enzymes as well as antibodies.[10–12] Not only researchers confirmed safety of PEG for *in vivo* application[13], several PEGylated pharmaceutics have been approved by regulatory authorities like the U.S. Food and Drug Administration (FDA) and the European Medicines Agency (EMA).

However, more and more scientists express concerns with respect to the immunogenicity and biocompatibility of PEG and PEGylated therapeutics.[14–18] Vacuolation of PEG and PEGylated proteins in long-lasting cells like macrophages and histiocytes of various tissues as well as renal tubular cells and ependymal cells of the choroid plexus has been observed.[2, 19–22]

Several groups reported anti-PEG antibodies of varying percentage in healthy blood donors ranging from 0.2 % in 1984[23] and 4 % in 2011[24] up to 25 % in 2008[25, 26]. Thus, PEG itself may induce antigenic and immunogenic response in individuals bearing anti-PEG antibodies, resulting in rapid clearance and reduced efficacy of PEGylated therapeutics.[27] However, according to Brinks *et al.* the reliability and specificity of anti-PEG binding assays has to be critically questioned and an appropriate standardization is lacking to date.[28] Furthermore, immunogenic reactions to PEG after intravenous injections to rats were shown to be dependent on the attached protein as well as the size and terminus of the PEG moiety,[29] thus contradicting a *bona fide* antibody response. Nevertheless, approaches circumventing PEGylation or offering alternatives require intensive investigations in order to elude a prospective reliance on PEG.[17]

Another and major disadvantage of PEG is its lack of biodegradability, thus necessitating the use of low-molecular-weight PEG. However, PEG oligomers with a molar mass less than

400 g/mol (DP < 10) trigger fatal blood poisoning by sequential oxidation of PEG yielding diacid and hydroxy acid metabolites catalyzed by alcohol and aldehyde dehydrogenase, a process decelerating with increasing molar mass.[14, 30] Studies investigating the oxidation of unbranched alkane diols by equine alcohol dehydrogenase revealed similar effects of decreasing oxidation rates with increasing distances between the terminal hydroxy groups probably attributable to the substrate specificity of alcohol dehydrogenase.[31]
Ideally, alternatives to PEG comprise structures similar to endogenous macromolecules, thus ensuring high biocompatibility and potentially enabling their *in vivo* degradation yielding non-toxic metabolites. It has to be noted, however, that structures highly similar to endogenous macromolecules also bear the risk of unintended side effects and require thorough investigations. Two promising candidates for the replacement of PEG in biomedical applications, namely POx and polypeptoids, are discussed in the following sections.

2.1.2 Poly(2-alkyl-2-oxazoline)s

Poly(2-alkyl-2-oxazoline)s (POx) are a versatile class of peptide-like polymers first reported by four independent groups more than 50 years ago.[32–35] Obtained via a living cationic ring-opening polymerization of 2-alkyl-oxazolines (Figure 2.2), POx shine with narrow molecular weight distributions, high biocompatibility and easily fine-tuned properties like solubility, chemical functionality, architecture and size as highlighted in a number of excellent reviews.[36–40] Bearing smaller aliphatic side chains like methyl or ethyl groups, POx possess characteristics quite similar to PEG regarding hydrophilicity, protein repellent effects and *stealth* behavior.[41–45] The attachment of longer side chains introduces a thermoresponsive behavior, with a lower critical solution temperature (LCST) decreasing from ≈ 70 °C for poly(2-ethyl-2-oxazoline) (PEtOx) and ≈ 45 °C for poly(2-isopropyl-2-oxazoline) (P^{i}PrOx) to ≈ 25 °C for poly(2-propyl-2-oxazoline) (PPrOx), while poly(2-butyl-2-oxazoline) (PBuOx) and POx with even longer aliphatic side chains are insoluble in water at any temperature.[46, 47] Furthermore, POx are non-toxic[46, 48, 49] as well as non-immunogenic[46, 50] and the FDA approved PEtOx as an indirect food additive.
In particular, POx excel PEG regarding their extraordinary versatility. The possibility to not only modify both chain ends but also the side chains provides the opportunity to gradually fine-tune hydrophobicity and other properties. Studies by Luxenhofer and

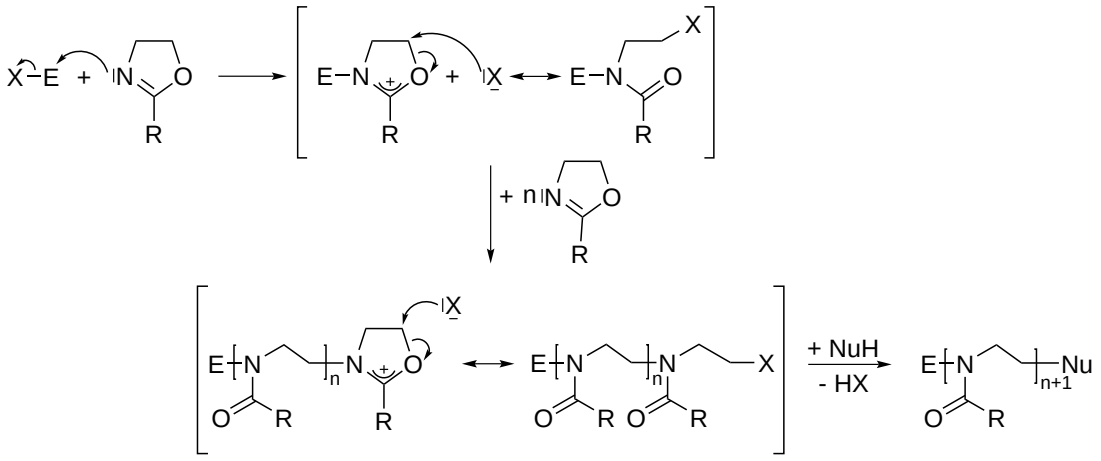

Figure 2.2: Mechanism of living cationic ring-opening polymerization of 2-alkyl-2-oxazolines. (X-E = electrophilic initiator, NuH = nucleophilic terminating agent).

coworkers revealed the extraordinary high drug solubilization capacity of the double-amphiphilic triblock copolymer P(MeOx$_{37}$-*b*-BuOx$_{23}$-*b*-MeOx$_{37}$) with up to 45 wt.% drug loading of the cancer chemotherapeutic paclitaxel, whereas the currently applied clinical formulations Taxol® and Abraxane® possess drug loadings of only 1 wt.% or 10 wt.%, respectively.[46]

In the beginning of 2016, the first POx conjugate SER-214 (acPEtOx-rotigotine) developed by Serina Therapeutics, Inc. entered phase I clinical trials in patients suffering from Parkinson's disease.[51] Promising preliminary results indicate the conjugate to be safe and well tolerated after single injections, final results will be available after completion of the phase I studies which was initially expected in may 2017 but is still pending.[52]

Overall, POx take advantage of a facile and defined synthesis, high biocompatibility and easily adjustable characteristics, thus being ideal candidates for biomedical applications especially in the realm of drug delivery. Nevertheless, in order to broadly apply POx based therapeutics, a more thorough understanding of the *in vivo* behavior, biodistribution and potential degradation is essential.

2.1.3 Polypeptoids

Regarding their chemical structure, polypeptoids closely resemble polypeptides as they differ solely in the position of their extending side chains. However, shifting the attachment point of a side chain from C$_\alpha$ to the nitrogen atom as a part of the amide bond has tremen-

dous impact on the polymer characteristics and functionality. Due to the introduction of a tertiary amide bond, polypeptoids lack the center of chirality. Furthermore, NMR studies revealed *cis* and *trans* conformation of the peptide bonds.[53, 54] The inability of polypeptoids to form hydrogen bonds further limits the tendency to assemble secondary structures like β-sheets and α-helices. For this purpose, especially polypeptoids bearing short aliphatic side chains like methyl or ethyl moieties exhibit random coil structures and offer excellent solubility in water and a variety of organic solvents.[55]

Polypeptoids are non-toxic[56, 57] and presumably non-immunogenic[58, 59], however, Kimura and coworkers observed accelerated blood clearance of lactosome nanoparticles comprising poly(lactic acid)-*b*-poly(sarcosine) after multiple injections and identified polysarcosine (PSar) as the responsible epitope[60]. The biodegradability of polypeptoids remains controversial and will be elucidated in more detail within the scope of this work, however, N-methylation is a widely applied approach to enhance the proteolytic stability of (poly)peptides.[61–63]

Depending on the desired chain length and sequence specificity, polypeptoids are accessible by various synthetic strategies. Similar to the synthesis of polypeptides from α-amino acid *N*-carboxyanhydrides (NCAs), the living nucleophilic ring-opening polymerization of *N*-substituted α-amino acid *N*-carboxyanhydrides (NNCAs) (Figure 2.3) is a convenient and facile strategy to obtain well-defined polypeptoids in a wide range of molecular weights from either solution, bulk or solid-phase. Recently, Ling and coworkers reported on the

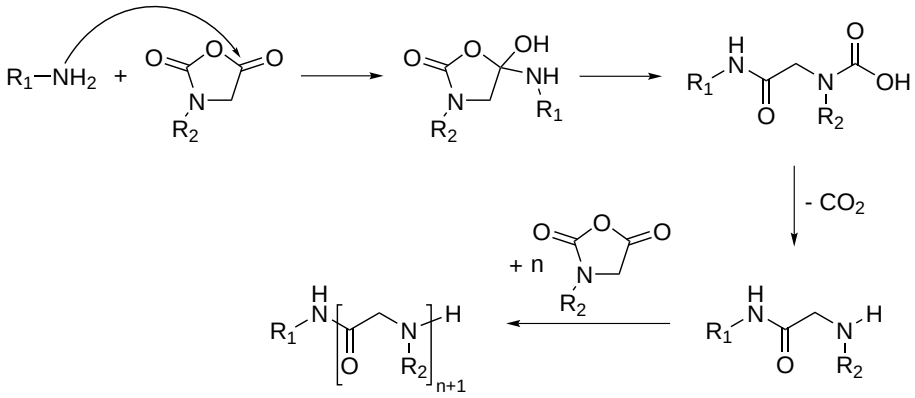

Figure 2.3: Normal amine mechanism of primary amine initiated living nucleophilic ring-opening polymerization of NNCAs (R_1, $R_2 \neq H$).

synthesis of polypeptoids from N-substituted *N*-thiocarboxyanhydrides (NTAs), which

are less sensitive to moisture than the wider applied NNCAs.[64–66] Applying a slightly elevated temperature of 60 °C, well-defined homopolymers as well as block copolymers with a DP in good agreement to the monomer-to-initiator ratio are obtained. Although amines are the initiator of choice aiming for polypeptoids with Poisson-type molar mass distributions, alternatives like rare earth borohydride complexes[65] and *N*-heterocyclic carbenes (NHCs)[67–69] are also applied, the latter one yielding cyclic polypeptoids. Based on the model of solid-phase peptide synthesis introduced by Merrifield[70], uniform sequence-specific (poly)peptoids are accessible via stepwise solid-phase submonomer synthesis (SPSS) by alternating bromoacetic acid and the desired primary amines.[71, 72] However, remarkable and precise control over both sequence and chain length comes along with the price of high expenditure of time, limited degree of polymerization (DP, < 50 monomer units) and low yields (< 20 %).
A detailed overview of (poly)peptoids as potential biomaterials is outside the scope of this thesis, however, the current state of the art is well summarized in a variety of reviews[71–78].

2.2 Potentials Pathways of Polymer (Bio-)Degradation

2.2.1 Oxidative Degradation

2.2.1.1 Oxygen as a Source of Life and Stress

Oxygen is one of the most essential elements of life on earth. Roughly four billion years ago, the atmosphere on earth strongly differed from what we are used to today. Outgassing from volcanism generated an atmosphere mostly consisting of water vapor, carbon dioxide, hydrogen sulfide and traces of nitrogen, hydrogen, carbon monoxide, helium, methane as well as ammonia, whereas oxygen was entirely lacking.[79, 80] Once photosynthetic organisms evolved, increasing levels of oxygen enabled the development of complex living organisms. Our modern atmosphere comprises 78 % nitrogen, 21 % oxygen, 0.93 % argon and 0.03 % carbon dioxide. The vast majority of oxygen derives from photosynthesis by marine as well as terrestrial plants, however, smaller amounts of oxygen are also produced through light dependent oxidation (referred to as photolysis) of water in the atmosphere.
Molecular oxygen has a key function in the metabolism of aerobic organisms.[81] Cellular

respiration essentially reflects a reverse photosynthesis, thus generating energy stored in form of adenosine triphosphate (ATP):

$$C_6H_{12}O_6 + 6\ O_2 \rightarrow 6\ CO_2 + 6\ H_2O + 2880\ kJ/mol$$

Ironically, oxygen is not only an existential basis for life on earth, but may also have severely harmful effects under certain conditions. Not only decreased (hypoxia) but also increased levels (hyperoxia) of oxygen are a potential stress factor for living organisms.[82] For instance, hyperoxia is associated with retinopathy of prematurity, a potentially blinding disease of the retina affecting 50 000 premature infants each year.[83] However, the lion's share of damage associated with oxygen is caused by so called reactive oxygen species (ROS), a type of free radicals and unintended by-product of aerobic metabolism elucidated in greater detail within the following sections.

2.2.1.2 Physiology and Pathology of Free Radicals

Contemporary literature applies the generic term 'free radicals' in a rather broad sense.[84] In general, free radicals are capable of independent existence and possess either unpaired electrons or unstable bonds. Occasionally, molecules in excited state or species resulting from free radical reactions are also referred to as free radicals. The majority of free radicals is highly reactive and unstable, with half-lives in a range of milli-, micro- or nanoseconds.[85] Free radicals are able to donate or accept electrons from other molecules, thus acting as oxidants or reductants.[86]

Physiology

A major portion of free radicals are represented by reactive oxygen species (ROS) and reactive nitrogen species (RNS), both of which are generated *in vivo* in a regulated manner by healthy tissues. Indeed, produced on demand, ROS and RNS play a beneficial role in physiology and are incorporated in various essential processes, such as apoptosis of defective or effete cells, oxidative phosphorylation within mitochondria to generate ATP from adenosine diphosphate (ADP), detoxification of xenobiotics by Cytochrome P450 oxidizing enzymes, generation of prostaglandins and leukotrienes and associated regulatory functions through oxygenases as well as disposal of microorganisms, fungal, bacteria or degenerated cells by macrophages and lymphocytes.[84, 87, 88] ROS further limit inflammation and

immune response, as evidenced by hyperinflammation and enhanced immune activation in patients suffering from chronic granulomatous disease (CGD), an autoimmune defect characterized by a lack of the ROS generating phagocyte NADPH oxidase NOX2.[89, 90] Capturing iodide for the biosynthesis of thyroid hormones in mammals, hydrogen peroxide is a crucial cofactor of thyroperoxidase.[91] In redox biology, tiny increases of ROS levels activate signaling pathways through specific covalent protein modifications with functional consequences, thus regulating fundamental biological processes including cell growth, differentiation, proliferation and apoptosis.[88, 92–94] On the other hand, increased levels of free radicals are associated with a myriad of pathologies. As a result, evolution created a versatile defense system based on antioxidants.

Antioxidants

Substances capable of neutralizing free radicals and reducing potential damage are referred to as antioxidants.[84, 85] In healthy tissues, each cell is provided with protective mechanisms suitable to prevent harmful effects caused by free radicals. Examples of antioxidants include enzymes like superoxide dismutase (SOD), glutathione peroxidase, glutathione reductase and thioredoxin as well as non-enzymatic substances that are either endogenous or micronutrients such as vitamin E (α-tocopherol), vitamin C (ascorbic acid), carotenoids, flavonoids, polyphenols, α-lipoic acid, glutathione, ubiquinol, uric acid and melatonin.[95, 96] Mechanisms of antioxidant action are just as various as antioxidants themselves. Primary antioxidants act by donating electrons to or accepting electrons from free radicals, thus quenching the initial free radical.[85] Although by this means the antioxidant is converted to a free radical itself, damage is prevented due to the antioxidants ability to accommodate the electron loss without becoming highly reactive. For instance, antioxidants comprising aromatic ring structures can easily delocalize unpaired electrons.[97] Secondary antioxidants act by inactivating ROS and RNS generating processes and include metal chelating agents and inhibitors of free radical producing enzymes.

Antioxidants of the defense system can be classified into three stages: preventive, radical scavenging and repair.[85]

Preventive antioxidants suppress free radical generation by scavenging metal ions or reducing hydroperoxides as well as hydrogen peroxide before they might form more deleterious species. For instance, lipid hydroperoxides are decomposed yielding the respective alcohols by several enzymes such as glutathione peroxidase, glutathione-S-

transferase, phospholipid hydroperoxide glutathione peroxidase and peroxidase, while hydrogen peroxide can be reduced to water by glutathione peroxidase and catalase.
Radical scavenging antioxidants inactivate radicals or terminate chain propagation reactions. A well known and the most potent lipophilic radical-scavenging antioxidant is vitamin E, however, ubiquinol as well as numerous hydrophilic agents such as vitamin C, uric acid, bilirubin and albumin are further examples of endogenous antioxidants in this stage of defense.
At the last stage of repair and reconstitution, oxidatively altered proteins are recognized and degraded by proteolytic enzymes, proteinases, proteases and peptidases to prevent accumulation, while damaged DNA is repaired by enzymes like glycolases and nucleases.

Pathology

Overproduction of free radicals and lack of antioxidant efficacy give rise to an imbalance referred to as oxidative stress, a pathologic condition contributing to a wide range of severe diseases. Prolonged elevated levels of free radicals cause non-specific damage to DNA, RNA, lipids, carbohydrates and proteins.[98, 99] The *Free Radical Theory of Aging* (FRAT), first proposed by Harman in 1956, suggests oxidative damage to cells as a major root of aging,[100] however, recent studies suggest free radicals to be rather beneficial for aging and age-dependent damage being associated with a protective ROS-mediated stress-response.[101]
Nevertheless, oxidative stress is implicated in pathologies such as renal, breast and lung cancer,[102–104] infectious diseases like hepatitis C,[105] influenza[106] and HIV/AIDS,[107] chronic fatigue syndrome,[108] congestive heart failure[109] as well as neurological disorders like Parkinson's disease,[110] Alzheimer's disease,[111] amyotrophic lateral sclerosis,[112] Huntington's disease[113] and Schizophrenia[114] (*cf.* Figure 2.4).

Lipids like phospholipids, cholesterol, cholesterol esters and triglycerides are components of cell and subcellular membranes extraordinarily susceptible to free radical damage. Abstraction of a hydrogen atom from a fatty acid methylene group by any oxidative species results in the formation of a fatty acid radical and induces the profoundly deleterious chain reaction of lipid peroxidation (Figure 2.5).[84, 115, 116] Due to their large proportion of double bonds and methylene groups bearing highly reactive hydrogen atoms, polyunsaturated fatty acids are the most favorable substrates of lipid peroxidation *in*

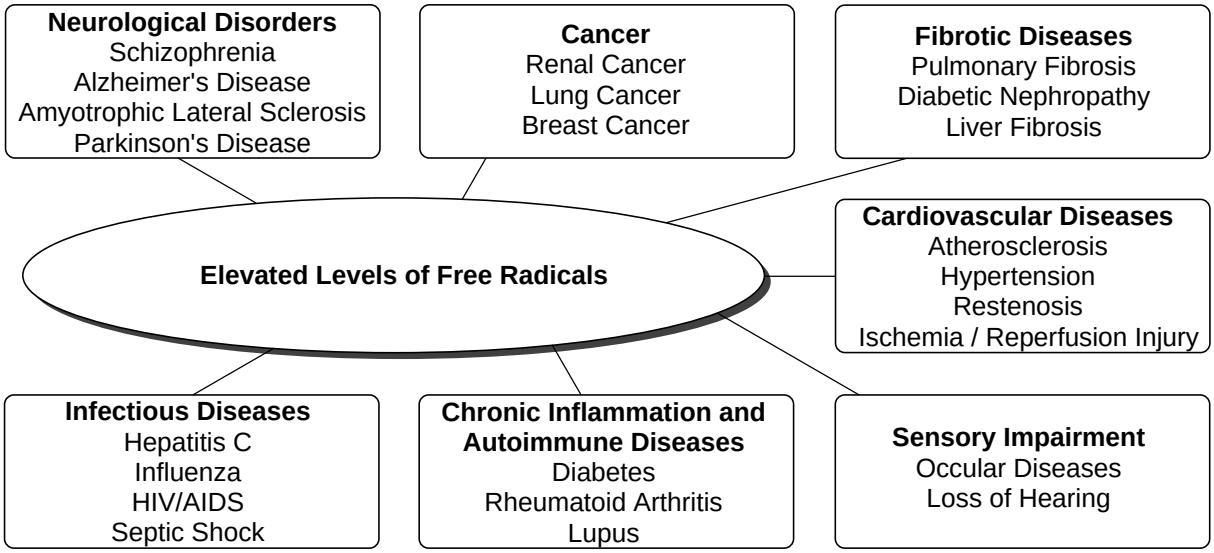

Figure 2.4: Elevated levels of free radicals are not only associated with the process of aging, but also with numerous severe diseases. Recreated from [88].

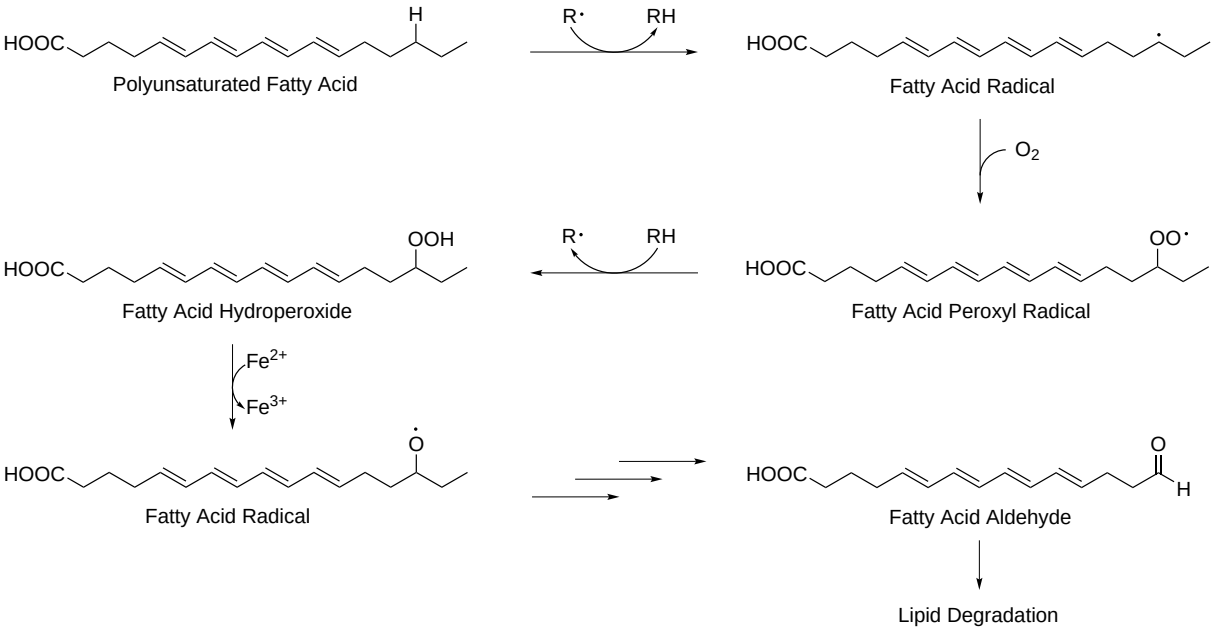

Figure 2.5: Lipid peroxidation is initiated by hydrogen abstraction from a polyunsaturated fatty acid yielding a fatty acid radical which reacts with oxygen to form a lipid peroxyl radical. Propagation proceeds via hydrogen removal from a second polyunsaturated fatty acid, thus generating a second fatty acid radical as well as a fatty acid hydroperoxide. The latter one can be reduced by Fe^{2+} forming a fatty acid aldehyde which is further metabolized. Recreated from [116].

vivo. Lipid peroxidation results in the formation of fatty acid aldehydes, which undergo metabolism yielding a number of toxic substances such as malondialdehyde, a highly

reactive dialdehyde or 4-hydroxynonenal, an α,β-unsaturated hydroxyaldehyde.[84]

DNA carries fundamental genetic information in all known forms of life. Oxidative modification of the DNA nucleobases adenine, guanine, cytosine and thymine is a diverse process and closely associated with carcinogenesis. Free radicals like the hydroxyl radical (·OH) may attack double bonds or abstract hydrogen atoms from the thymine methyl group or any C-H group of the sugar moieties.[84, 117] Highest oxidation potential is possessed by guanine, thus generating, among others, 8-hydroxyguanine, one of the major products of DNA oxidation (*cf.* Figure 2.6). Studies suggest implication of 8-hydroxyguanine in

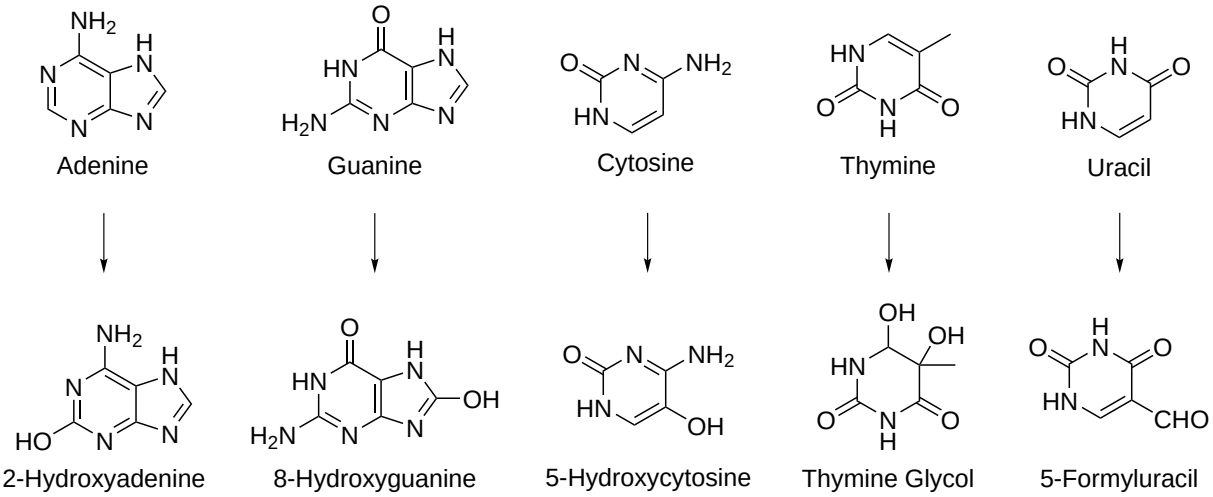

Figure 2.6: Depiction of the five DNA and RNA bases as well as some typical products of oxidative modification. A more comprehensive overview of oxidatively damaged DNA and RNA base lesions can be found in a review by Cooke and coworkers,[117] who list more than 20 substances.

carcinogenesis and consider it as a reliable marker for oxidative stress, DNA damage and cancer.[118, 119]

Proteins underlie oxidative degradation by various reactive species. Although oxidatively altered proteins are usually removed rapidly, a minor part is known to accumulate over time, thus contributing to damage associated with aging and severe diseases. The mechanism of protein oxidation will be discussed in detail in section 2.2.1.5.

2.2.1.3 Endogenous and exogenous Sources of Free Radicals

Free radicals are a typical by-product of essential metabolic processes and cellular respiration, but may also derive from external sources including ozone, air pollutants, X-rays, cigarette smoking, drugs and industrial chemicals.[120] Mitochondria, referred to as 'the powerhouse of the cell' supplying cells with energy in form of ATP, are a major location of free radical production *in vivo*, with enzymes like P450 cytochromes, xanthine oxidase and nitric oxide synthase generating various forms of ROS and RNS as adverse products. However, there are also a number of enzymes primarily generating ROS in an regulated manner, such as the membrane-bound NADPH oxidases (NOX) and dual oxidases (DUOX).

Mitochondria

Mitochondria are rod-shaped double membrane-bound organelles found in the cytoplasm of virtually all eukaryotic cells. Exploiting nutrients and oxygen to supply cells with energy in form of ATP, mitochondria are the site of aerobic cellular respiration. In a fourstaged process, glucose is broken down yielding carbon dioxide, water and ATP (Figure 2.7). While the first stage of glycolysis may also occur in absence of oxygen in a process

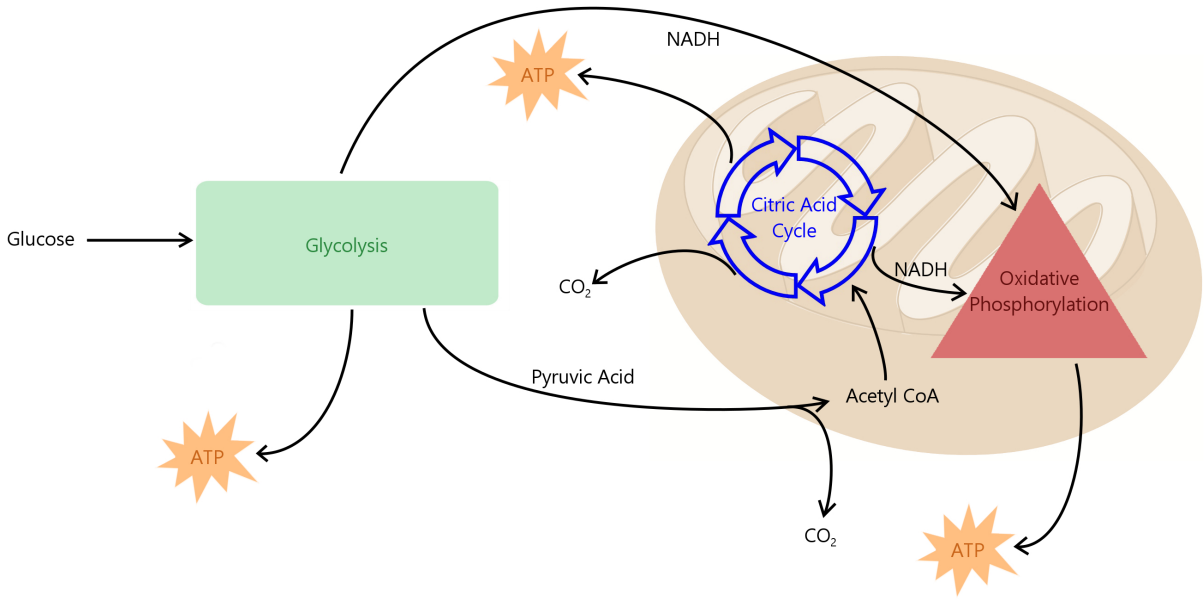

Figure 2.7: Simplified depiction of cellular respiration within cytoplasm and mitochondria.

called fermentation, the subsequent stages of pyruvate oxidation, the citric acid cycle and oxidative phosphorylation largely depend on oxygen, although it is only utilized directly

in the latter one.
In the final complex IV of oxidative phosphorylation, cytochrome C oxidase transfers electrons to oxygen, which is reduced yielding water:[121]

$$4 \text{ Cytochrome } C_{red} + O_2 + 4\ H^+ \rightarrow 4 \text{ Cytochrome } C_{ox} + 2\ H_2O$$

As more than 95 % of the total inhaled oxygen are utilized in this manner, it should be noted that the major role of oxygen in aerobic organisms is to act as a dumping ground for electrons.[122]
Although the whole process of cellular respiration is highly effective, the alternating one-electron oxidation-reduction reactions facilitate side reactions with molecular oxygen, thus generating toxic superoxide ($\cdot O_2^-$).[123, 124] Estimates assume about 1 - 2 % of the daily inhaled oxygen to be reduced within mitochondria yielding superoxide, which might disproportionate yielding hydrogen peroxide.[122] In case of a 60 kg woman with a daily oxygen consumption of 6.4 L/kg, this corresponds with a superoxide production of 160 - 320 mmol per day.
Another source of ROS within mitochondria is the outer membrane enzyme monoamine oxidase, which catalyzes the oxidative deamination of biogenic amines like serotonin, melatonin and adrenaline and generates significant amounts of hydrogen peroxide (H_2O_2).[125]
However, in order to assess steady state concentrations of mitochondrial ROS, several aspects should be taken into account. Levels of ROS not only depend on the local concentration of oxygen, but also on NADH/NAD^+ and coenzyme Q (COQ)/$COQH_2$ ratios, the proton motive force (δ_p) and levels of ROS consuming enzymes. For instance, peroxidases like glutathione peroxidases 1 and 4,[126] peroxiredoxins 3 and 5,[127] and catalase[128] are quite efficient antioxidants found within the mitochondria matrix.[129] Catalyzed by mitochondrial SOD (manganese SOD (MnSOD)), superoxide disproportionates yielding hydrogen peroxide.[130] Superoxide also contributes to the generation of peroxynitrite ($ONOO^-$) via reaction with nitric oxide ($NO\cdot$).
While *in vivo* measurements of ROS concentrations are considered more or less unreliable,[131] *in vitro* measurements are incapable of reflecting the specific conditions within a particular cell organelle. Mitochondrial levels of superoxide are estimated as $\approx 10^{-10}$ M,[122] which is in good agreement with reported steady state levels of superoxide in *Escherichia coli* (*E. coli*) of $2 \cdot 10^{-10}$ M.[132] Quite similar, intramitochondrial hydrogen peroxide concentrations are

calculated as $\approx 5 \cdot 10^{-10}$ M.[122]

NADPH Oxidases and Dual Oxidases

Enzymes of the NADPH oxidase (NOX) and dual oxidase (DUOX) family of NADPH oxidases play various roles in physiology and pathology as the key producers of free radicals. NOX and DUOX generate superoxide by transporting electrons across biological membranes, thus playing a vital role not only in host defense, but also in cellular signaling, regulation of gene expression, cell differentiation, growth, proliferation, migration and apoptosis as well as the post-translational processing of proteins.[133]

For many years it was thought that NOX activity is solely expressed in phagocytes as an efficient part of host defense. By today, seven members of the NOX family (namely NOX1 to NOX5, DUOX1 and DUOX2) have been identified in a wide variety of phagocytic and non-phagocytic cells of various organisms including mammals, nematodes, fruit fly, green plants, fungi and slime molds. In contrast, prokaryotes as well as most unicellular eukaryotes lack NADPH oxidases.[134, 135] As each of these seven isoforms of NADPH oxidases is unique regarding tissue distribution and mechanism of activation, a brief overview is given in Table 2.1 as well as in the following.

NOX2 is the most extensively studied species of NADPH oxidases and considered the prototype NOX or phagocyte NOX, as it was first described in neutrophils and phagocytes, however, it is actually rather widely distributed.[133, 136–138] Acting as a transmembrane redox chain, NOX2 transfers electrons from the donor NADPH within the cytosol towards oxygen as an electron acceptor on the outer side of the membrane, thus generating superoxide. NOX2 is activated by phosphorylation of the $p47^{phox}$ subunit.

The significance of NOX2 becomes evident in patients suffering from the previously mentioned CGD, which is characterized by a genetically determined lack of NOX2 caused by more than 410 different mutations of the NOX2 coding gene, resulting in insufficient levels of free radicals and the associated inability to kill bacteria.[89] Patients suffering from CGD experience recurrent infections (e.g. abscesses of skin, lungs or liver) and inflammations of lymphatic glands, lungs (pneumonia) and bones (osteomyelitis).[139]

NOX1 was the first described homologue of NOX2.[140, 141] Due to their high sequence identity of ≈ 60 %, it appears that NOX1 and NOX2 emerged from a comparatively

recent gene mutation.[140–142] Quite similar to NOX2, NOX1 generates superoxide and is widely expressed, among others, in colon and smooth muscle cells and also found in the colon tumor cell lines Caco-2, DLD-1 and HT-29.[133, 143, 144] Interestingly, expression of NOX1 in the gastric mucosa is largely species dependent. While no NOX1 activity is found in human stomach,[145] Rokutan *et al.* described its expression in the stomach of guinea pigs.[146] However, the physiological function of NOX1 is still a matter of hypothesis. Highly expressed in colon, a key function in host defense is very likely, however, NOX1 may also be involved in the regulation of blood pressure and smooth muscle proliferation.[147]

Table 2.1: NOX and DUOX tissue distribution and generated ROS according to ref.[133] and ref. [147].

	Tissue Distribution	**Generated Species**
NOX 1	colon, smooth muscle, endothelium, uterus, placenta, prostate, osteoclasts, retinal pericytes	$\cdot O_2^-$
NOX 2	phagocytes, thymus, small intestine, colon, spleen, pancreas, ovary, placenta, prostate, and testis B-lymphocytes, neurons, cardiomyocytes, skeletal muscle, hepatocytes, endothelium, hematopoietic stem cells, smooth muscle	$\cdot O_2^-$
NOX 3	inner ear, fetal kidney, fetal spleen, skull bone, brain	$\cdot O_2^-$
NOX 4	kidney, blood vessels, osteoclasts, endothelium, smooth muscle, hematopoietic stem cells, fibroblasts, keratinocytes, melanoma cells, neurons	$\cdot O_2^-$, H_2O_2
NOX 5	lymphoid tissue, testis, endothelium, smooth muscle, pancreas, placenta, ovary, uterus, stomach, various fetal tissues	$\cdot O_2^-$
DUOX 1	thyroid, airway epithelia, tongue epithelium, cerebellum, prostate testis	$\cdot O_2^-$, H_2O_2
DUOX 2	thyroid, salivary and rectal glands, gastrointestinal epithelia, airway epithelia, uterus, gall bladder, pancreatic islets, prostate	$\cdot O_2^-$, H_2O_2

NOX3 also shares ≈ 56 % of its amino acid sequence with NOX2,[133, 148] however, NOX3 is unique among the NADPH oxidases in terms of a comparatively restricted and specified tissue distribution. NOX3 is almost solely expressed in the inner ear, including the cochlear and vestibular sensory epithelia as well as the spiral ganglion.[147, 149, 150] Hence, superoxide generation by NOX3 is considered to be involved in the auditory system and hearing loss due to drugs, noises and aging as well as balance problems.

NOX4 is predominantly expressed in the kidney and was therefore also referred to as renal oxidase or renox.[147, 151] However, it is actually the most widely distributed NOX isoform and found in probably all vascular cells, typically within intracellular organelles like the endoplasmic reticulum, nuclear envelope and mitochondria. Interestingly, NOX4 is more distant from the evolutionary closely related subgroup of NOX1, NOX2 and NOX3 enzymes sharing only ≈ 39 % protein sequence identity with NOX2.[133, 152] NOX4 function has not been elucidated in detail yet, however, involvement in oxygen sensing, cell proliferation, differentiation, migration and apoptosis as well angiogenesis is suggested.[147, 151–153]

NOX5 is the latest identified member of the NOX family.[154, 155] First described by two independent groups in 2001, NOX5 is the genetically most distinct species.[156] It is highly expressed in lymphoid tissue (e.g. spleen, lymph nodes) and testis, but also found in various other tissues like vascular smooth muscle as well as B- and T-lymphocyte-rich areas.[133, 147, 154] However, as NOX5 is not expressed in both macrophages and dendritic cells and rodents express no NOX5 at all, an essential role of this NOX isoform in mammalian organisms and a key function in host defense are rather unlikely.

DUOX1 and DUOX2 are also referred to as thyroid oxidases (ThOXs) as they are highly expressed within the thyroid gland and involved in thyroid hormone synthesis.[147, 157] However, expression within epithelia of the respiratory and gastrointestinal tract indicates further contribution of both enzymes to oxidative host defense. Depending on presence or absence of their respective maturation factors (also known as mitose-promoting factors) DUOXA1 and DUOXA2, DUOX differ in their function regarding the generated reactive species. In their immature state, DUOX1 and DUOX2 produce superoxide, while the mature forms generate hydrogen peroxide.[158, 159]

Phagocytes

Phagocytes (Greek: *φαγεῖν*, phagein = devour, eat; -*κύτος*, -kytos = hollow vessel, cell) are an essential type of wide blood cells and a crucial part of the body's natural defense system. In a process referred to as opsonization, foreign particles, bacteria, parasites or apoptotic cells are marked with opsonin proteins like antibodies or complement factors. Professional phagocytes, including neutrophils, monophils, macrophages, mast cells and dendritic cells, are equipped with cell surface receptors specifically recognizing opsonized particles and pathogens.[160] The process of phagocytosis (Figure 2.8) involves binding of the phagocyte to the pathogen inducing engulfment and ingestion of the potentially harmful material, thus removing it from the bloodstream and forming a vesicle within the phagocyte which is known as phagosome. Non-professional phagocytes like fibroblasts and

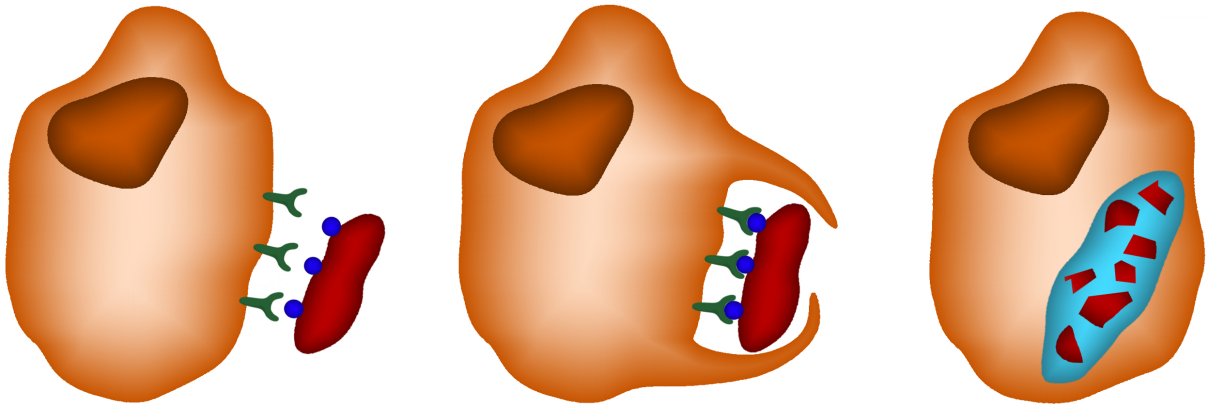

Figure 2.8: Schematic depiction of phagocytosis. Specific receptors (dark green) on a phagocyte (orange with nucleus depicted in brown) recognize the opsonin-marked (dark blue) particle (red). Binding of the opsonin proteins to the phagocyte receptors induces engulfment of the particle forming a phagosome (light blue). Finally, high amounts of oxidative species are released in a so called oxidative burst and initiate digestion of the foreign particle.

epithelial cells of bladder and thyroid lack opsonin-specific phagocytic receptors. Hence, they are very restricted in their range of ingestible particles, which is basically limited to foreign organisms and fading cells.[161] Furthermore, non-professional phagocytes do not generate ROS and RNS in response to particle uptake, which is a major feature in digestion of pathogens by professional phagocytes.

Intracellular digestion by professional phagocytes proceeds via both oxygen-dependent as well as oxygen independent pathways. Oxygen-independent pathways apply electrically charged proteins, lysozymes, lactoferrins, proteases and hydrolases, respectively, but are in

general considered less effective.[162] However, ingestion of foreign particles by professional phagocytes has tremendous influences on their oxygen management resulting in a state referred to as respiratory or oxidative burst. First, oxygen uptake is increased heavily up to 50-fold.[160, 163–165] Furthermore, high quantities of superoxide are generated by NOX2 within the phagosome:

$$O_2 + NADPH \rightarrow \cdot O_2^- + NADP^+ + H^+$$

In order to regenerate NADPH, large amounts of glucose are metabolized via the hexose monophosphate shunt. Although superoxide is quite innocuous, it rapidly dismutates yielding weakly microbicidal hydrogen peroxide:

$$\cdot O_2^- + 2\ H^+ + NADPH \rightarrow H_2O_2 + O_2$$

Concentrations of these immediate products of oxidative burst have been estimated by Winterbourn and coworkers by a kinetic model based on the reactions of superoxide to be $\approx 25\ \mu$M superoxide and $\approx 2\ \mu$M hydrogen peroxide in a neutrophil phagosome.[166] While superoxide is incapable to escape from the phagosome, hydrogen peroxide is able to diffuse freely but does probably not reach bactericidal levels. However, according to studies of Imlay and Linn, *E. coli* lacking hydrogen peroxide scavenging mechanisms are sufficiently killed by exposure to 1 μM hydrogen peroxide for a few hours.[167] In contrast, hydrogen peroxide added to the medium of *Cryptococcus neoformans* and *Candida albicans* to a final concentration of 30 mM even enhanced bacteria growth.[168] Thus, effective concentrations of hydrogen peroxide appear highly divergent and dependent on the attacked microorganism.
Irrespective of the above, although both superoxide and hydrogen peroxide are quite harmless species, they are the origin of various deleterious free radical species.

The Cascade of reactive Oxygen and Nitrogen Species describes the transitions between various free radical species evolving from the formation of superoxide ($\cdot O_2^-$)(Figure 2.9).[88] As mentioned previously, superoxide is generated by an one-electron-transfer to oxygen catalyzed by enzymes such as glucose oxidase, NADPH oxidase, lipoxygenase or NADH oxidase within numerous areas of organisms.[170] Due to its negative charge,

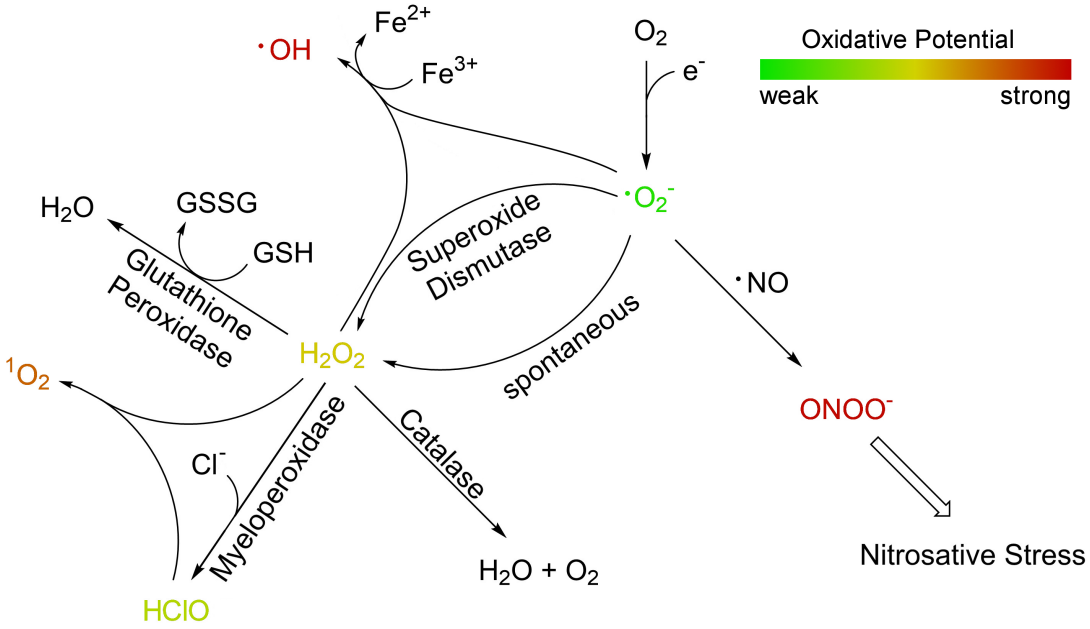

Figure 2.9: Transitions between ROS and RNS *in vivo* are mediated within a cascade of reactions. Modified from [169].

superoxide is incapable to cross membranes. A short half-life and low oxidative potential further limit harmful effects attributed to superoxide. However, superoxide undergoes spontaneous or enzyme-catalyzed dismutation yielding hydrogen peroxide (H_2O_2), an even less reactive ROS providing both the potential for membrane permeation as well as an extended half-life. In an alternative scenario, superoxide reacts with nitric oxide (·NO) to initiate the formation of RNS yielding highly reactive peroxynitrite ($ONOO^-$).
Hydrogen peroxide can be deactivated by either catalase generating water and oxygen or glutathione peroxidase under conversion of glutathione (GSH) to glutathione dimer (GSSG) yielding water. Nevertheless, catalyzed by myeloperoxidase (MPO), hydrogen peroxide reacts with ubiquitous chloride to form hypochlorous acid (HClO), which then may proceed to react with hydrogen peroxide and generate singlet oxygen ($^1O_2$). Both hydrogen peroxide and superoxide undergo iron or copper ion catalyzed Fenton reaction, thus yielding biologically exceedingly active and damaging hydroxyl radicals (·OH):[171, 172]

$$H_2O_2 + M^{n+} \rightarrow \cdot OH + OH^- + M^{(n+1)+}$$

Within neutrophils, hypochlorous acid formed by MPO acts as the primary reactive oxidizing agent, although minor proportions of hydroxyl radicals and singlet oxygen are

thought to be involved in phagocytic processes as well.[173–175] Winterbourn *et al.* estimated a hypochlorous acid production rate of 134 mM/min under assumption of a MPO concentration of 1 mM, however, the overwhelming share reacts instantly with neutrophil proteins.[176]

It should be noted though that these calculations were implemented for neutrophils and cannot necessarily be transferred to other phagocytic species. Oxidative conditions within the phagosomes of macrophages are considered to be quite harsh as well,[177, 178] while dendritic cells acting as a messenger between the innate and adaptive immune system apply much lower concentrations of reactive species in order to sustain antigenic materials for T cells.[179] As higher ROS production rates are associated with higher antimicrobial capacity,[180, 181] involvement of dendritic cells in oxidative polymer degradation is unlikely.

One milliliter of human blood contains about 7 million leukocytes (white blood cells).[182] With a daily production rate of $5 \cdot 10^{10}$ to $10 \cdot 10^{10}$ cells, neutrophils represent the most abundant ($\approx$ 60 %) species of leukocytes and might be potential candidates for the oxidative *in vivo* degradation of polymers.[183] Generated by stem cells in bone marrow, neutrophils circulate within the bloodstream with a half life of 6 to 8 h before they migrate into specific tissues such as liver, spleen and bone marrow, where they survive for only a few days.[184]

In contrast, macrophages are more long-lived and survive up to a total of several months in the human body. Monocytes are known to circulate about 3 days before they migrate into tissue and differentiate into macrophages or dendritic cells, a process largely determined by growth factors, microbial products and pro-inflammatory cytokines.[185, 186] Catalyzed by nitric oxide synthase (NOS), macrophages predominantly generate nitric oxide (NO·) which offers less oxidative potential compared to hypochlorous acid.[187, 188] However, in presence of superoxide, highly damaging species like hydroxyl radicals and peroxynitrite may be formed.[189, 190]

Tissue-specific macrophages are attributed to a specific purpose and established at strategically important sites of the body prone to accumulation of harmful material or microbial invasion (Table 2.2).

Regardless of the pathway of administration, following their uptake in the body polymers may be almost constantly exposed to phagocytic species. Whilst circulation in the bloodstream, neutrophils may potentially attack, ingest and finally digest polymeric particles by

producing hypochlorous acid. Once migrated into tissues, polymers are exposed to specific macrophages and associated oxidation by nitric oxide. Indeed, investigations by Ikada and coworkers support the concept of oxidative polymer biodegradation.[191]

Table 2.2: Specific tissue localization and associated functions of several important macrophages.

Location	**Macrophage**	**Function**
liver	Kupffer Cells	clearance of debris, regeneration of liver tissue
lung	Alveolar Macrophages, Dust Cell	immune surveillance
central nervous system	Microglia	active immune defense, clearance of plaques, damaged neurons and synapses
bone	Osteoclasts	resorption of bone cells for bone remodeling
intestine	Crypt Macrophages	immune surveillance
adipose tissue	Adipose Tissue Macrophages	elimination of dead adipocytes
kidney	Intraglomerular Mesangial Cells	ductual development
placenta	Hofbauer Cells	prevent passage of pathogens from mother to fetus
epidermis	Langerhans Cells	immune surveillance
granulomas	Epithelioid Cells	immure particles resistant to phagocytosis

Following intravenous injection of ^{125}I-labeled PEG into mice, blood circulation half-lives were largely dependent on the chain length of PEG. Increasing the molecular weight from 6 kg/mol to 190 kg/mol extended the circulation half life from 18 min to 1 day. Subsequent migration into tissue was observed to be irrespective of the molecular weight, however,

tissues like muscle, skin, bone and liver were more prone to polymer accumulation than other organs, thus corresponding well with the tissue distribution of macrophages. Indeed, while renal clearance decreased with increasing molecular weight, liver clearance enhanced due to ingestion of high molecular weight PEG (> 50 kg/mol) by Kupffer cells. However, although it can be hypothesized that PEG is digest within the Kupffer cells, this has not been proven reliably so far.
Overall, there are many good reasons to expect an oxidative degradation of polymers *in vivo*, at least down to a size easily excretable by, for instance, renal filtration.

2.2.1.4 Cytochrome P450 Hemoproteins

Cytochrome P450 hemoproteins (CYP) are a superfamily containing heme as a cofactor usually found as terminal oxidase enzymes in electron transfer chains.[192] They are named after their absorption maximum of 450 nm of in the reduced state of the enzymes and complexed with carbon monoxide. CYPs represent one of the largest and most functionally diverse superfamily of enzymes comprising more than 200 000 distinct proteins expressed in almost every class of organisms including animals, plants, fungi, protists, bacteria, *archaea* and viruses.[193]
CYPs hemoproteins do not primarily generate ROS but are involved in the oxidative, peroxidative and reductive metabolism of various smaller and larger exogenous and endogenous substrates. In general, reactions catalyzed by CYPs can be classified into four categories:
The most common and best understood reaction catalyzed by CYP hemoproteins acting as monooxygenases are hydroxylation reactions:

$$RH + O_2 + NADPH + H^+ \rightarrow ROH + H_2O + NADP^+$$

Quite similar, CYP hemoproteins catalyze the hydroxylation of methyl groups attached to oxygen or nitrogen atoms resulting in N- or O-dealkylation, thus facilitating the biotransformation of substrates.[192]
CYP enzymes also catalyze epoxidation reactions of olefines introducing oxygen into a carbon-carbon π-bond yielding the corresponding epoxides. Furthermore, under conditions of limited oxygen and availability of an alternate electron acceptor, CYP hemoproteins catalyze reduction reactions including the reduction of molecular oxygen yielding

superoxide.[194] Lastly, CYP hemoproteins catalyze heteroatom oxidations adding oxygen to a nitrogen, sulfur or other heteroatom.[192]

Due to their broad specificity and ubiquitous distribution, CYP enzymes may contribute the oxidative modification and degradation of polymers by both hydroxylation reactions and heteroatom oxidations.

2.2.1.5 Oxidative Modification and Degradation of Polymers

Poly(ethylene glycol)

Investigations on the oxidation of ethers have been a topic of organic chemistry since the early 20th century. Isham and Vail were the first who investigated the oxidation of diethyl ether vapor at high temperatures, yielding either acetaldehyde or acetic acid and water depending on the availability of oxygen.[195] The complex process of diethyl ether autoxidation (peroxidation) by absorption of oxygen from the air is a complex process unintentionally resulting in the explosion of diethyl ether containing bottles.[196–198] Gu and coworkers investigated the oxidation of methyl *tert*-butyl ether in aqueous solutions exposed to Fenton's reagent.[199] At room temperature and concentrations of 15 mM H_2O_2 and 2 mM Fe^{2+} at pH 2.8, 99 % of the methyl *tert*-butyl ether were decomposed within 2 h yielding *tert*-butyl formate, *tert*-butyl alcohol, acetone and methyl acetate (Figure 2.10).

In this context, it appears almost certain that PEG as a polyether is prone to oxidation as well. Indeed, in early studies by McGary Jr. the viscosity of aqueous PEG solutions (10 g/L) decreased significantly upon exposure to oxidizing agents such as hydrogen peroxide, potassium permanganate, bromine and peracetic acid for two days.[200] Ferrous sulfate, cuprous as well as cupric chloride and silver nitrate provoked a significant loss of viscosity as well, most probably by inducing autoxidation of the polyether. In particular, a 3 mM hydrogen peroxide solution supplemented with cupric chloride immediately decreased the viscosity by 98 %. However, presence of easily oxidizable primary and secondary alcohols such as allyl alcohol, isopropyl alcohol or ethanol impeded the oxidation of PEG significantly. Quite similar, compounds like amines, unsaturated molecules or nitriles could also exhibit a stabilizing effect.

Further studies examined the thermal oxidative decomposition of PEG in presence of oxygen with degradation rates increasing with temperature,[201–204] however, no degradation

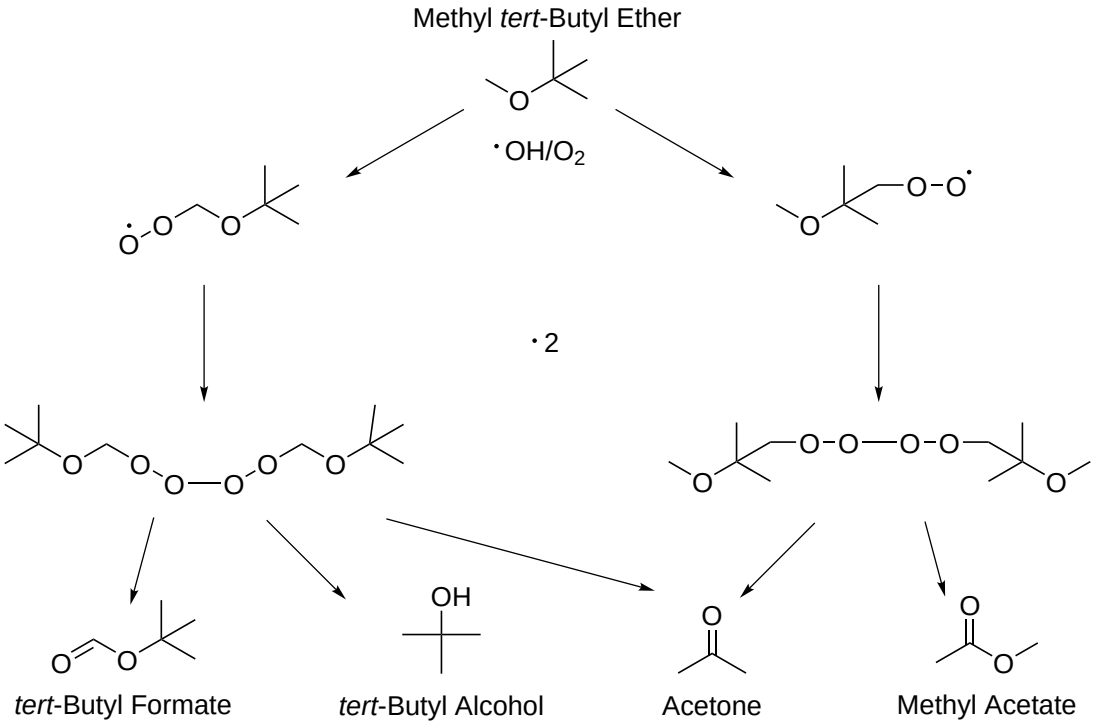

Figure 2.10: Mechanism of oxidative degradation of methyl *tert*-butyl ether by hydrogen peroxide and Fe^{2+} as proposed by Gu and coworkers[199].

was observed in vacuum.[201] NMR investigations on the thermal oxidative degradation of PEG during storage at 150 °C for 4 d conducted by Heatley and Mkhatresh revealed β-chain scission generating two formate ester chain ends as well as 2-hydroxyethyl formate and ethylene glycol diformate as small degradation products and, to a lesser extent, formation of in-chain esters, acetate chain ends, acetal links as well as peroxy groups.[202] Generation of formic acid and formaldehyde is also very likely, however, both possess boiling points below 150 °C (101 and -19 °C, respectively) and should have evaporated during the experiment as the test tubes applied by Heatley and Mkhatresh were open to ambient atmospheric conditions.

According to these investigations, the mechanisms of oxidative PEG degradation proceeds as follows: Initially, radicals such as ·OH or $\cdot O_2^-$ abstract any α-H atom from the PEG chain. Subsequent addition of O_2 and abstraction of a further H atom from another site generates a hydroperoxide (Figure 2.11).

The following generation of hemiacetal and formate ester end groups proceeds either directly via β-scission or involves the transition metal catalyzed formation of alkoxy radicals as an intermediate step (Figure 2.12).

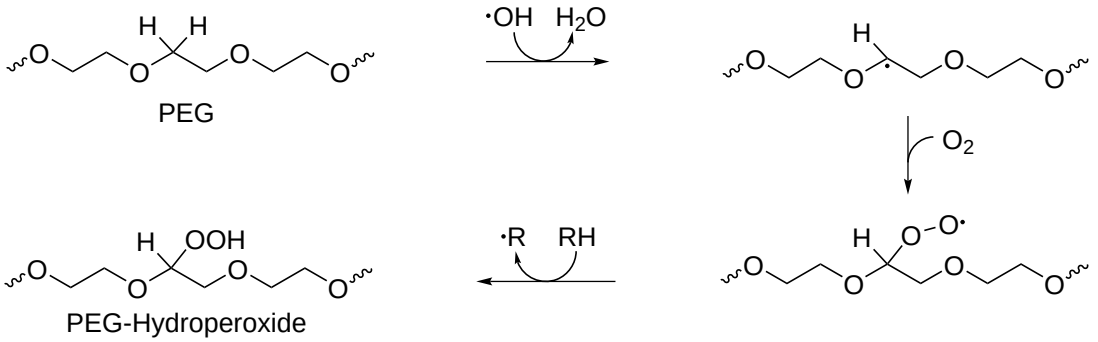

Figure 2.11: Formation of hydroperoxides by free radical mediated oxidation of PEG.

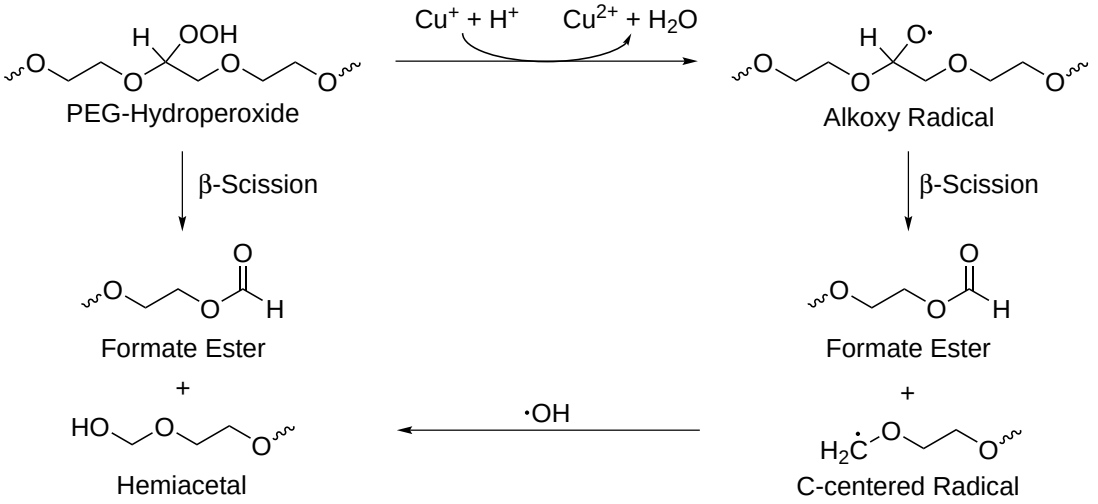

Figure 2.12: Pathways of formate ester and hemiacetal end group generation via β-scission of PEG hydroperoxides.

The labile hemiacetal chain end is highly susceptible to hydrogen atom abstraction and rearrangement resulting in the abscission of formaldehyde (Figure 2.13).

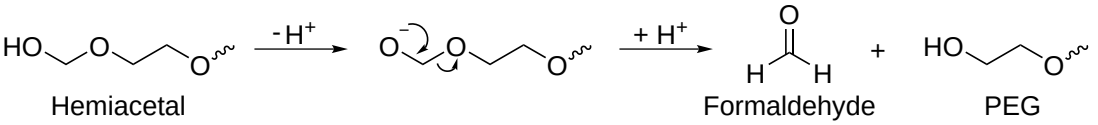

Figure 2.13: Rearrangement of the labile hemiacetal end group generates formaldehyde.

In consideration of the hypothesized oxidative milieu, formaldehyde could be oxidized yielding formic acid, thus inducing the formation of further formic acid chain ends via Fischer-Speier esterification (Figure 2.14).[205]

However, various side reactions may occur, for instance the generation of acetate end groups by β-scission of a C-centered radical (Figure 2.15).

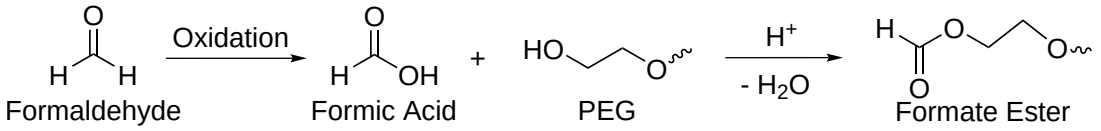

Figure 2.14: Formic acid generated via oxidation of formaldehyde initiates Fischer-Speier esterification yielding formate ester chain ends.

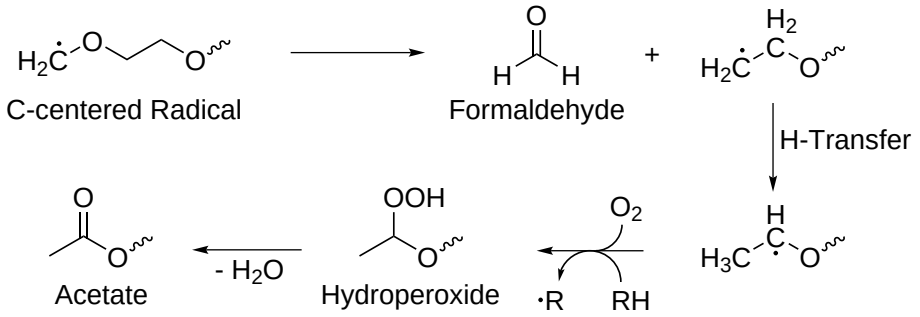

Figure 2.15: As a side reaction of oxidative PEG degradation, β-scission of C-centered radicals may generate acetate chain ends.

Poly(peptoid)s and Poly(2-alkyl-oxazoline)s

While the oxidation of proteins is a well known process associated with aging and various diseases (*cf.* section 2.2.1.2), the mechanism of polypeptoid and poly(2-oxazoline) oxidation has not been elucidated yet. However, the oxidation of similar structures such as proteins, proline residues or other tertiary amines may provide valuable indications regarding pseudo-polypeptide oxidation.

Protein oxidation is initiated quite similar to PEG oxidation by abstraction of a hydrogen radical resulting in the formation of a hydroperoxide (Figure 2.16).[206–208] It should be

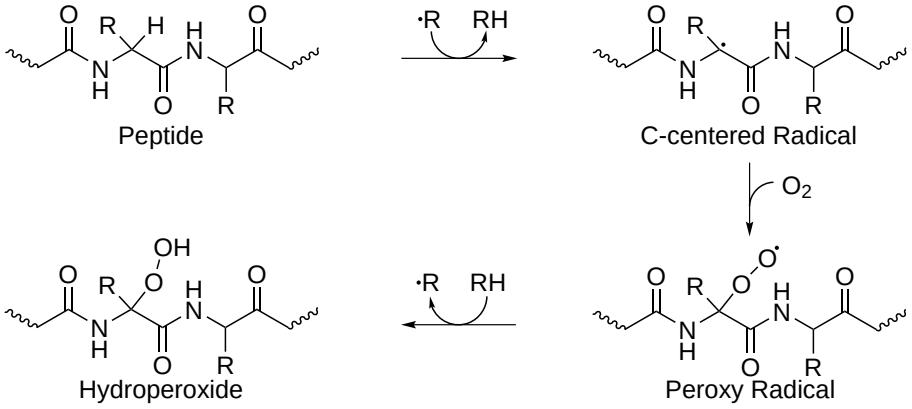

Figure 2.16: Abstraction of hydrogen induces the generation of peptide hydroperoxides.

noted that the abstraction of the α-hydrogen atom is facilitated by the + I - effect of the

substituent R. As both POx and polypeptoids lack the substituent on C_α, they might underlie less pronounced hydroperoxide generation.

Subsequent cleavage of the peptide bond and peptide decomposition proceed via either the diamide or the α-amidation pathway (Figure 2.17).[208] While the diamide pathway results

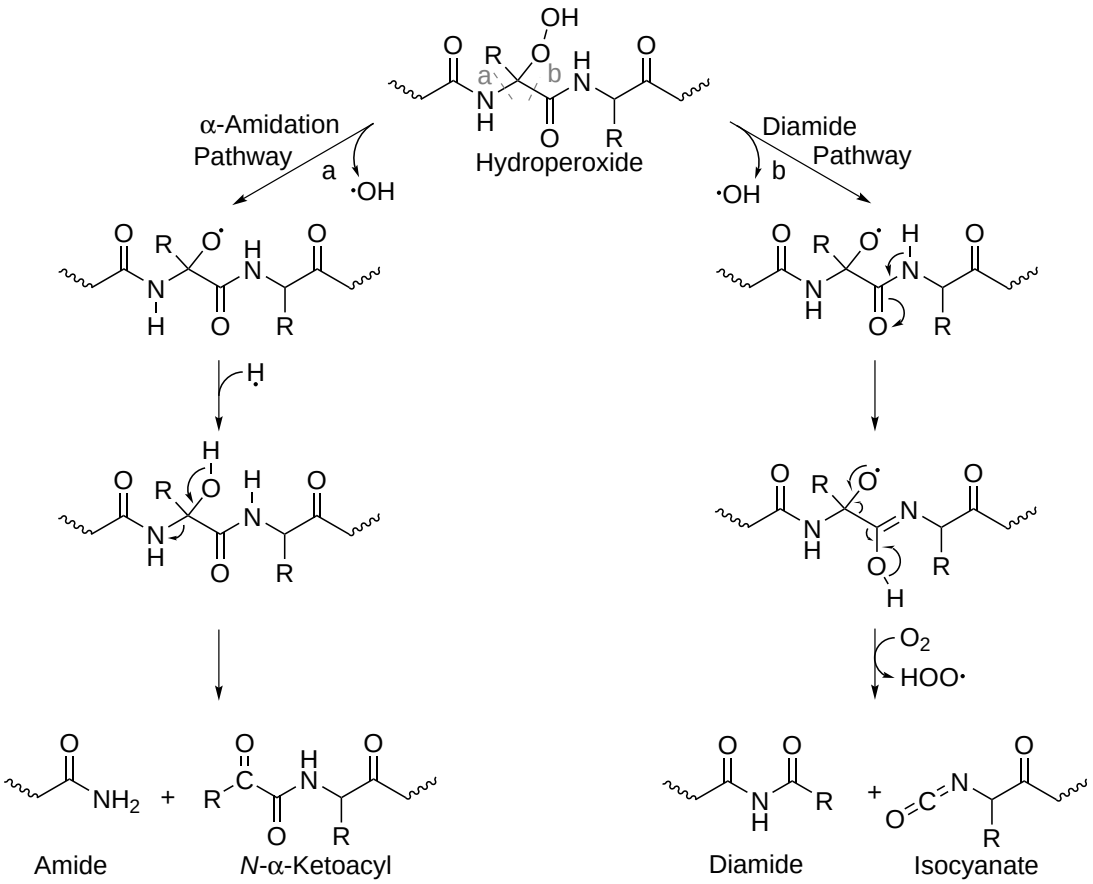

Figure 2.17: Decomposition of peptide hydroperoxides via the α-amidation pathway (a) and the diamide pathway (b).

in chain scission yielding a diamide and an isocyanate, oxidation via the α-amidation pathway generates an amide and a *N*-α-ketoacyl. In both cases, peptide bonds are not the primary target of oxidation.

It remains unclear, however, if similar mechanisms can be expected for pseudo-polypeptide oxidation. Not only the lack of a substituent on C_α, but also the introduction of a substituent rather than a hydrogen atom attached to nitrogen may impede similar processes and initiate alternative mechanisms.

Interestingly, studies on the oxidation of collagen, a proline-rich protein which will be discussed in more detail in section 2.2.3, various model peptides as well as polyproline revealed very pronounced oxidation of the peptide chains by both UV-irradiation and

exposition to Cu(II)/H_2O_2 at the sites of proline residues.[209, 210] Schuessler and Schilling reported similar observations regarding the cleavage of serum albumin exposed to γ-rays.[211] Sung and coworkers applied proline oligomers and biPEGylated proline oligomers as crosslinkers of scaffolds and observed their decomposition under physiological relevant conditions (5 mM H_2O_2, 50 μM $CuSO_4$).[212] It should be noted, however, that Sung *et al.* assumed oxidative stability of PEG in contradiction with results of McGary Jr., who reported rapid oxidation of PEG under comparable conditions as mentioned previously.[200] According to Uchida and coworkers, the mechanism of oxidation at proline residues proceeds quite similar to the diamide pathway yielding 2-pyrrolidone as a diamide as well as the respective isocyanate (Figure 2.18).[209, 210, 213]

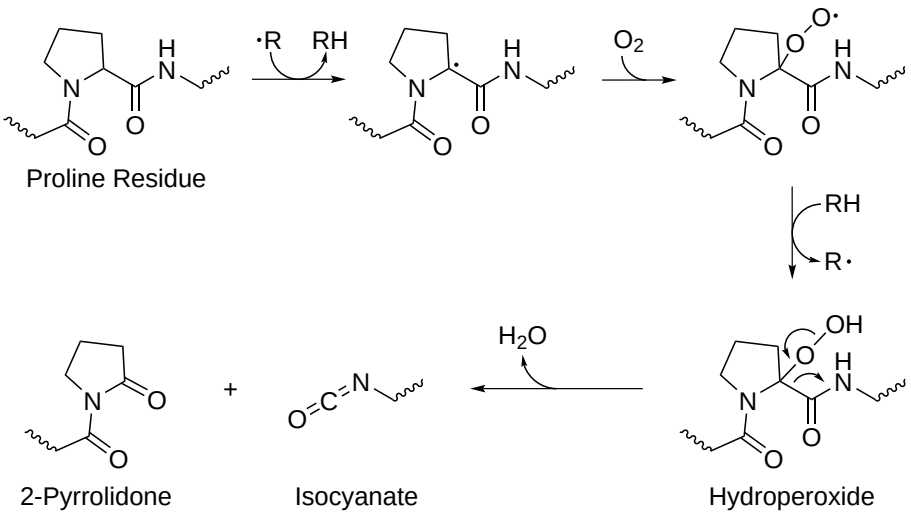

Figure 2.18: Mechanism of protein oxidation at the site of proline residues as proposed by Uchida *et al.*

Although proline residues bear tertiary amides and are therefore often considered as an intermediate between (poly)peptides and (poly)peptoids, the process of protein oxidation at the site of proline residues as proposed by Uchida *et al.* requires amino acid residues bearing secondary amides on the carboxyl site of proline. Hence, the oxidative degradation of neither polyproline nor pseudo-polypeptides are explicable in this way.

The metabolic pathway of tertiary amides such as *N*-methyl-2-pyrrolidone (NMP),[214] *N*,*N*-dimethylformamide (DMF)[215] and *N*,*N*-dimethylbenzamides[216] involves oxidation by cytochrome P450 enzymes. Oxidative dealkylation proceeds via a carbinolamide intermediate species, yielding a secondary amide and an aldehyde (Figure 2.19).[217]

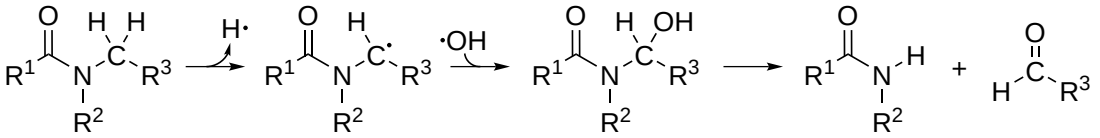

Figure 2.19: Oxidative dealkylation of tertiary amines via a carbinolamide intermediate ($R^3 \neq H$).

Applying the concept of oxidative dealkylation to polyproline, POx and polypeptoids, different sites of potential chain scission become obvious (Figure 2.20).

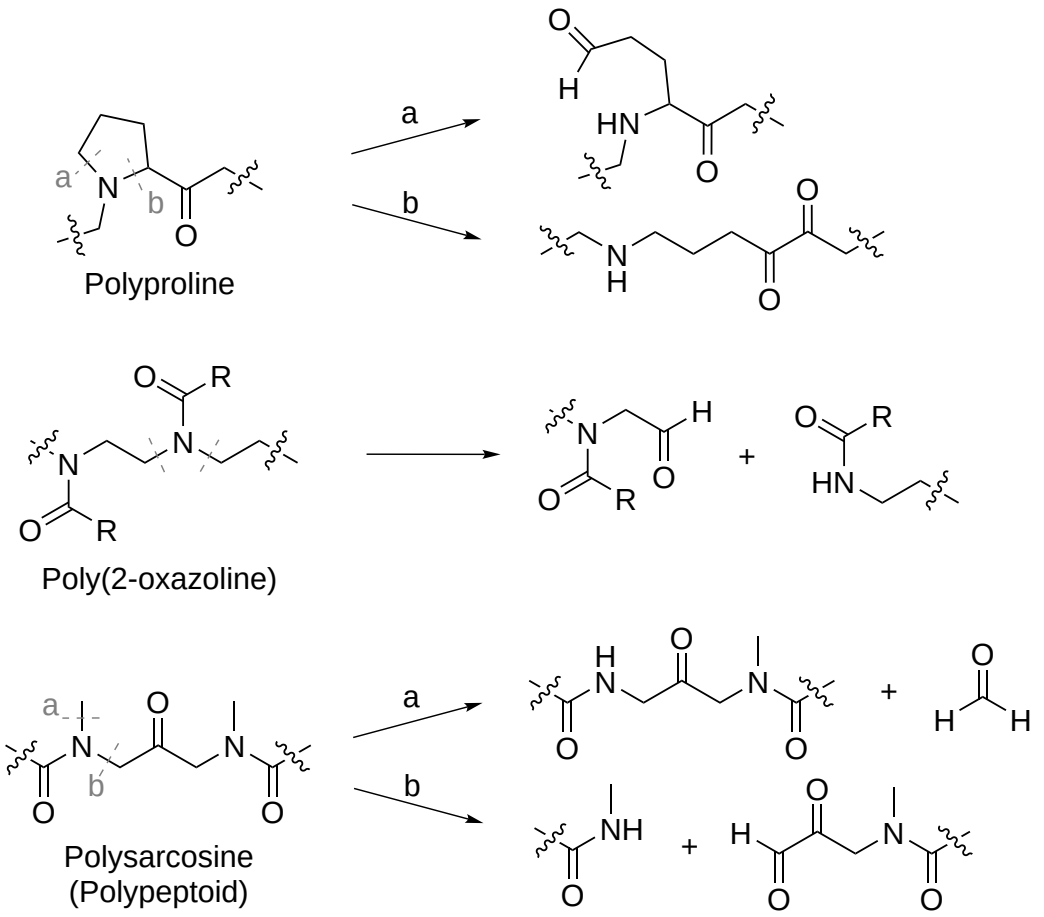

Figure 2.20: Potential sites and products of chain scission via oxidative dealkylation of polyproline, POx and polypeptoids.

In case of proline, both options open the five-membered ring, however, chain scission requires further steps to be involved. Conversely, cleavage of POx is achieved by both pathways, while the oxidative dealkylation of polypeptoids proceeds either via side chain cleavage or backbone scission with effectively equal probabilities.

Previous Studies on the oxidative Degradation of Polymers

Fundamentals of the oxidative degradation of PEG, PEtOx and poly(*N*-ethylglycine) (PEtGly) were already investigated within the framework of earlier studies[169, 218]. In this context, not only the susceptibility of all three polymer species towards oxidative deterioration by potentially biological relevant concentrations of hydroxyl radicals could be proven, but also clear correlations between the concentration of the reactive species, the DP of the respective polymer, incubation time as well as the apparent oxidation rate were observed.

For this purpose, polymers with a DP of ≈ 50 and ≈ 150 were synthesized or bought, respectively, dissolved in phosphate buffered saline (PBS) (1 g/L) and incubated at 37 °C. Subsequently, $CuSO_4$ was added to a concentration of 50 μM and daily replenished doses of H_2O_2 aiming for final concentrations of 0.5, 5 and 50 mM secured the continuous generation of highly reactive ·OH by an *in situ* Fenton-like reaction:

$$H_2O_2 \; + \; M^{n+} \; \longrightarrow \; \cdot OH \; + \; OH^- \; + \; M^{(n+1)+}$$

Under the examined conditions, PEtOx demonstrated highest susceptibility to oxidative degradation, closely followed by PEtGly. Probably due to the enhanced stability of PEG hydroperoxides, PEG proved to be slightly more resistant to oxidative deterioration.

Furthermore, a tremendous influence of the polymer chain length on the apparent oxidation rate was observed, with higher oxidation rates determined for polymers with a higher DP which is attributable to a lower relative concentration of oxidable chain ends.

Interestingly, incubation of the polymers with H_2O_2 without further addition of $CuSO_4$ revealed no significant differences regarding the extent of polymer degradation of the investigated polymers, thus indicating a dependence of the degradation rate on the type of the reactive oxygen species.

Unfortunately, ^{1}H-NMR turned out to be unsuitable to identify potential degradation products. However, a CellTiter-Glo® assay revealed no cytotoxicity of the partial degraded polymers at low concentrations, but was strongly affected by residual oxidative species inducing cytotoxicity at higher polymer concentrations.

Further studies conducted by Moritz Faust during the course of his master thesis confirmed the reproducibility of the previously described results and focused on the oxidative degradability of poly(*N*,*N*-dimethylacrylamide), polyglycidols and poly(*N*-vinylpyrrolidone)

(PVP).[219] Interestingly, polyglycidols exhibited even higher susceptibility towards oxidative degradation than PEtOx. In contrast, minor changes of the dispersity of both PVP as well as poly(*N*,*N*-dimethylacrylamide) accompanied by significant decreases of the molecular weight indicated side chain scission and rather stable C-C backbones.

2.2.2 Hydrolysis of Poly(2-alkyl-2-oxazoline)s and Polypeptoids

Hydrolysis of amide bonds cleaving the peptide backbone and yielding, if performed exhaustively, the respective amino acids, is known to require very harsh conditions (6 M HCl, pH -0.8, 110 °C)[220] and therefore not considered to be of relevance for peptide and protein degradation *in vivo*. Although similar conditions (6 M HCl, pH -0.8, 120 °C) have been applied for the hydrolysis of polypeptoids,[221] detailed kinetic studies are hitherto lacking. Nevertheless, hydrolysis of polypeptoids proceeds similar to the hydrolysis of polypeptides via backbone scission releasing the respective tertiary amino acids (Figure 2.21). The hydrolysis of POx under both strong acidic[222–225] as well

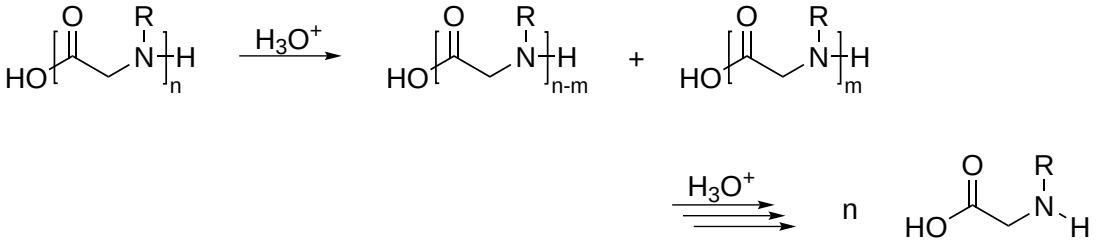

Figure 2.21: Hydrolysis of polypeptoids results in backbone scission and yields tertiary amino acids if performed exhaustively.

as strong basic[32, 226] conditions has attracted more attention, not least as an effective way to generate linear polyethylenimine (PEI) (Figure 2.22) as the cationic ring-opening polymerization of ethyleneimine yields highly branched PEI. However, both linear PEI as well as partially hydrolyzed P[(2-ethyl-2-oxazoline)-*co*-(ethyleneimine)] comprising at least 56 mol-% PEI are reported to show cytotoxicity against NIH 3T3 fibroblast cells,[224] HeLa human cervix carcinoma cells[227] and ATCC CRL-2522 human dermal fibroblast cells[228]. In order to elucidate if low pH values (1 - 4) as found in the human stomach may hydrolyze POx to an extent of health concern, Hoogenboom and coworkers conducted detailed kinetic investigations.[228] In both simulated gastric fluid (SGF) and simulated intestinal fluid (SIF) supplemented with digestive enzymes, the degree of hydrolysis after 6 h at 37 °C was found to be negligible (< 0.2 %). Considering the short passage time

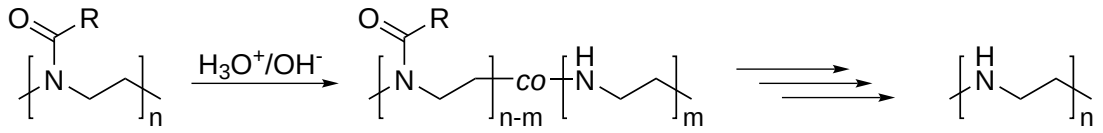

Figure 2.22: The hydrolysis of POx under either strong acidic or strong basic conditions is a fast and facile method for the synthesis of linear PEI.

through the stomach of around 4 h, *in vivo* hydrolysis of POx to a deleterious magnitude can more than likely be precluded.

According to Hoogenboom *et al.*, hydrolysis of POx follows a pseudo-first order kinetic, thus being independent of both the polymer amide concentration as well as the chain length and proceeding at higher rates with increasing temperature.[225, 228] However, higher hydrolysis rates of poly(2-methyl-2-oxazoline) (PMeOx) compared to PEtOx are observed, which can be attributed to the better hydration of the more hydrophilic PMeOx as well as the additional methylene group of PEtOx creating more steric hindrance in the tetrahedral intermediate.[225] Kinetic studies further revealed an inhibition period within the initial phase of POx hydrolysis, which was attributed to a neighboring group effect.[228] According to Hoogenboom and coworkers, once generated secondary amine moieties catalyze the hydrolysis of adjacent amides, thus suggesting that the hydrolysis of POx does not occur in a random fashion but rather block-like.[228, 229] Even under very harsh conditions (6 M HCl, 100 °C), cleavage of the POx backbone is not observed as evident from maintained narrow dispersities.[230]

Although hydrolysis appears to be not of relevance for the *in vivo* fate of POx, PPrOx-PEI copolymers were recently shown to form polyplex particles offering potential as DNA delivery carriers.[230]

2.2.3 Prospects for an enzymatic Degradation of Polypeptoids

During the evolution of peptide and protein structures more than three billion years ago, 20 amino acids emerged as the ideal building blocks of the biosynthetic chain. According to their structure, properties and bioavailability, these 20 amino acids can be further classified into several subclasses (*cf.* Figure 2.23). However, the imino acid proline holds an unique position with the side chain being attached to both the nitrogen and the C_α carbon, resulting in a five-membered cyclic structure comprising a secondary amine and an associated substantial impact on polarity and basicity of the amino acid itself as well

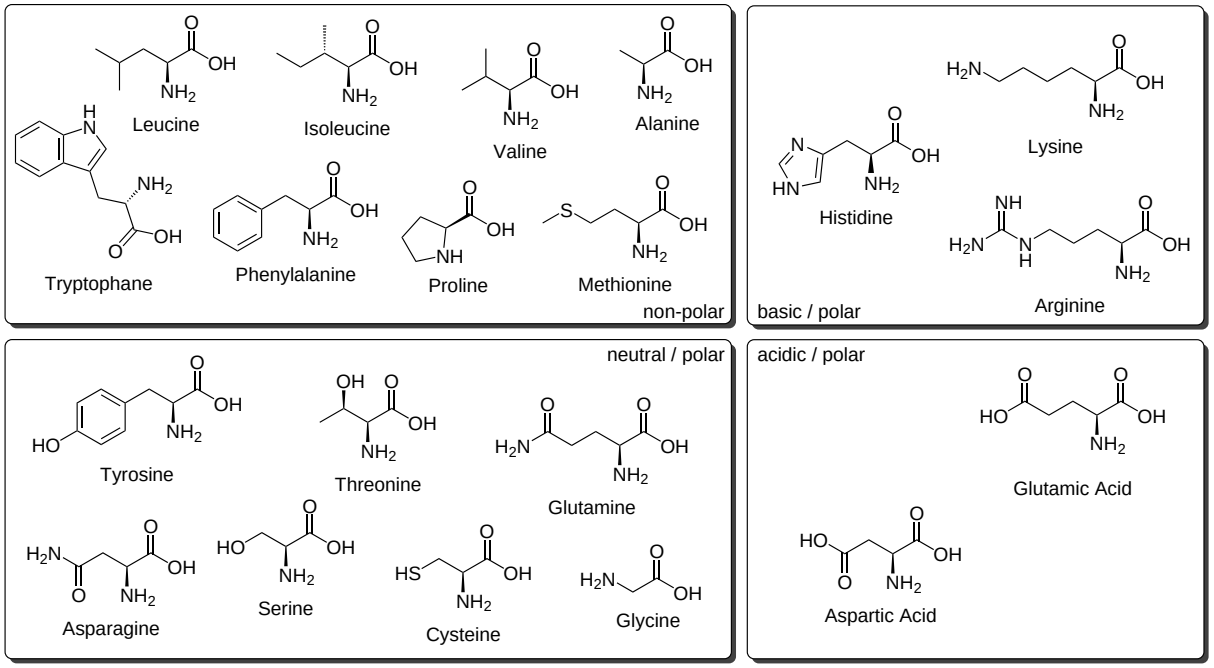

Figure 2.23: Depiction of the 20 proteinogenic amino acids, classified based on their polarity and pH-value.

as major constraints on peptide backbones bearing proline residues.[231, 232]

Due to the cyclic structure of proline, rotation around the C_α - N bond (ϕ), usually only affected by steric hindrance or electrostatic repulsion of adjacent side chains, is highly limited. Proline residues establish a fixed bend within a peptide chain, thus changing direction and affecting the global shape of a peptide or protein.

Furthermore, lack of functional groups impedes proline participation in hydrogen bonds and resonance stabilization of amide bonds, which is the reason why proline is the only amino acid not compatible with defined secondary structures like α-helices and β-sheets. Nevertheless, proline is a common residue in turns and also found quite often as the first residue of α-helices or within the edge strands of β-sheets.

As a result of its unique conformation and biochemistry, introduction of proline residues influences the interaction of peptides with enzymes tremendously, thus hindering proteolytic hydrolysis. For this purpose, a physiological key function of proline is the inhibition of enzymatic degradation of biologically active peptides.[233]

Within the human body, proline is first and foremost a fundamental component of collagen, a structural protein making up around 30 % of the total protein mass.[234] Collagen (Greek: $\kappa\acute{o}\lambda\lambda\alpha$, kólla = glue; -$\gamma\acute{\varepsilon}\nu$, -gen = producing), mainly found in bones, skin, tendons,

ligaments and connective tissue, possesses an atypical amino acid composition primarily consisting of glycine (33 %), proline (13 %), alanine (11 %) and hydroxyproline (10 %) residues, with Pro-Hyp-Gly being the most common triplet (11 %).[234, 235] With 23 % of the residues being either proline or hydroxyproline, not only entropic costs but also susceptibility against enzymatic degradation are reduced to a minimum.
Similar features are attributed to the N-functionalization of (poly)peptides in general and (poly)peptoids in particular. The introduction of tertiary amides via N-methylation is a common tool of biological and medicinal chemistry to enhance the *in vivo* half-life of peptides and improve their pharmacokinetic profile,[236] while (poly)peptoids are actually claimed to be thoroughly insusceptible to proteolytic hydrolysis.[237] Investigations by Zuckerman and coworkers focused on the enzymatic digestion of peptide and peptoid sequences by several prominent proteases, namely carboxypeptidase A, papain, pepsin, trypsin, elastase and chymotrypsin. For comparison, specific sequences comprising L-amino acids and their analogues either comprising D-amino acids or representing peptoids and reverse order retro-peptoids, respectively, were synthesized. As anticipated, L-amino acid sequences were cleaved by the respective enzymes, however, neither the corresponding D-amino acid nor peptoid and reverse-peptoid sequences were susceptible to degradation, which is easily intelligible in consideration of the high substrate specificity commonly possessed by proteases. Whether or not a particular substrate is hydrolyzed by a specific protease is determined by its sequence, conformation and the accessibility of cleavable bonds. Due to the distinct tertiary structures of enzymes, substrate access to the active site is easily inhibited by steric effects. In context of the above-mentioned study, slight alterations of the original sequence probably induce extensive adjustments of the respective secondary and tertiary structure, thus impeding proteolytic hydrolysis. Furthermore, it should be noted that all of the enzymes investigated by Zuckermann and coworkers rule out peptide chain scission at the site of a proline residue.[238] As already discussed, bearing a secondary amine proline is unique among the 20 proteinogenic amino acids, which is reflected by the low susceptibility towards enzymatic attacks of sequences comprising proline. Hence, proline residues resemble an intermediate between (poly)peptides and (poly)peptoids (Figure 2.24). In order to clarify whether or not (poly)peptoids are digested by natural enzymes, utilizing proteases that specifically recognize and cleave proline residues appears more promising. Indeed, nature evolved a great variety of appropriate

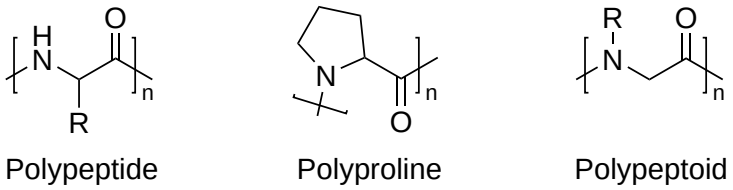

Figure 2.24: Line up of the chemical structures of polypeptides, polyproline and polypeptoids.

enzymes (Figure 2.25), of which the most essential ones will be highlighted hereafter.

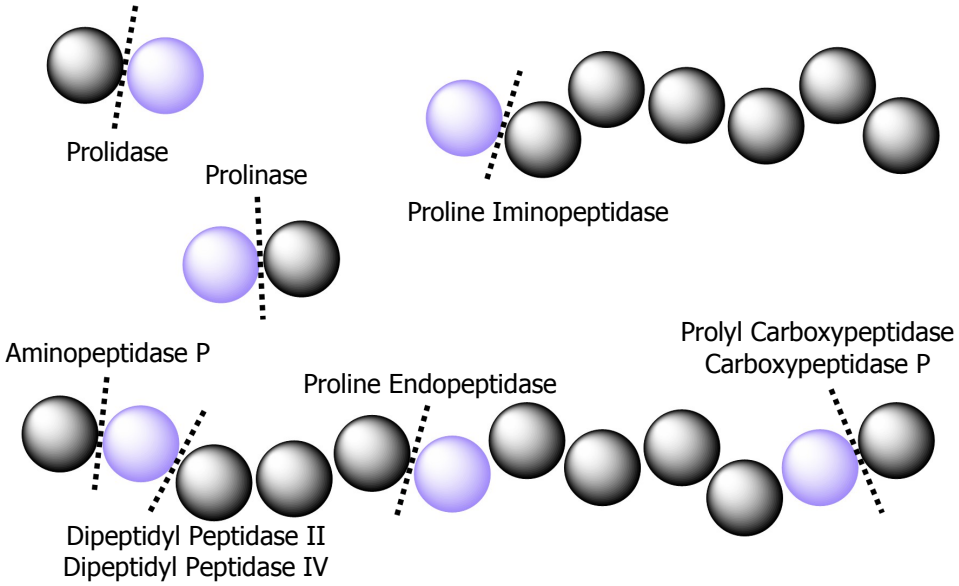

Figure 2.25: Based on the various positions in which proline residues may occur within peptides or proteins, a great variety of enzymes that are capable of recognizing and cleaving proline specifically evolved.

2.2.3.1 Proline-specific Peptidases

Proline Endopeptidases (PEP, EC 3.4.21.26)

Per definition, the serine protease family of proline endopeptidases (PEP) cleaves peptide bonds on the carboxyl side of internal proline residues:

$$Y - Pro + X$$

where Y is a peptide or protected amino acid and X an amino acid, peptide, amide, aromatic amine or alcohol and + marks the cleaved bond.[239, 240] First PEP activity was reported by Walter *et al.* in 1971, who observed hydrolysis of the proline-leucine bond of oxytoxin in human uterus homogenate.[241] Over the intervening years, PEP enzymes have been isolated from a variety of sources like eukaryotes (e.g. human, pork, bovine,

mouse, rat), bacteria (e.g. *Flavobacterium meningosepticum*, *Aeromonas hydrophila*) and archaea (e.g. *Pyrococcus furiosus*, *Sulfolobus tokodaii*).[242] Despite the ubiquitous presence of PEP enzymes in vertebrate organs, particularly high activities were found in testis, liver, lung, skeletal muscle and brain.[243] Elevated levels of PEP activity were also found in tumor tissue and body fluids (semen, serum and saliva, but not urine).[243, 244] Initial studies demonstrated the cleavage of low molecular weight peptides of less than 3000 g/mol by PEP enzymes, whereas high molecular weight proteins like albumin (66 kg/mol) and elastin (72 kg/mol) could not be hydrolyzed.[245, 246] More recent investigations suggest that the chain length limit of at least some PEP enzymes might be slightly higher,[247] however, cleavage by most species is restricted to oligomers. Although PEP enzymes are highly specific to proline, cleavage of the Y-Ala-X bond is also observed at a low rate of 1/100 to 1/1000 of that of Y-Pro-X bond.[248] However, PEP enzymes do not cleave Pro-Pro bonds, which most probably precludes the digestion of (poly)peptoids as well.[239, 249]

Proline-specific N-terminal Exopeptidases

Dipeptidyl Peptidase IV (DPP IV, EC 3.4.14.5) cleaves N-terminal dipeptides from oligopeptides with penultimate proline or alanine:

$$\mathrm{Y - Pro + X}$$

where Y is an amino acid and X an amino acid (except from proline and hydroxyproline), peptide, aromatic amine or alcohol.[232, 250, 251] Also referred to as post-proline dipeptidyl aminopeptidase, dipeptidyl peptidase IV (DPP IV)was first discovered in rat liver by Hopsu-Havu and Glenner and identified as glycylproline naphthylamidase.[252] The membrane-bound serine-type DPP IV appears to be ubiquitous in vertebrates[253] and was purified from a great variety of tissues, like rat liver[250, 254, 255], porcine liver[256] and kidney[253, 256–258], lamb kidney[259], porcine small intestine[260] and human submaxillary gland[261]. Highest activities of DPP IV were observed in kidney, however, activity was also found in liver, skin, spleen and jejunum.[239] Rejecting the cleavage of Pro-Pro as well as Pro-Hypro, DPP IV is most likely incapable of cleaving (poly)peptoid sequences.

Dipeptidyl Peptidase II (DPP II, EC 3.4.14.2) was only demonstrated to be distinct from DPP IV through detailed biochemistry and substrate specificity studies. Just as DPP IV, dipeptidyl peptidase II (DPP II) cleaves N-terminal dipeptides from sequences

with penultimate proline or alanine:

$$\text{Y} - \text{Pro} + \text{X}$$

where Y is an unprotected amino acid and X is an amino acid or dipeptide. Interestingly, unlike any other proline specific peptidase mentioned here, DPP II (Figure 2.26) tolerates alanine substituting for proline very well and with comparable cleavage rates.[262] However, substrates with hydroxyproline instead of proline at the penultimate position are not hydrolyzed.[263] DPP II prefers basic over neutral amino acid residues at the N-terminus, whereas 100-fold reduced enzyme activity is reported for acidic amino acids in the ultimate position.[262] In contrast to DPP IV, DPP II was shown to cleave Pro-Pro bonds, although with reduced efficiency, and might therefore also be capable of cleaving (poly)peptoids.[262] Furthermore, decreasing cleavage rates with increasing chain length and no activity at all towards sequences of more than 11 residues are observed.[262, 264, 265]

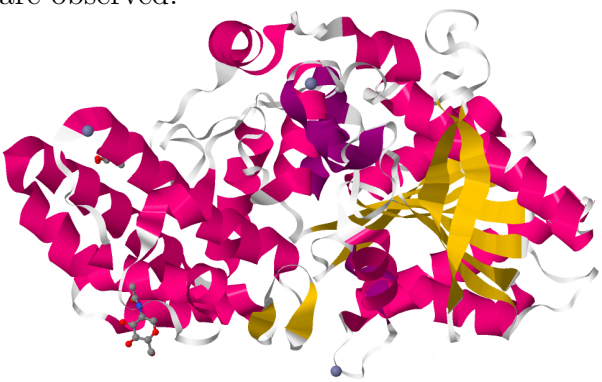

Figure 2.26: Biological assembly and ligands of human DPP II. Created with RCSB Protein Data Base according to ref. [266].

DPP IV is resistant to sulphydryl blocking and chelating agents but inhibited by addition of diisopropyl fluorophosphate (DFP), which classifies DPP II as a serine protease.[262, 267, 268] Further inhibitory effects have been observed after addition of mercury and zinc ions.[264, 267, 269] Reported pH optima range from 4.5 to 6.3, with maximum activity observed at pH 5.5.[267, 268, 270, 271] DPP II is widely distributed and was isolated from inter alia *Schistosoma japonicum*,[272] rat brain,[262, 264, 268, 271] rat kidney,[264] porcine spleen,[269] bovine anterior pituitary gland[270] and human placenta[267].

Proline Iminopeptidase (EC 3.4.11.5) is an aminopeptidase that releases N-terminal proline residues from large peptides such as poly-L-proline as well as from small peptides like Pro-Gly or Pro-Gly-Gly:

$$\text{Pro} + \text{X}$$

where X is an amino acid or peptide.

Proline iminopeptidase (Figure 2.27), also known as cytosol aminopeptidase V, was first identified in proline-less mutants of *E. coli* and purified by Sarid, Berger and

Katchalski.[273, 274] It is described to be highly specific to proline as, among others, N-terminal hydroxyproline is not attacked, and strictly an exopeptidase, since N-substituted proline residues are not cleaved and cleavage of poly-L-proline solely yields proline. Proline iminopeptidase has a wide pH-optimum of 7.8 to 9.5 and is activated by Mn^{2+} while addition of Cd^{2+}, Co^{2+}, Cu^{2+}, Fe^{2+}, Fe^{3+}, Hg^{2+} or Zn^{2+} inhibits enzymatic activity. After proline iminopeptidase was found to be also present in cell-free extracts of wild type *E. coli*, it was also detected in *Brevibacillus brevis*, chicken, rat, rabbit and pork tissues as well as in chicken egg white.[273, 274, 276, 277] In general, highest activities were observed in liver and kidney tissue, but lower activities were also found in spleen, heart, lung and testis.

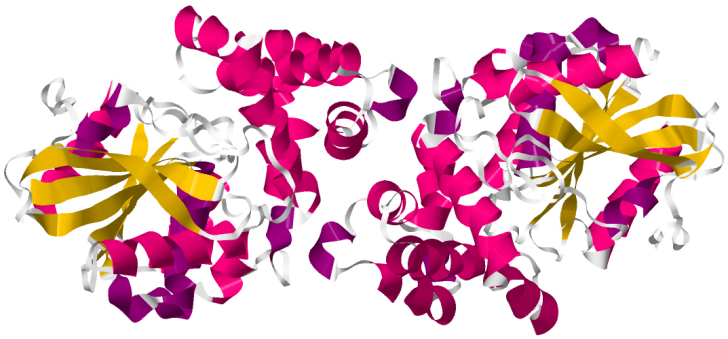

Figure 2.27: Biological assembly and ligands of Proline Iminopeptidase from *Xanthomonas campestris pv. citri*. Created with RCSB Protein Data Base according to ref. [275].

However, the high enzyme specificity towards L-proline as assumed by Sarid et al. remains doubtful. To prove their hypothesis, they investigated the exhaustive digestion of random copolymers comprising L-proline and D-proline, hydroxyproline, glycine, or sarcosine, respectively.[273] A colorimetric assay was used to determine the amount of released L-proline, which was compared with values calculated based on statistical considerations. While for both D-proline and hydroxyproline comonomers their calculation corresponds well with the amount of released L-proline detected by the colorimetric assay, in case of sarcosine as the comonomer the amount of free L-proline is 4.4 times higher than expected according to calculation. This becomes even more surprising considering investigations by Fasman and Blout focused on the copolymerization of sarcosine and proline, yielding gradient copolymer with a higher percentage of sarcosine at the N-terminus.[278] In this context, the high amount of released L-proline can merely be attributed to the release of sarcosine as well. It should be noted that neither this assumption has been examined in further experiments yet, nor does any indication of proline iminopeptidase activity against any other (poly)peptoid exist.

Aminopeptidase P (APP, EC 3.4.11.9) is a metallo-exopeptidase catalyzing cleavage of the N-terminal amino acid in peptides with penultimate proline:

$$\text{Y} + \text{Pro - X}$$

where Y is an N-unsubstituted amino acid and X is an amino acid, peptide or -OH.[279, 280] Yaron and Mlynar were the first who isolated aminopeptidase P (APP) (Figure 2.28), also named X-prolyl aminopeptidase, from *E. coli*.[281] Since then, APP has been purified

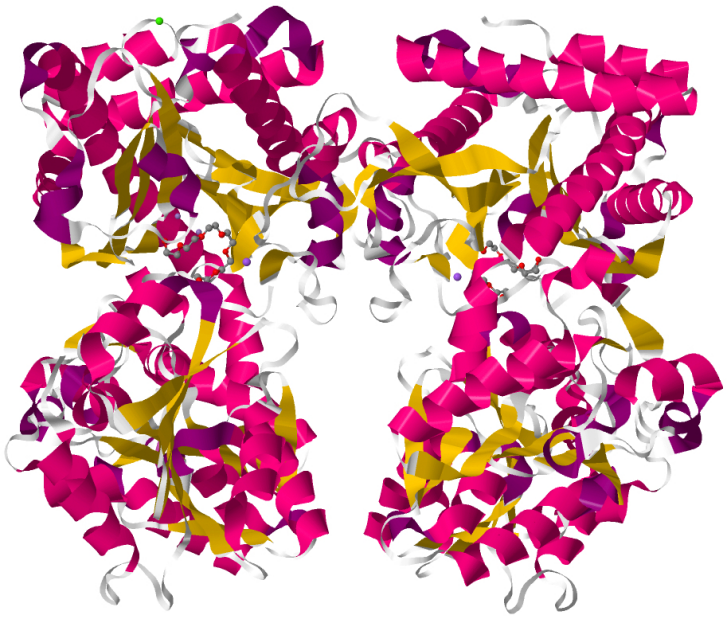

Figure 2.28: Biological assembly and ligands of human cytosolic APP. Created with RCSB Protein Data Base according to ref. [282].

not only from other bacteria (e.g. *Lactococcus lactis*,[283] *Streptomyces lividans*[284]), but also from mammalian tissues like porcine kidney,[285, 286] bovine lung,[287] rat brain[288] and lung[289] as well as human erythrocytes,[290] leukocytes,[291] kidney[292] and lung[293]. Highest activities are observed at an optimum pH range of 7.0 to 8.5 and an optimum temperature of 43 °C. Peptides containing penultimate hydroxyproline are not cleaved,[239] however, APP was shown to cleave sequences with proline in the N-terminal and penultimate position as in Pro-Pro or Pro-Pro-Pro-Pro,[294] thus implying a potential relevance for the cleavage of (poly)peptoids.

Proline-specific C-terminal Exopeptidases

Prolylcarboxypeptidase (EC 3.4.16.2) was first identified in the lysosomal fraction of porcine kidney as an enzyme catalyzing the cleavage of phenylalanine from C-terminal Pro-Phe of angiotensin II and is thus also referred to as angiotensinase C.[295, 296] With proline at the penultimate position, prolylcarboxypeptidase cleaves C-terminal amino acids with a rather broad specificity:

X - Pro + Y

where Y is an amino acid with a free carboxyl group and X is a protecting group or peptide.[239, 297] However, Z-Pro-Gly is only hydrolyzed at a slow rate and Z-Pro-Pro as well as Z-Pro-Hyp are not hydrolyzed at all. It is therefore very unlikely that prolylcarboxypeptidase is capable to cleave (poly)peptoids.

Carboxypeptidase P (EC 3.4.17.16) was first identified and purified from porcine kidney by Dehm and Nordwig.[298] It cleaves C-terminal amino acids from penultimate proline residues with a specificity quite similar to prolylcarboxypeptidase:

X - Pro + Y

where Y is an amino acid and X is a protecting group or peptide.[239, 286] Carboxypeptidase P is not strictly specific to proline as low hydrolysis rates for Z-Ala-Tyr and Z-Gly-Phe are observed, however, proline is preferred and hydroxyproline cannot substitute for proline. Although a dipeptidase activity towards Pro-Ala and Pro-Phe was described, the enzyme does not exhibit activity towards Z-Pro-Pro which most probably precludes a potential digestion of (poly)peptoids.

Proline-specific Dipeptidases

Prolidase (EC 3.4.13.9) cleaves N-terminal amino acids from iminodipeptides:

Y + Pro

where Y is an unprotected amino acid other than proline. It is therefore unlikely that prolidase is involved in the digestion of dipeptoids. Although with significant losses in hydrolytic activity, hydroxyproline substitution does not impede prolidase catalyzed hydrolysis.[299]

Prolidase has a vital role in the hydrolysis of collagen degradation products and other

Y-Pro dipeptides, followed by subsequent recycling of proline. Lack of prolidase, and thus the inability to recycle proline from dipeptides, is a rare pathological state referred to as prolidase deficiency (PLD-D). PLD-D is associated with abnormalities of all collagenous tissues, including ulcerations of the skin on the face, palms, lower legs and soles, as well as facial dysmorphy, frequently accompanied by recurrent infections and mental retardation.[300] Patients suffering from PLD-D excrete tremendous amounts of Y-Pro dipeptides, especially Gly-Pro.

Prolinase(EC 3.4.13.18) hydrolyzes dipeptides with N-terminal proline or hydroxyproline:

$$\text{Pro} + \text{Y}$$

where Y is an unprotected and preferentially hydrophobic amino acid.[301, 302] The enzyme neither cleaves amides of proline or hydroxyproline nor tripeptides and is therefore also referred to as iminodipeptidase.[301, 303] Stabilization of the highly labile prolinase is achieved by addition of Mn^{2+}. Presence of Ag^{+} appears to inhibit enzymatic activity, whereas activation by Mn^{2+} and Cd^{2+}[304, 305] and a rather basic pH optimum of 8.5 to 9 are observed.[306] Prolinase was purified from yeast[307] as well as mammalian tissues such as porcine,[302, 303] bovine[306] and human[308] kidney. However, prolinase appears to possess only moderate specificity regarding proline at the N-terminus, as for instance substitution by glycine is well tolerated.[309]

2.2.3.2 Non-Proline-specific Peptidases cleaving at Proline

Aside from the great variety of more or less proline-specific peptidases capable of hydrolyzing peptide sequences comprising proline in various constellations (*cf.* Figure 2.25) described previously, there are numerous peptidases not specific to proline, but nevertheless able to cleave peptides at proline residues. Although certainly not exhaustive, the following section will give a number of examples of interesting non-proline-specific peptidases. Cleavage of proline comprising dipeptides, however, appears to be a unique function of rather specific enzymes.

Endopeptidases

In general, peptide bonds containing proline are considered resistant to proteases commonly applied for protein sequencing. However, in some cases trypsin (EC 3.4.21.4) is capable of

cleaving Lys-Pro as well as Arg-Pro bonds.[310–313] *Armillaria mellea* neutral proteinase[314] (EC 3.4.24.20) and lysyl endopeptidase (EC 3.4.21.50)[315] specifically cleave peptides on the carboxyl side of lysine, including the Lys^{8}-Pro^{7} bond of vasopressin and the Lys^{29}-Pro^{28} bond of the insulin B chain. The serine endopeptidase lactocepin (EC 3.4.21.96) isolated from *Lactococcus lactis* catalyzes the fragmentation of β-casein[316] as well as κ-casein[317] into oligopeptides with a very broad specificity, including the cleavage of proline comprising dipeptide bonds such as His-Pro, Tyr-Pro, Pro-Phe, Pro-Gly, Pro-Ile, Pro-Thr, Leu-Pro, Pro-Leu and Pro-Pro and might therefore also cleave (poly)peptoids. Another potential candidate for the digestion of (poly)peptoids are members of the astacin family (EC 3.4.24.21), multidomain zinc metalloendopeptidases isolated from the crayfish *Astacus fluviatilis* described to hydrolyze Pro-Ala, Pro-Ser, Pro-Gly, Pro-Thr and Pro-Pro.[318] The metalloendopeptidase thermolysin (EC 3.4.24.27) is reported to hydrolyze peptide bonds on the carboxyl side of proline, e.g. Pro-Ala, Pro-Ile and Pro-Val in alcohol dehydrogenase[319], Pro-Tyr and Pro-Val in ferredoxin[320] and Pro-Trp in a bone-marrow-proteoglycan[321]. Cathepsin L (EC 3.4.22.15), a lysosomal cysteine endopeptidase, has a high preference for aromatic residues in the P2 position, but tolerates proline at P1 in sequences such as in Pro-Ala, Pro-Gly, Pro-Met and Pro-Pro and is therefore also likely to exhibit activity against (poly)peptoids.[322]

N-terminal Exopeptidases

Possessing a high preference for alanine at the N-terminal position, the zinc aminopeptidase N (EC 3.4.11.2) is reported to release amino acids from peptides, amides and arylamides. Albeit slower, cleavage of N-terminal proline from sequences such as Pro-Phe and Pro-Trp dipeptides is not ruled out either.[323] In certain cases, Y-Pro dipeptides are released from sequences comprising hydrophobic N-terminal residues and proline in the penultimate position, however, Pro-Pro is not cleaved.[238, 324] With quite similar yet broad specificity regarding alanine at the N-terminal position, cytosol alanyl aminopeptidase (EC 3.4.11.14), a Co^{2+} and Zn^{2+}activated metalloexopeptidase widely distributed in mammalian tissues and body fluids, releases proline from Pro-Phe-Arg-AMC (7-amido-4-methylcoumarin).[325]

C-terminal Exopeptidases

A variety of carboxypeptidase enzymes including carboxypeptidase Y (carboxypeptidase C or cathepsin A, EC 3.4.16.5) from yeast[326] and carboxypeptidase O from *Aspergillus*

niger[327] possess very broad specificity and hydrolyze C-terminal peptide bonds where proline is either the penultimate or terminal residue, however, Pro-Pro is not cleaved. Peptidyl-dipeptidase A (angiotensin-converting enzyme compound peptidase, EC 3.4.15.1) isolated from *E. coli*[328] as well as various mammalian sources[329] releases C-terminal dipeptides from oligo- and polypeptides. While the enzyme does not catalyze peptide bond scission on the amino side of proline and thus excludes proline at the penultimate position, it is capable of cleaving the peptide bonds on the carboxyl side of proline. By this means, peptidyl-dipeptidase A cleaves the C-terminal His^9-Leu^{10} dipeptide from angiotensin I yielding the octapeptide angiotensin II, a potent vasopressor with penultimate proline at the carboxyl terminus, which is therefore insusceptible to further hydrolysis by peptidyl-dipeptidase A.[309] In a similar way, the enzyme inactivates the vasodilator bradykinin by successively releasing Phe^8-Arg^9 and Ser^6-Pro^7 from the C-terminus. However, precluding the cleavage of Pro-Pro bonds peptidyl-dipeptidase A is not of relevance for the cleavage of (poly)peptoids.

2.2.4 Sarcosine

Justus von Liebig, born 1803 in Darmstadt, is considered as the founder of organic chemistry and a major contributor to agricultural and biological chemistry.[331] *Liebig's Extract of Meat*, a highly concentrated beef meat stock, is used and acknowledged worldwide for adding meat flavor to a range of dishes (Figure 2.29). During his work on the second edition of *Animal Chemistry* in 1847, Liebig isolated a new organic base obtained by boiling creatine and creatinine and named it sarcosine (Greek: $\sigma\acute{\alpha}\rho\xi$, sarx = flesh).[332]

Only 15 years later, Liebig's nephew Jacob Volhard recognized sarcosine as *N*-methylglycine and described its synthesis from methylamine and monochloroacetic acid.[333, 334]

Sarcosine is a natural, non-proteinogenic amino acid and ubiquitous in biological materials, as it is found in muscles and body fluids such as blood (0.06 - 2.67 μmol/L in serum),[335] saliva, urine (5.3 - 177 μmol/L)[335] and feces as well as various

Figure 2.29: Poster advertising *Liebig Company's Extract of Meat.* Taken from ref [330].

kinds of food like turkey, ham, egg yolk, vegetables and legumes. It exhibits excellent solubility in water, has a sweet taste and forms colorless hygroscopic crystals.

A rare metabolic disorder known as sarcosinemia is characterized by elevated levels of sarcosine in plasma and urine caused by a mutation of the sarcosine dehydrogenase (EC 1.5.8.3) coding gene or severe folate deficiency, as folate is essential for the demethylation of sarcosine yielding glycine.[336, 337] Although some studies associate the disorder with neurologic problems and mental retardation,[336, 338, 339] clinical abnormalities are most likely no phenotypic manifestations of sarcosinemia with no known toxicity of sarcosine.[340]

Within the scope of the present work, sarcosine is first and foremost of significance as the product of exhaustive enzymatic as well as hydrolytic degradation of PSar. However, sarcosine is also known to play a vital role in physiological as well as pathological processes, some of which are discussed briefly in the following section.

2.2.4.1 Metabolic Pathway

Sarcosine is incorporated in a number of metabolic processes. Within mitochondria, sarcosine is an intermediate product of both the choline and glycine metabolism (Figure 2.30). Generation of sarcosine in the course of the choline metabolism is based on the methylation of phosphatidylethanolamine by S-adenosylmethionine (SAM) yielding phosphatidylcholine. During a subsequent multi-stage process, betaine (trimethylglycine) is formed as an intermediate product and further oxidized yielding dimethylglycine via betaine-homocysteine S-methyltransferase (BHMT).[342] Subsequent oxidative demethylation of dimethylglycine catalyzed by dimethylglycine dehydrogenase (DMGDH) results in the formation of sarcosine.[343, 344]

As a part of the glycine metabolism, glycine is converted to sarcosine during the demethylation of SAM yielding S-adenosylhomocysteine (SAH) via glycine *N*-methyltransferase (GNMT), a SAM regulatory enzyme highly expressed in mammalian liver, kidney, exocrine pancreas and prostate.[345–348] During a subsequent oxidative phase, sarcosine is demethylated yielding glycine by sarcosine dehydrogenase (SARDH) or sarcosine oxidase (SAROx), respectively.[343] Both SAROx and SARDH as well as DMGDH generate methylene tetrahydrofolate, which is required for the conversion of serine to glycine via serine hydroxymethyltransferase (SHMT).

Furthermore, sarcosine is the product of creatine degradation via creatinase (Figure

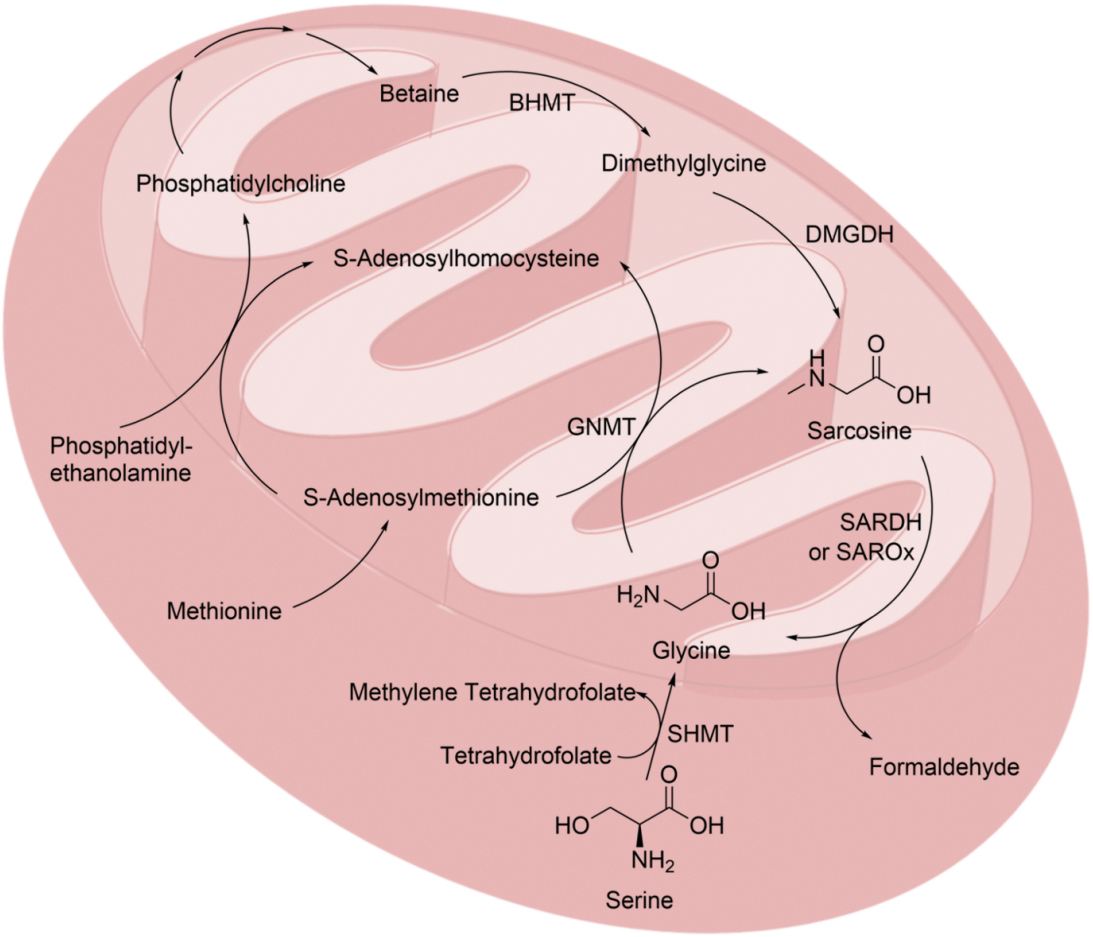

Figure 2.30: Metabolism of sarcosine within mitochondria. SHMT: serine hydroxymethyltransferase (EC 2.1.2.1), SARDH: sarcosine dehydrogenase (EC 1.5.8.3), SAROx: sarcosine oxidase (EC 1.5.3.1), GNMT: glycine *N*-methyltransferase (EC 2.1.1.20), BHMT: betaine-homocysteine S-methyltransferase (EC 2.1.1.5), DMGDH: dimethylglycine dehydrogenase (EC 1.5.8.4). Modified from [341].

2.31).[349] Creatine is a naturally occurring nitrogenous organic acid and an essential component of the energy supply system in vertebrates. Phosphorylation of creatine via creatine kinase yields phosphocreatine, a fundamental and the most rapid source of energy in form of ATP in skeletal muscles and brain.

Recent investigations by several groups portray enhanced sarcosine production and increased levels of sarcosine metabolites in prostate cancer.[350–353] Sarcosine therefore offers tremendous potential as a reliable biomarker for prostate cancer progression, especially as it can be detected conveniently and non-invasively in human urine.[354]

Furthermore, antidepressant-like properties of sarcosine were observed in animal behavior models with naive rats including acute behavioral tests like the forced swim test and tail suspension test as well as anxiety-based tests such as the elevated plus maze test.[355] By

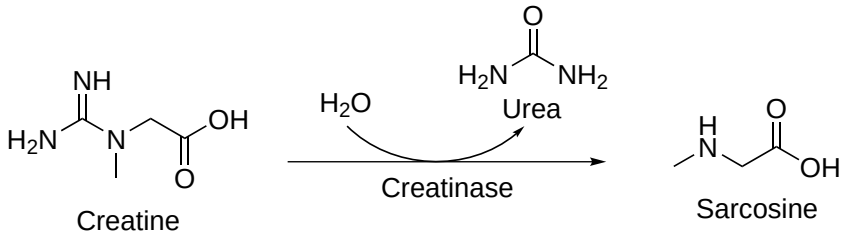

Figure 2.31: Degradation of creatine yielding sarcosine via creatinase (EC 3.5.3.3).

and large, sarcosine displayed effects similar to conventional antidepressants. Chronic sarcosine administration also reversed chronic unpredictable stress-induced behavior caused by a sucrose preference test as well as a novelty suppressed feeding test. An affiliated proof-of-concept clinical trial in 40 predominantly taiwanese men in their mid-30s diagnosed with major depressive disorder proved significant higher effectiveness of sarcosine compared to citalopram, a typical antidepressant inhibiting the serotonin re-uptake, in all assessments thus demonstrating the potential of sarcosine as a novel antidepressant.[355] Recently, sarcosine is also discussed for the treatment of schizophrenia with doses of 1 g/d in addition to conventional antipsychotics inducing significant improvement of cognitive and negative symptoms in a 23-year-old male patient.[356, 357]

3 Motivation

Naturally occurring polymers have formed life on earth since time immemorial. However, only in the last century mankind discovered the overwhelming potential of synthetic polymers specifically designed for the desired application. With their enormous versatility and easy accessibility, polymers became true all-rounders and accelerated technological progress like no other material.

By today, polymers are applied in all spheres of daily life. Countless electronic devices and vehicles are entirely or partly made of polymers. Although rather disputed, polymeric packaging materials are unbeatable in terms of efficiency, flexibility and durability. Furthermore, polymers are not only well established in construction (e.g. windows, floors, pipes, glazing etc.) but also highly valued in the leisure and apparel industry. It is scarcely surprising then, that polymers also conquered the fields of medicine, healthcare and cosmetics. From surgical supplies, sutures, implants (e.g. dentures and artificial joints) and emulgators in lotions, creams, shampoos as well as toothpastes to drug carriers and scaffolds for tissue engineering, biocompatible polymers are applied to save lives and make them more convenient.

Especially poly(ethylene glycol) (PEG), a water-soluble polyether offering a multitude of desirable features for biomedical applications, attracted great interest and became an almost ubiquitous component of medical and cosmetic formulations. However, the extensive application of PEG lately evoked serious criticism (*cf.* section 2.1.1). A key aspect in this context is its lack of biodegradability and concomitant accumulation of PEG *in vivo*.

Among the most promising candidates for replacing PEG in biomedical applications are poly(2-alkyl-2-oxazoline)s (POx) and polypeptoids, which are characterized by their similarity to natural polypeptides. However, although the enormous synthetic versatility and application potential of these so-called pseudo-polypeptides are subject of intensive research, very little is currently known on their stability *in vivo*.

Biodistribution and clearance of foreign particles is largely depending on their size. While small polymers ($R_h \leq 6$ nm) are rapidly filtered and cleared by the kidneys, larger ones ($R_h \geq 125$ nm) tend to accumulate in various tissues like liver, spleen and bone marrow, where they may trigger adverse effects and toxicity.[358–362] Nevertheless, various tissues and organelles of the mammalian body possess conditions upon which pseudo-polypeptides may potentially deteriorate.

The aim of this work is to investigate the stability of POx, polypeptoids and PEG against biologically relevant oxidative, hydrolytic and enzymatic degradation.

Oxidation

Oxidative species like hydrogen peroxide, hydroxyl radicals and hypochlorous acid are, for instance, formed as a byproduct of cellular respiration, but also generated on purpose by neutrophils and macrophages in order to destroy foreign particles. In the context of the preceding master thesis, susceptibility of all three polymer species towards oxidative degradation by a Fenton-like reagent has already been ascertained and shown to be highly depending on the polymer chain length.[169, 218] Building on these results, a more comprehensive understanding of oxidative polymer decomposition should be gained by enlarging the range of both the investigated polymers as well as the applied oxidative species. Furthermore, it is intended to identify species resulting from oxidative polymer degradation applying GC/MS spectroscopy in order to confirm or reject previously hypothesized mechanisms.

Hydrolysis

Although the largest part of the body has a slightly basic pH value (e.g. blood has an optimum pH of 7.4), specific areas like the stomach (gastric acid pH 1.2 - 1.3) and tumor tissues (pH 5.8 - 7.0)[363] possess acidic conditions under which polymers comprising hydrolytically labile amide bonds might decompose. Hoogenboom and coworkers suggested the *in vivo* side chain scission of POx yielding toxic PEI to be negligible,[225, 228] however, hydrolysis of polypeptoids would result in significant degradation by backbone scission yielding non-toxic amino acids.

Kinetic investigations performed in the framework of the present thesis should clarify whether or not the hydrolytic degradation of polypeptoids can be expected to affect their stability *in vivo* for instance during passage of the stomach and intestine.

Enzymatic Degradation

The proteolytic digestion of (poly)peptides and proteins by both highly specific as well as rather unspecific digestive enzymes is an essential part of metabolism. However, the minor modification of N-methylation is known and widely applied to decelerate if not completely prevent the breakdown of (poly)peptides.[61–63] Therefore, it is usually - and probably

prematurely - assumed that polypeptoids are insusceptible to enzymatic degradation in general.
In this respect, the medium-term stability of polypeptoids as well as POx and PEG within biological environments will be evaluated.

The present thesis is intended to provide a comprehensive overview on the most important pathways of polymer digestion *in vivo*. Within this framework, potential mechanisms and degradation products will be discussed and assessed regarding their effects on the human body. Eventually, this thesis will facilitate the appraisal of polypeptoids and POx regarding their stability and safety as future biopolymers.

4 Results and Discussion

4.1 Oxidative Degradation of Polymers

The oxidative degradation of PEtOx, PEG and PEtGly was already investigated within the framework of the preceding master thesis (see section 2.2.1.5).[169, 218] Although the susceptibility of all three polymer species towards oxidative degradation by hydroxyl radicals was proven, many questions were left unanswered and motivated further investigations on this topic.

4.1.1 Utilization of Iron instead of Copper for the Generation of Hydroxyl Radicals by a Fenton-Reaction

For previous investigations, hydroxyl radicals were generated by a Fenton-like reaction of hydrogen peroxide and copper sulfate:

$$Cu^{2+} + H_2O_2 \longrightarrow Cu^{+} + \cdot OOH + H^{+}$$

$$H_2O_2 + Cu^{+} \longrightarrow \cdot OH + OH^{-} + Cu^{2+}$$

However, Fenton reactions are most intensively studied with iron[364] and the high affinity of cupric ions to ligands containing nitrogen questioned the comparability of the oxidative degradation rates of POx and PEG. Indeed, Ringsdorf and coworkers observed the development of a hexagonal columnar mesophase by PMeOx using X-ray scattering and suggested a helix structure comprising internal nitrogen atoms.[365] Therefore, complexation of copper by POx helices is quite conceivable and might have significant effects on the degradation rate. On the one hand, complexation may decelerate the oxidative degradation by a shielding effect, on the other hand the resulting spacial proximity could also accelerate oxidative deterioration of the POx.

In order to assess influences of a potential complexation of copper by PEtOx, the oxidative degradation of $PEtOx_{51}$ and $PEtOx_{108}$ by 50 μM ammonium iron(II) sulfate and 50 mM hydrogen peroxide at 37 °C was investigated. After predefined intervals of time, aliquots of 5 mL ($\widehat{=}$ 5 mg polymer) were withdrawn, freeze-dried and analyzed via gel permeation chromatography (GPC) in hexafluoroisopropanol (HFIP).

The obtained elugrams (Figure 4.1) reveal the development of a strong bimodal distribution within only 8 h of incubation. With prolonged incubation time, the ratio between

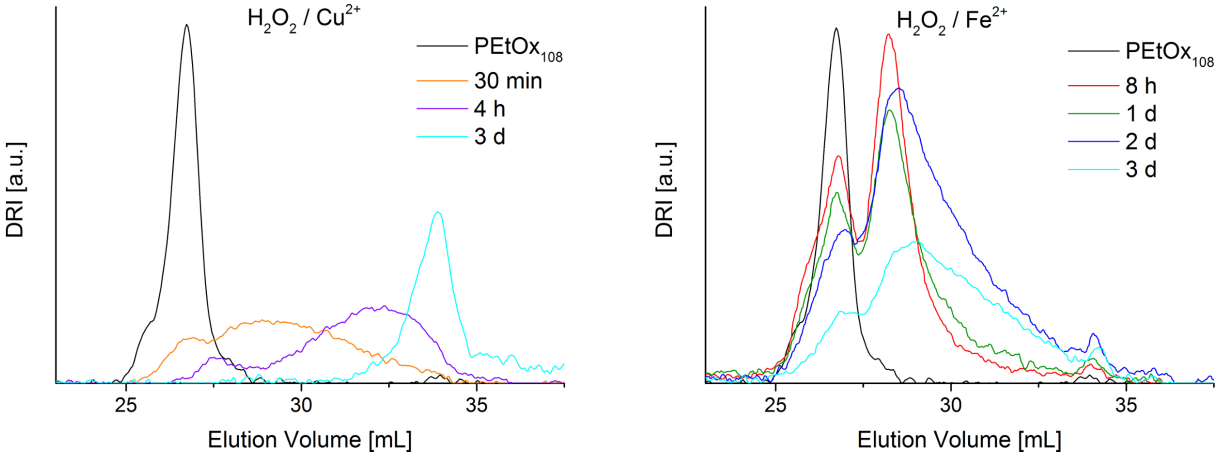

Figure 4.1: Elugrams of $PEtOx_{108}$ after incubation with 50 mM hydrogen peroxide and 50 μM copper(II) sulfate (left) or ammonium iron(II) sulfate (right) at 37 °C.

both signals continuously shifts towards the lower molecular weight distribution which simultaneously evolves a low molecular weight tailing, indicating a preferred chain scission in the center of the polymer rather than sequential oxidation of the chain ends. Apart from the significantly slower degradation of $PEtOx_{108}$ when ammonium iron(II) sulfate instead of copper(II) sulfate is applied for the generation of hydroxide ions, patterns of the elugrams are comparable regarding the emerging bimodal distribution.

Determination of the mass average molar mass (M_w) from the elugrams allows comparison with the previously obtained results on the oxidative degradation by $CuSO_4$ and H_2O_2 (Figure 4.2).[169, 218] Direct comparison shows significantly lower apparent degradation rates of $PEtOx_{51}$ and $PEtOx_{108}$ when iron instead of copper is applied for the generation of hydroxyl radicals via Fenton reaction. The resulting decrease of the apparent degradation rate via substitution of copper by iron is quite similar to a reduction of the H_2O_2 concentration by 90 %. One likely reason for this is the higher reaction rate constant of a Fenton-like reaction with copper ($4.7 \cdot 10^3$ $mol^{-1}sec^{-1}$[366]) compared to iron (76 $mol^{-1}sec^{-1}$[367]).[368] Although the potential complexation of copper by PEtOx cannot be ruled out, the tremendously higher Fenton reaction rate constant of copper far outweighs the effects of a possibly existing complexation.

Nevertheless, both iron and copper are available for the generation of hydroxyl radicals *in vivo*. The adult human body contains about 4 g of iron and 80 mg of copper, with the vast majority being bound to proteins but at disposal for Fenton-like reactions.[368] Indeed, Cederbaum and Dicker proved the generation of hydroxyl radicals in rat liver

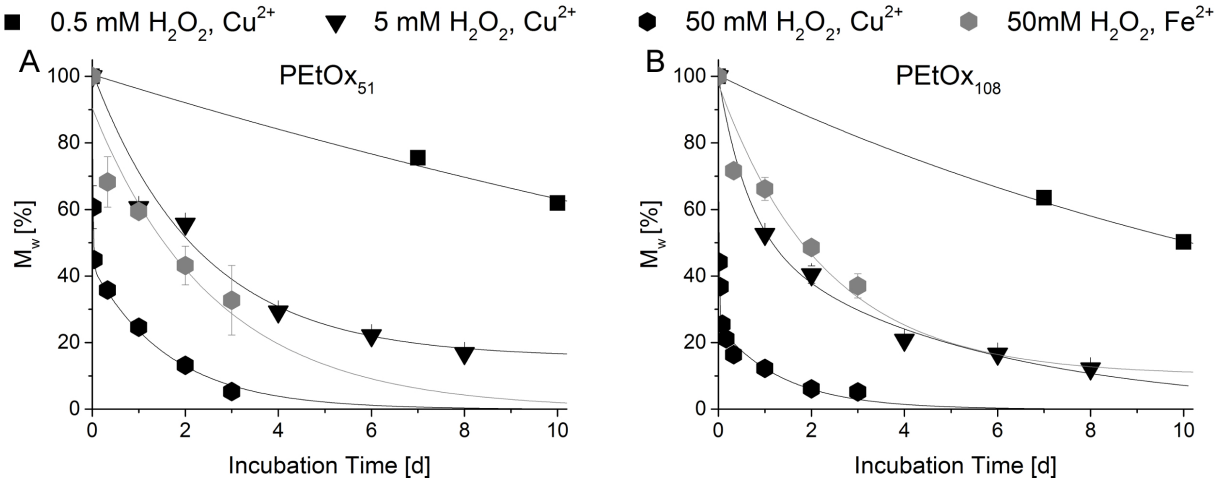

Figure 4.2: Decrease of M_w during oxidative degradation of $PEtOx_{51}$ and $PEtOx_{108}$ by hydroxyl radicals generated from H_2O_2 and Cu^{2+} or Fe^{2+}, respectively. Data are normalized to the pristine polymers and presented as mean ± SEM (n = 3). Lines are intended as a guide to the eye.

microsomes by an iron involing Fenton-reaction.[369] It can therefore be reasonably assumed that both copper and iron induced generation of hydroxyl radicals might be implicated in the oxidative degradation of POx *in vivo*.

4.1.2 Correlation of apparent Degradation Rate and Polymer Chain Length

Previous investigations revealed a strong dependency of the apparent degradation rate on the DP and molar mass of the respective polymer, with longer polymer chains being degraded faster than shorter ones.[169, 218, 219] In order to examine these correlations over an enhanced range of chain lengths, polymers with molar masses from 3.5 to 500 kg/mol were exposed to oxidative conditions and analyzed via GPC in HFIP.

By this means, previously obtained data of PEG_{45} (2 kg/mol) and PEG_{136} (6 kg/mol) were complemented with PEG_{230} (10 kg/mol), PEG_{800} (35 kg/mol) and PEG_{9100} (400 kg/mol), data of $PEtOx_{51}$ (5 kg/mol) and $PEtOx_{108}$ (11 kg/mol) were complemented with $PEtOx_{500}$ (50 kg/mol) and $PEtOx_{5000}$ (500 kg/mol). In contrast, data on the oxidative degradation of high molar mass PVP_{360} (40 kg/mol) and PVP_{3250} (360 kg/mol) acquired by Moritz Faust were complemented by the investigation of lower molar mass PVP_{30} (3.5 kg/mol)

and PVP_{90} (10 kg/mol).

Exemplary elugrams obtained after oxidative degradation of high molar mass PEtOx and PEG as well as low molar mass PVP applying 50 mM H_2O_2 and 50 μM $CuSO_4$ reveal extremely rapid deterioration especially of the high molar mass polymers (Figure 4.3).

Similar to the previously investigated $PEtOx_{51}$ and $PEtOx_{108}$, the formation of a characteristic bimodal distribution in case of $PEtOx_{500}$ and $PEtOx_{5000}$ is observed,[218] which indicates chain scission in the center of the polymer chain during the initial phase of oxidative deterioration. However, a strong shift of the peak elution volumes to higher elution volumes further implies the involvement of chain end oxidation processes at an advanced stage of the experiment.

Interestingly, oxidative degradation of both PEG_{800} and PEG_{9100} results in multimodal distributions with distinct signals at elution volumes of 27.5, 29, 30 and 32 mL regardless of the molar mass of the pristine polymer. Due to the absence of significant shifts of the individual signals, an oxidative cleavage in the center of the PEG chains appears most likely. Although less pronounced probably due to the lower polymer chain lengths and corresponding closer proximity of the signals to lower molar mass limit of the GPC system, a similar trend was observed during previous investigations.[218]

Earlier investigations on the oxidative degradation of high molar mass PVP revealed hardly any changes of the dispersity during oxidation and suggested a comparably high stability of the backbone but side chain scission yielding linear polyethylene to occur.[219] Although elugram patterns of PVP_{30} and PVP_{90} do not reflect these findings at first glance, a significant signal broadening and the development of low molar mass tailings accompanied by slight shifts towards higher elution volumes are most probably due to the close proximity of the polymer signals to the system peak of the applied GPC system. Nevertheless, considering increased proportions of oxidable chain ends with decreasing molar mass of PVP, side chain scission may not be the sole factor in the oxidative deterioration of low molar mass PVP.

Quantitative analysis of oxidative polymer degradation is feasible by plotting the % residual M_w obtained from the GPC elugrams against the incubation time (Figures 4.4, 4.5 and 4.6).

As expected from the elugrams, the apparent degradation rate increases with increasing concentration of H_2O_2. A highly significant weight loss of 93 % of the initial molar mass

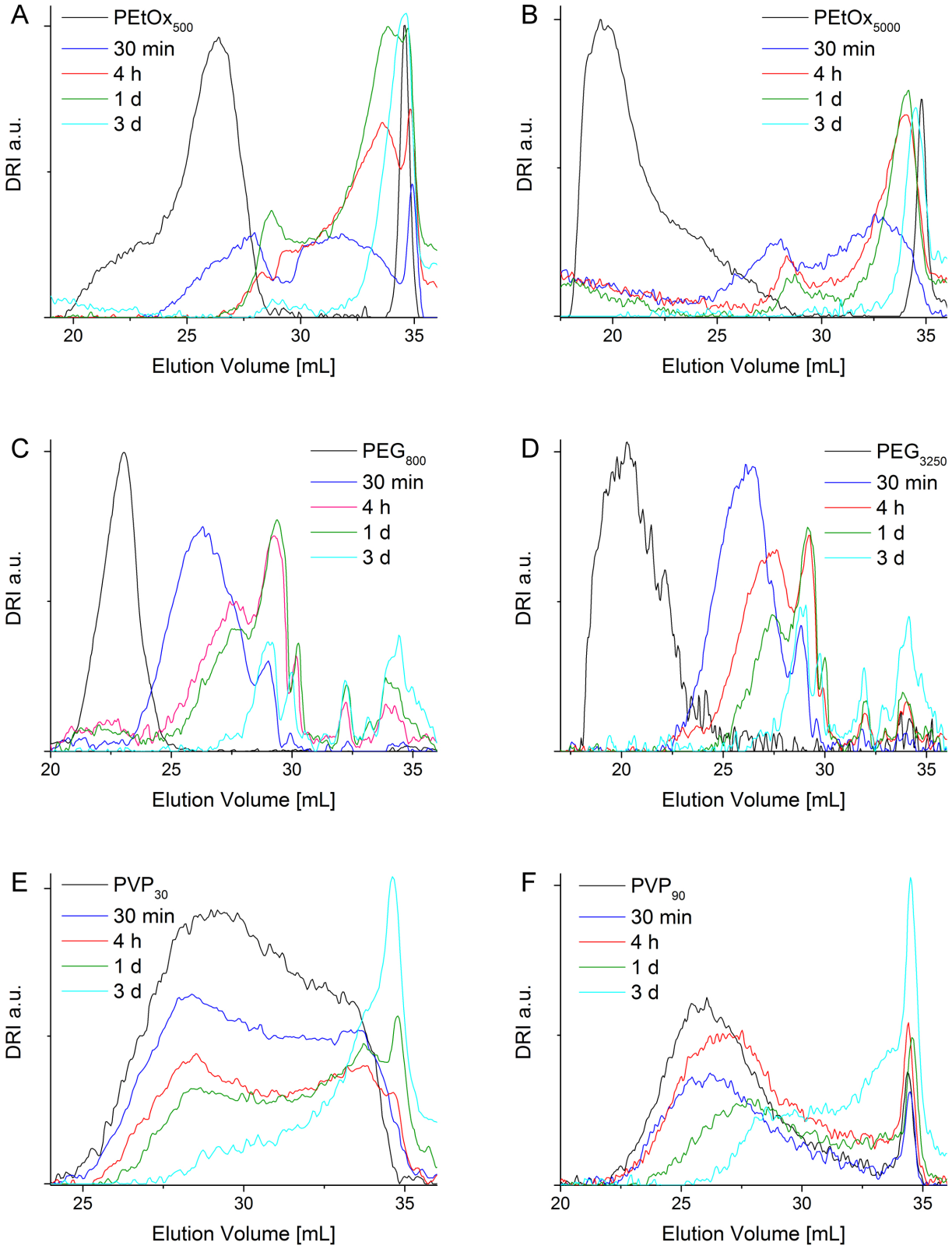

Figure 4.3: Exemplary elugrams of high molar mass **A** $PEtOx_{500}$, **B** $PEtOx_{5000}$, **C** PEG_{800} and **D** PEG_{9100} as well as low molar mass **E** PVP_{30} and **F** PVP_{90} after incubation with 50 μM $CuSO_4$ and 50 mM hydrogen peroxide at 37 °C.

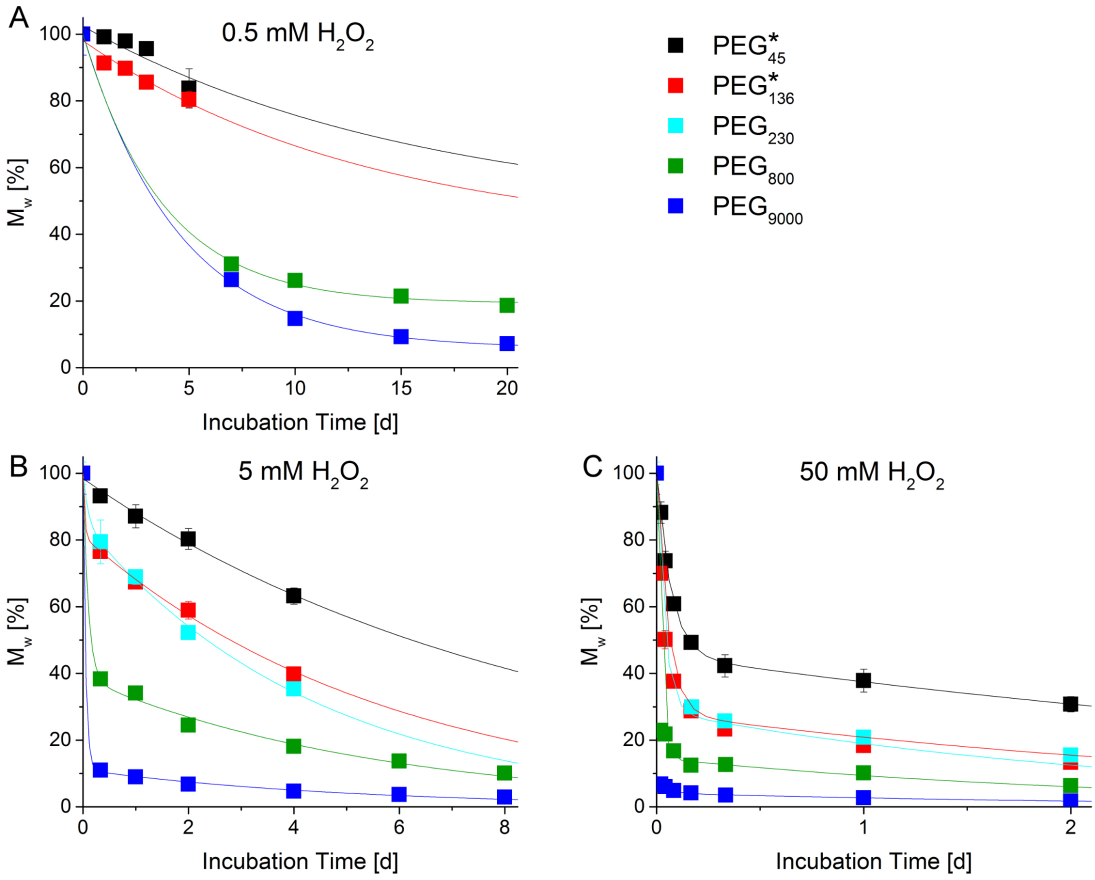

Figure 4.4: Molar mass development of PEG depending on the DP of the pristine polymer upon incubation with 0.5 to 50 mM H_2O_2 and 50 μM $CuSO_4$. Data are presented as mean ± SEM (n = 3). Lines are intended as a guide to the eye. * Data taken from ref. [169].

of PEG_{3250} is observed within only 30 minutes of incubation applying a concentration of 50 mM H_2O_2. Identical conditions resulted in an even higher weight loss of 97.5 % observed for POx_{5000}. Nevertheless, following a rapid initial weight loss degradation rates of both PEG and POx decelerate considerably. Somewhat contradictorily, the apparent degradation rate of PEG_{230} closely resembles the apparent degradation rate of PEG_{136}, which is, however, attributable to the application of an older charge of hydrogen peroxide for experiments involving PEG_{230} and inactivation of H_2O_2 during prolonged storage time resulting in lower oxidative activity. With the exception of PEG_{230}, all of the presented degradation experiments were carried out with fresh H_2O_2 solution.

Interestingly, the early phase of oxidative PVP degradation is characterized by a slight increase of M_w. Although only evident at low concentrations of H_2O_2, this phase is proba-

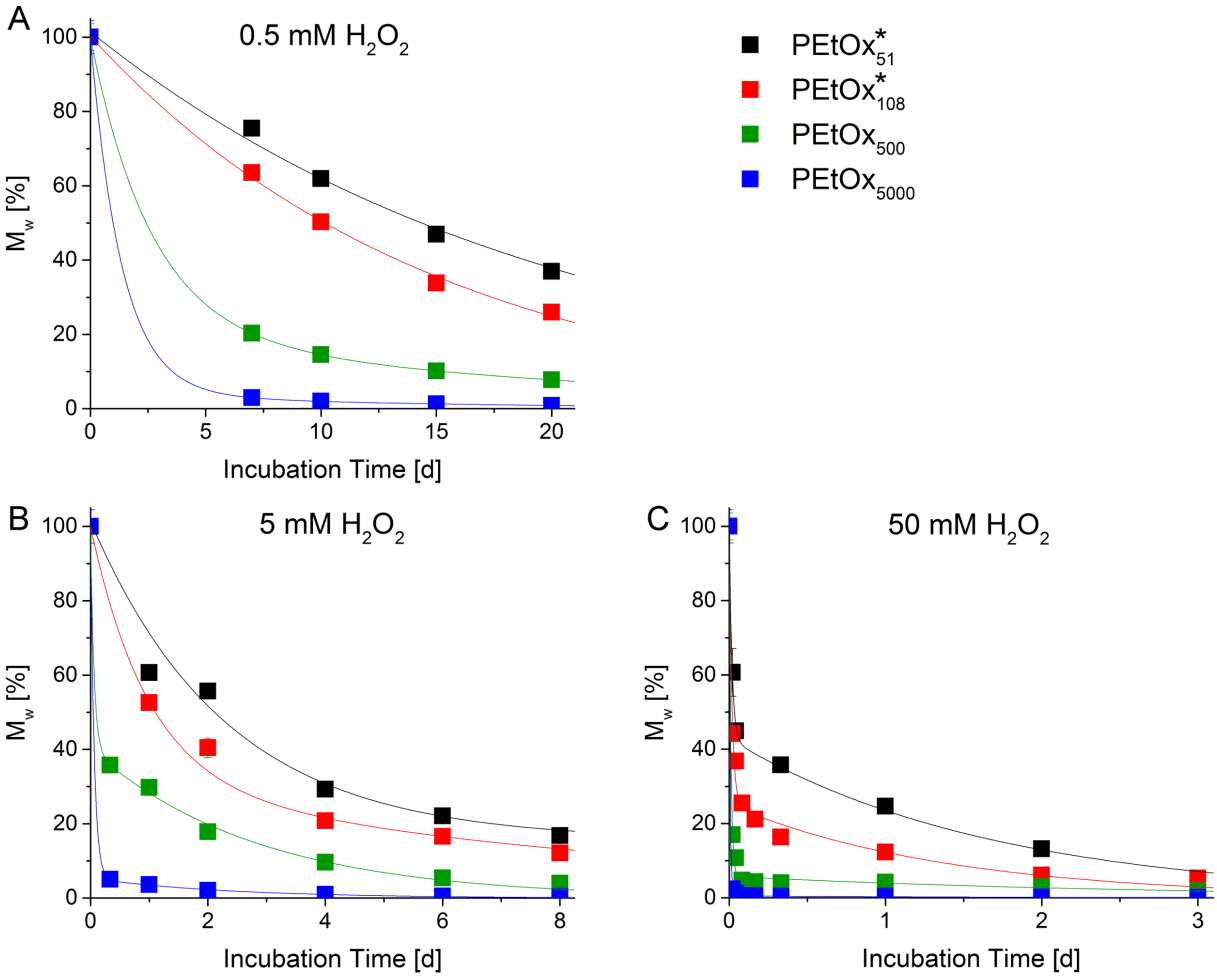

Figure 4.5: Molar mass development of PEtOx depending on the DP of the pristine polymer upon incubation with 0.5 to 50 mM H_2O_2 and 50 μM $CuSO_4$. Data are presented as mean ± SEM (n = 3). Lines are intended as a guide to the eye. * Data taken from ref. [169].

bly also existent when 50 mM H_2O_2 are applied, though not discernible within the scope of this experiment due to the fast oxidation rate. These findings may indicate a previously discussed side chain scission occurring in the first phase of oxidative deterioration. GPC measurement is first and foremost based on the hydrodynamic radius of the polymers. Therefore, obtained M_w values do not reflect the true molar mass, but are relative values referred to the applied standard. If partial side chain cleavage results in enhanced solubility in HFIP, higher values for M_w are obtained regardless of the actual existing weight loss and would explain the observed initial increase of M_w.

As expected and already ascertained in previous investigations,[169, 218, 219] rates of oxidative polymer degradation are further strongly depending on the applied concentration of H_2O_2.

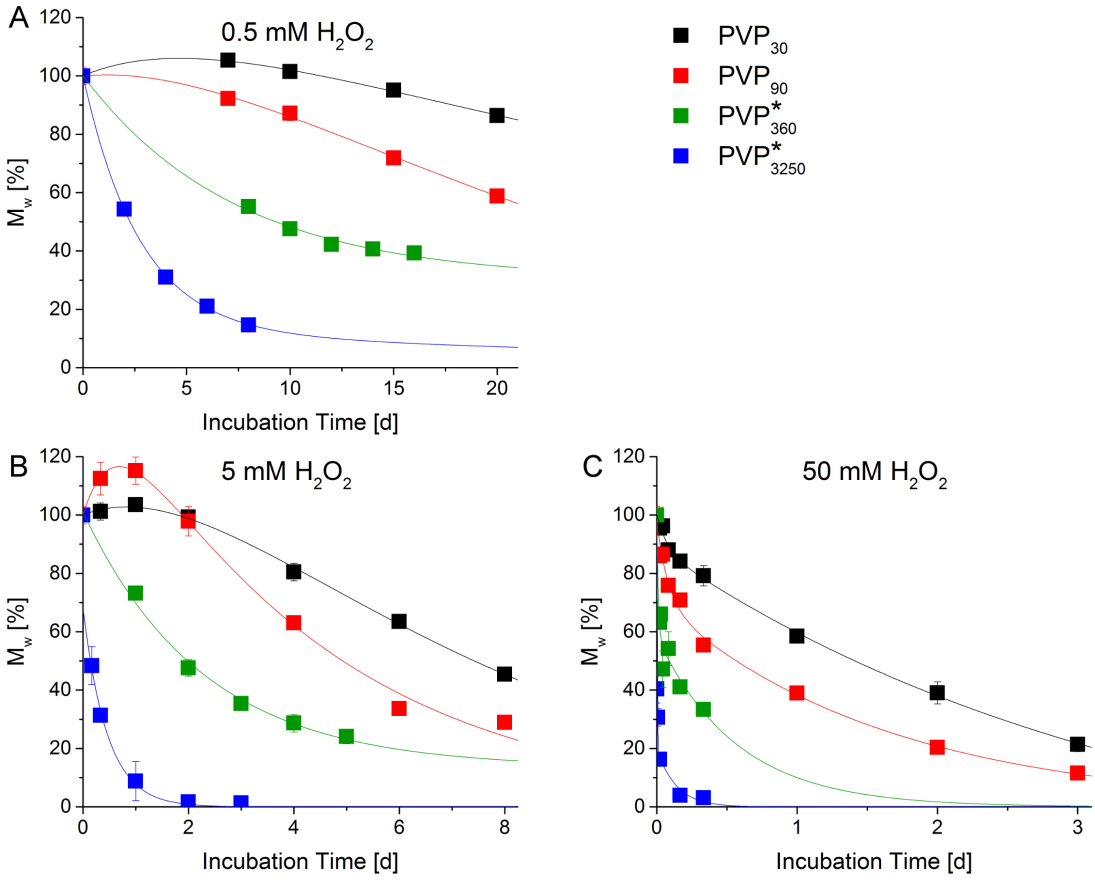

Figure 4.6: Molar mass development of PVP depending on the DP of the pristine polymer upon incubation with 0.5 to 50 mM H_2O_2 and 50 μM $CuSO_4$. Data are presented as mean ± SEM (n = 3). Lines are intended as a guide to the eye. * Data acquired by Moritz Faust.

While the oxidative degradation of PEG, PEtOx and PVP proceeds extremely rapid at a concentration of 50 mM H_2O_2, significantly lower rates are observed at 0.5 mM H_2O_2. Unfortunately, estimations on the H_2O_2 concentration *in vivo* are rather inconsistent and unreliable. Zhang *et al.* state a concentration of 100 μM H_2O_2 to be biologically relevant,[370] which is in good agreement with presumptions of Almutairi and coworkers of 50-100 μM H_2O_2[371]. However, although it is very likely that all types of human cells are exposed to some level of H_2O_2, the exact extent remains uncertain.[372] Interestingly, some beverages like black tea and instant coffee contain concentrations exceeding 100 μM H_2O_2,[373–375] and even higher concentrations can be found in freshly voided human urine even of newborn infants.[376–378]

Although concentrations of H_2O_2 in healthy human tissue are supposedly much lower, a

slow oxidative degradation of the investigated polymers *in vivo* can be reasonably expected. Enlarging the spectrum of investigated PEG, PEtOx and PVP molar masses confirms an increase of the apparent degradation rate with increasing degree of polymerization as experienced in earlier studies.[169, 218, 219] Interestingly, these results are in contradiction with investigations on the alcohol and aldehyde dehydrogenase catalyzed sequential oxidation of PEG, which revealed decelerating degradation with increasing degree of polymerization.[30] Although experiments on the oxidative degradation of polymers conducted in the scope of this work did not involve oxidative enzymes, these findings suggest internal backbone scission rather than sequential chain end oxidation to be the major cause of degradation. Indeed, this assumption is in excellent agreement with the observation of lower apparent degradation rates of shorter polymer chains. While in polymers with a DP of ≈ 50 the proportion of terminal monomer units amounts to 4 %, this proportion decreases with increasing chain length to 1.3 % at DP 150, 0.4 % at DP 500 and merely 0.04 % at a DP of 5000. This, in turn, reduces the influence of end group oxidation reactions decelerating backbone degradation. Nevertheless, each backbone scission increases the proportion of terminal monomer units, thus explaining decreasing apparent degradation rates during advanced stages of the experiment by a self-inhibitory effect.

4.1.3 Oxidative Degradation of Poly(ethylene glycol) and Polysarcosine by H_2O_2, ClO^- and $\cdot O_2^-$

The spectrum of ROS and RNS *in vivo* enfolds several further reactive species (*cf.* section 2.2.1.3) that might be capable to oxidatively alter the structure of polymers. Studies on the oxidative degradation of PEG_{45} (2 kg/mol), PEG_{136} (6 kg/mol) as well as $PSar_{60}$ (4.5 kg/mol) and $PSar_{138}$ (10 kg/mol) by H_2O_2 with and without further addition of $CuSO_4$, ClO^- and $\cdot O_2^-$ were conducted by Julian Schreck during his bachelor thesis and re-evaluated for the present thesis.[379]

Unfortunately, $PSar_{60}$ was obtained with a bimodal distribution probably caused by impurities introduced during polymer synthesis. Thus, $PSar_{60}$ and PEG_{45} degradation data are only comparable to a limited extent and are not discussed hereafter.

H_2O_2 vs. $H_2O_2/CuSO_4$

In order to estimate the influences of low concentrations of copper ions on the oxidative

degradation of PEG and PSar, polymers were exposed to H_2O_2 in concentrations of 0.5 mM, 5 mM and 50 mM with and without further addition of 50 μM $CuSO_4$. As discussed previously, marginal quantities of copper react with H_2O_2 in a Fenton-like reaction yielding highly reactive hydroxyl radicals.

Exemplary elugrams of $PSar_{138}$ and PEG_{136} (Figure 4.7 and 4.8) reveal no significant differences between the elugram patterns subjected to the addition of $CuSO_4$.

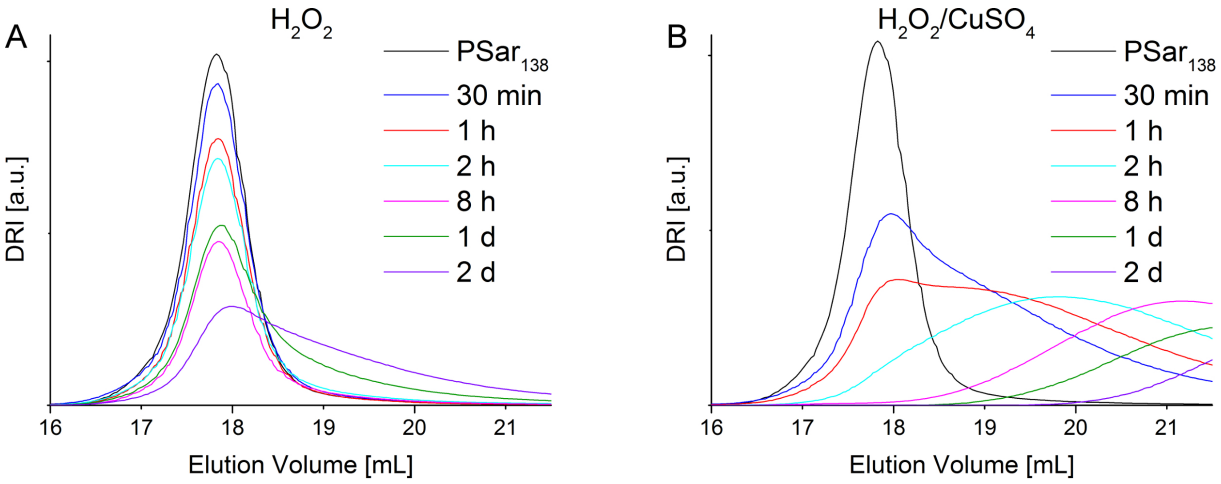

Figure 4.7: Elugrams of $PSar_{138}$ obtained after incubation with **A** 50 mM H_2O_2 and **B** 50 mM H_2O_2 supplemented with 50 μM $CuSO_4$ at 37 °C. Experiments conducted by Julian Schreck.

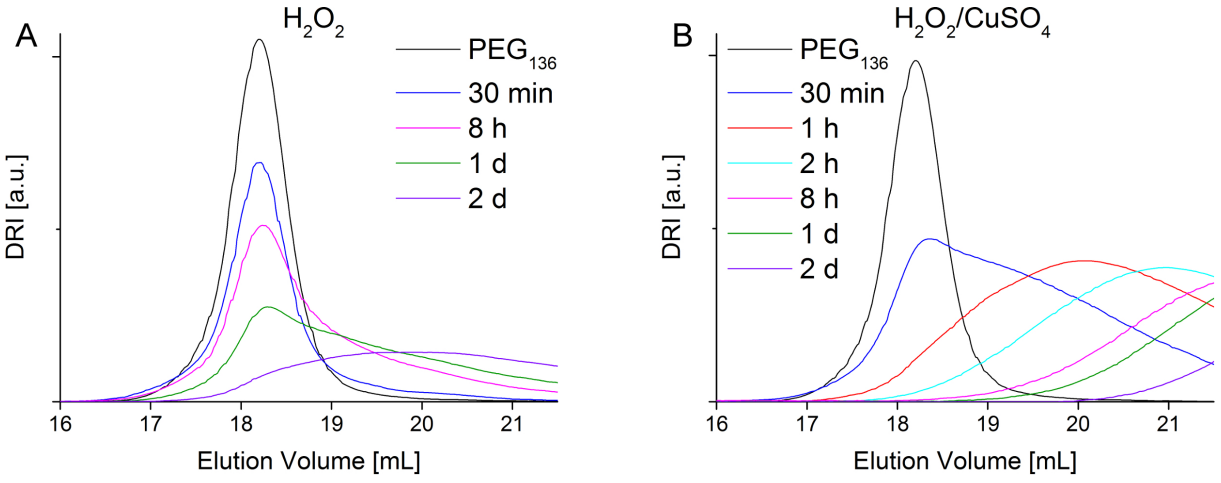

Figure 4.8: Elugrams of PEG_{136} obtained after incubation with **A** 50 mM H_2O_2 and **B** 50 mM H_2O_2 supplemented with 50 μM $CuSO_4$ at 37 °C. Experiments conducted by Julian Schreck.

For both polymers, the development of a low molecular weight tailing and subsequent

shift of the peak elution volume towards higher elution volumes is observed. In case of $PSar_{138}$, this is in good agreement with the results obtained for PEtGly in earlier studies.[169, 218] However, previous investigations further revealed the development of multimodal distributions during oxidative degradation of PEG which are not apparent within the current elugrams. Although this is partly attributable to the relatively low molar mass of PEG, a major difference compared to previously investigations is the application of DMF instead of HFIP as eluent of the GPC system. Based on the principles of GPC and the tremendous effects of the individual polymer-solvent system, comparability of results obtained from different GPC systems is rather limited.
Nevertheless, although no significant effects on the elugram patterns caused by the addition of $CuSO_4$ are observed, a major increase of the apparent degradation rate is apparent (Figure 4.9).

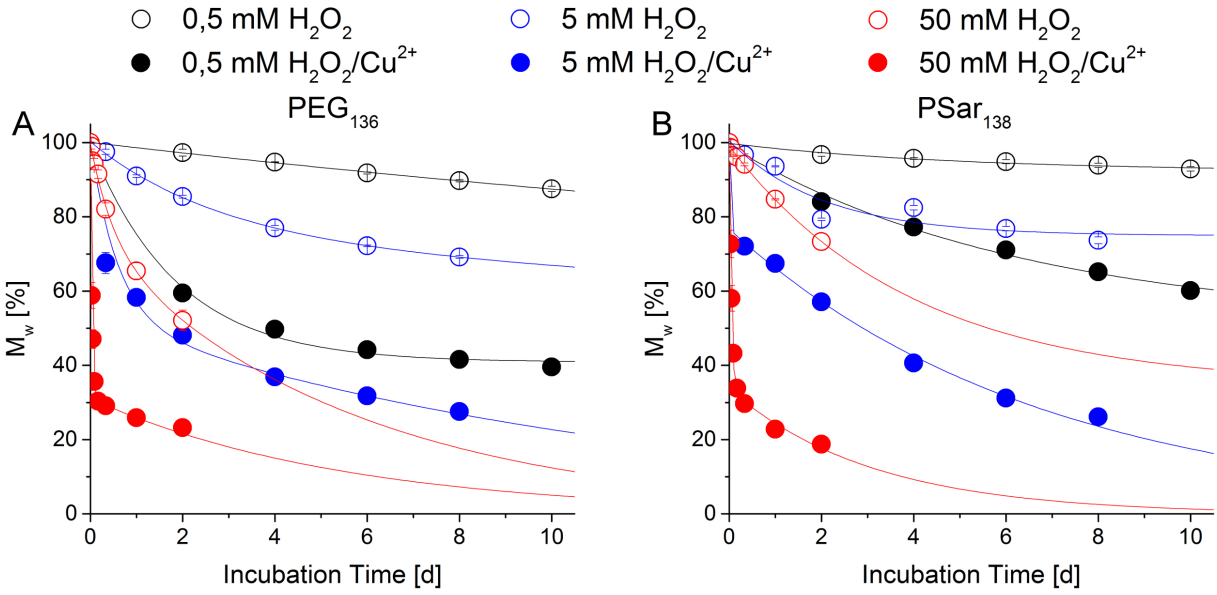

Figure 4.9: Molar mass development of **A** PEG_{136} and **B** $PSar_{138}$ upon incubation with 0.5 to 50 mM H_2O_2 or 0.5 to 50 mM H_2O_2 and 50 μM $CuSO_4$. Data are presented as mean ± SEM (n = 3). Lines are intended as a guide to the eye. Experiments conducted by Julian Schreck.

While incubation of PEG_{136} with 50 mM H_2O_2 results in a weight loss of ≈ 50 % within two days, further addition of 50 μM of $CuSO_4$ resulted in a weight loss of ≈ 75 % within the same period. Even greater discrepancies are observed during incubation of $PSar_{138}$ with a weight loss of ≈ 25 % without $CuSO_4$ compared to ≈ 80 % when $CuSO_4$ is supplemented. It should be noted, however, that the H_2O_2 concentration of the system comprising H_2O_2

and $CuSO_4$ was replenished daily, while no further H_2O_2 was added to the system without $CuSO_4$ due to constant ROS concentrations.[169, 379] Nevertheless, with regard to the clear differences between the apparent degradation rates of both systems observed during the initial 24 h of the experiment, repeated addition of H_2O_2 appears not to distort the obtained results.

These findings are little surprising as hydroxyl radicals generated *in situ* via reaction of H_2O_2 with Cu^{2+} are known to be far more reactive then H_2O_2 itself (*cf.* section 2.2.1.3). Apart from this trend, oxidative degradation of PSar and PEG, respectively, by H_2O_2 and ·OH appears to proceed via identical mechanisms, with the abstraction of hydrogen radicals by the applied ROS generating polymeric hydroperoxides being the rate determining step depending on the reactivity of the applied species.

Superoxide

Superoxide is a highly reactive ROS, however, compared to other ROS investigated in the scope of this thesis it is rather harmless and rapidly deactivated by SOD *in vivo*. However, as discussed in section 2.2.1.3, superoxide acts as a precursor for several highly damaging species.

Superoxide can be generated *in situ* under non-physiological conditions using a system comprising hypoxanthine (HX) and xanthine oxidase (XO).[380]

$$Hypoxanthine \; + \; 2\, O_2 \; + \; H_2O \; \xrightarrow{XO} \; Xanthine \; + \; 2 \; \cdot O_2^- + 2\, H^+$$

The present study was conducted applying 0.5 mM HX and 20 U/L XO. However, GPC elugrams obtained of both PEG_{136} and $PSar_{138}$ display identical signals independent on the incubation time (Figure 4.10).

Unfortunately, estimating the amount of superoxide generated by the HX/XO system is unfeasible due to the short half life of superoxide. It might be reasonably assumed that the generated amounts of superoxide are simply insufficient for the oxidative degradation of PEG and PSar. Furthermore, incubation times were limited to a maximum of 24 h due to suggested inactivation of XO. It can be hypothesized that prolonged incubation times would result in a noticeable degradation of the polymers, however, it cannot be ruled out that the reactivity of superoxide is to low to induce the oxidative degradation of PEG and PSar.

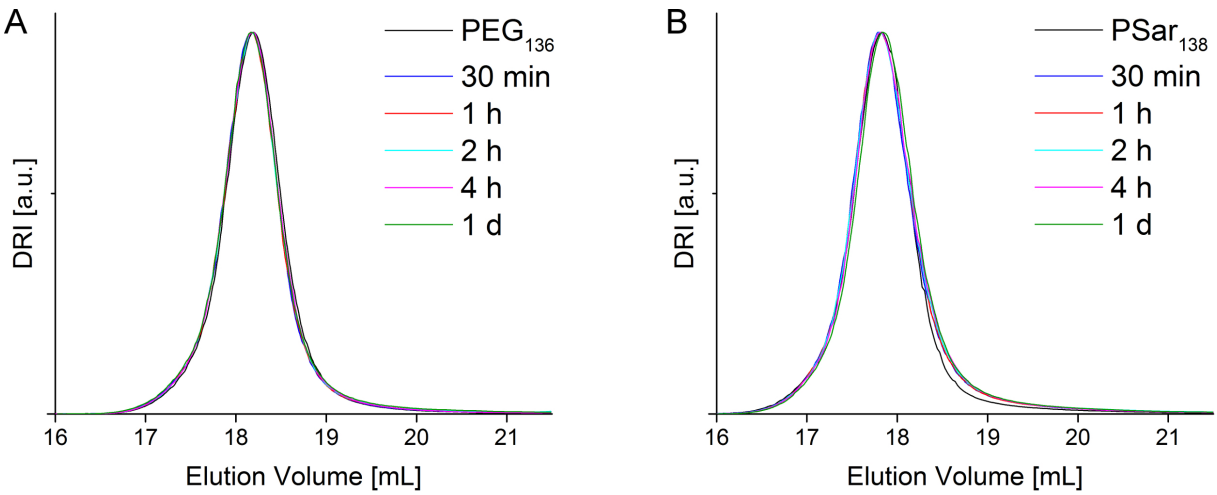

Figure 4.10: Normalized elugrams of **A** PEG_{136} and **B** $PSar_{138}$ obtained after incubation with 0.5 mM HX and 20 U/L XO at 37 °C. Experiments conducted by Julian Schreck.

Hypochlorite

Hypochlorite

a counter ion, it represents the most commonly encountered household bleaching agent and is also used for the disinfection of public swimming pools. *In vivo*, hypochlorite is generated by leukocytes to induce the digestion of foreign particles engulfed within the phagosome.

The degradation of PEG_{136} and $PSar_{138}$ by hypochlorite anions was investigated at concentrations ranging from 0.5 to 50 mM with respect to NaClO. It should be noted that NaClO was only added at time zero and not replenished daily.

No significant modifications of $PSar_{138}$ upon incubation with 0.5 and 5 mM ClO^- are apparent, which is well reflected by nearly constant plots of M_w (Figure 4.11 **B**). However, quite distinct elugram patterns are observed upon incubation with 50 mM ClO^- (Figure 4.11 **A**). Initially, rapid deterioration the polymer characterized by a shift of the peak elution volume towards higher elution volumes as well as the development of a pronounced low molecular weight tailing are evident and further reflected by a weight loss of $\approx$ 50 %. Subsequently, the peak elution volume shifts back towards lower elution volumes and M_w levels off at about 60 % with respect to the pristine $PSar_{138}$ which is most probably caused by chain recombination reactions.

In case of PEG_{136}, both low as well as high molecular weight tailings are apparent even upon incubation with low concentrations of 0.5 mM ClO^- (Figure 4.12). At both 0.5 and 5 mM ClO^-, the development of low molecular weight tailings is noticeable and attributable

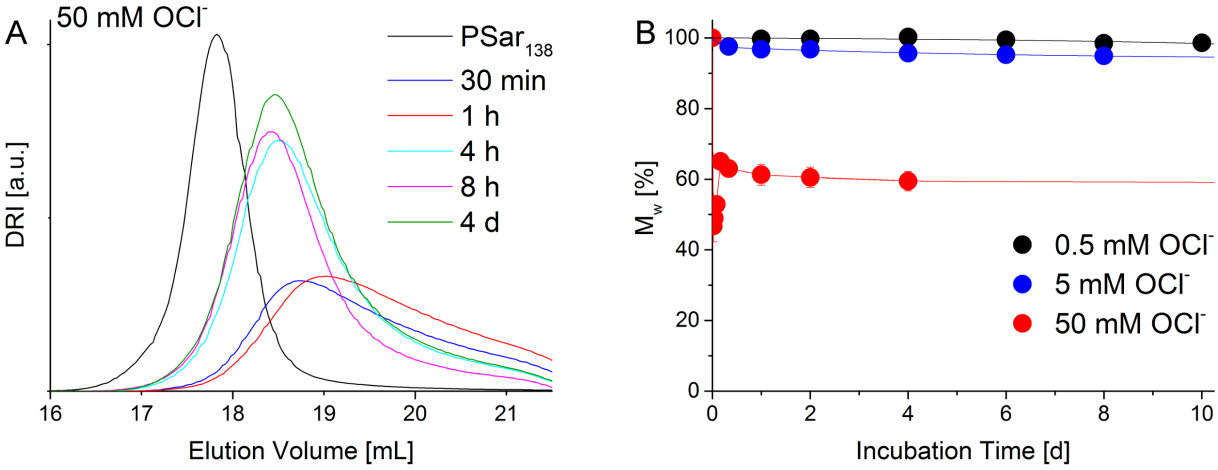

Figure 4.11: GPC elugrams (**A**) and M_w (**B**) development of $PSar_{138}$ upon incubation with hypochlorite at 37 °C. Experiments conducted by Julian Schreck.

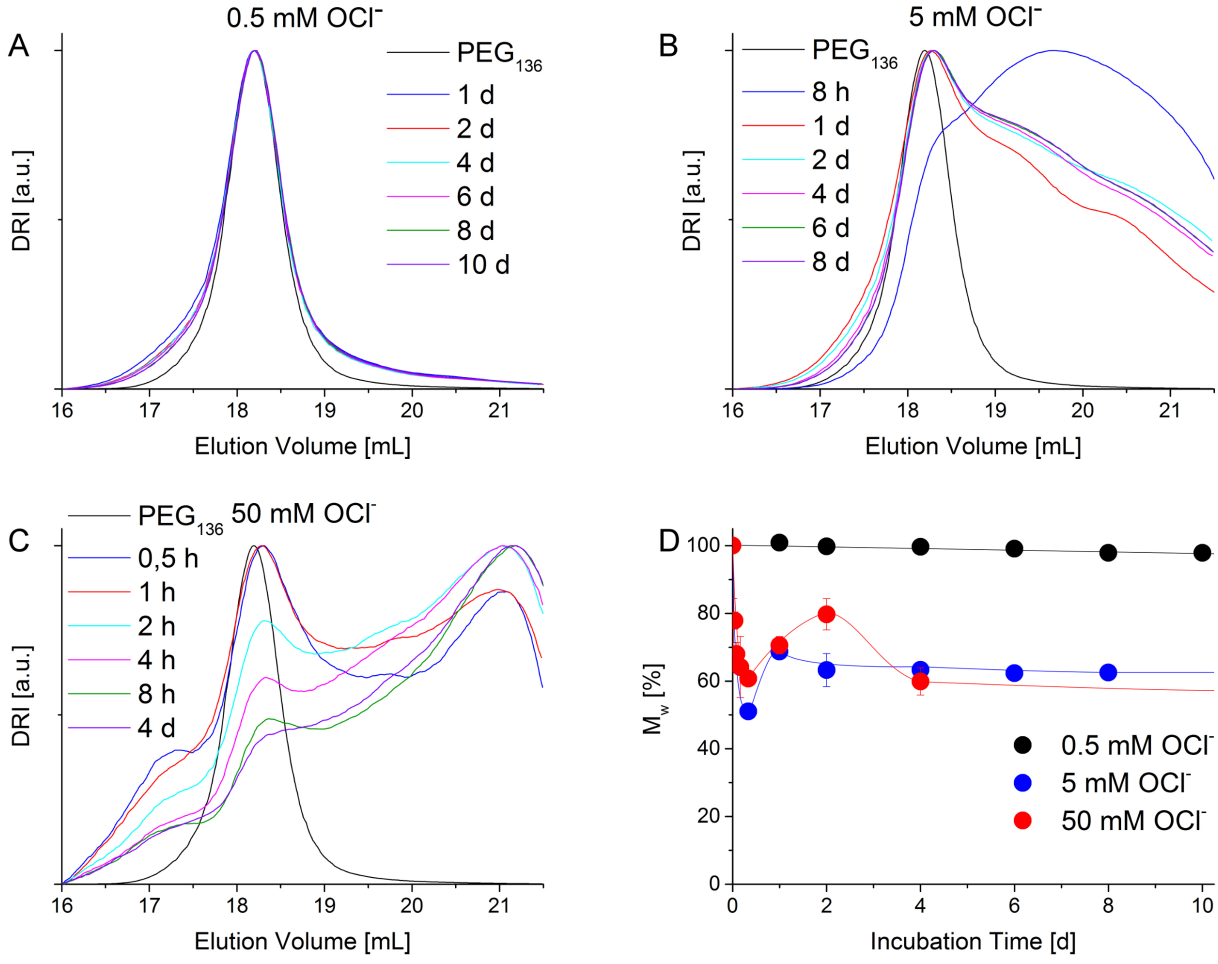

Figure 4.12: GPC elugrams (**A** to **C**) and M_w (**D**) development of PEG_{136} upon incubation with hypochlorite at 37 °C. Experiments conducted by Julian Schreck.

to chain recombination reactions. Further increase of the ROS concentration to 50 mM ClO^- reveals a multimodal distribution with peak elution volumes at higher as well as lower elution volumes compared to the elugram of the pristine polymer being formed. Interestingly, while M_w remains constant upon incubation with 0.5 mM ClO^-, an initial drop of M_w followed by a slight increase and final equilibration at $\approx$ 60 % are observed in accordance with the results obtained for $PSar_{138}$ at 50 mM ClO^-.
Interestingly, investigations on both polymers agree regarding conspicuous aspects. First of all, a maximum weight loss of $\approx$ 40 is observed regardless of the species of the polymer or the concentration of ClO^-. Furthermore, a rapid deterioration and weight loss within the initial 8 h of the experiment is followed by a sharp increase of M_w before the equilibrium of about 60 % is reached. Two days after addition of ClO^-, no significant alterations of the elugrams and determined molar masses are observed. This is, however, most probably attributable to the slow decomposition of ClO^- in water releasing sodium ions, chloride ions and hydroxyl radicals:

$$NaClO + H_2O \longrightarrow Na^+ + Cl^- + 2 \cdot OH$$

As discussed previously, ·OH radicals generated in this manner are potent oxidants inducing the degradation of both PEG and PSar. Moreover, an equilibrium between ClO^- and HClO is established:

$$ClO^- + H_2O \rightleftharpoons HClO + OH^-$$

Therefore, the solution responds basic and may hydrolyze PSar amide bonds. Hypochlorous acid acts as an oxidizing agent constituting the foundation for the bleaching and disinfecting properties possessed by sodium hypochlorite:

$$HClO + H^+ + 2\,e^- \longrightarrow Cl^- + H_2O$$

Furthermore, hypochlorous acid also decomposes yielding singlet oxygen oxidant which also has an oxidizing effect:

$$2\,HClO \longrightarrow 2\,HCl + {}^1O_2$$

With regard to the great range and variety of reactive species generated by sodium hypochlorite, the quite uncommon patterns of the elugrams and evolution of M_w are more comprehensible.
In case of $PSar_{138}$, both oxidative and hydrolytic processes can be suggested to induce and affect degradation. Especially the observed increase of M_w between 1 h and 4 h may indicate recombination of generated hydroperoxides. This is even more evident in case of PEG_{136}, where hydrolysis is not expected and radical recombination results in multimodal distributions with in some cases even higher molecular masses than the pristine polymer. Furthermore, the rapid and suddenly ending weight loss observed for both polymer species within the first hours of the experiment indicates fast consumption of the available ClO^-. It can be hypothesized that the repeated addition of NaClO mimicking a constant generation of ClO^- *in vivo* might result in complete decomposition of the polymers even at low concentrations of the oxidant.

It remains to be emphasized that both PEG and PSar are susceptible to oxidative degradation to various oxidants generated *in vivo*. However, not only rates of oxidative degradation but also the underlying mechanisms appear to be strongly dependent on the applied ROS. Although the extent of ROS generation *in vivo* has not been properly evaluated yet, oxidative degradation of the investigated polymers upon prolonged exposure to minute biologically relevant concentrations of ROS can be reasonably assumed.

4.1.4 Analysis of Degradation Products via GC/MS

While quantification and determination of the apparent degradation rates of oxidative polymer degradation via GPC is a feasible and viable approach, this method does not allow insights into the inherent mechanisms. In order to verify previously proposed mechanisms (*cf.* section 2.2.1.5), polymers were dissolved to a concentration of 1 g/L in PBS and incubated with 50 μM $CuSO_4$ and 50 mM H_2O_2 (replenished daily) for 14 d to ensure complete oxidation of the respective polymers. Subsequently, samples were frozen and stored at - 18 °C until analysis via GC/MS, a method combining vaporization of the samples and separation of the individual components based on their affinity towards the stationary phase of the GC column as well as the subsequent mass spectrometry incorporating ionization and separation based on the mass-to-charge (m/z) - ratio.

Poly(2-alkyl-2-oxazoline)s

GC/MS measurement was performed for three different POx species, namely $PMeOx_{60}$, $PMeOx_{90}$ and $PEtOx_{51}$. Potential residues of not or partially degraded polymers are considered non vaporizable and should therefore not influence the measurement.

The obtained chromatograms (Figure 4.13) display a multitude of signals and strong similarities, however, noticeable differences between PMeOx and PEtOx are apparent while PMeOx chromatograms are practically identical regardless of the DP. Oxidative

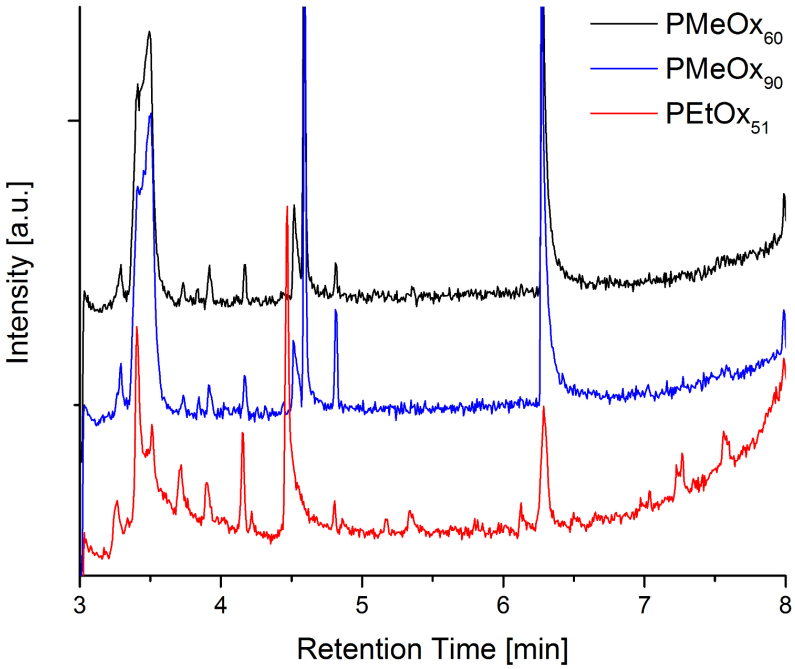

Figure 4.13: GC/MS chromatograms obtained for $PMeOx_{60}$, $PMeOx_{90}$ and $PEtOx_{51}$.

deterioration of POx may yield a variety of different structures (Figure 4.14). Chain ends bearing aldehydes or secondary amides may be cleaved via α-cleavage (*cf.* Figure 4.15) yielding **1**, **2**, **3** and **4** (**a** for methyl substituents, **b** for ethyl substituents). Indeed, m/z 85 assignable to **3a** is found in the mass spectra not only of PMeOx, but also in the mass spectrum of PEtOx at a retention time of 4.8 min which questions the generation of **3a** via α-cleavage. Furthermore, neither **3b** nor any other potential structures generated from α-cleavage of oxidized chain ends are found individually or as H_2O, H^+, Na^+ or K^+ adducts.

However, mass spectra of PMeOx and PEtOx contain signals characteristic of acetamide (**5a**, m/z 59, 6.3 min), a potential product of exhaustive oxidation. Furthermore, rather conspicuous signals at m/z 44 observed for both POx species at various retention times

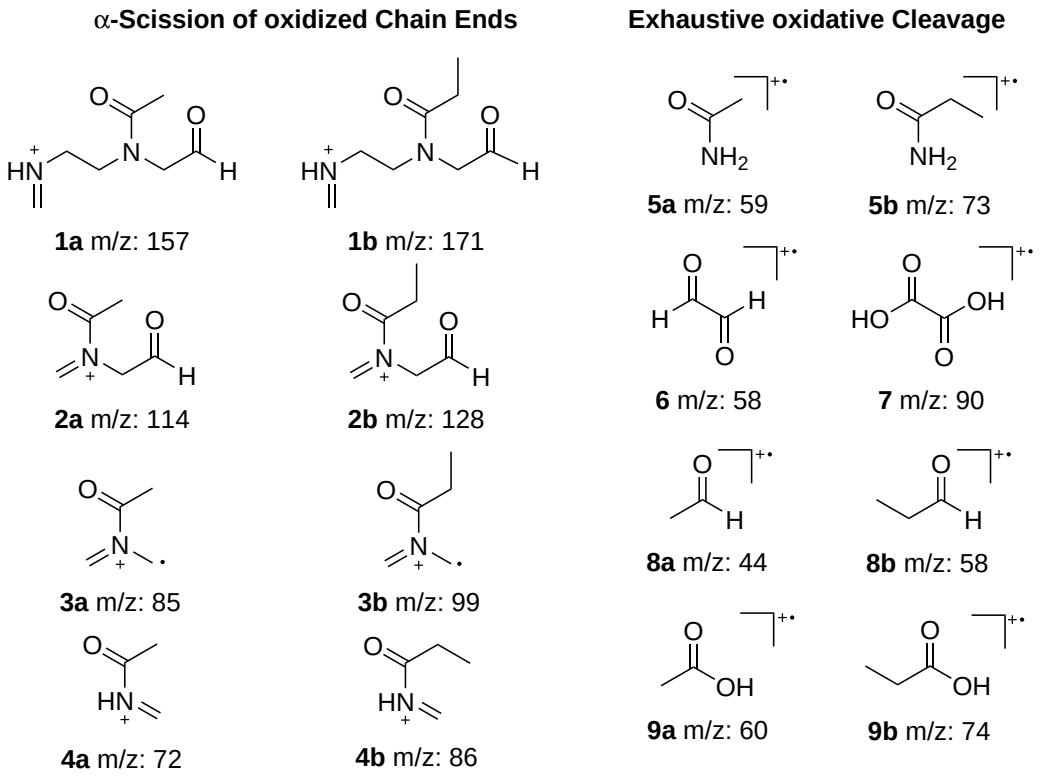

Figure 4.14: Potential products of oxidative POx cleavage. Oxidized chain ends may undergo α-cleavage (**1** - **4**), while smaller degradation products can be determined directly (**5** - **9**). Structures labeled **a** are generated from PMeOx, while **b** labeled structures can be assigned to PEtOx.

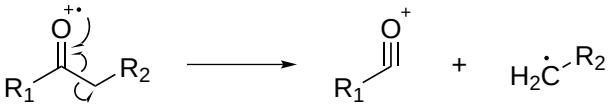

Figure 4.15: The mechanism of α-cleavage describes the cleavage of a carbon-carbon bond adjacent to a carbon atom bearing a functional group.

(PMeOx: 3.3, 3.4, 3.9, 4.2, 4.81, 6.27 mL; PEtOx: 3.2, 3.4, 3.5, 5.3, 6.1, 6.3 mL) indicate the generation of acetaldehyde (**8a**) as a product of fission, but may also be attributable to carbon dioxide or the McLafferty peak of an aldehyde (*cf.* Figure 4.16). However, m/z 58 at a retention time of 3.9 mL found in spectra of both POx species also suggests the generation of propionic aldehyde (**8b**) or oxoaldehyde (**6**). Signals at m/z 60 (PMeOx, 3.5 and 3.6 mL) and m/z 74 (PEtOx, 5.3 mL), respectively, indicate the generation of acetic acid and propionic acid probably via oxidation of acetaldehyde and propionic aldehyde.

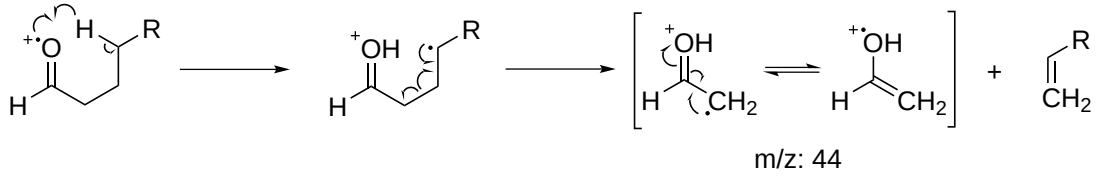

Figure 4.16: Mechanism of a McLafferty rearrangement as observed upon mass spectrometry with the example of an aldehyde yielding a fragment with m/z 44.

In summary, several signals indicate the oxidative degradation of POx in conformity with previously proposed mechanisms generating, among others, acetaldehyde, acetamide and carbon dioxide.[169, 218] Nevertheless, a number of prominent signals such as m/z 79 (PMeOx: 4.5 mL and 4.6 mL) and 96 (PMeOx: 3.4 mL, PEtOx 3.4 and 6.3 mL) which were found in a number of POx mass spectra, could not be assigned to any potential degradation product thus suggesting further mechanisms or side reactions to occur.

Polypeptoids

Chromatograms of the investigated polypeptoid species $PSar_{45}$ and $PEtGly_{44}$ differentiate particularly in the area of low retention times of 3 to 4 min (Figure 4.17), which is further reflected by quite different mass spectra. Analog to the previously discussed POx, potential products of oxidative polypeptoid deterioration are summarized in Figure 4.18. However, most of the observed signals cannot be assigned to any of the structures or their H_2O, H^+, Na^+ or K^+ adducts. While m/z 44 (PSar: 4.2, 3.1, 7.3 mL; PEtGly: 3.3, 3.5, 3.7, 6.3, 9.4 mL) potentially corresponding with acetaldehyde **13**, carbon dioxide or the McLafferty peak of an aldehyde (*cf.* Figure 4.16) was found in almost every mass spectrum, only **12** (m/z 86) (4.2 mL) was found in a mass spectra of PSar and the water adduct of **14** (m/z 91, PSar: 6.1 mL; PEtGly: 3.5 mL) was found in mass spectra of both polypeptoids.
Based on these data and with respect to the rather ambiguous allocation of m/z 44, the mechanism of oxidative polypeptoid degradation as proposed in previous studies[169, 218] can neither be confirmed nor rejected. Formaldehyde (m/z 30), a potential product of oxidative PSar dealkylation, could not be clearly identified as m/z 30 was found in every obtained spectrum. Due to a large variety of signals with rather low intensity, it cannot be reasonably assumed which signals are caused by degradation products and impurities, especially as many signals indicating column bleeding (including m/z 51, 69, 119, 131, 18, 219) are observed. The investigation of further polypeptoid species bearing different side

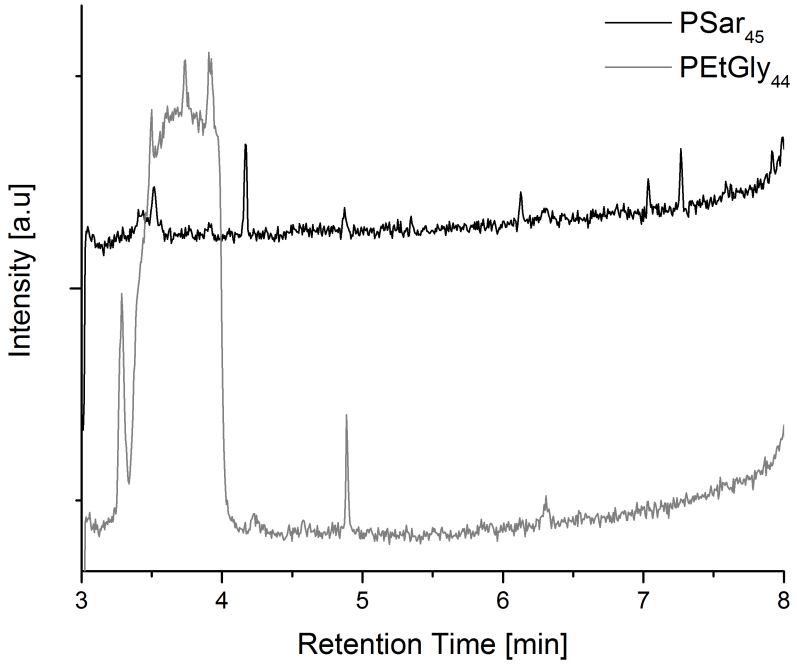

Figure 4.17: GC/MS chromatograms obtained for $PSar_{45}$ and $PEtGly_{44}$.

chains both before and after exhaustive oxidation appears promising to further elucidate the mechanism of oxidative polypeptoid deterioration via GC/MS.

Poly(*N*-vinylpyrrolidone)s

GC chromatograms of oxidatively degraded PVP_{30} and PVP_{90} (Figure 4.19) show considerable differences although they only differ regarding the chain length of the substrate. Particularly noticeable is a rather broad signal at a retention time of 3.4 to 4 min, which was also apparent in the chromatogram of $PEtGly_{44}$ and might therefore indicate major impurities. Previous investigations suggested γ-aminobutyric aicd (**18**), 2-pyrrolidone (**19**) and succinimide (**20**) to be products of exhaustive oxidative PVP degradation (Figure 4.20).[219, 381–383] However, while m/z 85 (2-pyrrolidone, **19**, 4.8 mL) and m/z 99 (succinimide, **20**, 9.4 mL) are found in mass spectra of PVP_{90}, they are lacking in the mass spectra of PVP_{30}. Ring opening would yield γ-aminobutyric acid (**18**) which is not found in any mass spectrum of PVP_{30} or PVP_{90}, however, McLafferty rearrangement of the carboxylic acid yields a McLafferty peak with m/z 60, which is found in mass spectra of both PVP species at a retention time of 4.8 mL. As discussed before m/z 44 is present in nearly all

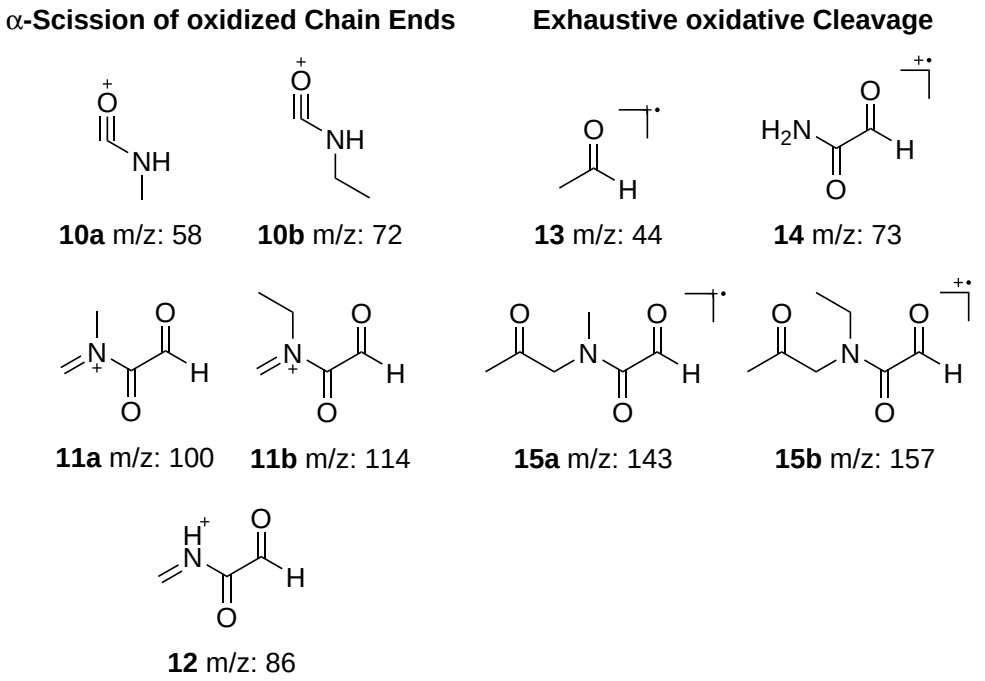

Figure 4.18: Potential products of oxidative polypeptoid cleavage. Oxidized chain ends may undergo α-cleavage (**10** - **12**), while smaller degradation products can be determined directly (**13** - **15**). Structures labeled **a** are generated from PSar, while **b** labeled structures can be assigned to PEtGly.

mass spectra and indicates the generation of a number of potential structures. In case of PVP, m/z 44 could represent the McLafferty peak **17** after rearrangement of aldehyde chain ends. However, neither *N*-vinylpyrrolidone **21** as the product of depolymerization nor **16** as the product of α-chain scission or their H_2O, H^+, Na^+ or K^+ adducts are found in mass spectra of PVP.

By and large, data on the oxidative degradation of PVP are in good agreement with previously proposed mechanisms.[381–383]

Unfortunately, GC/MS measurements on oxidatively degraded PEG were conducted immediately following repair of the applied device. The obtained mass spectra first and foremost indicate the presence of dichloromethane and toluene, both applied for thorough cleansing of the device upon repair, to an extent impeding detailed assessment of the GC/MS data.

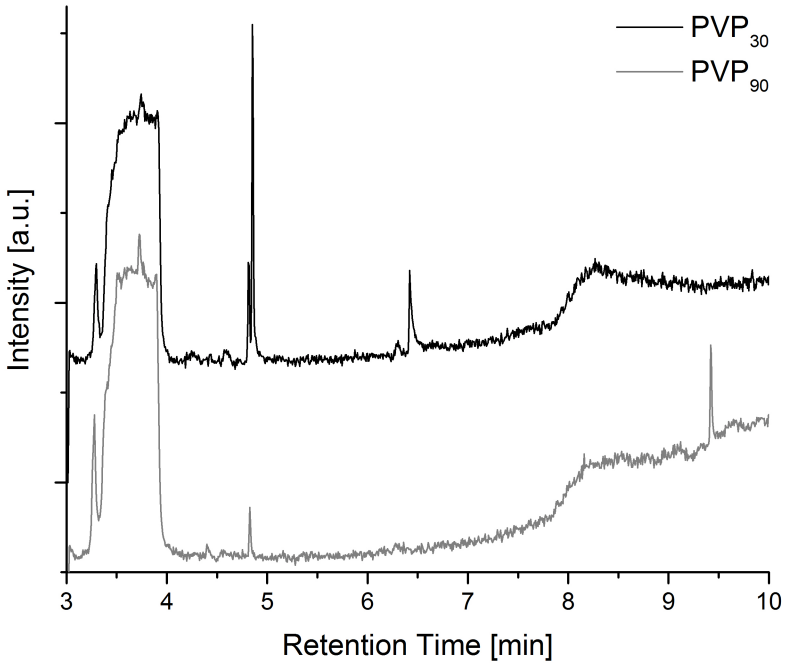

Figure 4.19: GC/MS chromatograms obtained for PVP_{30} and PVP_{90}.

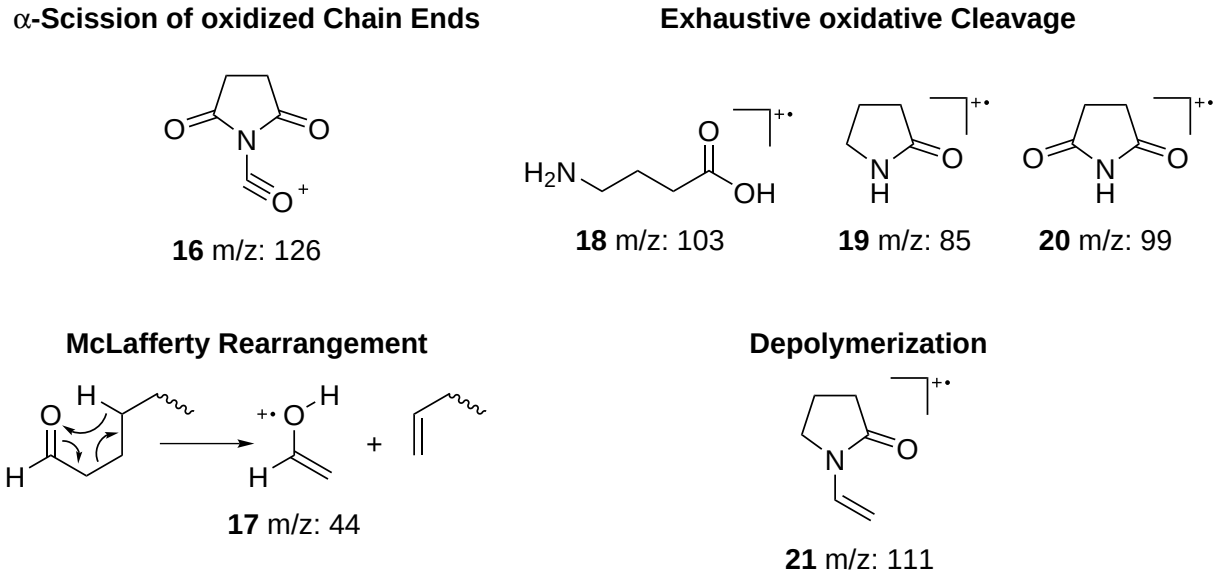

Figure 4.20: Potential products of oxidative PVP cleavage. Oxidized chain ends may undergo α-cleavage (**16**) or McLafferty Rearrangement (**17**) while smaller degradation products can be determined directly (**18** - **20**). Depolymerization yields the monomer *N*-vinylpyrrolidone.

4.2 Acidic Hydrolysis of Pseudo-Polypeptides

4.2.1 Hydrolysis of $PMeOx_{90}$

Hydrolysis of POx under strong acidic[222–225] as well as strong basic conditions is a straightforwar approach towards linear PEI[32, 226] (*cf.* section 2.2.2).
Based on earlier studies conducted by Hoogenboom and coworkers,[225, 228, 230] the hydrolysis of $PMeOx_{90}$ under acidic conditions was investigated. The polymer was dissolved in 6 M HCl to a concentration of 50 g/L (equivalent to an amide concentration of 0.58 mol/L) and incubated at 90 °C for up to 6 h. Cleavage of the amide bond yields PMeOx-*co*-PEI or, if performed exhaustively, pure PEI as well as acetic acid (Figure 4.21). After defined

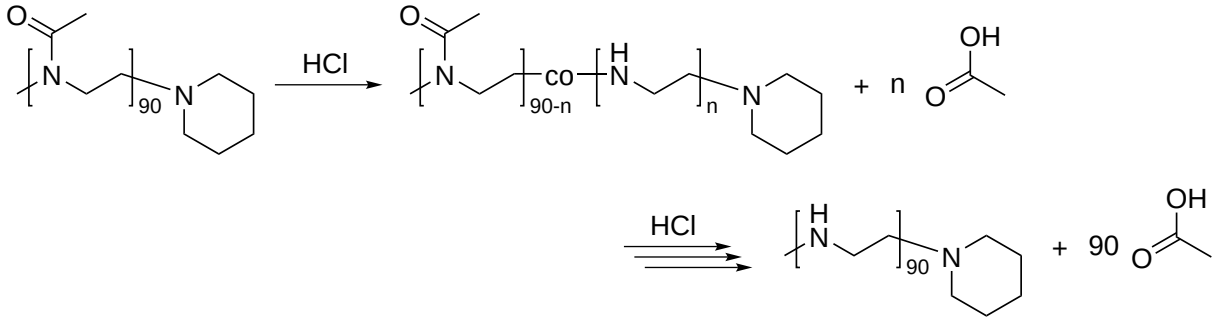

Figure 4.21: Acidic hydrolysis of $PMeOx_{90}$ yielding PMeOx-*co*-PEI and finally PEI as well as acetic acid.

intervals of time, samples were withdrawn, cooled on ice and neutralized by addition of sodium hydroxide to terminate the reaction and ensure full deprotonation of the generated acetic acid in order to prevent its vaporization during subsequent evaporation of the solvent at 100 °C. Finally, the solid residual was dissolved in deuterated methanol and ^{1}H-NMR spectroscopy was applied to determine the conversion of PMeOx to PEI using the signals of the released acetic acid (-CH_3 at $\delta = 1.9$ ppm) and the remaining PMeOx side chains (-CH_3 at $\delta = 2.1$ ppm) as illustrated in Figure 4.22.
Plotting conversion as a function of the incubation time (Figure 4.23 **A**) reveals an initial delay followed by a linear correlation, until a conversion of ≈ 80 % is reached. Subsequently, the hydrolysis rate slows down significantly, which is in excellent agreement with earlier reports and can be attributed to the precipitation of PMeOx-*co*-PEI decelerating hydrolysis at high conversion rates.[225, 384]

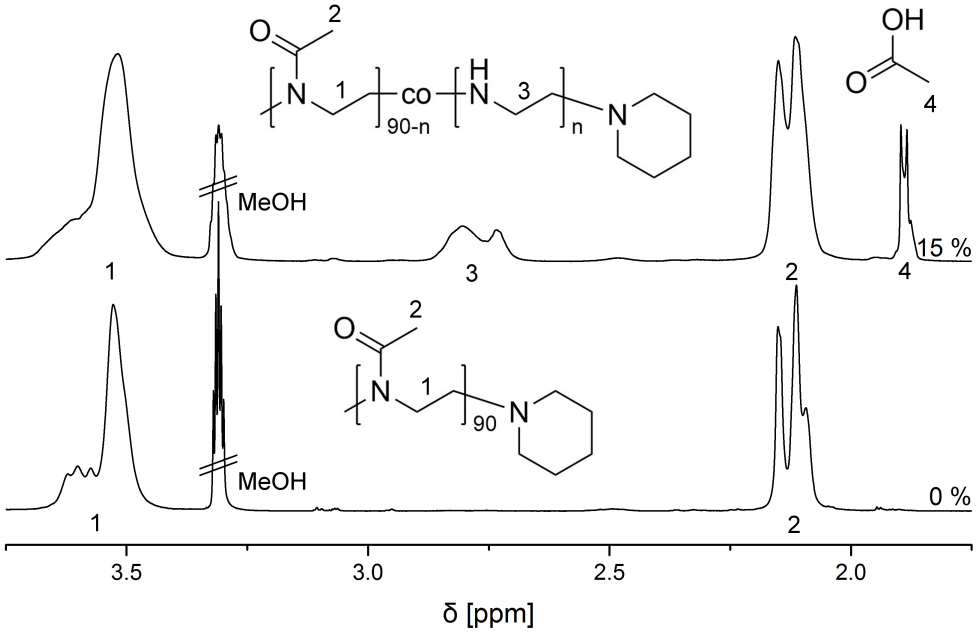

Figure 4.22: ^{1}H-NMR spectra of the initial $PMeOx_{90}$ and PMeOx-*co*-PEI with a degree of hydrolysis of ≈ 15 %.

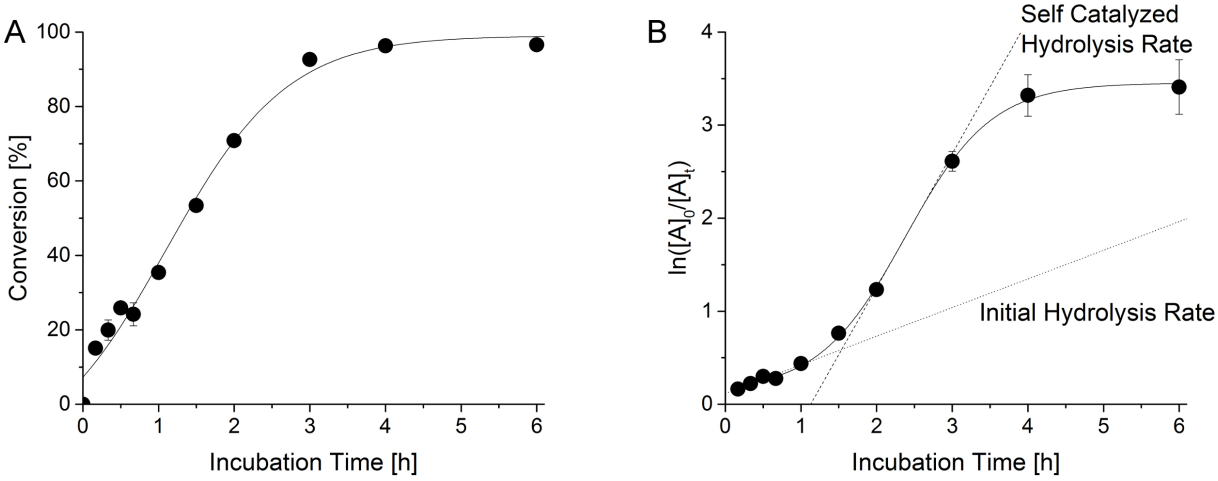

Figure 4.23: A Conversion vs. incubation time plot for the acidic hydrolysis of $PMeOx_{90}$ yielding PEI at 90 °C. Data are presented as mean ± SD (n = 3). Sigmoidal fit is intended as a guide to the eye. **B** Resulting pseudo-first order kinetic plot revealing a sigmoidal curve progression and tangent through the point of inflexion for the amide hydrolysis conversion of $PMeOx_{90}$ at 90 °C. Data are presented as mean ± SD (n = 3).

A second-order kinetic rate law can be determined as:

$$-\frac{d[A]}{dt} = k \cdot [H_3O^+] \cdot [A]$$

where [A] is the polymer amide concentration and k the rate constant. As H_3O^+ is present in large excess and acts as a catalyst, $[H_3O^+]$ is approximately constant and can be

conflated with the rate constant k to obtain the hydrolysis rate constant k_h yielding a pseudo-first order rate law:

$$-\frac{d[A]}{dt} \;=\; k_h \;\cdot\; [A]$$

Rearrangement results in:

$$-\frac{d[A]}{[A]} \;=\; k_h \;\cdot\; dt$$

Earlier studies further demonstrated the hydrolysis rate to be independent from the polymer amide concentration [A], thus also indicating that the reaction proceeds via a pseudo-first order kinetic.[225] Integration yields:

$$-\int_{[A]_0}^{[A]} \frac{d[A]}{[A]} \;=\; k_h \;\cdot\; \int_0^t dt \qquad\qquad (with \int \frac{dx}{x} \;=\; ln\ x)$$

$$ln\frac{[A]_0}{[A]_t} \;=\; k_h \;\cdot\; t$$

The hydrolysis rate constant k_h can be calculated using the slope of a tangent through the point of inflexion as well as the concentration of H_3O^+:

$$k \;=\; \frac{k_h}{[H_3O^+]} \;=\; \frac{a}{[H_3O^+]}$$

However, the pseudo-first order kinetic plot ($\ln([A]_0/[A]_t$ vs. time, Figure 4.23 **B**) reveals a sigmoidal relationship. In the initial phase of the experiment, a self-inhibitory effect due to neighboring group effects is observed. As reported by Hoogenboom *et al.*, hydrolysis of POx does not occur in a random fashion but rather block-like.[228] Once first secondary amine moieties are generated, they catalyze the hydrolysis of adjacent amides, thus accelerating side chain cleavage. In the later course of the experiment, the hydrolysis slows down again due to insufficient solubility of PEI as mentioned earlier.

The hydrolysis rate constant k for the acidic hydrolysis of PMeOx at 90 °C was therefore determined at two different stages of the experiment as labeled in Figure 4.23. In the initial phase of the experiment, the non-catalyzed hydrolysis rate k_1 is calculated as follows:

$$k_1 \;=\; \frac{(0.30784 \;\pm\; 0.04951)\ h^{-1}}{6\ mol\ L^{-1}} \;=\; 1.43 \;\pm\; 0.23 \;\cdot\; 10^{-5}\ Lmol^{-1}s^{-1}$$

During the self-catalyzed phase of the experiment, k_2 is calculated as follows:

$$k_2 = \frac{1.43914\ h^{-1}}{6\ mol\ L^{-1}} = 6.66 \cdot 10^{-5}\ Lmol^{-1}s^{-1}$$

Unfortunately, a direct comparison of the obtained values with the hydrolysis rate as determined by Hoogenboom and coworkers is not feasible due to an error in the calculation of k_h as published by Hoogenboom *et al.* However, comparison of the pseudo-first order kinetic plots (Figure 4.24) reveals significantly faster hydrolysis of PMeOx compared to PEtOx at 90 °C as expected due to the higher hydrophilicity of PMeOx and therefore better hydration. This is also in good agreement with similar findings comparing the

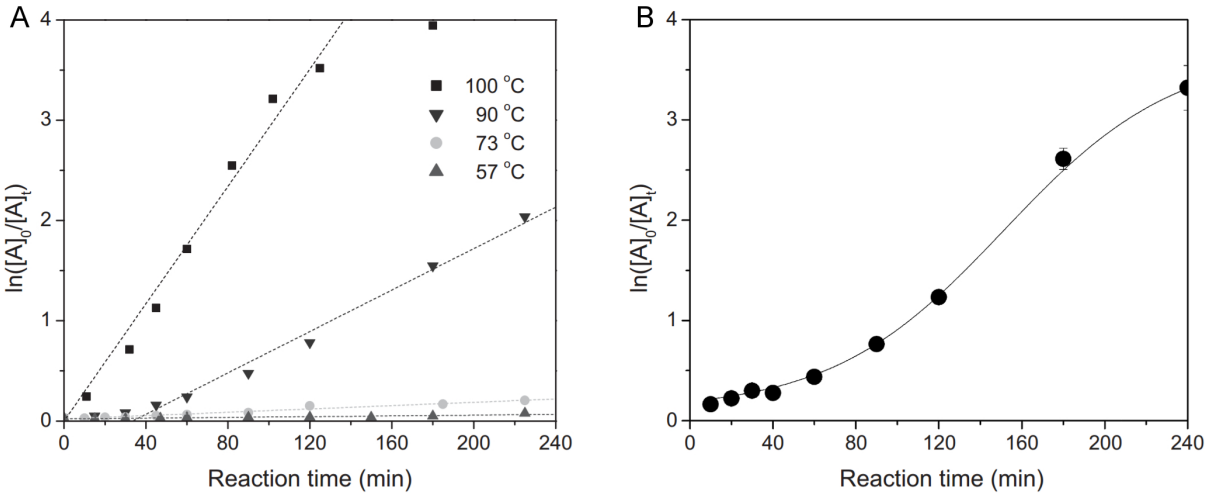

Figure 4.24: A Pseudo-first order kinetic plot of PEtOx hydrolysis using 5.8 M HCl as determined by Hoogenboom and coworkers, taken with permission from ref. [228]. **B** Pseudo-first order kinetic plot of PMeOx hydrolysis at 90 °C using 6 M HCl. Data in **B** are presented as mean ± SD (n = 3) Sigmoidal fit is intended as a guide to the eye.

hydrolysis rates of PEtOx and PMeOx at 100 °C, which confirm faster modification of PMeOx.[225] Due to the high excess of HCl in both experimental set ups, slight differences of the concentration of HCl (5.8 vs. 6 M) are supposedly negligible.

Furthermore, the slope of the line at 90 °C in Figure 4.24 **A** can be estimated to be 0.01 min^{-1} or 0.62 h^{-1}, respectively. Thus, the hydrolysis rate of PEtOx at 90 °C can be calculated as follows:

$$k_{\mathrm{EtOx,90\ °C}} = \frac{0.62\ h^{-1}}{5.8\ mol\ L^{-1}} = 2.97 \cdot 10^{-5}\ Lmol^{-1}s^{-1}$$

The obtained value is between k_1 and k_2, however, it is considered to be only a vague estimation as the curve progression as shown in Figure 4.24 **A** appears to follow a sigmoidal instead of a linear function as well.

4.2.2 Hydrolysis of $PSar_{25}$

As the previously described experimental set up proved to provide reliable and comparable data on the hydrolysis of pseudo-polypeptides, the acidic hydrolysis of $PSar_{25}$ was investigated in the same way and order but more detailed. In case of polypeptoids, hydrolysis of amide bonds initially results in cleavage of the backbone rather than the side chain. Only later, once a certain amount of amide bonds is cleaved, the respective tertiary amino acids are released (Figure 4.25).

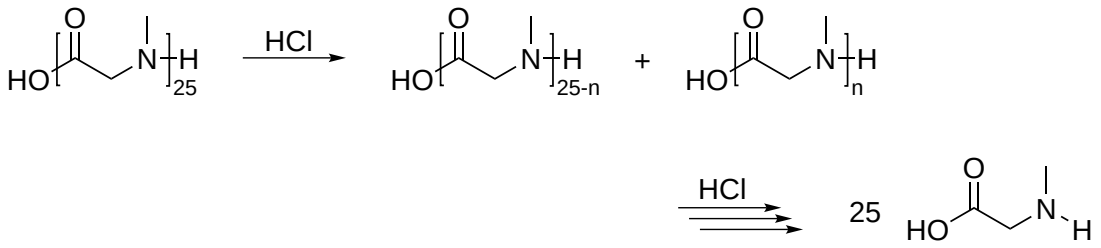

Figure 4.25: Acidic hydrolysis of $PSar_{25}$ yielding shorter PSar chains and finally sarcosine.

The amount of released sarcosine can be determined via ^{1}H-NMR spectroscopy (Figure 4.2.2). By this means, the proportion of sarcosine can be quantified using the signals of the methylene side chain (-CH_3 at δ = 3.0 ppm) and the C_α methylene group of sarcosine (-CH_2- at δ = 3.5 ppm). It has to be noted, though, that the chemical shift of the latter signal varies based on the protonation state of sarcosine. However, ^{1}H-NMR spectra further reveal two further sharp peaks δ = 4.0 ppm and δ = 3.0 ppm indicating the presence of additional low molar mass degradation products. Recorded reference spectra enable the assignment of these signals to sarcosine anhydride, a typical by-product of sarcosine *N*-carboxyanhydride (Sar-NCA) synthesis usually obtained with a proportion of less than 5 %. Sarcosine anhydride does not interfere the living nucleophilic ring opening polymerization of Sar-NCA yielding PSar and is eliminated during purification of the polymer, which is confirmed by the ^{1}H-NMR of $PSar_{25}$ (Figure 4.25) prior to hydrolysis not revealing signals corresponding with sarcosine anhydride. Thus, it can be reasonably

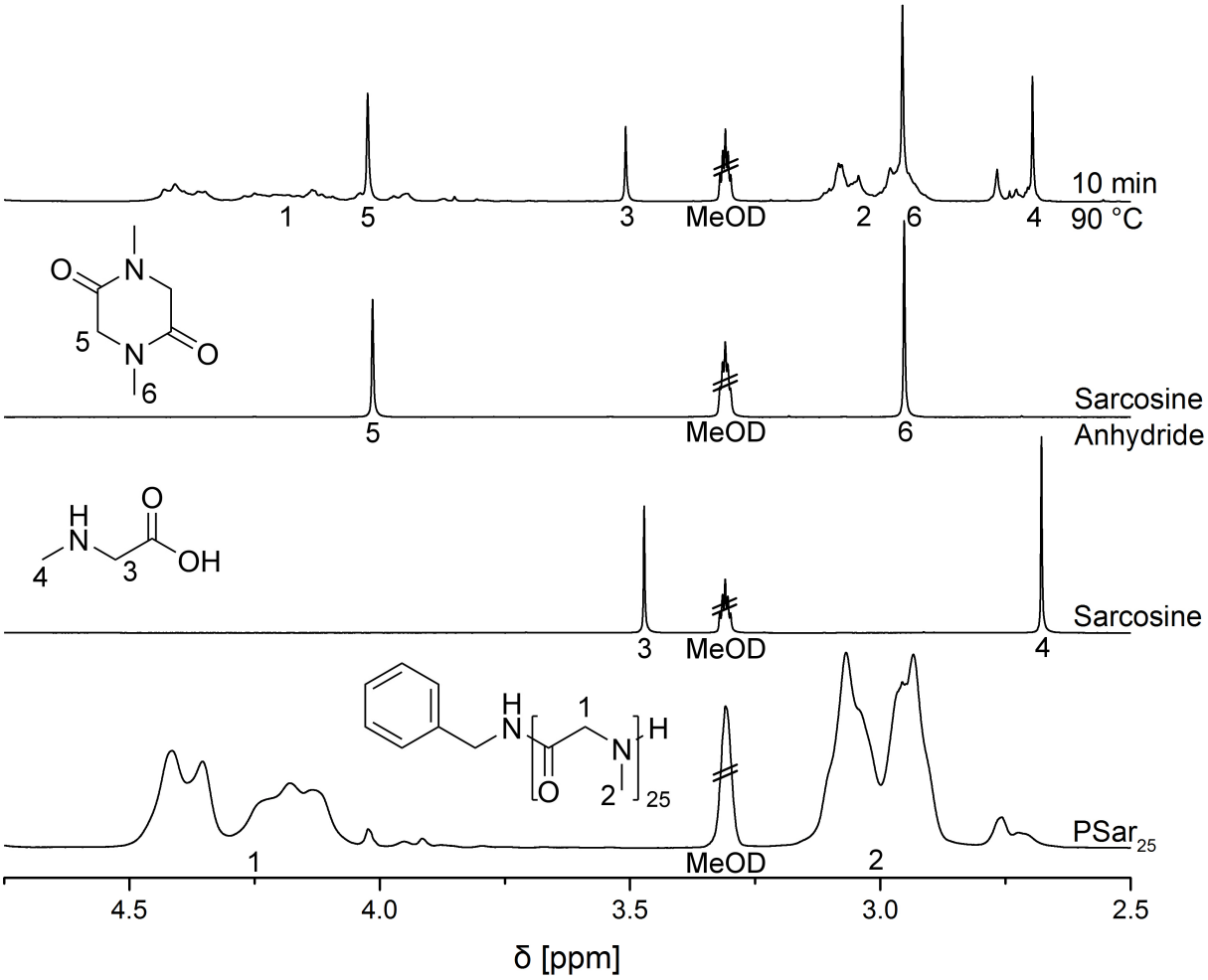

Figure 4.26: ^{1}H-NMR spectra of the initial $PSar_{25}$, sarcosine, sarcosine anhydride as well as $PSar_{25}$ hydrolyzed for 10 min at 90 °C.

concluded that sarcosine anhydride is obtained as a product of $PSar_{25}$ hydrolysis.

As mentioned earlier, cleavage of polypepoid amide bonds does not result in the immediate release of the respective amino acids. Assuming a perfectly random chain scission, the early phase of $PSar_{25}$ hydrolysis should primarily yield oligomers whose length decreases with advancing chain scission. In the same manner, the likelihood that the random hydrolysis of an amide bond releases sarcosine increases. It is therefore also important to note that the determinable release of sarcosine cannot be applied as a direct measure for the hydrolysis rate of $PSar_{25}$.

However, as unpublished studies conducted by our group reveal, sarcosine dimers are rather unstable. In view of the present data on the hydrolysis of $PSar_{25}$, it can be reasonably assumed that formed dimers cyclize yielding sarcosine anhydride (Figure 4.27). In a control

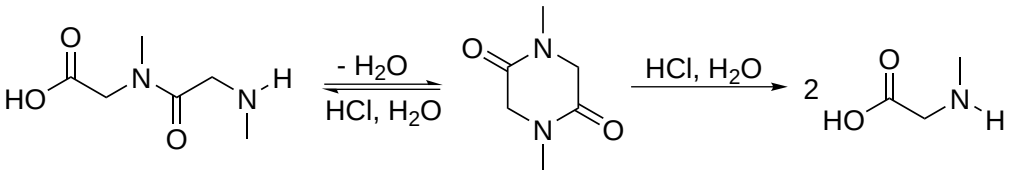

Figure 4.27: Instable dimers of sarcosine generated during hydrolysis of PSar cyclize yielding sarcosine anhydride, which is prone to further hydrolysis yielding sarcosine.

experiment, sarcosine anhydride was hydrolyzed during incubation in 6 M HCl at 99 ° for 6 h. As determined via ^{1}H-NMR spectroscopy, the conversion of sarcosine anhydride to sarcosine amounted to 95.7 % with respect to nitrogen. Indeed, it is likely that the ring opening hydrolysis of sarcosine anhydride yielding a sarcosine dimer exists in equilibrium with the cyclization of the latter yielding sarcosine anhydride. The actual generation of sarcosine thus requires the more or less simultaneous cleavage of both sarcosine anhydride amide bonds. Therefore, the intermittent generation of sarcosine anhydride probably decelerates but does not prevent the formation of sarcosine. Although no information regarding the *in vivo* fate and metabolism of sarcosine anhydride are available, it can be assumed to be physiologically harmless and is likely eliminated from the body in a natural way.

Proportions of nitrogen bound within PSar, sarcosine anhydride and sarcosine, respectively, were determined from the ^{1}H-NMR spectra and plotted against the incubation time at temperatures ranging from 55 to 99 °C (Figure 4.28). Like the acidic hydrolysis of POx, the acidic hydrolysis of PSar is a heavily temperature-dependent process. Especially at the highest investigated temperature of 99 °C, the residual M_w decreases to ≈ 15 % within only 10 min of incubation, while the proportion of nitrogen bound in PSar decreases at a similar rate. The proportion of nitrogen bound in sarcosine anhydride increases until reaching a maximum after 20 min of incubation and subsequently decreases again due to further hydrolysis yielding sarcosine in excellent agreement with the previously discussed mechanism. Simultaneously, more and more sarcosine is generated. With decreasing temperature, the process of acidic PSar hydrolysis slows down significantly. While the residual M_w still reaches its minimum of ≈ 15 % after 20 min at 90 °C, it is only reached after 1 h of incubation at 75 °C or 6 h at 55 °C. Likewise, the maximum proportion of nitrogen bound in sarcosine anhydride is only reached after 40 minutes at 90 °C and 4 h at

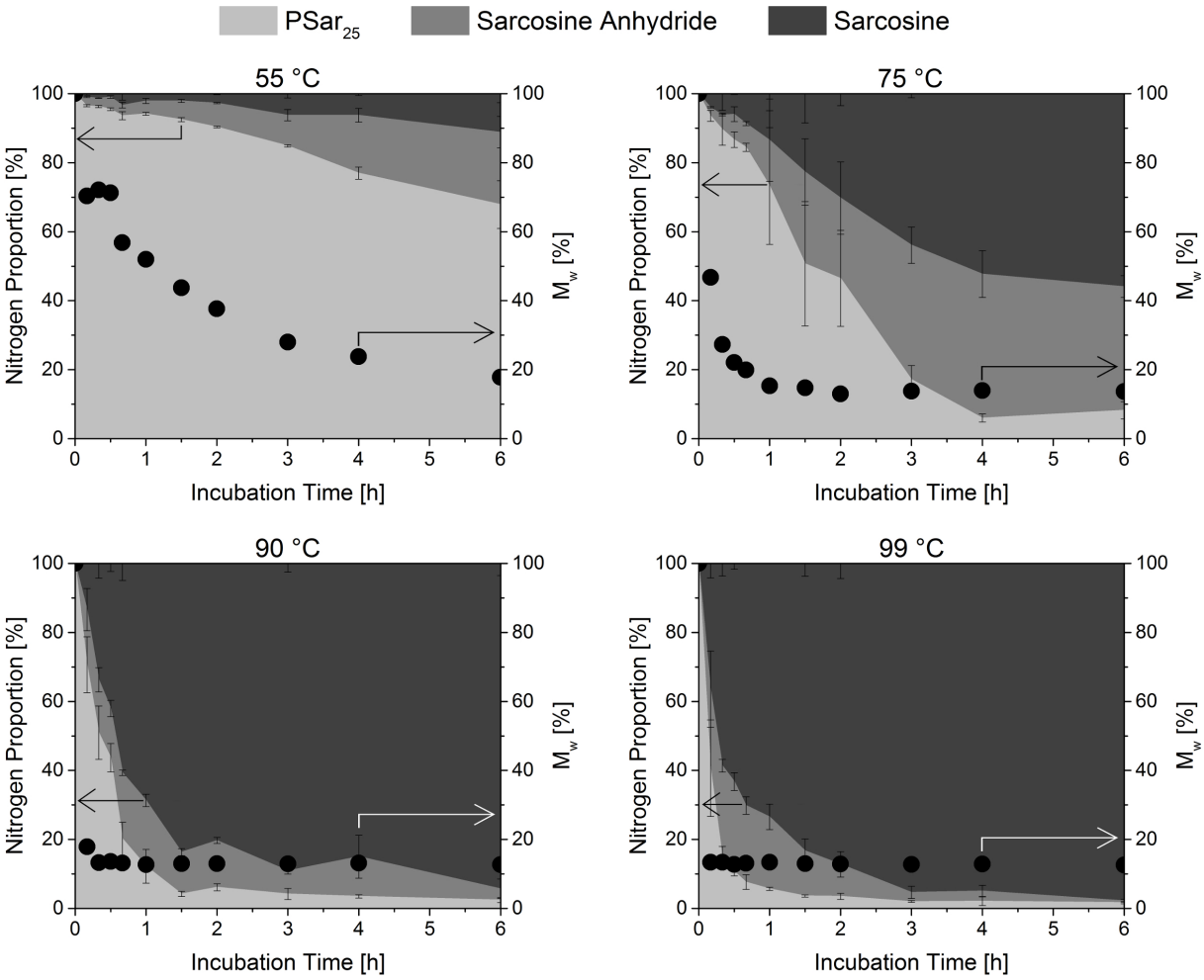

Figure 4.28: Kinetic plots showing the proportions of nitrogen bound within PSar (light grey), sarcosine anhydride (grey) and sarcosine (dark grey) as determined via ^{1}H-NMR spectroscopy as well as residual M_w as determined via GPC for the acidic hydrolysis of $PSar_{25}$ by 6 M HCl at 55 to 99 °C. Data are presented as mean ± SD (n = 3).

75 °C, while no maximum is apparent at 55 °C during 6 h of incubation. As expected, rates of polymer degradation as well as sarcosine release decrease with decreasing temperature. In order to estimate the relevance of PSar hydrolysis at a physiological temperature of 37 °C, similar experiments with prolonged incubation times of up to 14 d applying 6 M HCl as well as simulated gastric fluid (SGF) and simulated intestinal fluid (SIF) without further addition of digestive enzymes were conducted (Figure 4.29). Upon incubation in 6 M HCl, a very pronounced degradation is observed. Already during the initial 4 h of incubation, a molar mass decrease of ≈ 30 % is apparent, although only a very small proportion of 3.7 % sarcosine is generated. After 14 d of incubation, the minimum residual weight of ≈ 15 % and a sarcosine proportion of 55 % are reached, while only 10 % of the

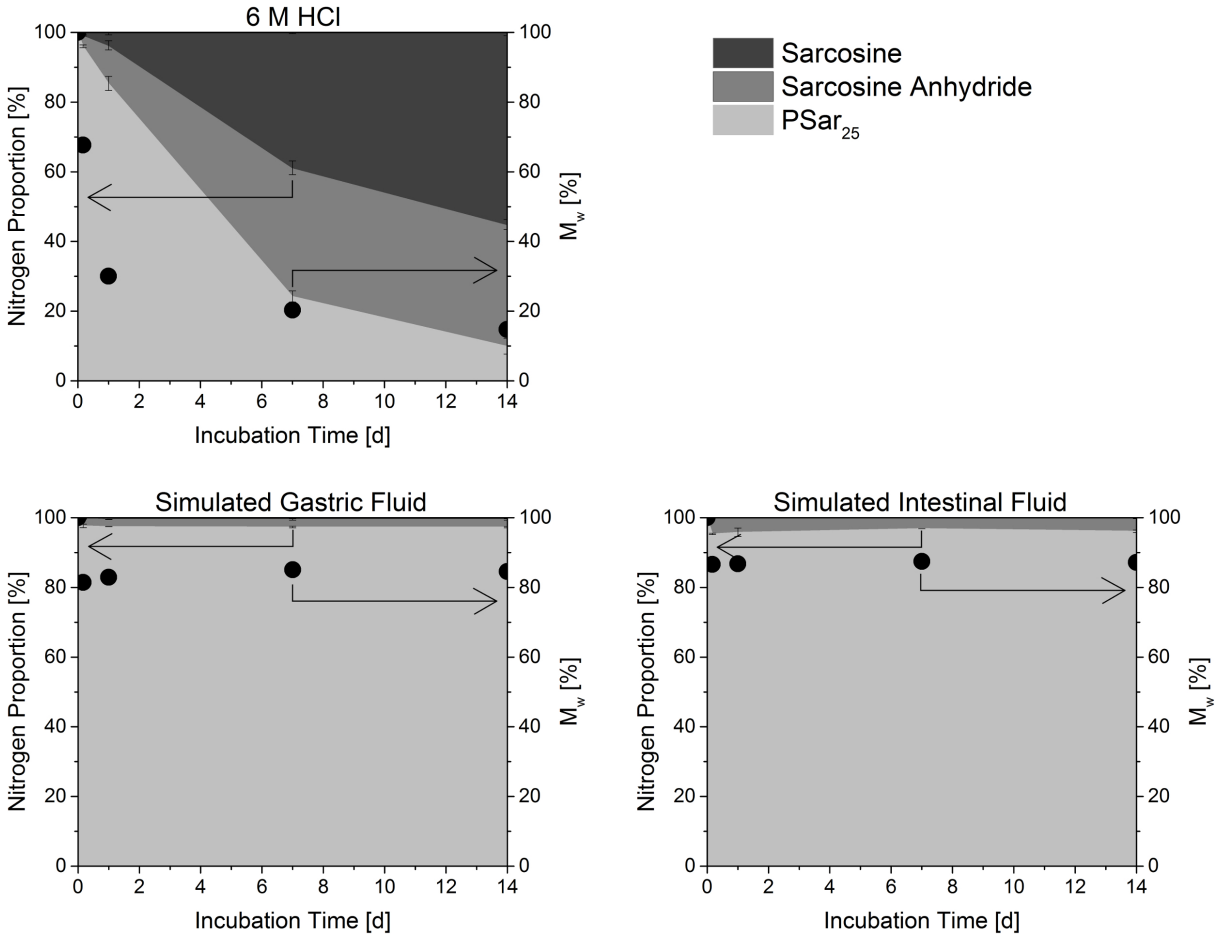

Figure 4.29: Kinetic plots showing the proportions of nitrogen bound within PSar (light grey), sarcosine anhydride (grey) and sarcosine (dark grey) as determined via ^{1}H-NMR spectroscopy as well as residual M_w as determined via GPC for the acidic hydrolysis of $PSar_{25}$ by 6 M HCl, SGF and SIF at 37 °C. Data are presented as mean ± SD (n = 3).

nitrogen is still bound within PSar.

In contrast, degradation of $PSar_{25}$ in both SGF (pH 1.1 - 1.3) and SIF (pH 6.50 - 6.60) is not particularly remarkable. Over an incubation period of 14 d, the quantity of generated sarcosine remains below the limit of detection (< 0.1 %). Nevertheless, significant amounts of sarcosine anhydride corresponding with a nitrogen proportion of 2 - 4 % are formed, while M_w decreases to about 85 %. Quite surprisingly though, no further alterations are observed after the first four hours of incubation.

One likely cause for these findings could be the very diverse ratios of polymer and acid. Hydrolysis experiments were conducted with a constant polymer concentration of 5 g/L corresponding to a polypeptoid amide concentration of 0.07 mol/L. Thus, hydrolysis in 6 M HCl resulted in a large excess of acid with an amide-to-H_3O^+ ratio of 1 : 86. If SGF is

applied, this ratio decreases tremendously to only 1 : 0.9. In case of SIF, the concentration of HCl is almost negligible with an amide-to-H_3O^+ ratio of $1 : 4 \cdot 10^{-6}$.

The initial step of acidic amide hydrolysis (Figure 4.30) is an acid-base reaction, where H_3O^+ is attacked by the amide carbonyl resulting in protonation of the latter one, thus increasing the electrophilicity of the carbon atom. Subsequently, the electrophilic carbon

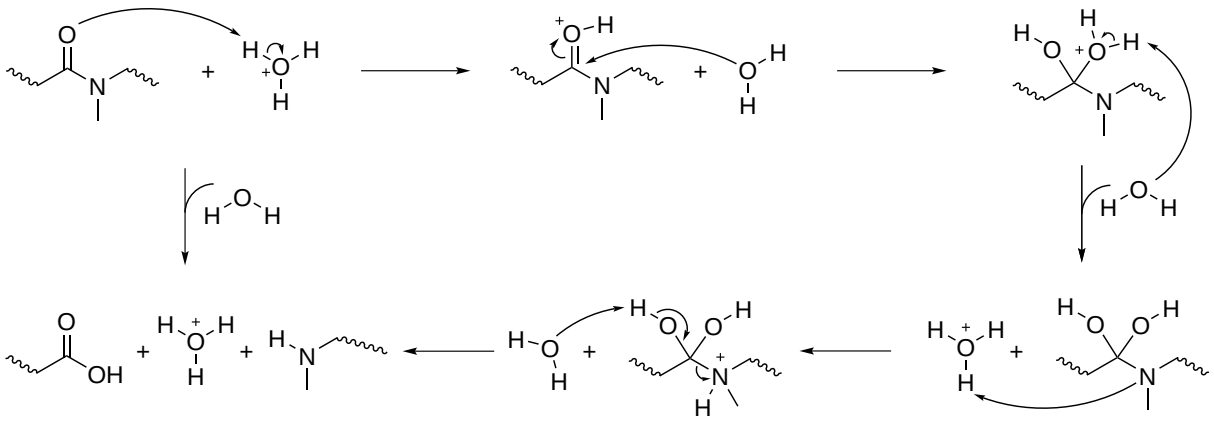

Figure 4.30: Mechanism of the acid-promoted hydrolysis of tertiary amides resulting in cleavage of the amide bond yielding the respective acid and secondary amide.

atom is attacked by the oxygen of water forming a tetrahedral intermediate, which is known as the rate-determining step and is followed by a number of fast non-rate-determining steps resulting in the cleavage of the amide bond. Although H_3O^+ only act as a catalyst until cleavage of the amide bond, a subsequent acid-base reaction of the generated secondary amines and H_3O^+ removes the latter one from the system (Figure 4.31). Thus, H_3O^+ does

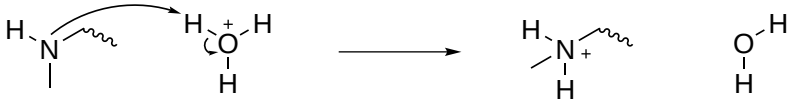

Figure 4.31: The acidic hydrolysis of amides is followed by a subsequent acid-base reaction removing H_3O^+ from the system.

not act as a catalyst but as a promoter of amide hydrolysis and its available quantity has a tremendous impact on the accessible degree of hydrolysis. With the large excess of 6 M HCl, all amide bonds comprised by $PSar_{25}$ can be cleaved theoretically. In contrast, SGF only offered the potential to cleave about 90 % of the available amide bonds while SIF only comprised H_3O^+ for the cleavage of less than 0.0005 %. Furthermore, hydrolytic ring opening of sarcosine anhydride and subsequent cyclization of the generated dimer

as discussed previously decelerate the generation of sarcosine tremendously. Especially when low amounts of acid are available, the simultaneous hydrolysis of both amide bonds comprised by sarcosine anhydride yielding sarcosine is very unlikely. Nonetheless, the generation of sarcosine from sequential chain end scission remains conceivable.

It is striking, however, that against all expectations the apparent hydrolysis rates of $PSar_{25}$ in both SGF and SIF are approximately the same. A pH measurement right after addition of the fluids revealed a pH of ≈ 7 in SIF and ≈ 6.5 in SGF. Apparently, $PSar_{25}$ comprising a benzylamine moiety at the C-terminus as well as a secondary amine at the N-terminus neutralized the added SGF, thus resulting in similar apparent degradation rates. In contrast, pH measurements after dissolving the same quantity of neopentylamine-$PSar_{90}$-Ac in SGF revealed an unaltered pH of ≈ 1.5. Interestingly, neither sarcosine nor sarcosine anhydride were released to reach the minimum detectable limit of ≈ 0.1 % within 4 h at 37 °C.

Overall, the experimental set up applied to investigate the acidic hydrolysis of $PSar_{25}$ sufficiently demonstrated the high temperature-dependency of acidic amide cleavage by an excess of HCl. Albeit very slow, $PSar_{25}$ is also cleaved at a physiological temperature of 37 °C by 6 M HCl as well as SGF and SIF. Control experiments incorporated the addition of HCl to a concentration of 6 M and subsequent neutralization and evaporation of the solvent at 100 °C and proved sufficient stability of $PSar_{25}$ under the described circumstances.

However, the applied amide-to-H_3O^+ ratios for both SGF and SIF proved to be ineligible to model a potential *in vivo* hydrolysis. In order to obtain reliable results, similar experiments should be conducted in excess of the acid. Nevertheless, the partial cleavage of $PSar_{25}$ by both SGF and SIF within only 4 h of incubation indicated by a decrease of M_w as well as the generation of sarcosine anhydride was successfully demonstrated. It can therefore be reasonably assumed that PSar is susceptible to acidic hydrolysis during passage through the stomach with a maximum retention time of 4 h. Cleavage of $PSar_{25}$ in SIF further suggests a potential hydrolysis under rather moderate conditions. Further experiments investigating the stability of PSar in PBS as well as under basic conditions could help to confirm and clarify these findings.

4.3 Enzymatic Degradation

Polypeptoids, POx and PEG are generally considered to be insusceptible to endogenous enzymes. In case of PEG, this is easily comprehensible in view of the polyether structure which does not resemble an endogenous polymer. However, POx and particularly polypeptoids bearing amide bonds within the side chain and backbone, respectively, exhibit strong similarities with polypeptides. Investigations on the enzymatic digestion of oligopeptoids conducted by Zuckermann and coworkers revealed their resistance against hydrolysis by carboxypeptidase A, papain, pepsin, trypsin, elastase and chymotrypsin.[237] It must be noted, though, that some of these enzymes are rather specific towards defined amino acid sequences and all of them rule out peptide chain scission next to a proline residue[238], which, in a certain way, resembles (poly)peptoids as it is the only essential amino acid bearing a tertiary amine.

Nevertheless, as reflected previously (see section 2.2.3) the specific selection of enzymes potentially capable to hydrolyze polypeptoids or POx without any further indications is rather complicated. It was therefore considered reasonable to apply more genuine conditions to investigate the stability of pseudo-polypeptides against enzymatic degradation. Since proline iminopeptidase, an N-terminal exopeptidase and interesting candidate for the hydrolysis of PSar as outlined in section 2.2.3.1, is expressed, among others, in liver and kidney of rats as well as in chicken egg white, these media where investigate with respect to their capability to digest polypeptoids and POx as well as PEG for reference.

4.3.1 Degradation of Polypeptoids in Homogenates of Rat Kidney and Liver

N-terminal labeled $PSar_{333}$-FITC

First experiments on the enzymatic degradation of polypeptoids in homogenates of rat kidney and liver were conducted by Fabian Wieghardt and Johanna Eisenreich in the context of their bachelor theses.[385, 386]

The N-terminus of benzylamine-initiated $PSar_{333}$ was labeled with fluorescein isothiocyanate (FITC), a fluorescin derivative with maximum excitation and emission wavelengths of 494 and 518 nm, respectively.[387] Subsequently, $PSar_{333}$-FITC was incubated with homogenates of freshly harvested rat liver and kidney at 37 °C for 24 h. Via Sephadex

LH-20 columns, the obtained homogenate-polymer-mixtures were separated into small fractions by size and the fluorescence of the individual fractions was measured to gain insights into the size distribution of the FITC-labeled fragments (Figure 4.32).

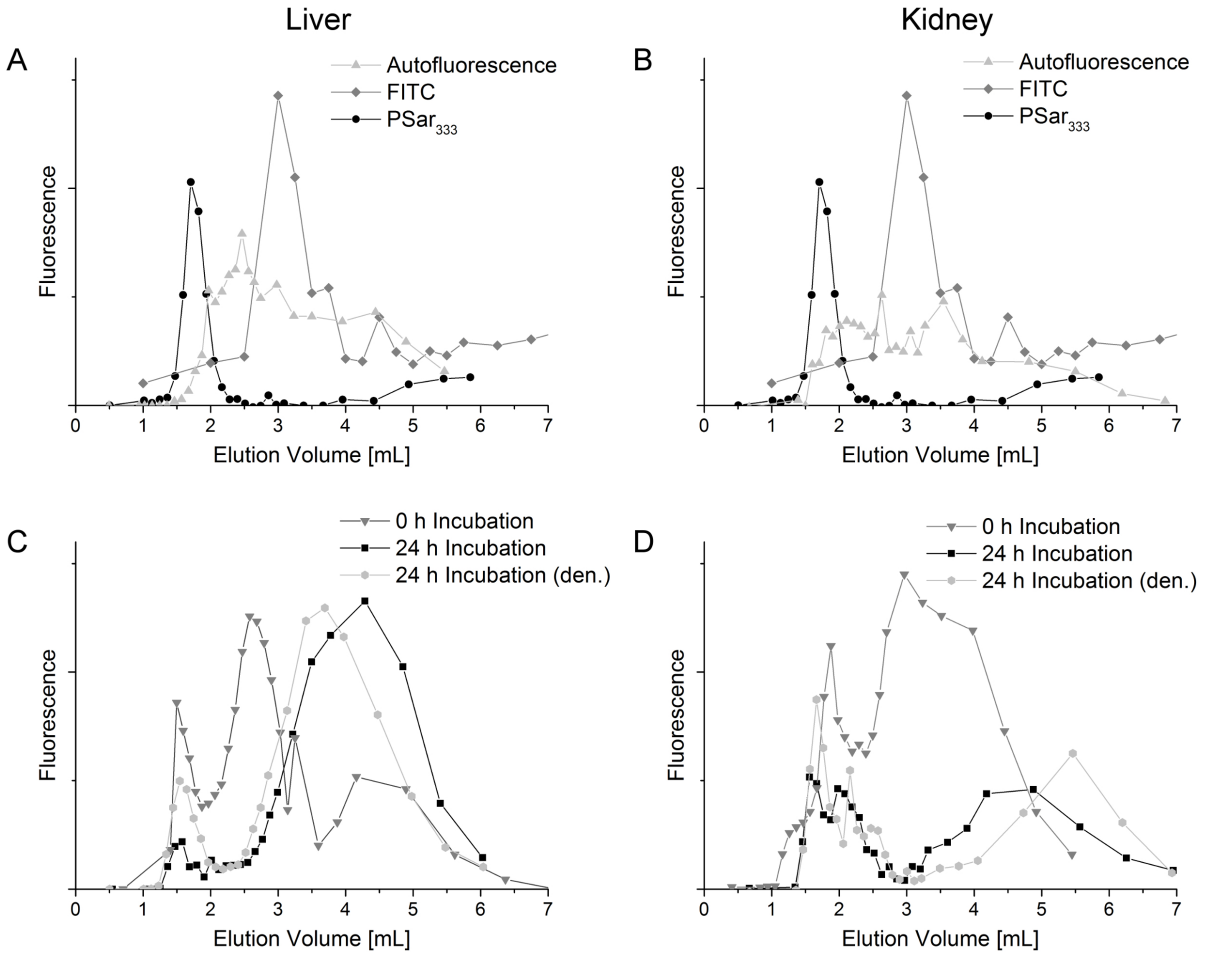

Figure 4.32: Fluorescence of $PSar_{333}$-FITC before and after incubation with rat organ homogenates for 24 h. **A** and **B** non-incubated polymer and FITC as well as the autofluorescence of liver and kidney, respectively. **C** and **D** elugrams of $PSar_{333}$-FITC after incubation with organ homogenates for up to 24 h. Data taken from ref. [385] and ref. [386].

Unfortunately, evaluation of the obtained results is complicated by the high autofluorescence of both liver and kidney as evident from Figure 4.32 **A** and **B**. Nevertheless, the elution volumes of non-incubated $PSar_{333}$-FITC and FITC are certainly separated, a possible degradation of the polymer should thus be clearly discernible. For both organ homogenates, three scenarios of incubation were performed:

- 0 h incubation, implicating thorough blending of homogenate and polymer and

subsequent analysis without prior incubation

- 24 h incubation of the homogenate-polymer-mixture at 37 °C
- 24 h incubation (den.) of the homogenate-polymer-mixture at 37 °C after prior denaturation of the organ homogenate for 2 h at 100 °C

In the assumption of effective deactivation of the involved enzymes, elugrams of the 0 h incubation and 24 h incubation with denatured homogenates should in essence reflect the elugram of $PSar_{333}$-FITC. Indeed, all elugrams display peaks at ≈ 1.7 mL well corresponding with $PSar_{333}$-FITC, thus excluding the entire cleavage of FITC from the N-terminus of the polymer. However, the 0 h incubation samples of both liver and kidney also show signals matching the elution volume of free FITC at ≈ 3.0 mL, while the 24 h incubated samples exhibit broad peaks at even higher elution volumes which cannot be explained by cleavage of FITC alone.

Although these results may indicate the enzymatic modification of $PSar_{333}$-FITC, they need to be examined rather critically. First of all, cleavage of FITC in both the 0 h incubated and denatured 24 h incubated sample is striking. The thiourea bond formed by labeling $PSar_{333}$ with FITC (Figure 4.33) is very stable under *in vivo* conditions, hence the undesired cleavage of FITC during the course of the experiment can be excluded. The

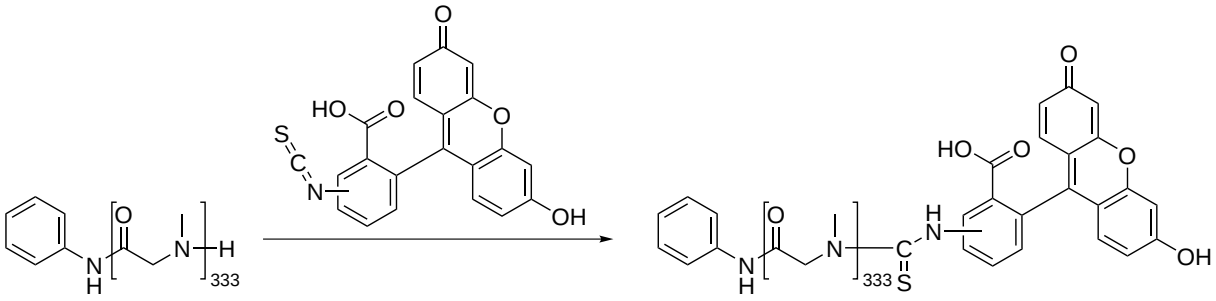

Figure 4.33: Reaction scheme for the labeling of $PSar_{333}$ with FITC creating a stable thiourea bond.

fluorescence quantum yield of FITC is known to be highly pH-dependent and decreases substantially under acidic conditions. Furthermore, the stability of the peptoid amide bonds towards the applied experimental conditions is questionable and possibly influenced by a slightly hydrolytic or oxidative milieu. It should be noted, however, that the fairly high autofluorescence observed in the control experiments (Figure 4.32 **A** and **B**) is astonishingly not mirrored within the elugrams of the homogenate-polymer-mixtures (Figure 4.32 **C**

and **D**). Furthermore, consideration must be given to the fact that the displayed elugrams do not reflect the actual size distribution of the polymer, but only the size distribution of FITC labeled fragments. Thus, potentially formed smaller PSar chains are not detected unless they still bear the FITC-labeled N-terminus.

Notwithstanding the aforementioned, a decisive disadvantage of this experiment might be in the synthesis and labeling of the polymer itself. Initiating the polymerization with benzylamine and attachment of the FITC dye introduces sterically demanding end groups to both the C-terminus as well as the N-terminus of PSar. Digestion of the $PSar_{333}$-FITC conjugate by exopeptidases like proline iminopeptidase can therefore more than likely be excluded.

C-terminal labeled SulfoPBI-$PSar_{185}$

In order to circumvent the latter issue, follow-up experiments conducted by Maria Krebs for her master thesis were based on dye-initiated PSar, thus ensuring accessibility of the N-terminus to enzymatic digestion by exopeptidases.[388] Therefore, the polymerization of Sar-NCA was initiated by a fluorescent sulfo perylene bisimide (SulfoPBI) bearing a primary amine group with maximum excitation and emission wavelengths of 620 and 566 nm (Figure 4.34 **A**), respectively, and SulfoPBI-$PSar_{185}$ was obtained with a rather broad dispersity of 1.3. Again, the dye-labeled polymer was incubated with freshly harvested

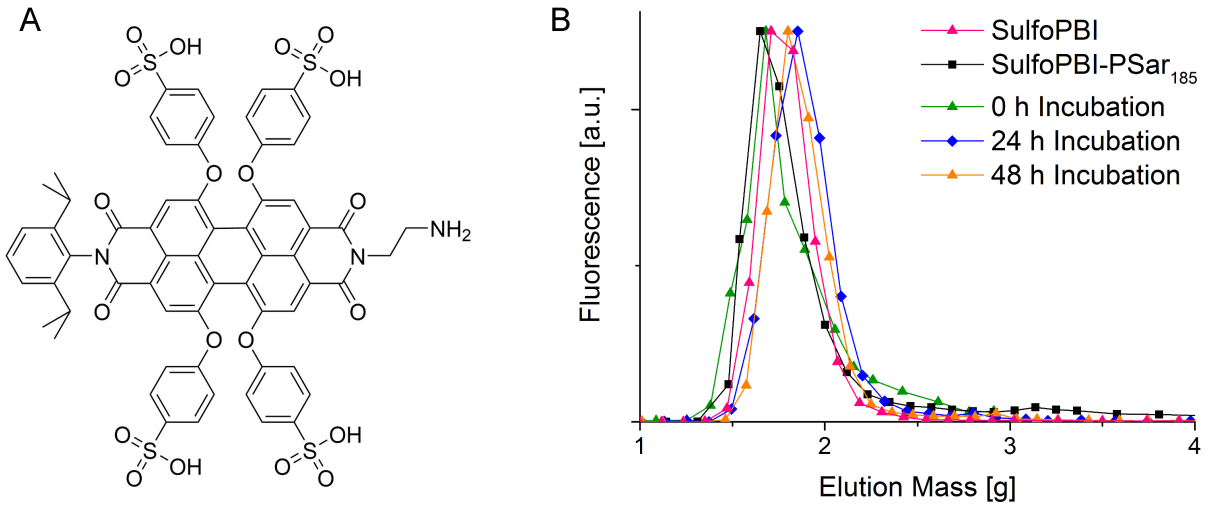

Figure 4.34: A Chemical structure of the fluorescent initiator SulfoPBI. **B** Normalized elugrams obtained for SulfoPBI-$PSar_{185}$ before and after incubation with rat liver homogenate. Data taken from ref. [388].

and blended rat liver homogenate and subsequently fractionated using a Sephadex LH-20 column (Figure 4.34 **B**). Surprisingly, not only SulfoPBI-PSar$_{185}$ and the incubated samples but also the SulfoPBI dye were eluted at very similar masses. As SulfoPBI was successfully attached to the PSar C-terminus as proved by NMR spectroscopy, the elution mass and therefore the hydrodynamic radius of the SulfoPBI-PSar$_{185}$ appears to be independent on the presence and molar mass of the polymer. This is most probably attributed to the formation of aggregates by SulfoPBI,[389] which showed up in a NOESY spectrum of SulfoPBI-PSar$_{185}$. Furthermore, aggregation of SulfoPBI as well as SulfoPBI-PSar$_{185}$ were verified via concentration-dependent UV/Vis spectra in millipore water and PBS (Figure 4.35). The initial solution of SulfoPBI-PSar$_{185}$ was consecutively diluted by half

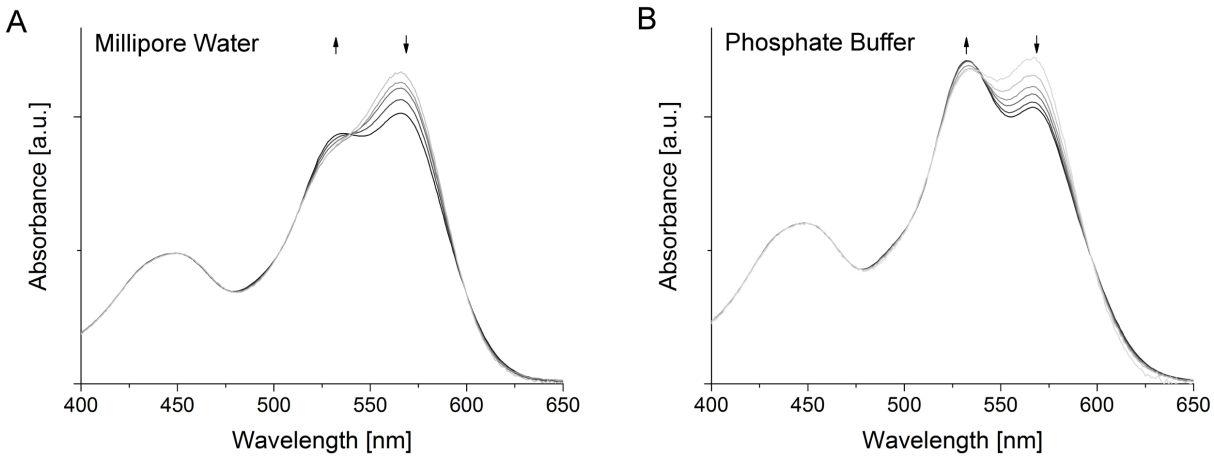

Figure 4.35: Concentration-dependent UV/Vis spectra of SulfoPBI-PSar$_{185}$ measured in **A** millipore water ($3.46 \cdot 10^{-5}$ M – $2.16 \cdot 10^{-6}$ M) and **B** PBS ($2.23 \cdot 10^{-5}$ M – $2.16 \cdot 10^{-6}$M). Arrows indicate increasing concentrations. Data taken from ref. [388].

and the obtained spectra were multiplied with the corresponding dilution factors to obtain overlapping bands at 449 nm with intensities directly proportional to the concentration of the dye-polymer conjugate according to the Beer–Lambert law. In addition, two further bands at 533 nm and 566 nm which change their appearance as a function of the concentration of SulfoPBI-PSar$_{185}$ are apparent. With increasing concentration, increase of the fluorescence intensity at 533 nm, simultaneous decrease of the fluorescence intensity at 566 nm and an isosbestic point at 540 nm are observed and indicate the formation of aggregates.[390]

At this point, *in vitro* examinations on the degradation of dye labeled PSar in rat liver

and kidney were discontinued for a number of reasons. Due to the low availability and quantity of rat organs, a reasonable polymer-to-organ ratio necessitates the use of very low concentrations of the polymer. In order to enable the detection of these low amounts of polymer, labeling accompanied by modification of at least one terminus and therefore not only alteration of the polymer structure but also its susceptibility to enzymatic digestion is inevitable. As mentioned previously, labeling of the polymer further only facilitates the detection of dye-labeled fragments. Therefore, a complete overview on the degradation state and size-distribution of the polymer is not possible at any time. Moreover, it is highly questionable whether a significant degradation of PSar within the time scope of these experiments can be anticipated at all. Although incubation was performed for up to 48 h, during incubation at 37 °C the organ homogenates began to rot very fast and may have lost their enzymatic activity within only a few hours. If at all, the enzymatic degradation of polypeptoids is expected to proceed at a steady but very slow pace, which requires far longer periods to be considered in order to obtain measurable modifications.

4.3.2 Degradation of Polypeptoids, Poly(2-alkyl-2-oxazoline)s and Poly(ethylene glycol) in Chicken Egg White

4.3.2.1 *In vitro* Investigations with dye-labeled $PSar_{333}$-FITC and unlabeled $PSar_{333}$

First experiments with chicken egg white and fluorescent $PSar_{333}$-FITC were carried out analog to the corresponding studies in organ homogenates by Fabian Wieghardt.[385] Again, the validity of the elugrams is affected bye a comparably high autofluorescence of the chicken egg white and all of the incubated samples possess signals well corresponding with FITC and $PSar_{333}$-FITC. As already discussed in detail within the previous section, the reliability of these data is doubtful.

However, the application of chicken egg white greatly benefits from its excellent availability in large quantities and enables the investigation of unlabeled polymer. Therefore, samples of each 1 g chicken egg white and 5 mg $PSar_{333}$ were blended, incubated for 24 h at 37 °C with and without prior denaturation for 2 h at 100 °C (in compliance with earlier experiments conducted by Neumann and Sela[276]), freeze dried and subsequently analyzed

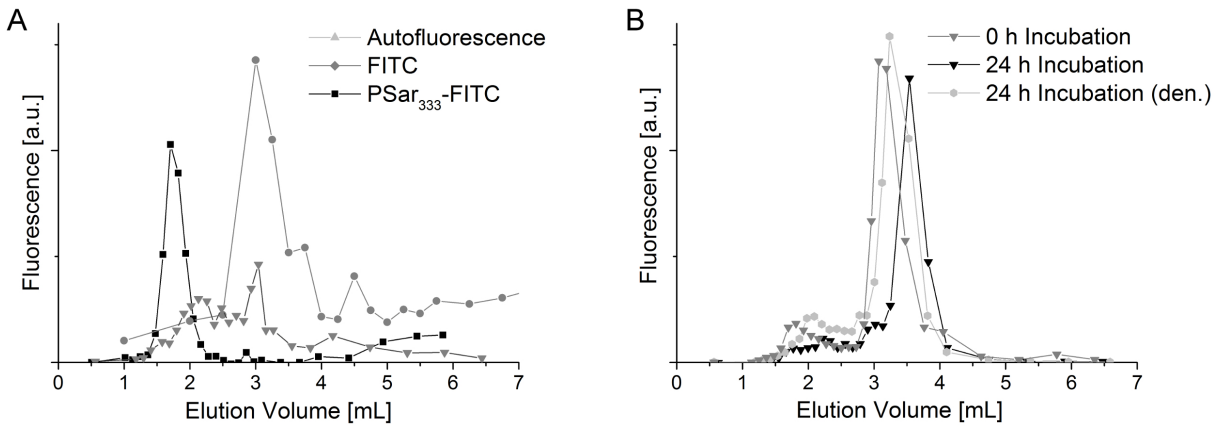

Figure 4.36: Fluorescence of $PSar_{333}$-FITC before and after incubation with chicken egg white for 24 h. **A** non-incubated polymer and FITC as well as the autofluorescence of chicken egg white. **B** elugrams of $PSar_{333}$-FITC after incubation with chicken egg white for up to 24 h. Data taken from ref. [385].

via GPC in DMF (Figure 4.37). GPC elugrams of all samples closely resemble each other,

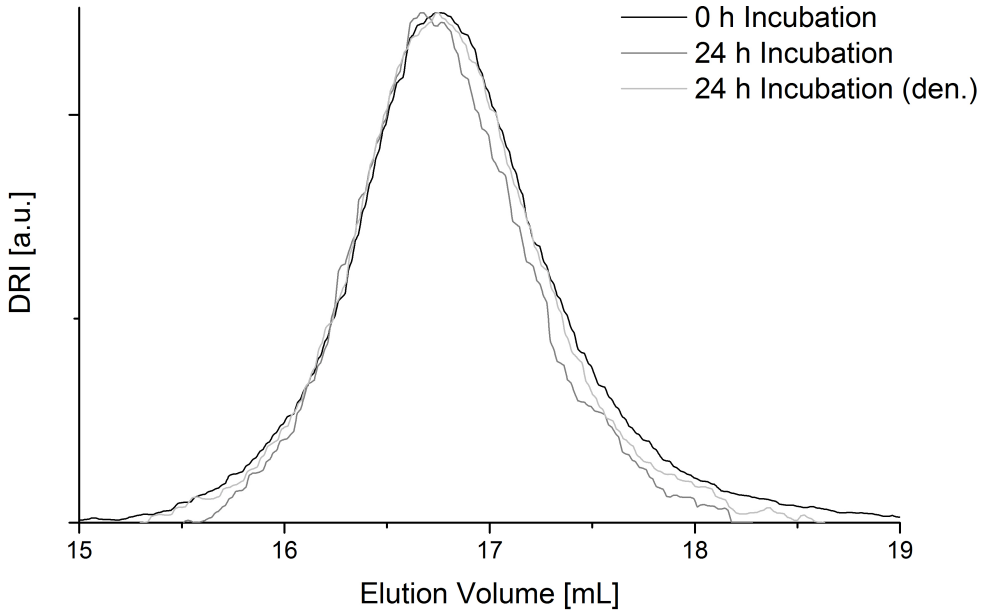

Figure 4.37: Normalized GPC elugrams of $PSar_{333}$ before and after incubation with chicken egg white for 24 h. Data taken from ref. [385].

thus indicating no significant degradation of $PSar_{333}$ in chicken egg white within 24 h to occur. Under similar conditions but applying substantially lower amounts of polymer (0.5 mg as opposed to 5 mg), Neumann and Sela observed the digestion of various peptides including poly-L-proline and poly-L-hydroxyproline to an extent of more than 30 % as analyzed colorimetrically.[276] It is conceivable that the unfavorable polymer-to-egg white

ratio impeded a potential significant degradation of PSar. Furthermore, the incubation time applied for this experiment is still limited to 24 h. Although both poly-L-proline and poly-L-hydroxyproline were significantly digested within this time frame as reported by Neumann and Sela, PSar might degrade at a much slower pace, if at all. In order to entirely rule out or confirm the digestion of PSar in chicken egg white, incubation for a prolonged period of time remains essential.

4.3.2.2 Preliminary Investigations on the *in ovo* Stability of Poly(ethylene glycol) and Polysarcosine

Injection of the polymer into the egg white of fresh whole chicken eggs was considered as a solution to both of the aforementioned problems. Due to the excellent solubility of both PEG and PSar in water, it can be assumed that both polymers do not remain localized at the site of injection but distribute homogenously over the whole egg, which was also observed in control experiments with food coloring. By this means, the polymer-to egg white ratio was greatly diminished from 5 mg polymer per 1 mL egg white as applied in the *in vitro* experiments to as little as 10 mg polymer per ≈ 50 mL egg white in the *in ovo* experiment, thus corresponding with an increase of the volume of egg white per mg of polymer of 2500 %. Furthermore, the application of whole eggs enabled the incubation for much prolonged periods of time to up to 20 d, which essentially resembles the breeding time of chicken eggs of about 21 d.

First experiments on the *in ovo* degradation of PSar and PEG were conducted by Maria Krebs,[388] however, in order to increase the reliability of these results, a comprehensive re-evaluation was necessary.

Solutions of 10 mg of polymer ($PSar_{68}$, $PPro_{80}$ or PEG_{45}) in 0.2 mL PBS containing 0.5 mM $MnCl_2$ were injected into the egg white of freshly laid chicken eggs. The resulting holes in the egg shell were sealed with instant adhesive and eggs were incubated for 0 d (≙ no incubation), 10 d and 20 d at 37 °C. To serve as a control, some of the eggs were denatured by boiling at 100 °C for 1 h prior to incubation for 20 d. Further eggs were injected with 0.2 mL PBS containing 0.5 mM $MnCl_2$ without addition of polymer.

Following the incubation, eggs were cooled in the refrigerator for about 4 h to facilitate subsequent separation of egg white and yolk. While the yolks were discarded, egg whites were freeze dried and extracted with MeOH/$CHCl_3$ (2/1 v/v). The solvent was evaporated

and samples analyzed via GPC measurement in DMF.

In order to ensure comparability of the obtained data and ascertain their reproducibility, all elugrams obtained from eggs injected with polymer solutions were normalized to the polymer signal and are depicted as mean (solid line) ± standard deviation (semi-transparent area) in the following figures. It has to be noted, however, that the extraction of egg white with MeOH/$CHCl_3$ (2/1 v/v) is not as specific to the polymer as it would be desirable and significant amounts of egg components are extracted as well. Nevertheless, GPC elugrams of control experiments with PBS injected egg white incubated for 20 d only show signals corresponding with egg components above an elution volume of 21 mL, while the examined polymers are eluted earlier (Figure 4.38).

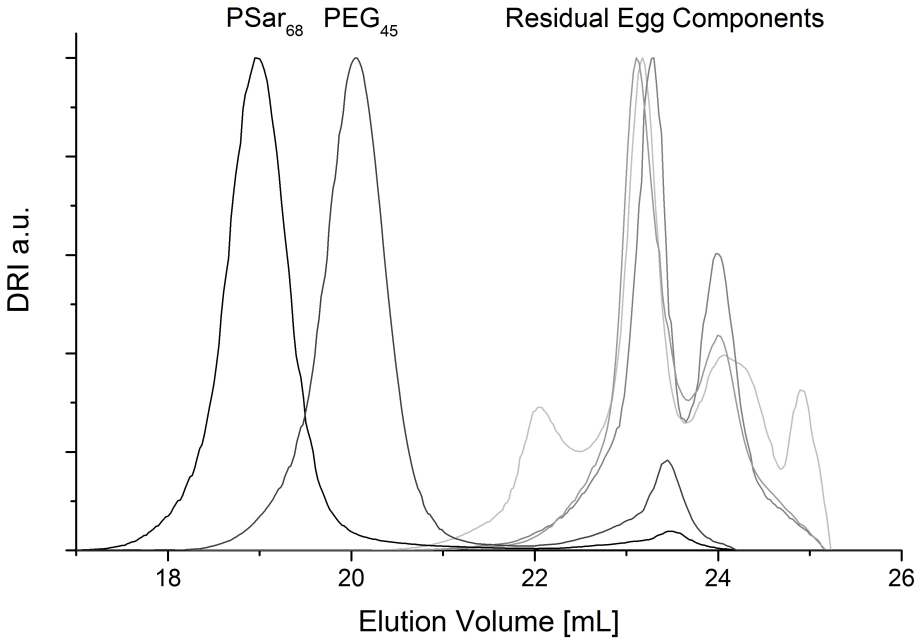

Figure 4.38: GPC elugrams of pristine $PSar_{68}$ (black) and PEG_{45} (grey) as well as three PBS-injected eggs after 20 d of incubation at 37 °C (light grey) normalized to the signal of the polymer or egg components, respectively. Data acquired by Maria Krebs.

$PPro_{80}$

Unfortunately, analysis of the $PPro_{80}$ samples was impeded by their poor solubility. Prior to injection, $PPro_{80}$ solutions in PBS were diluted to 44 % by addition of millipore water to ensure complete dissolution of the polymer. As PPro is insoluble in DMF, GPC measurements were performed in water (containing 0.1 M $NaNO_3$ and 0.02 w-% NaN_3). However, extraction of freeze dried egg whites with MeOH/$CHCl_3$ (2/1 v/v), which worked

out very well for both $PSar_{68}$ and PEG_{45}, was unsuccessful for $PPro_{80}$ as GPC elugrams in water reveal no signals corresponding with the polymer. In literature, glacial acetic acid is described as a good solvent for PPro,[278] however, extraction of freeze dried egg whites with glacial acetic acid was not successful either and resulted in no polymer signals apparent within GPC elugrams in water. Therefore, evaluation of $PPro_{80}$ degradation in chicken egg white, which would have served as an excellent control experiment corresponding with earlier studies by Neumann and Sela,[276] was unfortunately not possible.

PEG_{45}

As apparent from the GPC elugrams obtained after incubation of eggs injected with PEG_{45} (Figure 4.39), size distributions of the non-denatured PEG samples closely resemble each other with very low standard deviations. In contrast, elugrams obtained from the 20 d incubated denatured sample not only possess higher standard deviations, but the signal corresponding with PEG_{45} is also shifted to a higher elution volume corresponding with a lower molar mass. Unfortunately, while the non-denatured samples are, in essence, well separated from the signals caused by remaining egg components, this is not the case for the denatured samples where signals of PEG_{45} and egg components markedly overlap.
However, the potential degradation of PEG_{45} in denatured chicken eggs cannot be attributed to an digestion by egg white enzymes and will be discussed in more detail in another section.
In order to enable a quantitative assessment of the acquired GPC data, number average molar mass (M_n), mass average molar mass (M_w) and peak molecular weight (M_p) were determined within defined limits of 18.35 to 21 mL and are summarized in Table 4.1 as well as plotted in Figure 4.40.
All data except for the M_n values of PEG_{45} after 20 d follow a normal distribution and trends of both M_p and M_w suggest slight degradation of the polymer during incubation in contradiction to the elugrams discussed earlier. Indeed, highly significant decreases ($p = 0.001$) of M_w over a 20 d period of incubation in non-denatured eggs are evident, while no significant differences ($p = 0.05$) between the values obtained M_p are observed over the same period of time.
It has to be noted, however, that the reliability of both the M_n and M_w is compromised by a substantial overlap of polymer and egg content signals in the GPC elugrams resulting in

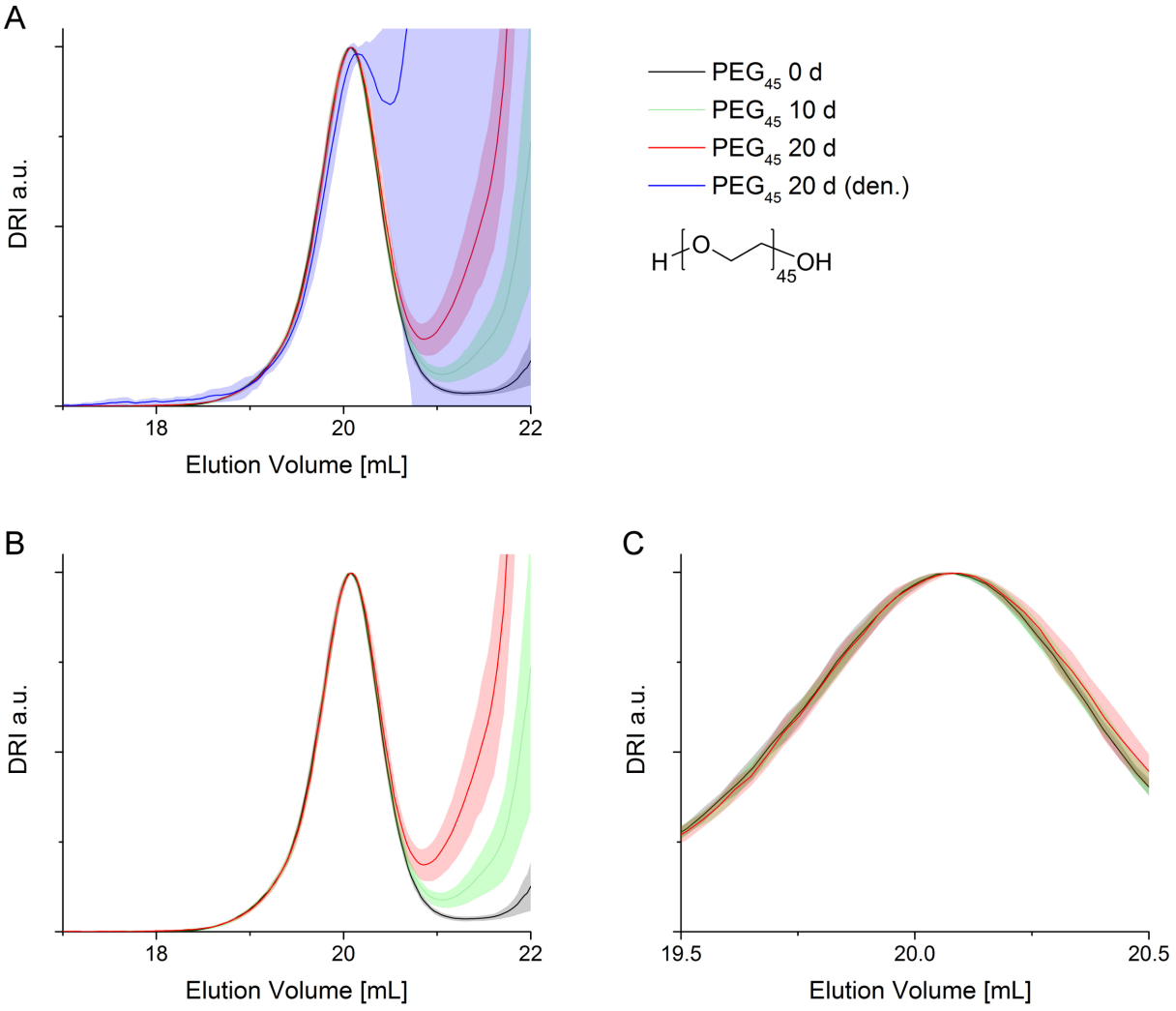

Figure 4.39: Normalized GPC elugrams of eggs injected with PEG_{45} and incubated at 37 °C. **A** Overview. **B** Overview without the denatured 20 d incubation. **C** Magnified view of the non-denatured samples incubated for 0 d, 10 d and 20 d. Data are presented as mean ± standard deviation (n = 5). Data acquired by Maria Krebs.

a distortion of the determined M_n and M_w values towards lower molar masses. Therefore, the determined decrease of M_n and M_w most probably not reflects the instability of PEG_{45} but actually the increasing amount of extracted egg components.

As indicated by the constant M_p of PEG_{45} which is not influenced by the overlap of signals, the performed experiments provide no evidence for an enzymatic digestion of PEG in fresh whole chicken eggs during incubation at 37 °C over a period of up to 20 d.

Unfortunately, both M_n and M_w of the denatured samples were not determinable due to poor separation between polymer and egg white signals. However, comparison of the M_p values of 0 d incubated samples and denatured 20 d samples reveals a highly significant

Table 4.1: M_n, M_w and M_p obtained from eggs injected with PEG_{45} and incubated at 37 °C. Data acquired by Maria Krebs and presented as mean ± standard deviation (n = 5).

Incubation Time [d]	**M_n ± SD [%]**	**M_w ± SD [%]**	**M_p ± SD [%]**
0	2243 ± 18	2378 ± 16	2226 ± 11
10	2224 ± 30	2363 ± 35	2218 ± 34
20	2182 ± 43	2330 ± 45	2220 ± 23
20 (denatured)	n.d.	n.d.	2108 ± 113

n.d. not determinable

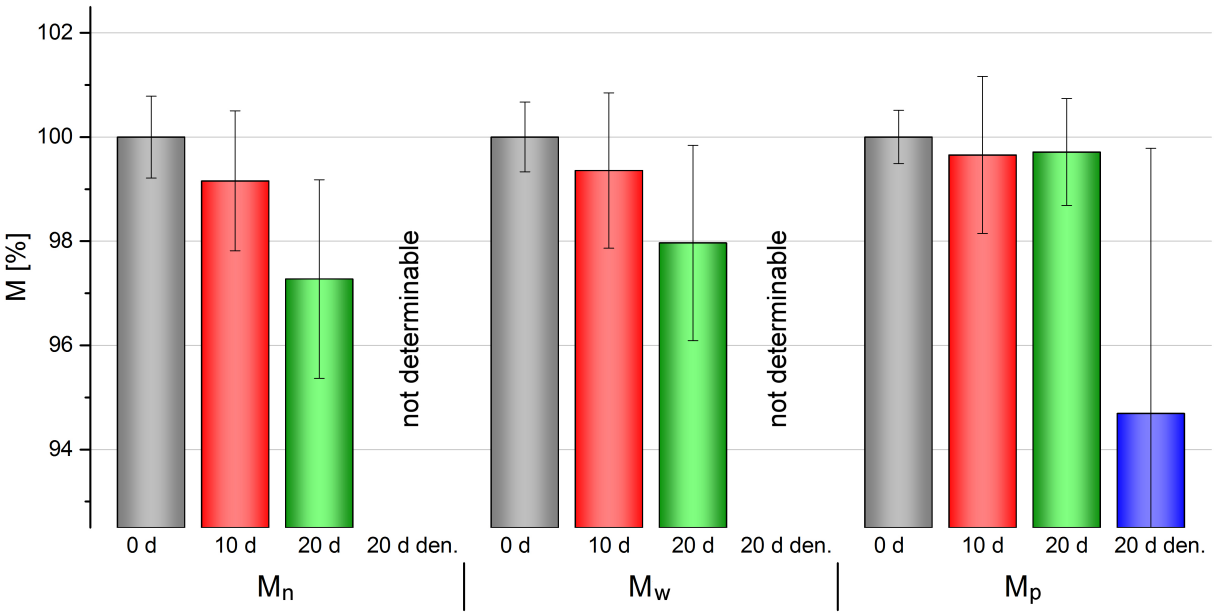

Figure 4.40: Column diagram displaying the percentage change of M_n, M_w and M_p obtained from eggs injected with PEG_{45} and incubated for up to 20 d at 37 °C. Data acquired by Maria Krebs and presented as mean ± standard deviation (n = 5).

decrease (p = 0.001). Nevertheless, degradation of PEG_{45} in denatured chicken eggs is still very low with a percentage loss of M_p of only 5.3 % accompanied by a relatively high standard deviation of 5.1 %.

$PSar_{68}$

At first glance, polymer signals of all elugrams obtained from eggs injected with $PSar_{68}$ closely resemble each other (Figure 4.41 **A**). As already mentioned for PEG_{45}, low standard

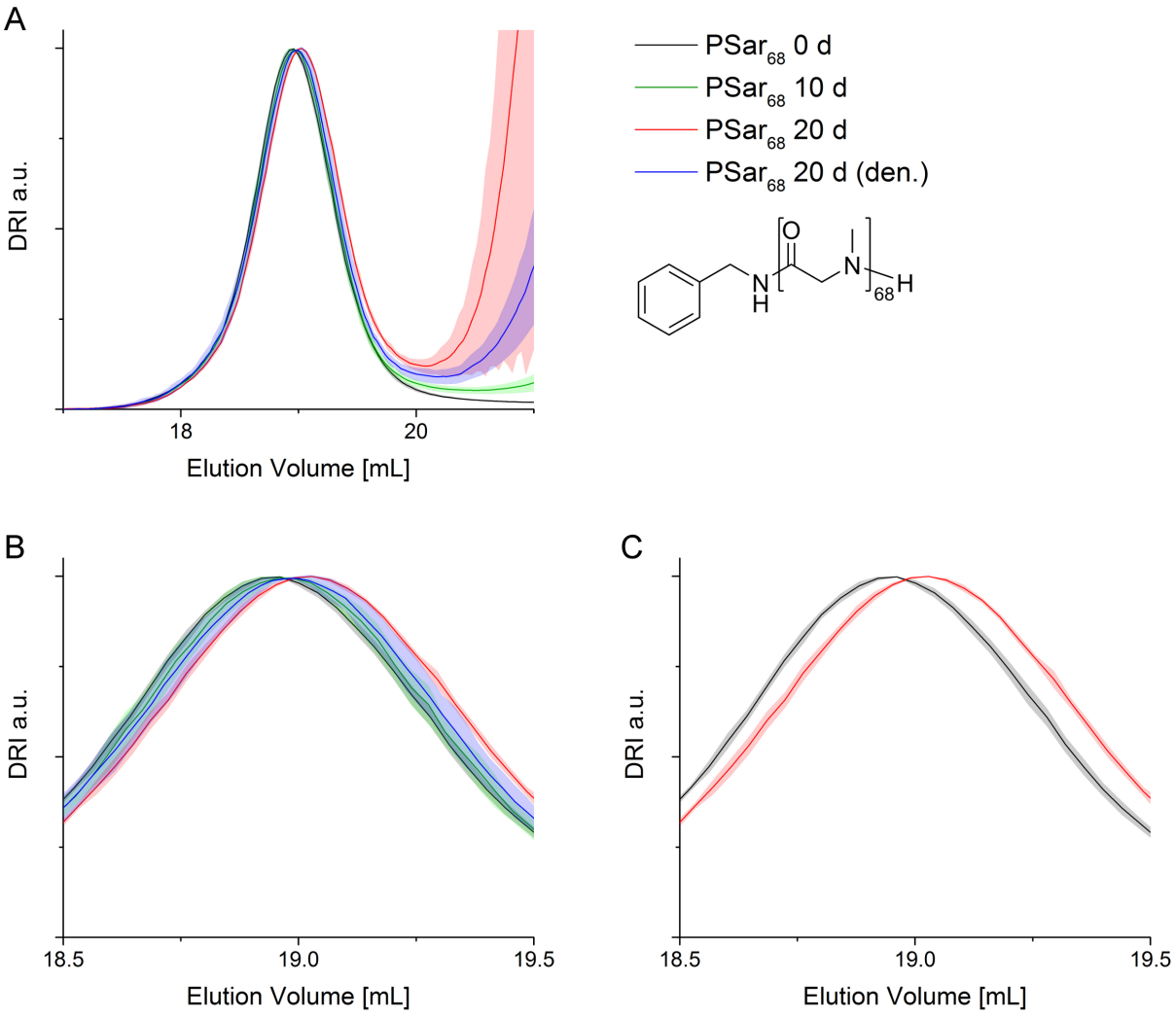

Figure 4.41: Normalized GPC elugrams of eggs injected with $PSar_{68}$ and incubated at 37 °C (mean ± standard deviation, n = 5, $PSar_{68}$ 0 d: n = 8). **A** Overview. **B** Magnified view of the polymer signal. **C** Magnified view showing only the 0 d and 20 d incubated samples. Data acquired by Maria Krebs.

deviations indicate excellent reproducibility and polymer signals are clearly separated from the signals caused by residual egg components.

However, on closer examination (Figure 4.41 **B** and **C**) slight differences between the polymer signals become apparent. Whereas the elugrams of the 0 d and 10 d incubated samples are more or less overlapping, the polymer signals of the 20 d incubated samples are shifted to slightly higher elution volumes indicating deterioration of $PSar_{68}$ during incubation. Albeit to a much lesser extent than observed for PEG_{45}, denatured samples again possess an increased standard deviation compared to the non-denatured ones.

Based on the available data, both non-enzymatic degradation and enzymatic digestion of $PSar_{68}$ in whole chicken eggs over the course of 20 d can be assumed. Nevertheless, the observed shifts of the polymer signals are rather small and do not allow any definitive conclusions at this stage of the investigations.
As discussed earlier, determination of M_n, M_w and M_p data enables the quantitative assessment of the acquired GPC data. Based on the obtained elugrams, limits of 17 to 20 mL where specified and molar mass averages were determined as summarized in Table 4.2 and plotted in Figure 4.42.

Table 4.2: M_n, M_w and M_p obtained from eggs injected with $PSar_{68}$ and incubated at 37 °C. Data acquired by Maria Krebs and presented as mean ± standard deviation (n = 5, $PSar_{68}$ 0 d: n = 8).

Incubation Time [d]	**M_n ± SD [%]**	**M_w ± SD [%]**	**M_p ± SD [%]**
0	4293 ± 22	4564 ± 22	4394 ± 32
10	4247 ± 68	4512 ± 78	4330 ± 58
20	4105 ± 8	4381 ± 14	4188 ± 28
20 (denatured)	4209 ± 68	4492 ± 90	4292 ± 86

Except for the M_p values of $PSar_{68}$ after 20 d of incubation in denatured eggs, all data are normally distributed. In accordance with the obtained elugrams, M_n, M_w and M_p reveal a slight decreasing trend during incubation in whole chicken eggs for 20 d. Highly significant ($p = 0.001$) decreases of M_n, M_w and M_p after 20 d of incubation in non-denatured eggs are evident, however, after 10 d of incubation highly significant ($p = 0.001$) decreases are only indicated by M_p, whereas no significant differences are detected in case of M_n and M_w even though a trend appears observable. Due to the increased molar mass and hydrodynamic radius of $PSar_{68}$ compared to PEG_{45}, overlaps of polymer and egg content signals are negligible and should not affect the determined molar mass values significantly, thus ensuring the reliability of the received data.
Although lower than observed for PEG_{45}, slight decomposition of $PSar_{68}$ during incubation in denatured eggs is indicated by highly significant ($p = 0.001$) decreases of both M_n and M_w.

A major aim of this experiment was the proof of a potential degradation of PSar by

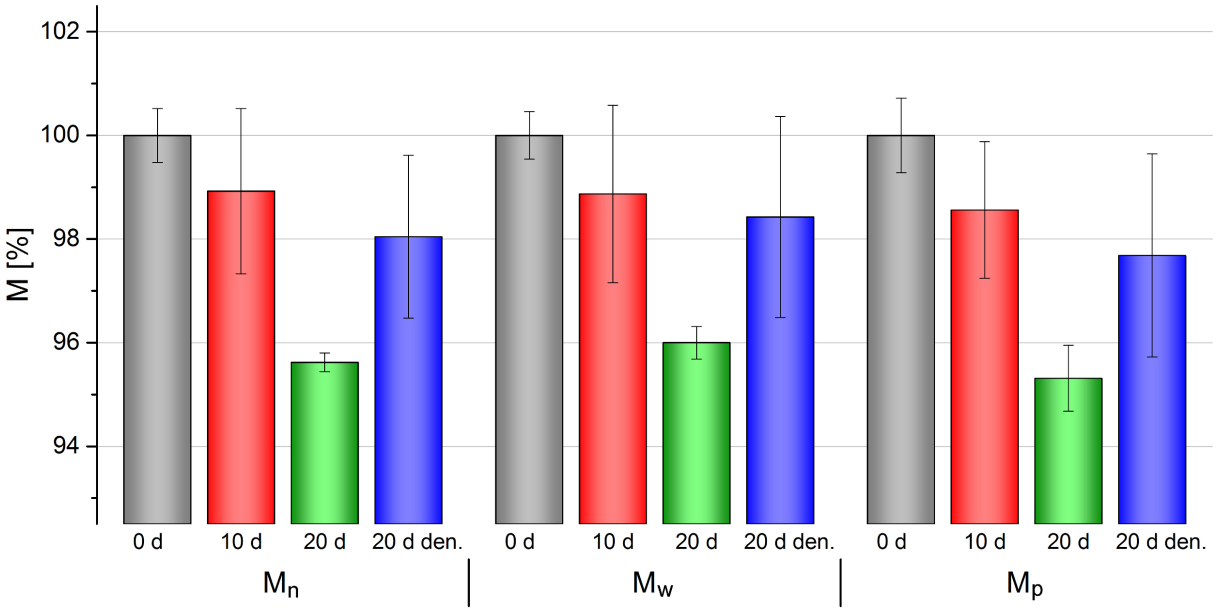

Figure 4.42: Column diagram displaying the percentage change of M_n, M_w and M_p obtained from eggs injected with $PSar_{68}$ and incubated for up to 20 d at 37 °C. Data acquired by Maria Krebs and presented as mean ± standard deviation (n = 5, $PSar_{68}$ 0 d: n = 8).

proline iminopeptidase, an N-terminal exopeptidase described to be highly specific to proline residues (see section 2.2.3.1). Therefore, manganese in the form of $MnCl_2$ was added to the injected polymer solutions prior to injection in order to increase proline iminopeptidase activity.[273, 274] However, injection of 0.2 mL of solution containing 0.5 mM $MnCl_2$ results in the addition of as little as 5.5 μg manganese per egg. According to the *Nutrient analysis of eggs*[391] published by the *Institute of Food Research Norwich*, raw chicken egg white contains less than 10 μg manganese per 100 g of egg white, while raw yolk contains about 110 μg manganese per 100 g. Pursuant to an average of 50 g egg white and 18 g yolk as determined for the used extra-large chicken eggs, a natural manganese content of 25 μg can be assumed which is only increased by 22 % upon further injection of $MnCl_2$. Hence, supplementation of $MnCl_2$ most probably not influences the further course of the experiment.

The free amino terminus possessed by $PSar_{68}$ enables digestion by proline iminopeptidase and further appropriate N-terminal exopeptidases as well as endopeptidases, wheras digestion by C-terminal exopeptidases is most likely impeded due to the sterically demanding C-terminal benzylamine. Indeed, proline iminopeptidase activity would explain the apparently increasing digestion rate of $PSar_{68}$ during incubation. While newly laid chicken eggs

possess a pH of 7.6 to 8.5 and are saturated with CO_2 ($\approx$ 0.35 % wt/vol) mainly present in form of hydrogen carbonate, loss of CO_2 by diffusion through the shell during storage is accompanied by increase of the pH to up to 9.6.[392–394] Katchalski and coworkers observed a maximum activity of proline iminopeptidase at a pH of 8.0 to 9.5 during incubation at 40 °C.[273] It is certainly conceivable that increasing pH values during incubation over prolonged periods may have resulted in the increase of proline iminopeptidase activity and accompanying accelerated digestion rates.

However, observed molar mass decreases of $PSar_{68}$ during incubation amount to only 4 % over the course of 20 d and are therefore, despite the low standard deviations of the obtained data, not very pronounced.

Additional investigations on the digestion of PPro under similar circumstances would have been very valuable for an accurate understanding of the underlying mechanisms, but failed due to the particularly poor solubility of PPro as discussed earlier. As suggested by related investigations conducted by Neumann and Sela, the enzymatic digestion of PPro in egg white is pretty fast with more than 30 % released proline detected colorimetrically after only 24 h of incubation.[276] However, less sterically hindered amide bonds and greater flexibility as possessed by PSar compared to PPro not necessarily implies higher enzymatic digestion rates of the former. Applicable literature data on the enzymatic degradation of PSar or other polypeptoids are lacking as related experiments have not been carried out before.

At this stage of the investigations, a final assessment of the susceptibility of PSar towards enzymatic degradation is not possible.

In contrary, data concerning the stability of PEG_{45} provide a fairly clear picture. As indicated by essentially similar elugrams and constant M_p values, the significant enzymatic digestion of PEG_{45} by non-denatured chicken eggs can most likely be excluded.

4.3.2.3 Investigations on the *in ovo* Degradation of Polysarcosine, Poly(2-methyl-2-oxazoline) and Poly(ethylene glycol)

Preliminary investigations on the stability of PSar and PEG discussed in detail within the preceding section raised a number of issues inspiring the implementation of further extensive experiments.

Considering the low over all degradation observed for $PSar_{69}$ over a period of 20 d *in ovo*,

elongation of the incubation times was a crucial element of these follow-up studies. The critical factor limiting the feasible incubation time is defined by the shelf life of the used eggs. While the breeding time of chicken eggs is about 21 d at 37.5 to 38.0 °C, freshly laid they are claimed to be safe to eat for 30 d if stored at room temperature (RT) and 60 d if stored refrigerated. Indeed, egg white and yolk are not only protected mechanically by the egg shell enabling a controlled gas exchange, but also by antibacterial lysozyme.[395–397] Lysozyme is not only one of the major components of egg white, but also found in human body secretions and fluids like mucus, saliva, tears and milk.

In order to assess the shelf life of chicken eggs under the circumstances of the intended experiment, three eggs were incubated at 37 °C for 27 d, 37 d and 370 d, respectively. Although the weight of the eggs steadily decreased from ≈ 80 g prior to incubation to as little as 13 g after 370 d and a distinct reduction of the egg white volume was observed, no visual or olfactory attributes indicated an actual rotting of the eggs. Given these findings, the incubation time of polymer injected eggs was doubled to a maximum of 40 d at 37 °C. Furthermore, polymers were dissolved in millipore water instead of PBS to ensure excellent solubility. Considering the low injected volume of 0.2 mL in comparison to the volume of egg white and yolk totalling ≈ 70 mL, this corresponds with a percentage of less than 0.3 % added volume. Consequently, no significant effects induced by the change of the solvent are expected.

In order to prevent external contaminations introduced by the applied polymers or the lab environment, polymers were purified via dialysis and filtered sterile prior to incubation. Moreover, the whole process of drilling holes in the shells of the eggs, injecting the polymer solutions and sealing the holes with instant adhesive was conducted under the sterile conditions of laminar flow hood.

As proline was unsuitable to serve as a reference due to poor solubility as discussed in more detail in the previous section, the range of investigated polymers was enlarged by utilizing four PSar species bearing different C- and N-terminal groups as well as PMeOx bearing amide bonds within the side chains instead of the backbone and PEG bearing no amide bonds at all (Figure 4.43). However, to ensure proper comparability, polymers with similar chain lengths of ≈ 90 monomer units were synthesized or purchased, respectively. PSar chain ends were varied in order to gain insights into the involvement of both N- and C-terminal exopeptidases which might be restricted by sterically demanding end groups.

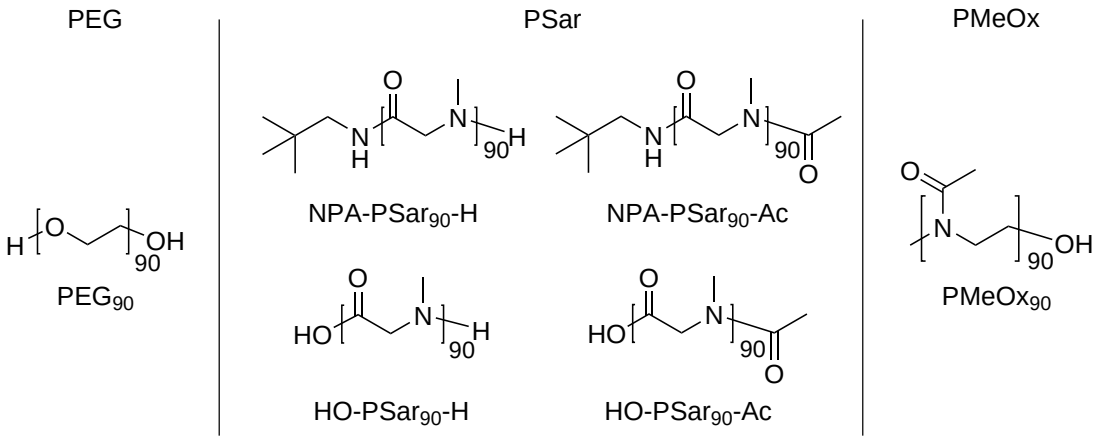

Figure 4.43: Chemical structures of the polymers applied for the incubation in chicken eggs for up to 40 d. NPA: neopentylamine.

For this purpose, the polymerization of Sar-NCA was initiated by neopentylamine (NPA) yielding NPA-PSar$_{90}$-H possessing an obstructed C-terminus as well as an easily accessible N-terminus. About half of this polymer was further modified applying acetic anhydride to obtain NPA-PSar$_{90}$-Ac possessing two obstructed termini. Vice versa, the water-initiated polymerization of Sar-NCA yielded HO-PSar$_{90}$-H bearing two termini susceptible to enzymatic digestion by exopeptidases. Again, about half of this polymer was further modified applying acetic anhydride to obtain HO-PSar$_{90}$-Ac possessing an easily accessible C-terminus but an obstructed N-terminus.

Control experiments involved the injection of pure millipore water prior to incubation. The corresponding elugrams (Figure 4.44) reveal signals of residual egg components as already observed in the preliminary investigations (see section 4.3.2.2) starting at an elution volume of 20 mL. Hence, all elugrams obtained after injection of polymers were cut at 20 mL. Nevertheless, as clearly apparent in the 20-fold magnification of the control elugrams (Figure 4.44 **C**), no interfering signals significantly surpassing the background noise and potentially interfering with polymer signals are observed. Rising curves as observed in the 20-fold magnification are independent of the incubation time and negligible compared to the signal heights of the polymer as will be shown in the following.

GPC elugrams of the utilized polymers (Figure 4.45) confirm no significant overlaps between polymer and egg component signals prior to incubation. However, due to the substantially lower molar mass of the PEG repetition unit of 44 g/mol compared to 71 g/mol for PSar and 85 g/mol for PMeOx, a higher elution volume corresponding with a

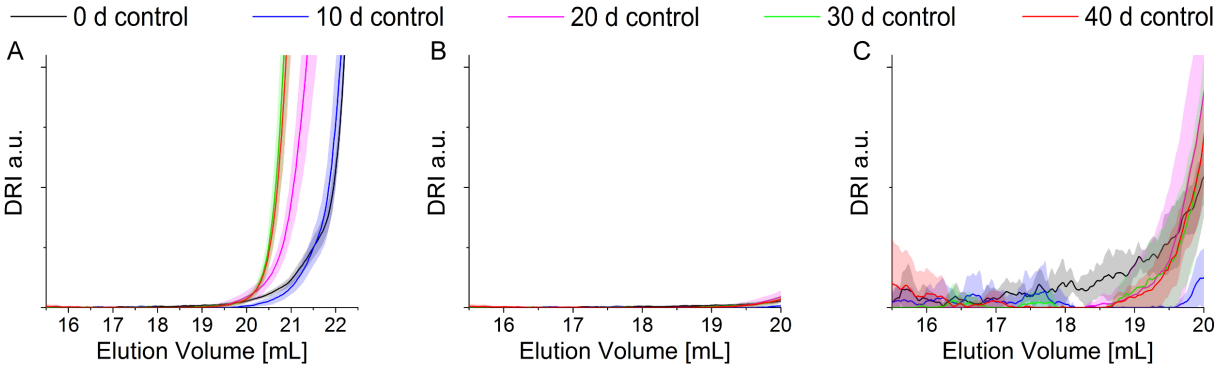

Figure 4.44: Elugrams of control experiments performed with pure millipore water. **A** Overview revealing signals corresponding with residual egg components starting at an elution volume of ≈ 20 mL. **B** Elugrams cut at an elution volume of 20 mL. **C** 20-fold magnification reveals no signals potentially interfering the evaluation of the polymer elugrams. Data presented as mean ± standard deviation (n = 6).

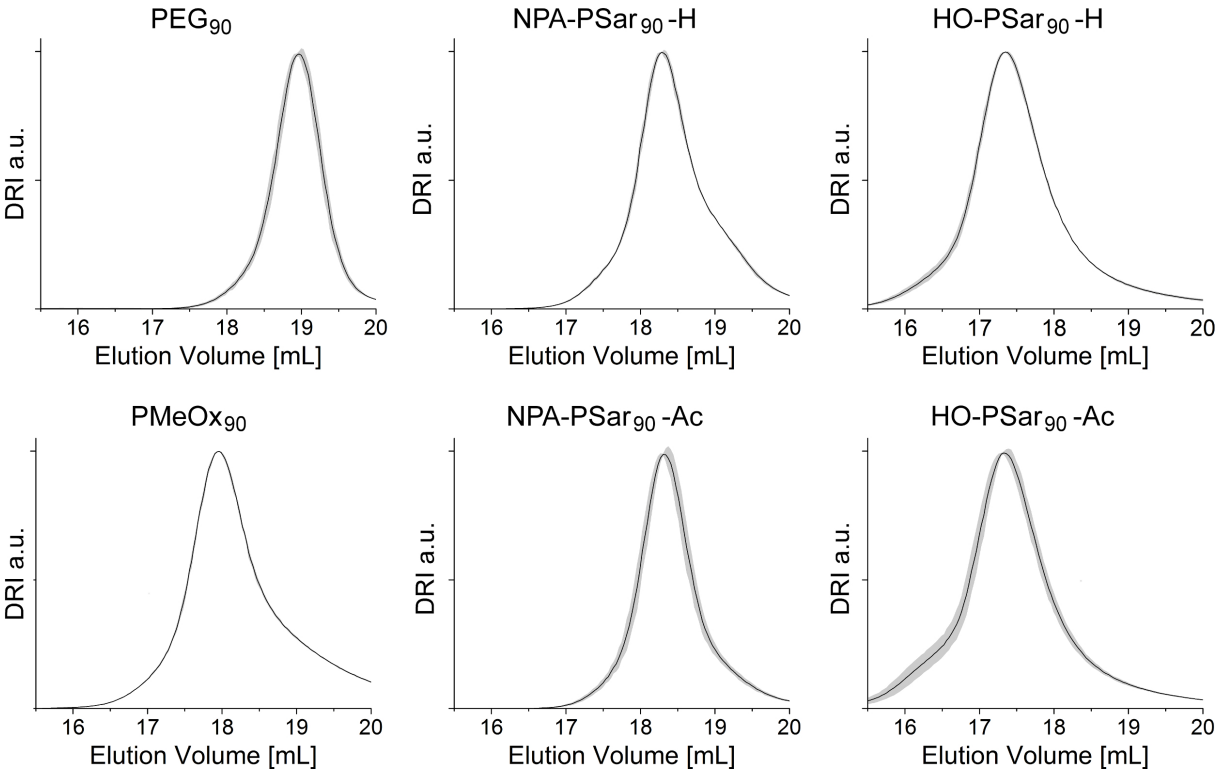

Figure 4.45: Elugrams of the priscine polymers applied for *in ovo* experiments. Data are presented as mean ± standard deviation (n = 4).

smaller hydrodynamic radius is apparent and digestion of PEG would result in an overlap of PEG and egg component signals rather fast.

Furthermore, the elugram of $PMeOx_{90}$ reveals a low molecular weight tailing which might

impair the evaluability of a potential digestion.

Compared to the NPA-initiated PSar samples, water-intiated PSar ones possess a significantly broader distribution as reflected by both the elugrams as well as the corresponding dispersity data (Table 4.3). This is attributable to the initiator water, which is, compared to the primary amines commonly applied to initiate the polymerization of NNCAs, significantly less nucleophilic. For this purpose, 2.5 equivalents of triethylamine (TEA) with respect to the initiator were supplemented in order to deprotonate water forming hydroxide ions resulting in an increase of its nucleophilicity accompanied by an increased initiation rate. Nevertheless, nucleophilicity of hydroxide ions is still relatively low as compared to primary amines, thus explaining the higher dispersity of the water-initiated PSar samples.

Table 4.3: Polymers applied for *in ovo* degradation experiments with molar mass averages, M_p as well as dispersity (Đ) as obtained via GPC in DMF.

Polymer	$\mathbf{M_n}$ ± **SD** [g/mol]	$\mathbf{M_w}$ ± **SD** [g/mol]	$\mathbf{M_p}$ ± **SD** [g/mol]	**Đ**
PEG_{90}	4237 ± 83	4417 ± 101	4218 ± 98	1.04
$PMeOx_{90}$	5899 ± 31	6715 ± 46	7135 ± 50	1.14
NPA-$PSar_{90}$-H	5319 ± 20	5784 ± 4	5960 ± 45	1.09
NPA-$PSar_{90}$-Ac	5470 ± 122	5823 ± 126	5879 ± 84	1.06
HO-$PSar_{90}$-H	8303 ±15	9711 ± 44	9766 ± 60	1.17
HO-$PSar_{90}$-Ac	8555 ± 255	10213 ± 377	9897 ± 221	1.19

It is noteworthy, however, that even short incubation times at temperatures lower than 37 °C induced significant alterations of the polymer elugrams (Figure 4.46). Initially, samples labeled 0 d* were prepared by injecting the polymer into the egg white followed by separation of egg white and egg yolk within 10 to 15 minutes at RT. Subsequently, samples were stored at - 18 °C until lyophilization. However, all polymers bearing amide bonds display significant changes of the elugrams particularly at lower elution volumes. Especially in case of $PMeOx_{90}$, NPA-$PSar_{90}$-H and HO-$PSar_{90}$-H, marked low molecular weight shoulders or tailings, respectively, are apparent.

For these reasons, further samples labeled 0 d were prepared following a slightly modified protocol implying separation of egg white and yolk and freezing of the former one prior to

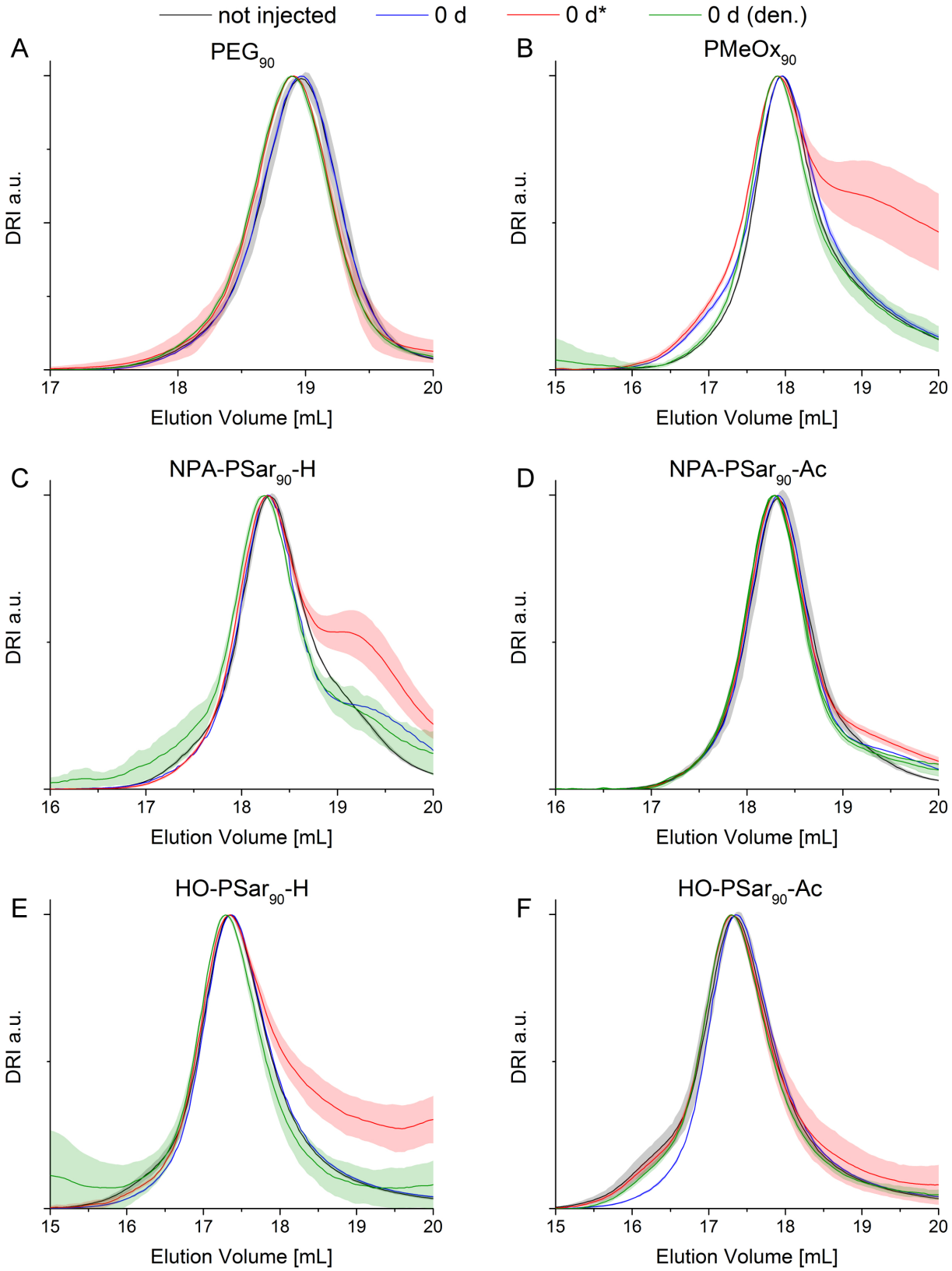

Figure 4.46: Elugrams of pristine polymers and control experiments obtained without incubation of the eggs. Data presented as mean ± standard deviation (n = 6, 0 d n = 3).

addition of the polymers and subsequent lyophilization. As apparent from Figure 4.46, this approach successfully reduced alterations of the polymer elugrams. Minor shifts of the elution volumes most probably result from variations of the eluent water content.
Denatured 0 d (den.) samples were prepared by injection of the polymer into the egg white and boiling of the eggs for 1 h at 100 °C. Subsequently, eggs were allowed to cool down to RT before egg white and yolk were separated and the former one stored at - 18 °C until lyophilization. With respect to the elugrams, this procedure proved to be effective as only minor differences between 0 d and 0 d (den.) curves are observed.

In summary, the set of samples was composed as follows:

- injection of six different polymers : PEG_{90}, $PMeOx_{90}$, NPA-$PSar_{90}$-H, NPA-$PSar_{90}$-Ac, HO-$PSar_{90}$-H and HO-$PSar_{90}$-Ac
- control injection of millipore water for reference
- incubation times up to 40 d in intervals of 10 d
- control incubations of polymers in eggs denatured by boiling at 100 °C for one hour prior to incubation for 0 d, 20 d and 40 d
- number of repetitions of n = 6

PEG_{90}

Preliminary investigations on the *in ovo* stability of PEG_{45} as discussed in section 4.3.2.2 revealed no hints towards an enzymatic digestion in chicken egg white. In order to verify this assumption, injection of PEG into freshly laid chicken eggs and incubation at 37 °C was repeated as a part of this more extensive study utilizing PEG_{90}.
Indeed, GPC elugrams in DMF (Figure 4.47) display highly similar curves even at a higher magnification (Figure 4.47 **B**). Elugrams obtained for PEG_{90} - 0 d (den.) and PEG_{90} - 20 d (den.) are not shown for the sake of clarity, but closely resemble the displayed elugrams. Nevertheless, direct comparison reveals a very slight shift towards higher elution volumes of PEG_{90} - 40 d as compared to PEG_{90} - 0 d (Figure 4.47 **B**), which is, in light of the prolonged incubation time, most probably not attributable to an actual digestion of the polymer but to the uncertainty of the method also reflected by partly overlapping standard deviations. Furthermore, intensities of the polymer signals as well as calculated values of M_n, M_w and M_p are depicted in Figure 4.48. As already concluded from the elugrams, no

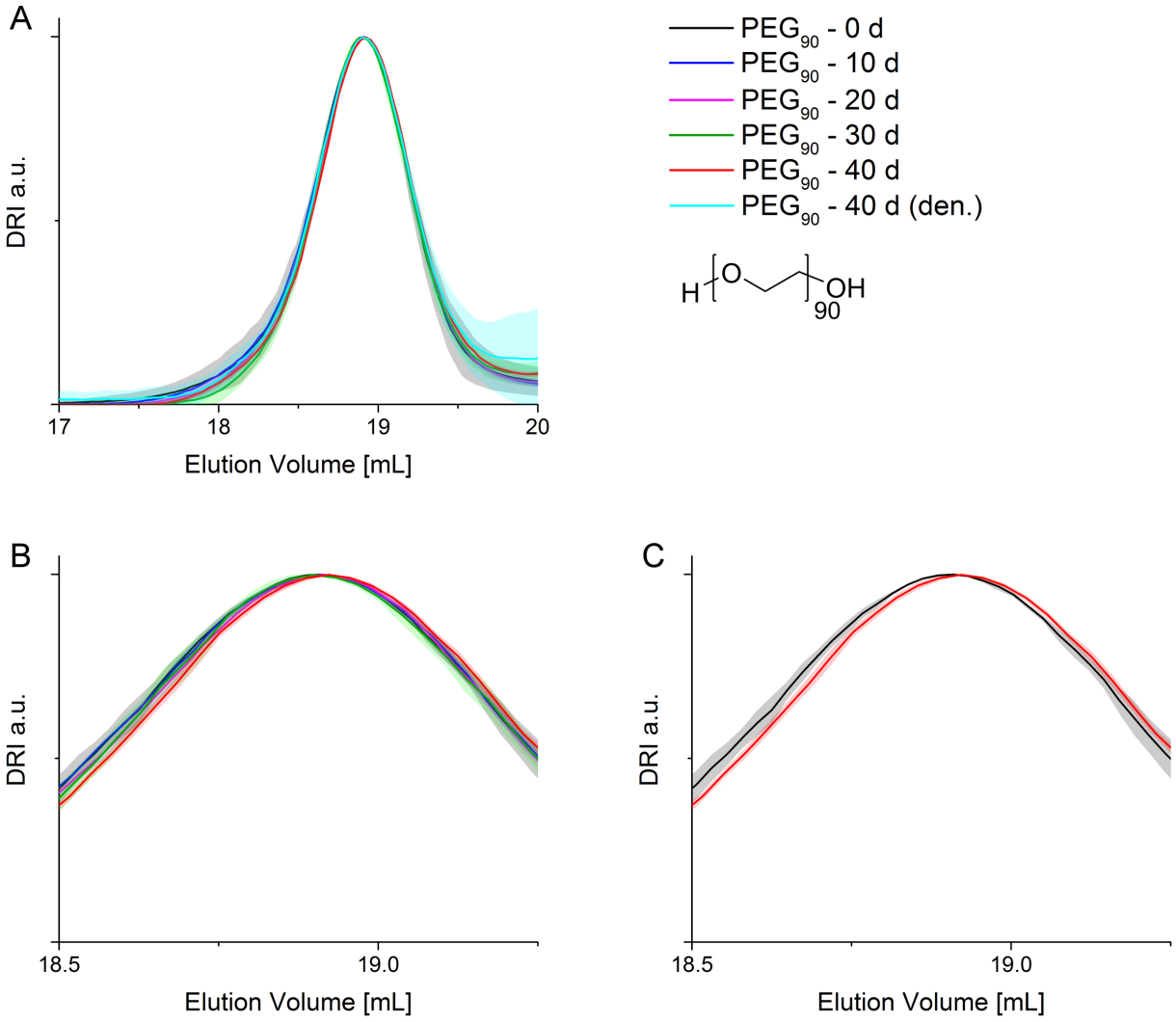

Figure 4.47: Normalized GPC elugrams of eggs injected with PEG_{90} and incubated at 37 °C. **A** Overview. **B** Magnified view of the polymer signal. **C** Magnified view showing only samples incubated for 0 d and 40 d. Data are presented as mean ± standard deviation (n = 6).

significant decreases of M_n, M_w and M_p are apparent as all values remain close to 100 % with respect to the 0 d incubated PEG_{90}, thus indicating stability of PEG_{90} in egg white. In contrast, polymer signal intensities of the elugrams obtained from raw incubated eggs remain constant at ≈ 100 % over the first 20 d of the experiment and immediately drop to ≈ 25 % once the natural breeding time is exceeded. Although this might indicate a sudden degradation of PEG_{90}, it is much more likely that the altered protein structure of the egg white obstructed extraction of the polymer. Furthermore, PEG_{90} might have diffused into the yolk due to significant losses of egg white volume. As the yolk was discarded right after

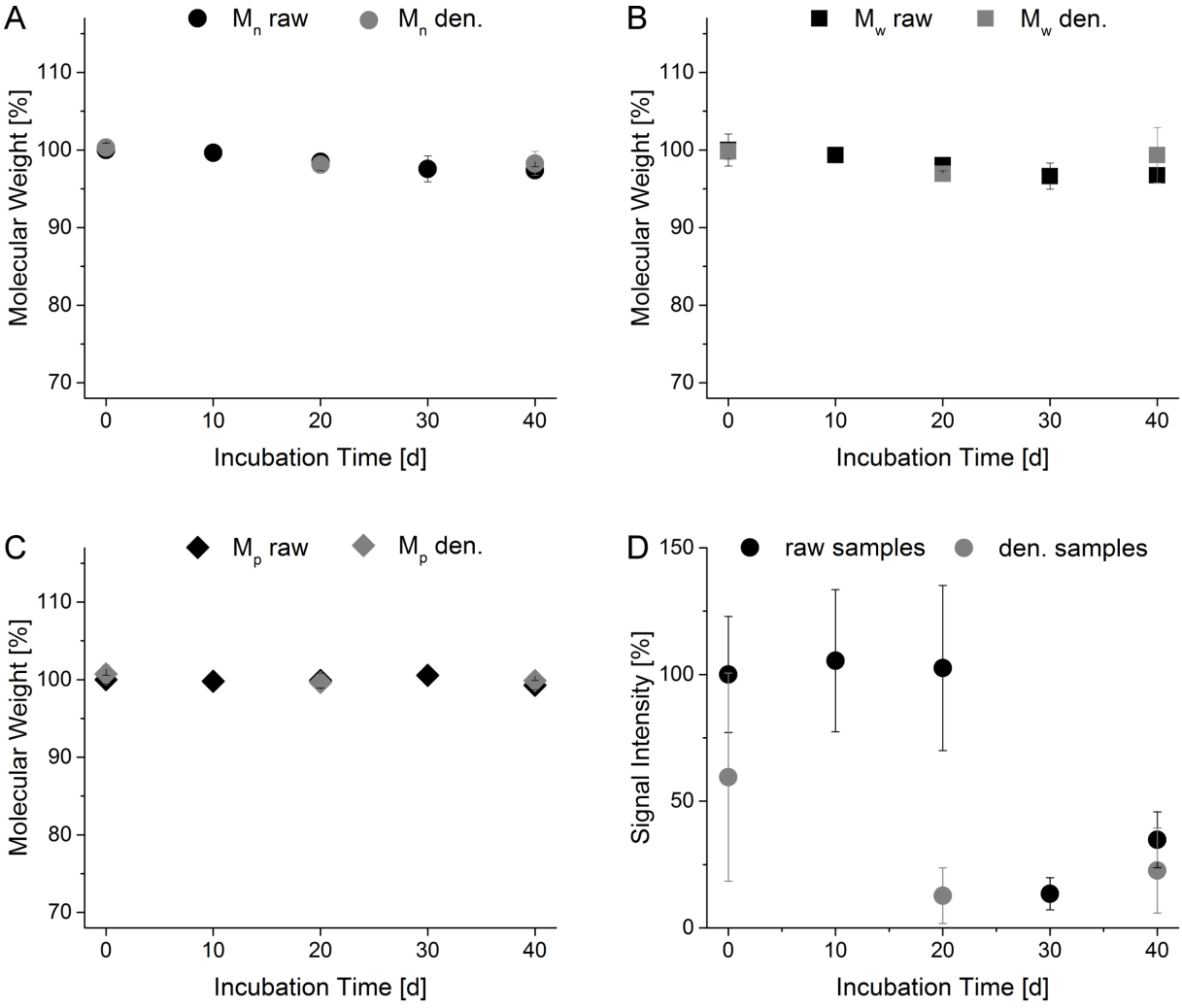

Figure 4.48: Percentage change of M_n, M_w and M_p (**A** - **C**)as well as signal intensity (**D**) obtained via GPC elugrams of eggs injected with PEG_{90} and incubated at 37 °C for up to 40 d. Data are presented as mean ± standard deviation (n = 6).

incubation, a large share of the polymer might have been discarded unintentionally. In case of the denatured eggs, polymer signal intensity decreases to ≈ 60 % even without further incubation and reaches ≈ 15 % after 20 and 40 d of incubation, respectively. Denaturation off the eggs and corresponding precipitation of the contained proteins not only results in the loss of any enzymatic activities but also alters the consistency of both egg white and yolk tremendously. While freeze-dried raw egg whites are brittle and easy to crumble, freeze-dried boiled egg whites possess remarkable elasticity and resistance to abrasion that might have impeded sufficient extraction of PEG_{90}. Moreover, diffusion rates increase exponentially with temperature and large proportions of the polymer already might have diffused into the yolk during boiling of the eggs.

In conformity with the outcomes of the preliminary study, the available results do not imply a potential digestion of PEG in freshly laid chicken eggs. First and foremost, this is attributable to a lack of hydrolyzable amide bonds, thus excluding the susceptibility of PEG as a polyether towards enzymatic digestion by peptidases in general.

Digestive enzymes *in vivo* not only include proteases and peptidases cleaving proteins, but also lipases splitting fat into three fatty acids and glycerol, amylases breaking down carbohydrates such as starch and polysaccharides into monosaccharides like glucose and fructose as well as nucleases responsible for the cleavage of nucleic acids into nucleotides. However, according to their specificity, none of these digestive enzymes posses the capability to cleave ether bonds as comprised by PEG.

Nevertheless, the enzymatic cleavage of ether bonds was described by a number of groups before. For instance, an enzyme preparation obtained from a soil *Arthrobacter* species was shown to cleave the ether linkage of 2,4-dichlorophenoxyacetate yielding 2,4-dichlorophenol via an oxidative pathway.[398] Schramm and Schink reported a strictly anaerobic ether-cleaving enzyme found in the cytoplasmic fraction of an *Acetobacterium* isolated from anoxic sewage sludges which degrades PEGs with molar masses ranging from 106 to more than 20 000 g/mol by a hydrogen shift to form unstable hemiacetal intermediates that decompose yielding acetaldehyde.[399] Furthermore, Haines and Alexander observed the extracellular depolymerization of PEG with molar masses of up to 20 000 g/mol yielding diethylene glycol by a hydrolyzing enzyme found in *Pseudomonas aeruginosa* isolated from soil,[400] however, attempts to reproduce these results carried out by other groups failed.[401, 402]

In conclusion, the enzymatic digestion of PEG *in ovo* can most likely be excluded as shown on the examples of PEG_{45} and PEG_{90}. Although results obtained *in ovo* are not fully transferable to *in vivo* conditions, with respect to the comprised polyether bonds an enzymatic cleavage of PEG *in vivo* is considered very unlikely. However, in order to verify this assumption, detailed *in vivo* investigations are inevitable.

$PMeOx_{90}$

In contrast to PEG, PMeOx comprises secondary amide bonds as an integral part of the side chain. Thus, digestion of PMeOx by peptidases cleaving the amide bonds is expected to yield toxic PEI similar to the acidic hydrolysis of POx discussed in section 4.2.1.

GPC elugrams obtained after incubation of $PMeOx_{90}$ *in ovo* (Figure 4.49) reveal no signif-

icant changes of the peak elution volume, but major modifications of the curve progression especially at higher elution volumes corresponding with lower molar masses. For the sake

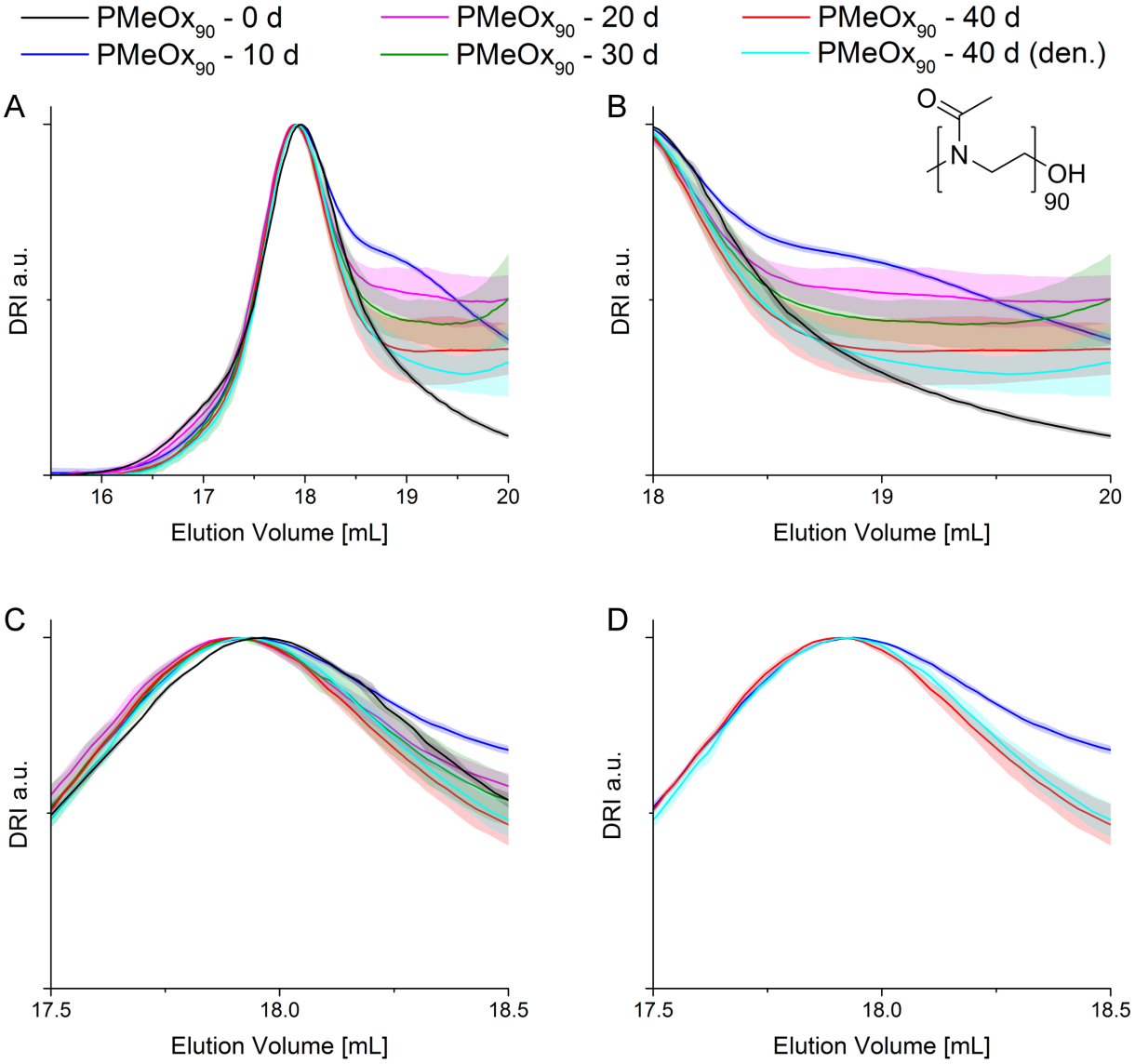

Figure 4.49: Normalized GPC elugrams of eggs injected with $PMeOx_{90}$ and incubated at 37 °C. **A** Overview. **B** Magnified view of the low molecular weight shoulder developed after 10 d of incubation. **C** Magnified view of the polymer signal. **D** Magnified view showing only samples incubated for 0 d and 40 d as well as 40 d (den.) for reference. Data are presented as mean ± standard deviation (n = 6, $PMeOx_{90}$ - 0 d n = 3).

of clarity, elugrams obtained for $PMeOx_{90}$ - 0 d (den.) and $PMeOx_{90}$ - 20 d (den.) are not shown, however, $PMeOx_{90}$ - 0 d (den.) closely resembles the elugram of $PMeOx_{90}$ - 0 d while $PMeOx_{90}$ - 20 d (den.) is very similar to $PMeOx_{90}$ - 40 d (den.).

A very pronounced low molecular weight shoulder apparent after 10 d of incubation (Figure

4.49 **A**) indicates modification of the polymer potentially due to side chain scission by enzymatic hydrolysis. Surprisingly though, this low molecular weight shoulder continuously decreases during prolonged incubation.

Considering results regarding the acidic hydrolysis of $PMeOx_{90}$ discussed in section 4.2.1, some interesting similarities are apparent (Figure 4.50). Elugrams of both experiments

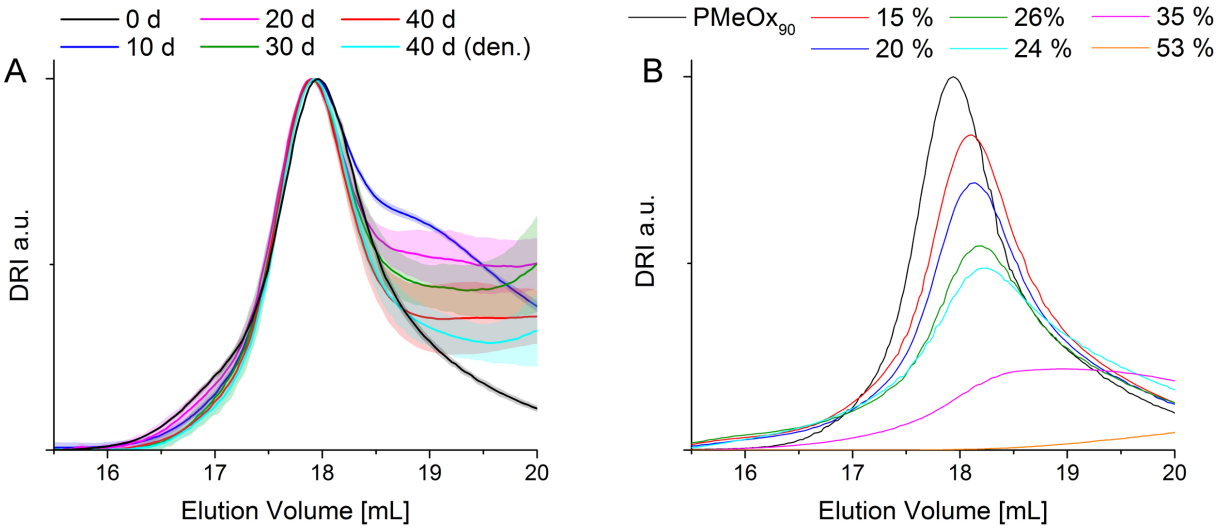

Figure 4.50: Elugrams of $PMeOx_{90}$ upon **A** incubation in freshly laid chicken eggs for up to 40 f and **B** acidic hydrolysis by 6 M HCl at 90 °C.

reveal the development of a low molecular weight shoulder at an elution volume of ≈ 19 mL which decreases again in the further course of the experiment. As discussed in more detail earlier (see section 4.2.1), acidic hydrolysis of $PMeOx_{90}$ results in side chain scission and generation of copolymers of PMeOx and PEI. Once a critical proportion of PEI is reached, poor solubility of PEI induces precipitation of the copolymer which is therefore not apparent within the elugrams.

The presence of a similar low molecular weight shoulder observed during *in ovo* experiments suggests that similar processes may be taking place. However, in contrast to the investigations on the acidic hydrolysis, the peak elution volume itself does not shift. This may indicate a potential preferential hydrolysis of already modified chains, thus maintaining a large proportion of the polymer chains in an unaltered condition. Furthermore, elugrams obtained from the *in ovo* experiments reveal a decrease of the high molecular weight tailing due to deterioration of the polymer. In contrast, elugrams obtained from acidic hydrolysis show an initial increase of the intensity at low elution volumes indicating chain coupling

reactions or modifications resulting in an increase of the hydrodynamic radius.
Intensities of the polymer signals and calculated values of M_n, M_w and M_p as well as signal intensities are plotted in Figure 4.51.

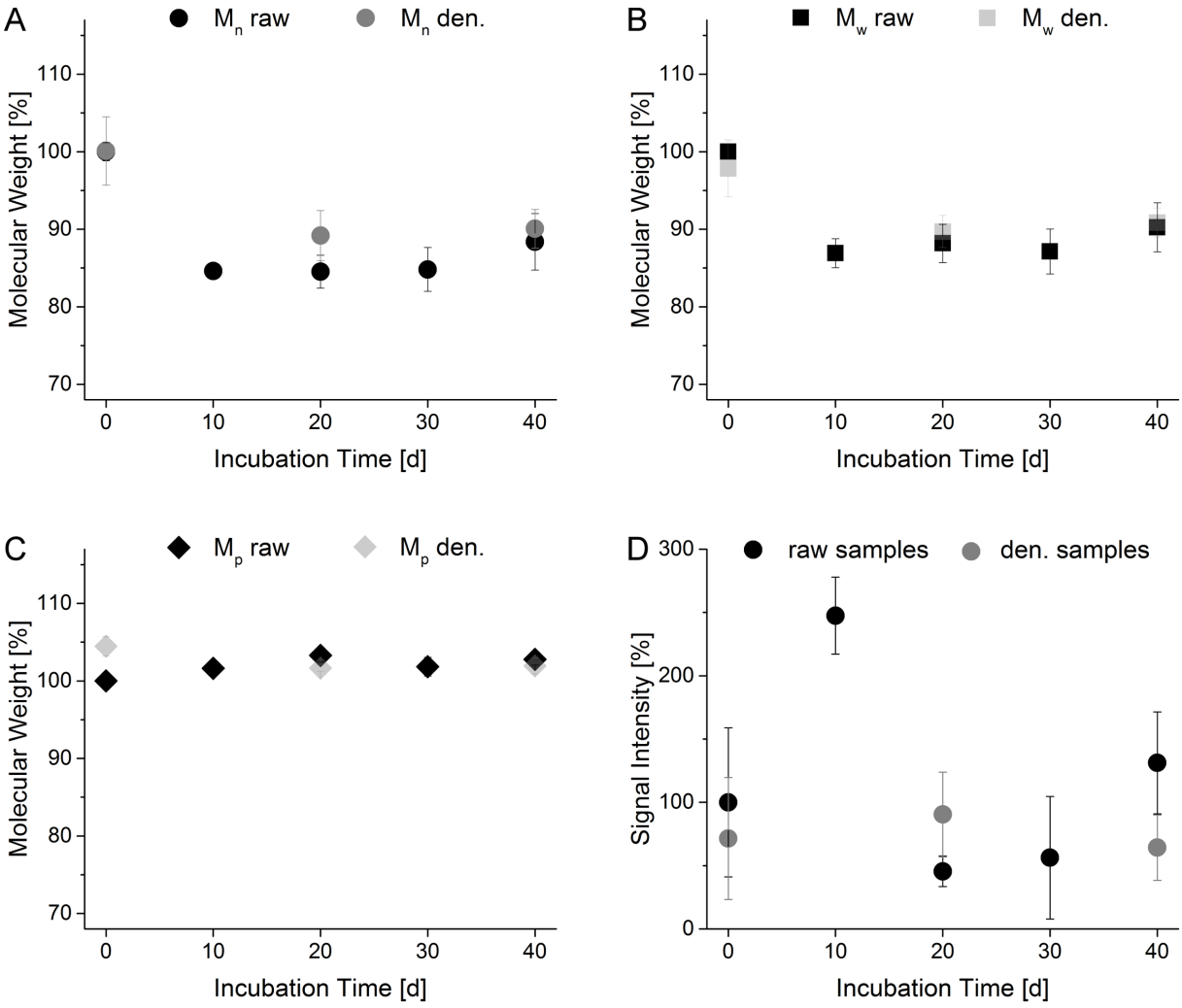

Figure 4.51: Percentage change of M_n, M_w and M_p as well as the signal intensity obtained from GPC elugrams of eggs injected with $PMeOx_{90}$ and incubated at 37 °C for up to 40 d. Data are presented as mean ± standard deviation (n = 6).

Indeed, the M_p of $PMeOx_{90}$ remains constant over the whole course of the experiment. This is further reflected by similar signal intensities, with the exception of $PMeOx_{90}$ - 10 d which is most probably attributable to artifacts.
In contrast, however, both M_n and M_w decrease to about 85 % within 10 d followed by a slightly increasing trend in accordance with the curve progressions of the elugrams. Strikingly, against the expectations M_n and M_w decreases are also observed in case of the denatured samples $PMeOx_{90}$ - 20 d (den.) and $PMeOx_{90}$ - 40 d (den.) which both drop

to ≈ 90 % of the initial values. This casts considerable doubts on the enzymatic origin of the observed degradation. As stated earlier, freshly laid chicken eggs possess a slightly basic pH value of about 7.6 to 8.5. Although not investigated in detail within the scope of this work, a significant basic hydrolysis of $PMeOx_{90}$ especially during boiling of the eggs is certainly conceivable.

On the whole, even though significant alterations of the elugrams and according decreases of M_n and M_w indicate deterioration of the investigated $PMeOx_{90}$, it is highly questionable whether these findings are attributable to an enzymatic digestion. In fact, strong similarities with the results obtained during acidic hydrolysis provide evidence that comparable processes may proceed *in ovo* as well. Although the generation of PEI results from either pathway, whether and, if so, to what extent PEI is formed during *in ovo* incubation could not be clarified in the scope of these investigations.

Based on the obtained results, estimating the degree and consequences of PMeOx hydrolysis *in vivo* precisely is difficult. However, an enzymatic digestion of PMeOx *in ovo* appears unlikely. Due to the shift of the amide bonds to the side chain of the polymer, the vast majority, if not all, of peptidases most probably rejects POx as a potential substrate despite the existing similarity to polypeptides.

In contrast, the acidic or basic hydrolysis is certainly conceivable, however, due to the relatively mild conditions regarding both pH value and temperature *in vivo*, hydrolysis of POx yielding toxic PEI in critical concentrations will hardly occur.

$PSar_{90}$

Preliminary investigations on the *in ovo* degradation of PSar conducted by Maria Krebs proved highly promising. As mentioned earlier, the introduction of different C- and N-terminal chain ends should help to further clarify ongoing mechanisms of a potential degradation of PSar in chicken egg white.

HO-$PSar_{90}$-H represents the least obstructed PSar species investigated in the scope of this work, bearing both a free carboxyl-terminus due to the initiation by water as well as a free secondary amine terminus allowing for a potential digestion by both C- and N-terminal exopeptidases as well as endopeptidases. As already apparent from Figure 4.46, a pronounced low molecular mass tailing is observable even without incubation at 37 °C. Elugrams obtained after incubation for prolonged periods of time illustrate these

findings even more clearly (Figure 4.52).

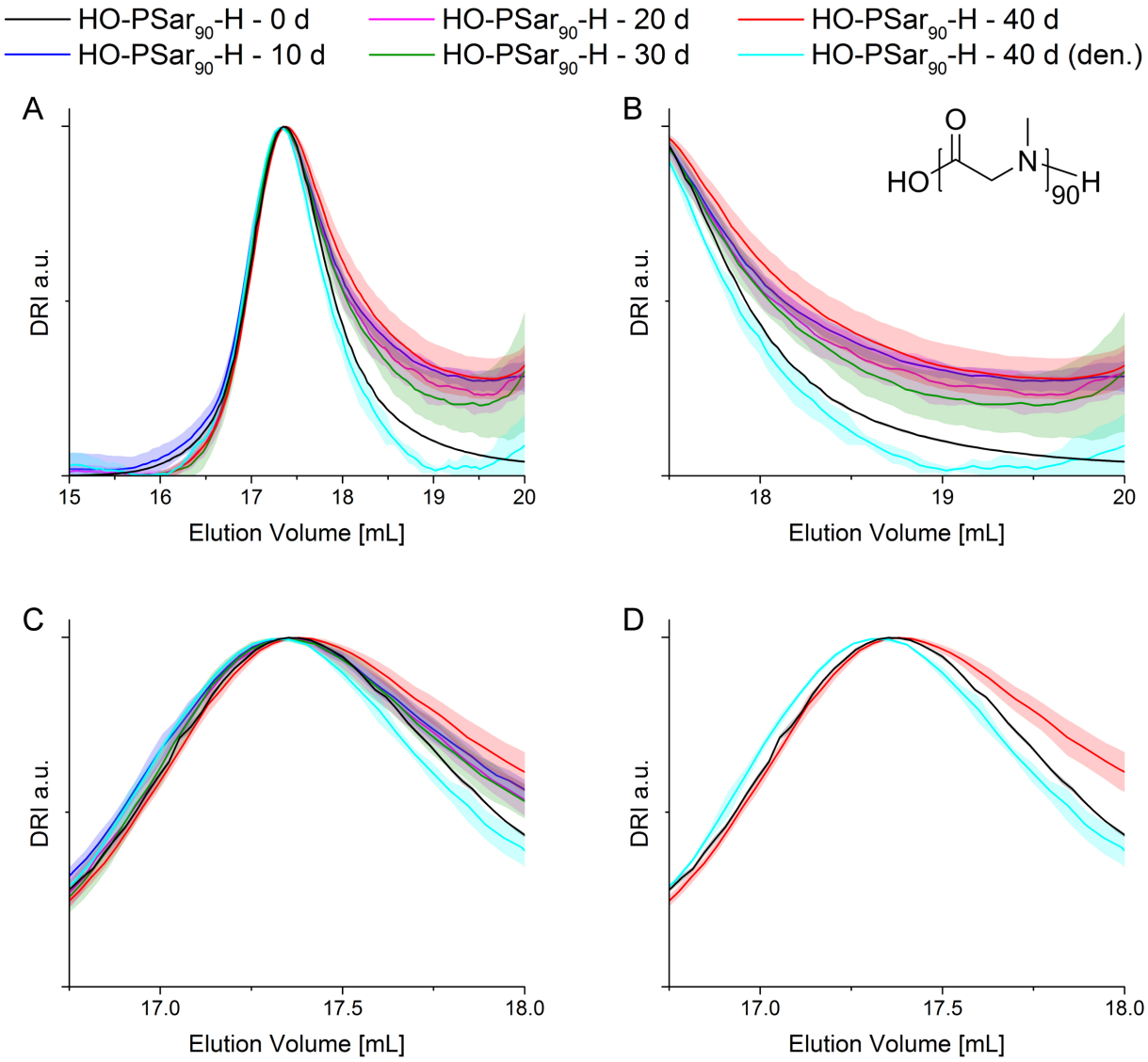

Figure 4.52: Normalized GPC elugrams of eggs injected with HO-PSar$_{90}$-H and incubated at 37 °C. **A** Overview. **B** Magnified view of the low molecular weight tailing evolving during incubation. **C** Magnified view of the polymer signal. **D** Magnified view showing only samples incubated for 0 d and 40 d as well as 40 d (den.) for reference. Data are presented as mean ± standard deviation (n = 6, HO-PSar$_{90}$-H - 0 d n = 1).

Nevertheless, due to the relatively high standard deviations displayed at higher elution volumes, no discernible trend of an increasing or decreasing molar mass can be identified. Indeed, with respect to the standard deviations elugrams appear to overlap indicating no further progressive change of the polymer structure with incubation time after the first 10 d, which is also reflected by M_n, M_w and M_p (Figure 4.53).

As already observed for PMeOx$_{90}$, M_p remains basically constant over the whole course

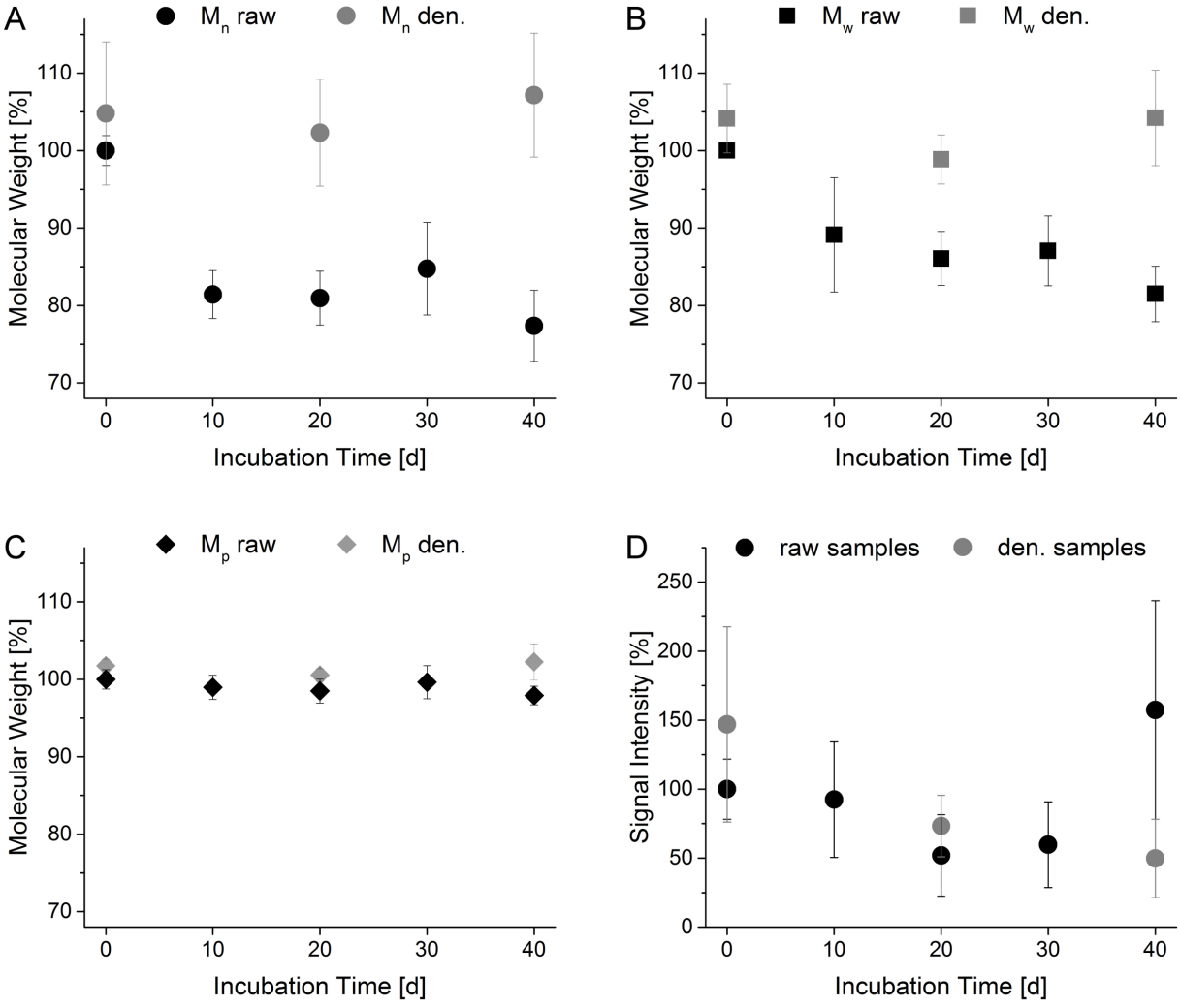

Figure 4.53: Percentage change of M_n, M_w and M_p as well as the signal intensity obtained from GPC elugrams of eggs injected with HO-PSar$_{90}$-H and incubated at 37 °C for up to 40 d. Data are presented as mean ± standard deviation (n = 6).

of the experiment, however, a slightly decreasing trend is emerging. Furthermore, both M_n and M_w drop to about 80 % and 90 %, respectively, within 10 d of incubation and display a declining trend in the further course. In contrast, molar mass averages of the denatured samples remain constant, thus hinting towards an enzymatic origin of HO-PSar$_{90}$-H deterioration.

Furthermore, a decreasing trend is also observed in case of the polymer signal intensities, with the exception of HO-PSar$_{90}$-H - 40 d which also possesses a very high standard deviation. Nevertheless, as discussed in more detail earlier, declining signal intensities may not only indicate degradation of the polymer but also diffusion into the yolk which was discarded without further analysis.

HO-PSar$_{90}$-Ac was obtained by post-polymerization modification of HO-PSar$_{90}$-H with acetic anhydride resulting in acetylation of the N-terminus. By this means, digestion of the polymer by N-terminal exopeptidases should be impeded. Indeed, the generation of a low molar mass tailing within the initial phase of the experiment is slowed down considerably (Figure 4.46 **F**), however, elugrams displaying the whole course of the experiment reveal a significant tailing developing after 10 d of incubation (Figure 4.54).

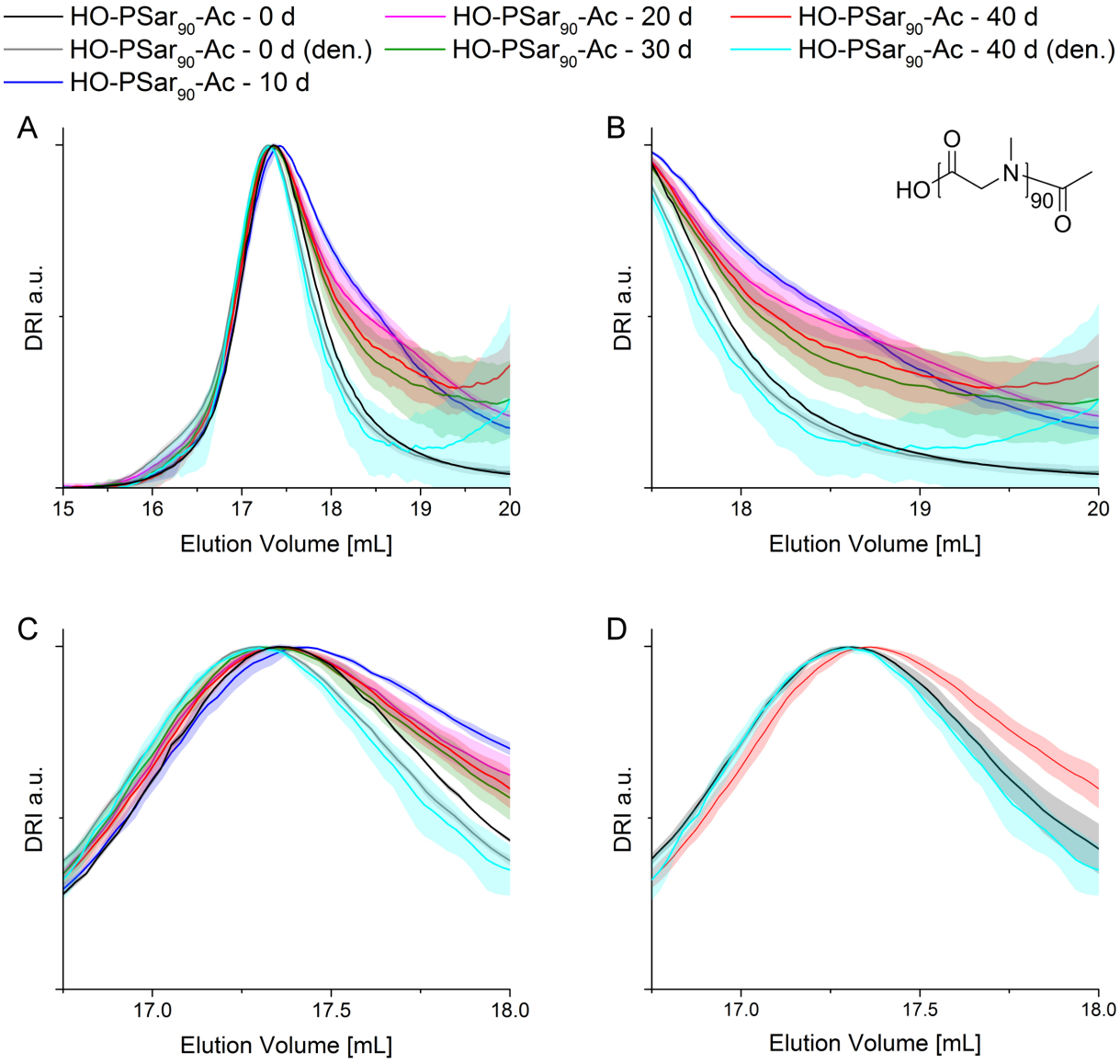

Figure 4.54: Normalized GPC elugrams of eggs injected with HO-PSar$_{90}$-Ac and incubated at 37 °C. **A** Overview. **B** Magnified view of the low molecular weight tailing developing during incubation. **C** Magnified view of the polymer signal. **D** Magnified view showing only samples incubated for 0 d and 40 d as well as 40 d (den.) for reference. Data are presented as mean ± standard deviation (n = 6, HO-PSar$_{90}$-Ac - 0 d n = 3).

However, the observed tailing constantly broadens during further incubation which becomes clearly visible in comparison of the signal heights at 18.25 mL and 19.5 mL. At 18.25 mL, shortly after the peak elution volume, signal heights decrease with increasing incubation time. In contrast, at a higher elution volume of 19.5 mL, the opposite trend is observed. Moreover, slight fluctuations of the peak elution volume are observed but appear to have no connection with the incubation time and may therefore be attributed to inaccuracies of the method. M_n, M_w and M_p values as well as signal intensities obtained from the elugrams (Figure 4.53) display a similar picture as noticed in case of HO-PSar$_{90}$-H. While

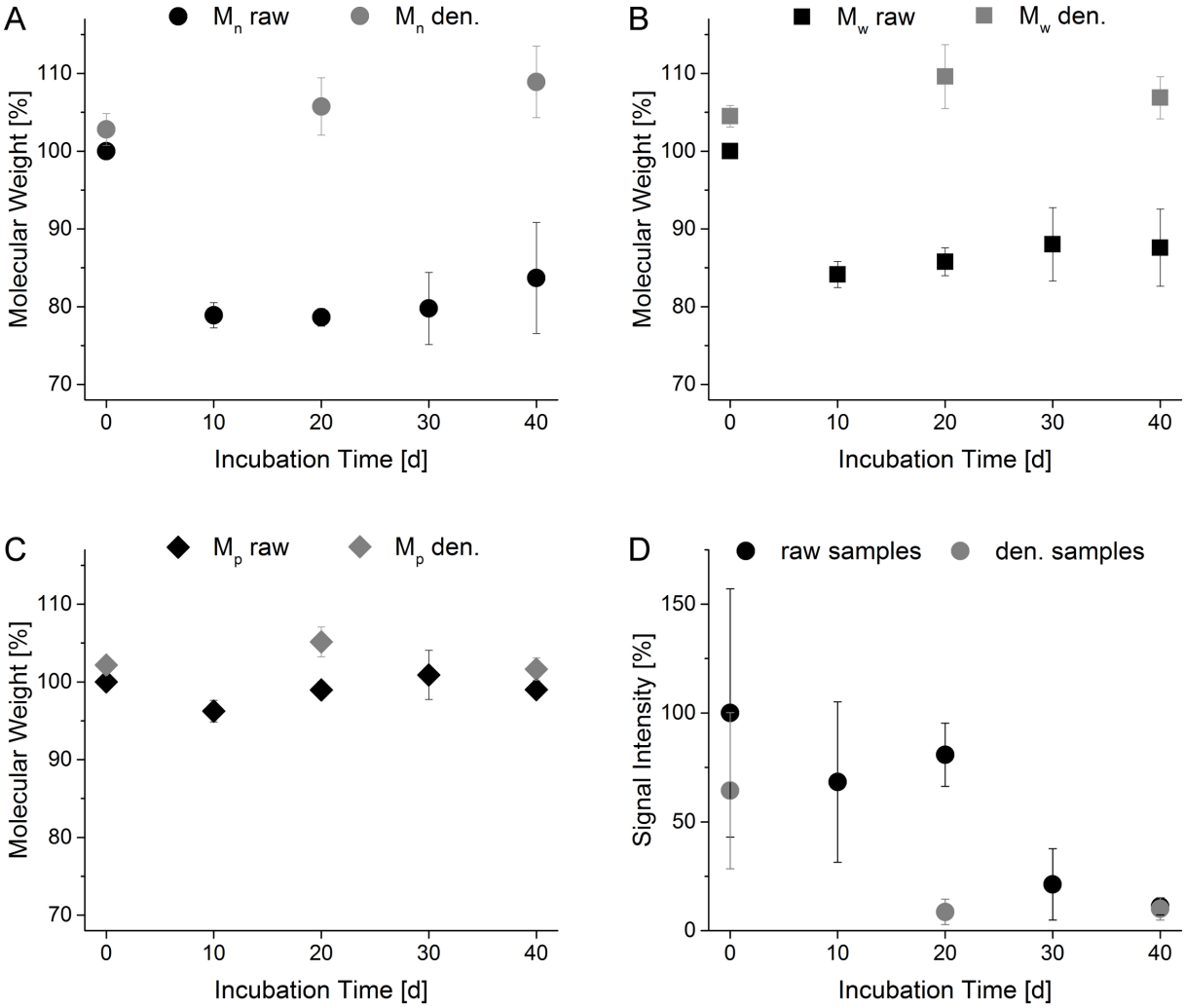

Figure 4.55: Percentage change of M_n, M_w and M_p as well as the signal intensity obtained from GPC elugrams of eggs injected with HO-PSar$_{90}$-Ac and incubated at 37 °C for up to 40 d. Data are presented as mean ± standard deviation (n = 6).

signal intensities continuously decrease over time, M_p remains essentially constant. Both M_n and M_w drop to about 80 % and 85 %, respectively, within the first 10 d of incubation

and display slightly increasing trends over the further course of the experiment caused by broadening of the observed tailing and the resulting overlap of tailing and signals corresponding with residual egg components. Interestingly, increasing trends are also apparent in case of the denatured samples, thus resulting in molar mass averages of up to 110 % which is attributable to slight shifts of the peak elution volume towards lower elution volumes corresponding with higher molar masses probably due to measurement inaccuracy. Apart from this, molar mass averages of the denatured samples are not changing with incubation time.

NPA-PSar$_{90}$-H was obtained by initiation of the polymerization with NPA, thus introducing a C-terminal obstruction to the PSar chain and potentially impeding digestion by C-terminal exopeptidases.
Even within a very short period of incubation, a significant low molecular weight shoulder or probably an underlying second distribution is apparent (Figure 4.46 **C**). Interestingly, elugrams reveal increasing intensity of this low molecular weight shoulder until 20 day of incubation followed by a decrease during the second half of the experiment (Figure 4.56). Alongside the low molecular weight shoulder indicating partial digestion of the polymer, no shift of the peak elution volume is observed which is further reflected by constant M_p values (Figure 4.57).
Nevertheless, slightly decreasing trends of M_n and M_w as well as the signal intensity indicate deterioration of NPA-PSar$_{90}$-H in accordance with the obtained elugrams. However, not only low signal intensities of the denatured samples probably caused by diffusion of the polymer into the yolk are observed, but also a slight decline of the molar mass averages, thus indicating the involvment of non-enzymatic processes in the degradation of NPA-PSar$_{90}$-H in egg white.
Compared with water-initiated HO-PSar$_{90}$-H and HO-PSar$_{90}$-Ac, the observed molar mass decrease is rather small, but appears to proceed continuously.

NPA-PSar$_{90}$-Ac represents the most obstructed of the investigated PSar samples bearing both NPA at the C-terminus and an acetyl group on the N-terminus potentially preventing enzymatic cleavage by N- and C-terminal exopeptidases.
Indeed, no extensive degradation within the initial phase of the experiment is observed (Figure 4.46 **D**). Furthermore, elugrams of the incubated samples (Figure 4.58) reveal a

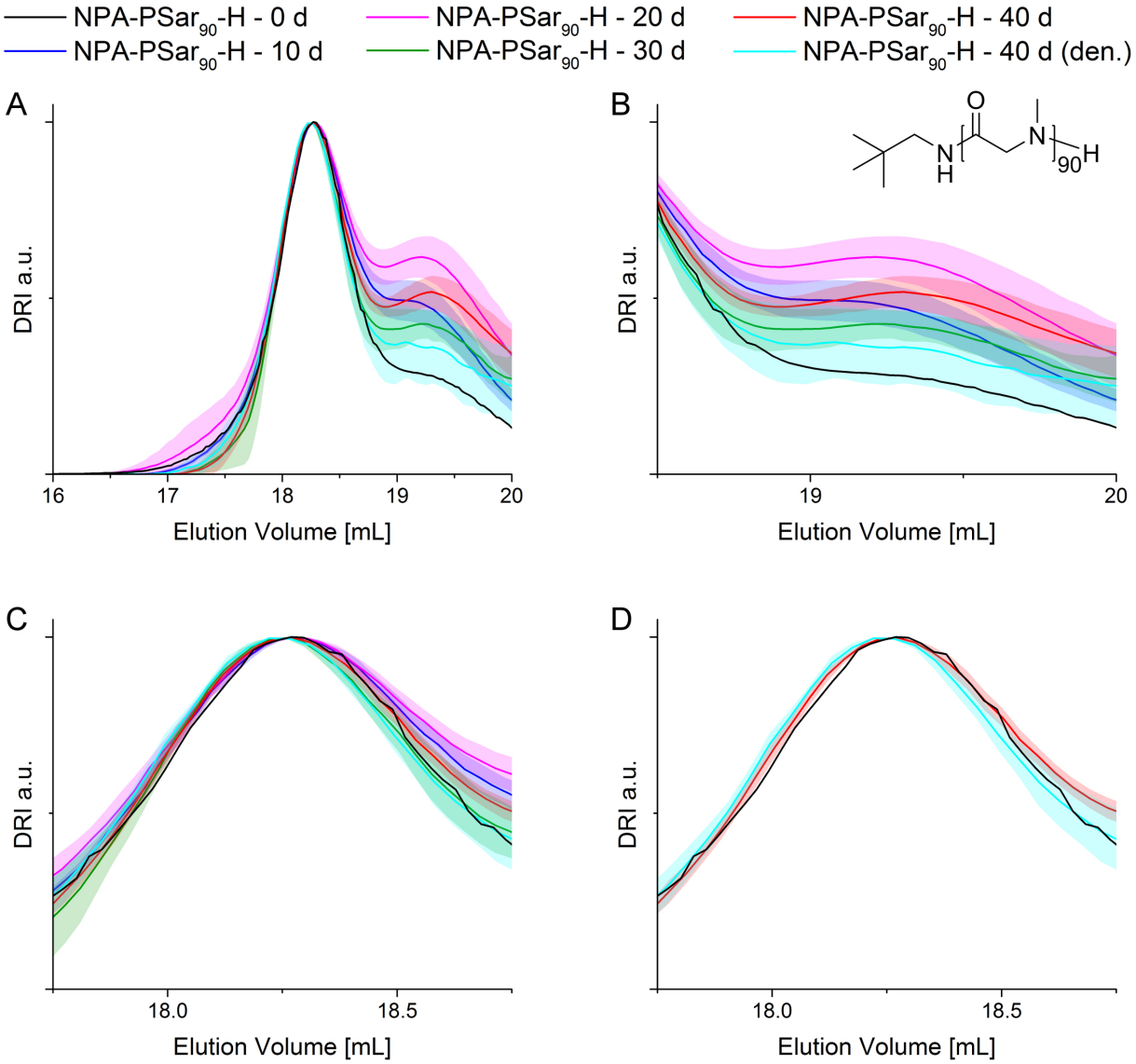

Figure 4.56: Normalized GPC elugrams of eggs injected with NPA-PSar$_{90}$-H and incubated at 37 °C. **A** Overview. **B** Magnified view of the low molecular weight shoulder developing during incubation. **C** Magnified view of the polymer signal. **D** Magnified view showing only samples incubated for 0 d and 40 d as well as 40 d (den.) for reference. Data are presented as mean ± standard deviation (n = 6, NPA-PSar$_{90}$-H - 0 d n = 3).

low molar mass shoulder or underlying second distribution evolving with incubation time. Interestingly, the peak elution volume of the low molar mass distribution is about half of the mass of the pristine polymer (≈ 3000 g/mol as compared to ≈ 6000 g/mol), thus indicating a potential backbone scission within the polymer chain. Again, corresponding molar mass averages and peak signal intensities are plotted in Figure 4.59. Likewise the previously discussed PSar species, hardly any alterations of the peak elution volume are

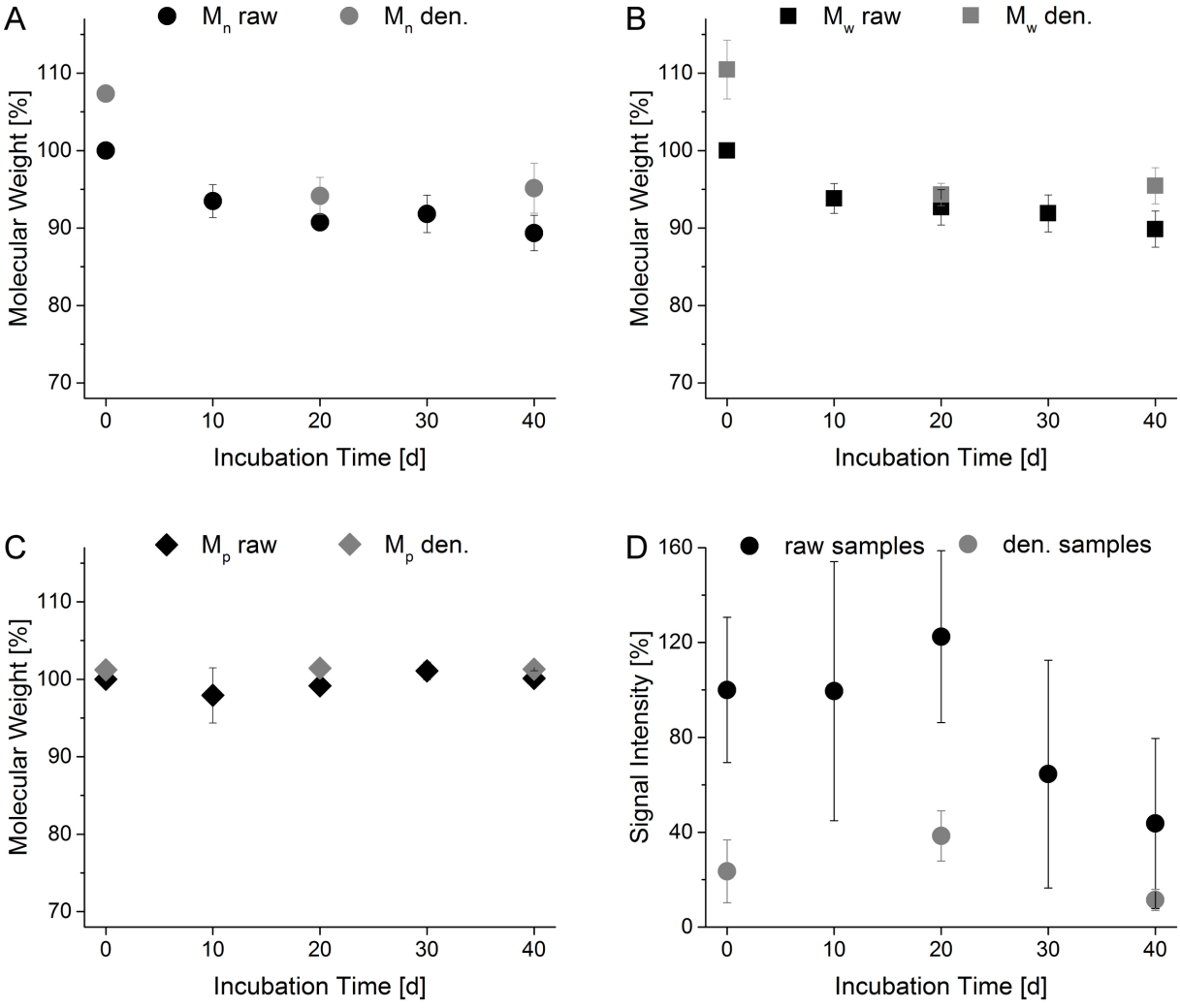

Figure 4.57: Percentage change of M_n, M_w and M_p as well as the signal intensity obtained from GPC elugrams of eggs injected with NPA-PSar$_{90}$-H and incubated at 37 °C for up to 40 d. Data are presented as mean ± standard deviation (n = 6).

observed. However, both M_n and M_w display a slow but steady decrease over the course of the experiment to about 90 % residual molar mass within 40 d. Furthermore, a significant loss of the signal intensity within the first 20 d is visible, which is, however, not very reliable in view of the markedly higher and erroneous data obtained for 30 and 40 d.

Considering the individual structures of the investigated PSar species and the corresponding patterns of the obtained elugrams, some clear correlations can be identified.
First of all, denatured samples exhibit no significant decreases of the molar mass averages corresponding with largely unaltered elugrams, thus implying an enzymatic origin of the modifications observed in case of the samples incubated without prior denaturation.

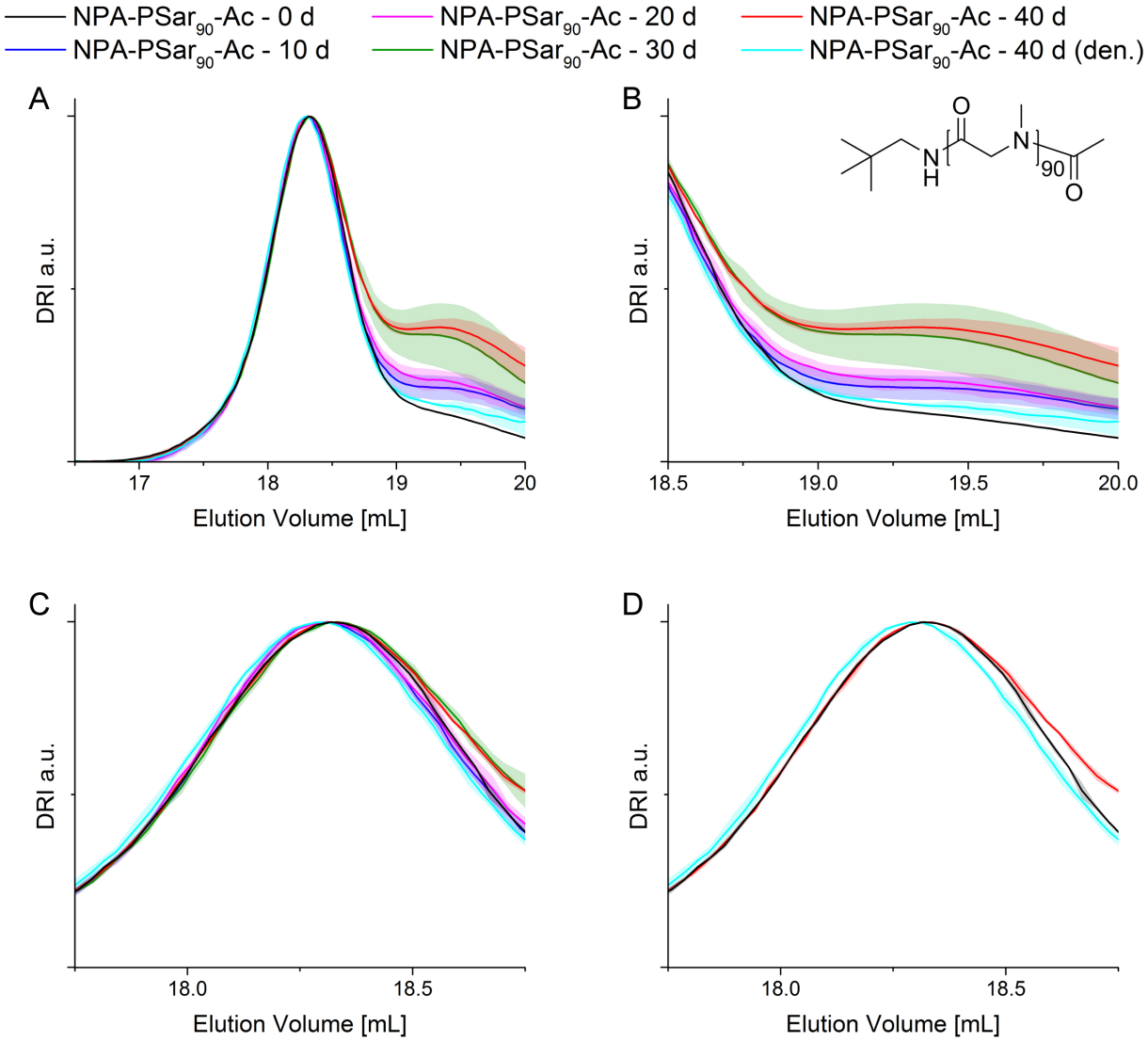

Figure 4.58: Normalized GPC elugrams of eggs injected with NPA-PSar$_{90}$-Ac and incubated at 37 °C. **A** Overview. **B** Magnified view of the low molecular weight shoulder developing during incubation. **C** Magnified view of the polymer signal. **D** Magnified view showing only samples incubated for 0 d and 40 d as well as 40 d (den.) for reference. Data are presented as mean ± standard deviation (n = 6, NPA-PSar$_{90}$-Ac - 0 d n = 3).

Furthermore, regardless of the respective C-terminus both acetylated species, namely NPA-PSar$_{90}$-Ac and HO-PSar$_{90}$-Ac, remain largely unaffected within the initial phase of the experiment, whereas NPA-PSar$_{90}$-H and HO-PSar$_{90}$-H possessing secondary amine termini rapidly evolve low molecular weight tailings and shoulders, respectively, even without incubation. This suggests an N-terminal exopeptidase activity specific to free amine termini within the first phase of the experiment. It should be noted though, that it is not possible to verify the sufficient post-polymerization acetylation of the PSar

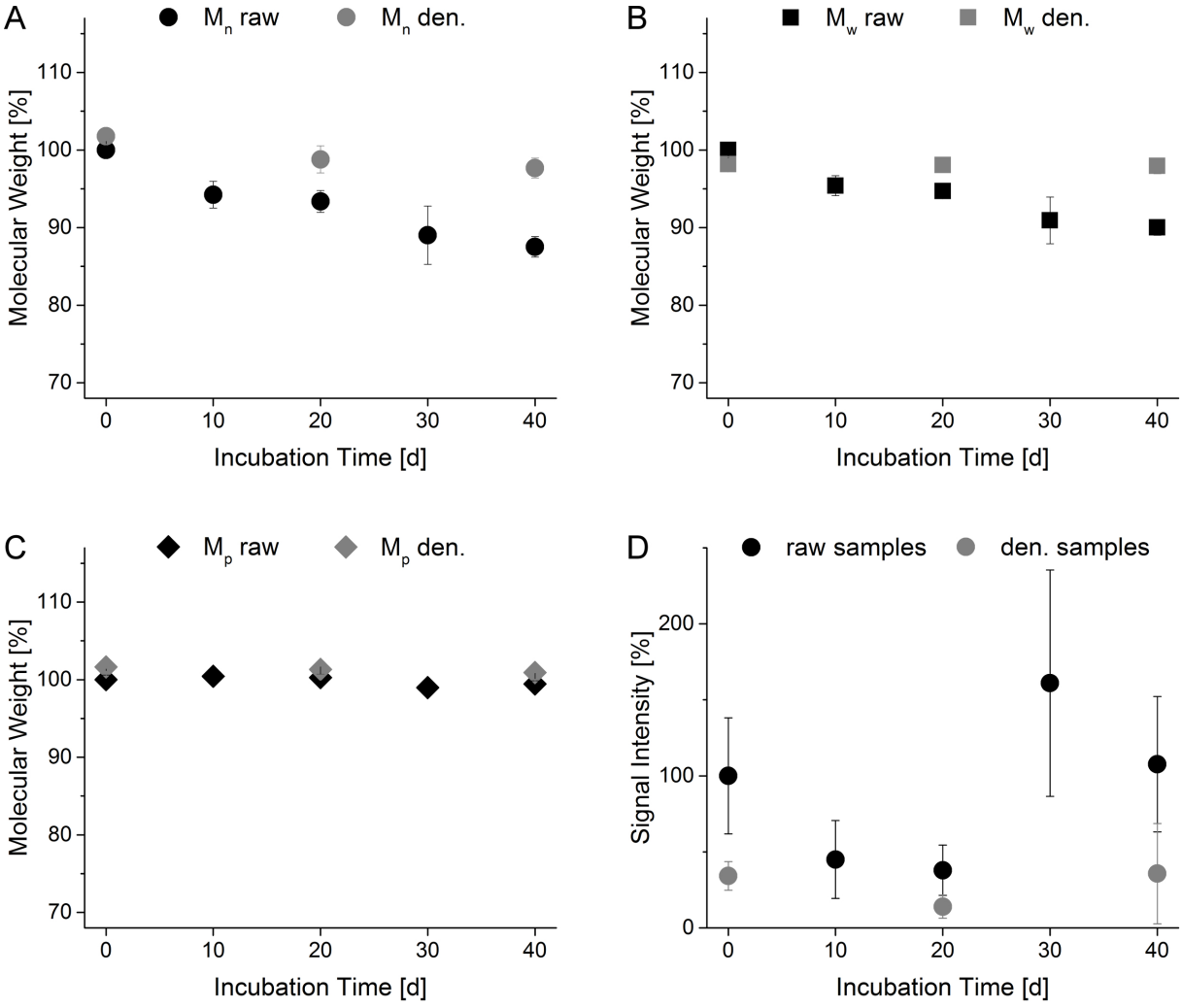

Figure 4.59: Percentage change of M_n, M_w and M_p as well as the signal intensity obtained from GPC elugrams of eggs injected with NPA-PSar$_{90}$-Ac and incubated at 37 °C for up to 40 d. Data are presented as mean ± standard deviation (n = 6).

samples via ^{1}H-NMR spectroscopy and matrix-assisted laser desorption/ionization time of flight (MALDI-ToF) mass spectrometry. Hence, a minor proportion of the polymer chains may still have possessed secondary amine termini enabling digestion by N-terminal exopeptidases.

Both water initiated polymers display a drop of M_n and M_w within the first 10 d followed by a slightly decreasing trend in case of HO-PSar$_{90}$-H and a slightly increasing trend observed for HO-PSar$_{90}$-Ac. However, increases of the molar mass averages of the latter are most likely misleading due to overlaps of signals corresponding with degradation products and egg components, respectively. Strong activity of a C-terminal exopeptidase may cause an instant molar mass loss reflected by continuous broadening of the signals accompanied

by significant low molecular weight tailings.
In contrast, NPA initiated samples possessing a modified C-terminus reveal elugram patterns indicating an underlying second distribution probably caused by fragmentation of the polymer chain. Particularly in case of NPA-$PSar_{90}$-Ac, which bears neither a free carboxy nor a free amine terminus and is thus considered insusceptible to exopeptidases, this suggests involvement of an endopeptidase cleaving internal amide bonds.

On the whole, investigations on the enzymatic digestion of PEG_{90}, $PMeOx_{90}$ and $PSar_{90}$ bearing different chain ends reveal quite distinct patterns of the elugrams depending on the chemical structure of the polymers. Comprising a polyether structure insusceptible to enzymatic hydrolysis by peptidases, PEG_{90} proved to be stable under the experimental conditions of this study.
It has to be noted, however, that animal studies suggest the involvement of alcohol and aldehyde dehydrogenases in the mammalian metabolism of PEG.[30] Alcohol dehydrogenase (EC 1.1.1.1) catalyzes the oxidation of primary and secondary alcohols yielding aldehydes or ketones, respectively, and is associated not only with the oxidation of methanol yielding toxic formaldehyde, but also with the oxidation of PEG chain ends triggering fatal blood poisoning.[403] High expression of alcohol dehydrogenase in liver is observed, however, no reports on an alcohol dehydrogenase activity in egg white are available which is in good agreement with the sufficient stability recognized within the scope of this study.
In contrast, $PMeOx_{90}$ bearing an amide bond within the side chain is known to be susceptible to hydrolysis under strong basic as well as strong acidic conditions yielding toxic linear PEI. Although elugrams of $PMeOx_{90}$ obtained after incubation *in ovo* indicate partial degradation, this is most probably not attributable to an enzymatic digestion as similar alterations of the samples incubated in denatured eggs are observed. Elevated temperatures during boiling on the one hand and prolonged incubation times on the other hand might have caused hydrolysis of $PMeOx_{90}$. However, based on the obtained results the presumption of an enzymatic digestion of $PMeOx_{90}$ in egg white can be rejected. Interestingly, studies conducted by Hsiue and coworkers suggest the susceptibility of PEtOx towards partial enzymatic hydrolysis by proteinase K (EC 3.4.21.64). While pronase, bromelain as well as lipase solely exhibited enzymatic activity towards poly(lactic acid) (PLLA) in a poly(L-lactide)-*block*-poly(2-ethyl-2-oxazoline)-*block*-poly(L-lactide) triblock copolymer, proteinase K was found to also remarkably hydrolyze the secondary

amide bond yielding PEI as determined via ^{1}H-NMR spectroscopy.[404] Proteinase K expressed by bacteria and fungi is known to digest hair (keratin) and catalyzes the hydrolysis of amide bonds on the carboxyl side of aliphatic and aromatic amino acids bearing blocked alpha amino groups with broad specificity. However, expression of proteinase K is neither reported within egg white nor organs and should therefore not be involved in the metabolism of POx *in ovo* and *in vivo*.

In case of $PSar_{90}$, hydrolysis results in backbone scission yielding, if performed exhaustively, the benign amino acid sarcosine. Indeed, while no deterioration upon incubation in denatured eggs is observed, elugram patterns suggest an enzymatic digestion probably involving an endopeptidase as well as C- and N-terminal exopeptidases.

It remains unclear, however, which enzymes might be involved in digestion of PSar *in ovo*. The following section will provide a short overview on the composition of chicken egg white and potential relations to *in vivo* conditions.

Relation to *in vivo* Conditions under Consideration of the Chicken Egg White Composition

Eggs serve as a staple in the diets of a vast majority of people and are valued not only for their nutritional but also functional purpose in modern recipes. Yolk, egg white and shell constitute the vital components of eggs. While the porous carbonate shell provides physical protection for the more fragile internal egg components and provides calcium for the developing chick, the yolk serves as an energy source comprising about 33 % fat and 17 % proteins.

The egg white, also known as albumen, makes up about two-thirds of an chicken egg and primarily consists of water (≈ 88 %) and proteins (≈ 11 %) supplemented by very low amounts of lipids (≈ 0.01 %).[405] Mine and coworkers identified and isolated more than 24 proteins from chicken egg white, including major proteins like ovalbumin (54 %, important for nutrition), ovotransferrin (12 %, binds iron), ovomucoid (11 %, trypsin inhibitor), ovomucin (3.5 %, trypsin inhibitor) and lysozyme (3.4 %, bactericidal enzyme).[405–407]

Using combinatorial hexapeptide libraries in conjunction with LC-ESI-IT-MS/MS, Mann *et al.* identified a total of 148 different proteins in albumen which are, unfortunately, not further specified yet.[408] As a part of the innate immune system, lysozymes act bactericidal by lysis of gram negative bacteria. Catalyzing the hydrolysis of β-1,4-glycosidic linkages between *N*-acetylmuramic acid and *N*-acetyl-D-glucosamine residues in peptidoglycan

and between *N*-acetyl-D-glucosamine residues in chitodextrins, they are not considered to cleave secondary amide bonds as found in PSar. To a lesser extent, expression of *N*-acetyl-β-D-glucosaminidase (EC 3.2.1.30), which hydrolyzes terminal non-reducing *N*-acetyl-D-hexosamine residues in *N*-acetyl-β-D-hexosaminides, and α-mannosidase (EC 3.2.1.24), which hydrolyzes terminal non-reducing alpha-D-mannose residues in alpha-D-mannosides, in egg white is observed, [409] however, both are also considered to possess no activity towards PSar.

Nevertheless, with respect to the number and diversity of proteins in egg white, the presence of enzymes capable of hydrolyzing secondary amide bonds cannot be excluded. However, it is obvious that egg white is incapable to reflect the greater variety of enzymes found *in vivo*. On the one hand, it is very likely that enzymes found *in ovo* which exhibit activity towards PSar are also expressed *in vivo*, on the other hand a lack of digestion of a polymer *in ovo* does not rule out a potential degradation by appropriate enzymes *in vivo*.

4.3.3 Stability of Poly(ethylene glycol), Poly(2-alkyl-2-oxazoline)s and Polypeptoids in rotten Chicken Eggs

Experiments on the enzymatic digestion of PEG, POx and polypeptoids incorporated the investigation of polymer stability in denatured eggs heated to 100 °C for 1 h prior to incubation. However, under these conditions not only potentially polymer digesting enzymes are heat inactivated, but also lysozyme protecting the egg from bacterial infestation.[410] Preliminary investigations conducted Maria Krebs under non-sterile conditions revealed rotting of denatured eggs during incubation at 37 °C for 20 d (Figure 4.60), which was to be expected as generally the storage of boiled eggs under refrigeration for a maximum of one week is recommended. It is conspicuous, however, that eggs injected with PEG_{45} appeared to be more affected by the rotting process than eggs injected with $PSar_{68}$. Although this could indicate a facilitation of the rotting process by injection of PEG, it is most probably attributable to the use of commercially acquired PEG without further purification, while $PSar_{68}$ was purified via dialysis. As apparent from the previously shown elugrams (Figure 4.39) and corresponding molar mass averages (Figure 4.40), a significant deterioration of

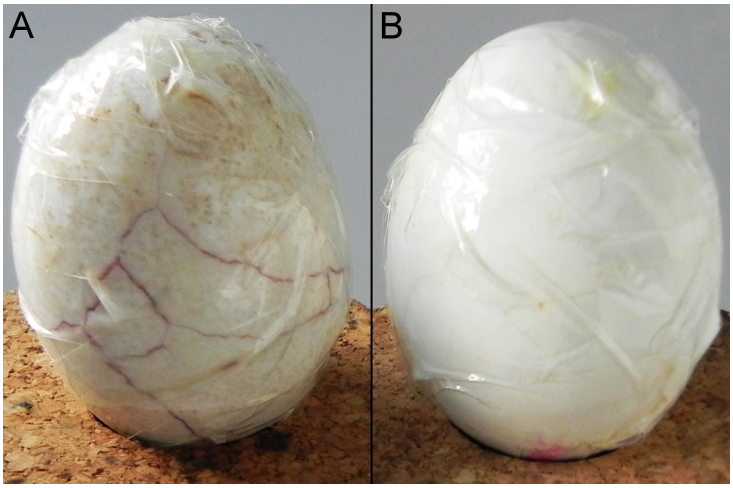

Figure 4.60: Rotten denatured chicken eggs injected with **A** PEG_{45} and **B** $PSar_{68}$ after incubation at 37 °C for 20 d.

PEG_{45} in rotten denatured chicken eggs is observed. In contrast, $PSar_{68}$ appears to be stable towards degradation in rotten denatured chicken eggs (*cf.* Figures 4.41 and 4.42). During further studies, thorough purification of the polymers via dialysis as well as sterile working conditions impeded rotting of the eggs in the majority of cases. Nevertheless, some eggs exhibited signs of rotting such as yellowish or purple discolorations, gel-like or slimy consistency and a strong characteristic odor (Table 4.4).

Table 4.4: Signs of spoilage and alterations of polymer elugrams in rotten denatured eggs.

Polymer	**Incubation Time**	**Signs of Spoilage**	**Elugram Alterations**
$PMeOx_{90}$	20 d	yellowish discolorations	-
	40 d	slimy consistency	-
PEG_{90}	20 d	slimy consistency	-
	20 d	slimy consistency	poor signal-to-noise ratio
	40 d	yellowish discolorations	-
	40 d	slimy consistency	-
NPA-$PSar_{90}$-H	20 d	yellowish discolorations	-
	20 d	purple discolorations	signal broadening

Continued on next page

Continued from previous page

Table 4.4: Signs of spoilage and alterations of polymer elugrams in rotten denatured eggs.

Polymer	Incubation Time	Signs of Spoilage	Elugram Alterations
NPA-PSar$_{90}$-Ac	20 d	purple discolorations, slimy consistency	poor signal-to-noise ratio
	40 d	slimy consistency	poor signal-to-noise ratio
HO-PSar$_{90}$-H	20 d	characteristic odor	-
HO-PSar$_{90}$-Ac	20 d	slimy consistency	-
	20 d	slimy consistency	no polymer signal
	20 d	slimy consistency	signal broadening
	40 d	characteristic odor	poor signal-to-noise ratio
	40 d	gel-like consistency	-
	40 d	slimy consistency	-
control	20 d	yellowish discolorations, slimy consistency	-
	20 d	yellowish discolorations, slimy consistency	-
	40 d	slimy consistency	-

In case of PMeOx$_{90}$, one of the 20 d and one of the 40 d incubated eggs revealed signs of spoilage, however, elugrams exhibited no irregularities. A total of four eggs rotted following injection of PEG$_{90}$. While elugrams obtained from three of these eggs revealed no differences compared with samples from non-rotten denatured eggs, one elugram of PEG$_{90}$ after incubation in an rotten egg characterized by a slimy consistency for 20 d possesses a comparatively poor signal-to-noise ratio but an unaltered M_p. About half of the elugrams obtained from rotten eggs injected with PSar$_{90}$ show certain abnormalities like a poor signal-to-noise ratio, significant signal broadening or, in one case, even a lack of the polymer signal. Interestingly, a remarkably high number of eggs injected with HO-PSar$_{90}$-Ac were subjected to rotting processes. For these experiments, a different instant adhesive was applied which dried much more slowly than the one used for all other

experiments. It can be assumed that this alternative instant adhesive failed to sufficiently seal the generated holes, thus facilitating the introduction and proliferation of bacteria inducing rotting of the eggs. Thus, the comparatively high proportion of rotten eggs in case of HO-PSar$_{90}$-Ac is most probably not caused by the polymer itself.

Although the quantity of samples is very low and reliable conclusions on the stability of the investigated polymers in rotten chicken eggs cannot be drawn at this stage of the investigations, the obtained results indicate a bacteria induced polymer deterioration upon spoilage of denatured chicken eggs. As discussed previously, polyethers like PEG are prone to enzymatic cleavage by both anaerobic as well as aerobic bacteria[411] such as *Pseudomonas aeruginosa*[400], *Pelobacter venetianus*[412], *Bacteroides* strain PG1[412], *Acetobacterium* sp. strain HA1[399] and *Sphingomonas terrae*[413]. Bond energies of C-O ether bonds (360 kJ/mol[414]) and N-C amide bonds (300 - 450 kJ/mol[415] depending on the respective substituent) are rather comparable. Even though investigations on the bacteria induced degradation of pseudo-peptides are hitherto lacking, cleavage of amide bonds by hydrolytic or oxidative enzymes released by bacteria is very likely.

Board isolated a total of 226 strains of bacteria from rotten eggs, with only 8 of the isolates being Gram positive rods.[416] Predominant species were identified as *Alcaligenes faecalis*, *Aeromonas liquefaciens*, *Proteus vulgarin*, *Cloaca* spp., *Citrobacter* sp. and *Pseudomonas fluorescens*.

Detailed investigations on the bacteria induced degradation of pseudo-polypeptides by oxidative or hydrolytic pathways are outside the scope of this work, however, obtained results are quite promising. Further studies focused on the deterioration of polymers by soil bacteria, putrefactive bacteria or yeasts may help to gain deeper knowledge on pseudo-polypeptide biodegradation.

5 Summary and Outlook

The present work aims towards the investigation of polymer degradation under biologically relevant conditions. In order to assess a potential degradation of polymers of interest for biomedical applications *in vivo* and associated effects on living tissue, representatives of poly(2-oxazoline)s and polypeptoids as well as poly(ethylene glycol) and poly(*N*-vinylpyrrolidone) for reference purposes are examined regarding their stability under oxidative and hydrolytic conditions as well as towards enzymatic degradation (*cf.* Figure 5.1).

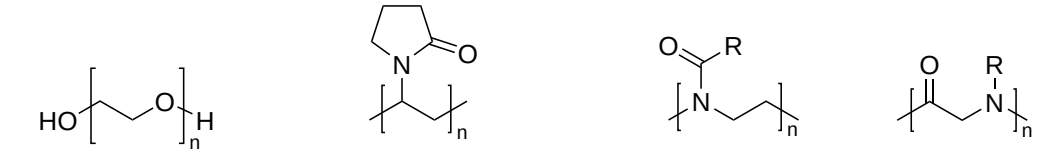

Poly(ethylene glycol) (PEG) | Poly(*N*-vinylpyrrolidone) (PVP) | Poly(2-alkyl-oxazoline) (POx) | Polypeptoid (POI)

Figure 5.1: Chemical structures of the polymers applied in the framework of the present thesis.

The polymers investigated in the framework of this thesis are generally considered to be non-biodegradable. Both poly(ethylene glycol) and poly(*N*-vinylpyrrolidone) are or were applied intensively *in vivo* provoking seriously harmful side effects like fatal blood poisoning from the oxidation of poly(ethylene glycol) chain ends or poly(*N*-vinylpyrrolidone) storage disease. Poly(2-alkyl-2-oxazoline)s and polypeptoids, both promising polymeric biomaterials for a wide variety of *in vivo* applications, are not clinically applied yet but undergo thorough investigations. However, comprising amide bonds within the backbone or the appending side chain, poly(2-alkyl-2-oxazoline)s and polypeptoids potentially offer a higher susceptibility towards (bio-)degradation. Representing the three most impactful initiators of degradation *in vivo*, the present study is focused on polymer deterioration by oxidative species, hydrolytic conditions and enzymes.

Oxidation

Oxidative species are generated in a variety of processes *in vivo*, both on purpose and as an unintentional by-product. Superoxide is a common by-product of cellular respiration within the mitochondria, while tissue specific NADPH oxidases generate superoxide and hydrogen peroxide to fulfill a multitude of functions. Spontaneously or catalyzed by enzymes, superoxide and hydrogen peroxide are metabolized yielding more harmful reactive oxygen

and nitrogen species such as hydroxyl radicals, hypochlorous acid or nitric oxide.
Previous investigations revealed the susceptibility of poly(ethylene glycol), poly(*N*-vinylpyrrolidone), poly(2-alkyl-2-oxazoline)s and polypeptoids to deterioration by hydroxyl radicals deriving from hydrogen peroxide and copper ions.[169, 218, 219] Results further showed a strong dependency of the apparent degradation rate on the polymer chain length. The present thesis is not only intended to confirm the aforementioned findings, but also to deepen the knowledge on oxidative polymer degradation by enlarging the investigated range of both polymer chain lengths as well as oxidative species.
Based on the established protocol, highly reactive hydroxyl radicals are generated by a Fenton-like reaction of hydrogen peroxide and copper ions:

$$H_2O_2 \; + \; Cu^+ \; \longrightarrow \; OH\cdot \; + OH^- \; + \; Cu^{2+}$$

However, the *in vivo* availability of copper ions of about 80 mg is significantly lower compared to about 4 g of iron ions which can also initiate the generation of hydroxyl radicals by a Fenton reaction. A direct comparison of both ions reveals significantly lower apparent degradation rates when iron instead of copper is applied, which is most probably caused by a lower Fenton reaction rate of 76 $mol^{-1}sec^{-1}$[367] compared to $4.7 \cdot 10^3$ $mol^{-1}sec^{-1}$[366] and the associated slower generation of hydroxyl radicals.
Furthermore, previously collected data on the hydroxyl radical induced oxidative degradation of poly(ethylene glycol), poly(*N*-vinylpyrrolidone) and poly(2-ethyl-2-oxazoline) are completed to obtain an overview about an enlarged molar mass range of 2 to 500 kg/mol. The obtained data confirm previous results of an apparent degradation rate increasing with increasing chain length due to self-inhibitory end group effects for all three polymer species (*cf.* Figure 5.2). Oxidation of chain ends rather than the backbone consumes reactive oxygen species and decelerates backbone scission, which is particularly influential for low molar mass polymers comprising a higher proportion of end groups. With each backbone scission generating two additional chain ends, their proportion increases tremendously during oxidation thus decelerating the apparent degradation rate.
Finally, the investigation of different oxidative species was intended to clarify the extent of oxidative degradation by less potent oxidants. A direct comparison of hydrogen peroxide with and without further addition of $CuSO_4$ reveals significantly lower apparent degradation rates of both poly(ethylene glycol) and polysarcosine if solely hydrogen peroxide is

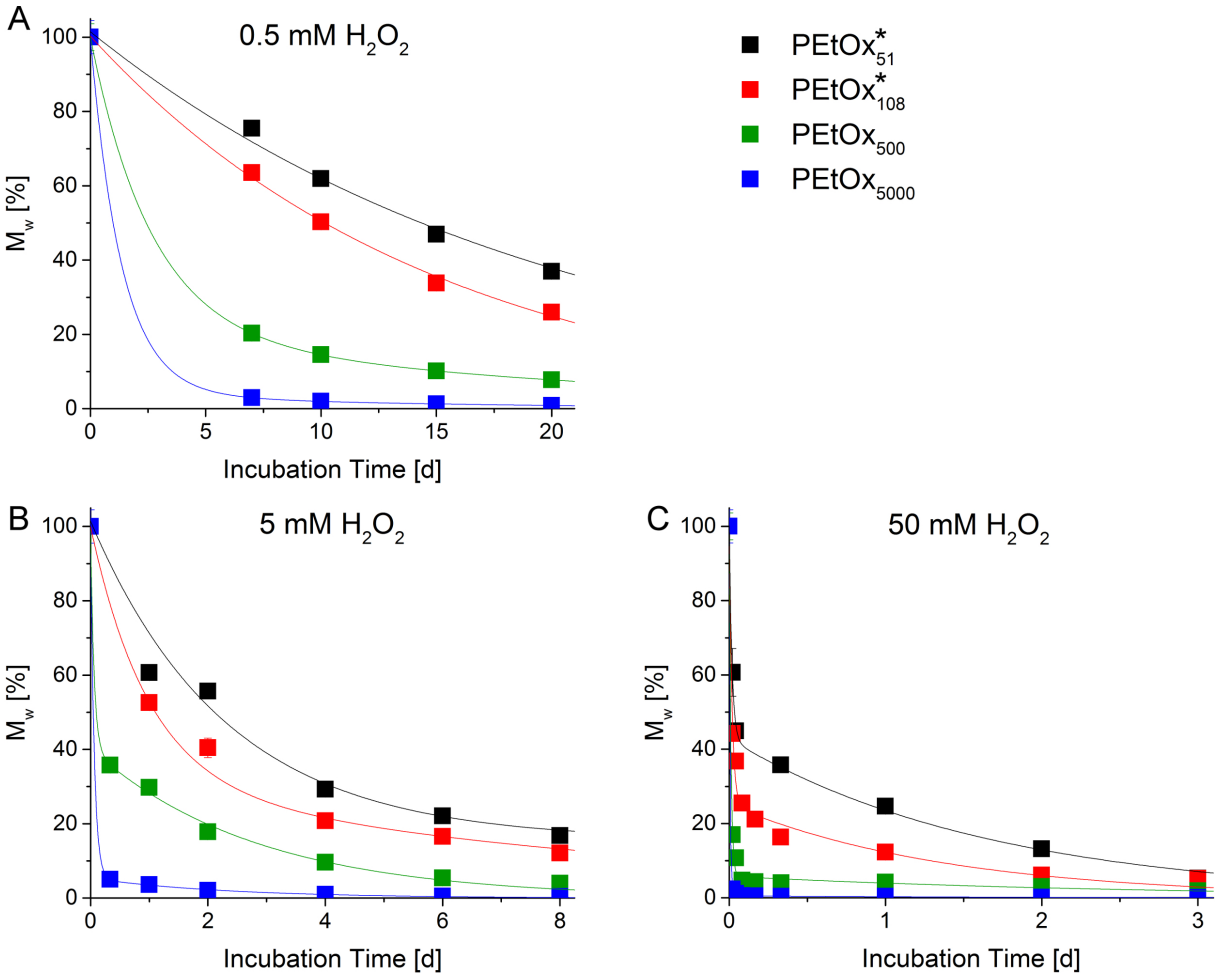

Figure 5.2: Molar mass development of polymers depending on the DP of the pristine polymer upon oxidative degradation by hydroxyl radicals deriving from 0.5 to 50 mM H_2O_2 and 50 μM $CuSO_4$ (**A** - **C**) with the example of PEtOx. Data are presented as mean ± SD (n = 3). Lines are intended as a guide to the eye. *Data taken from ref. [169].

applied, which is well comprehensible in view of the higher oxidative potential of hydroxyl radicals compared to hydrogen peroxide. Furthermore, amounts of superoxide generated from 0.5 mM hypoxanthine and 20 U/L xanthine oxidase have no significant effects on the molecular weight distribution of poly(ethylene glycol) and polysarcosine within 24 h of incubation. In contrast, incubation of both polymers with hypochlorous acid results in deterioration of the polymers. However, in case of poly(ethylene glycol) elugrams obtained after incubation in 50 mM HClO reveal a distinct high molecular weight shoulder probably caused by chain coupling. Reactions of hypochlorous acid in aqueous solution are quite diverse and generate not only hydroxyl radicals but also singlet oxygen and hydroxide allowing for a multitude of modification and degradation reactions.

GC/MS measurements of exhaustively degraded poly(ethylene glycol), poly(2-alkyl-2-oxazoline), polypeptoid and poly(*N*-vinylpyrrolidone) species are not particularly meaningful in case of poly(ethylene glycol) and the polypeptoids, however, results obtained for poly(*N*-vinylpyrrolidone) are in good agreement with previously postulated mechanisms of oxidative poly(*N*-vinylpyrrolidone) degradation. Results obtained for poly(2-alkyl-2-oxazoline)s are less conclusive, however, they indicate both backbone and side chain scission to occur, yielding, among others, acetaldehyde, acetamide and carbon dioxide.

Although the exact concentrations of oxidative species *in vivo* are very controversial, with respect to their great variety and wide distribution the investigated polymers are likely prone to oxidative deterioration to some extent, with rates, mechanisms and degradation products strongly depending on the respective reactive species, polymer structure and chain length.
Further studies should focus on elucidating the mechanisms of oxidative degradation especially of polypeptoids and poly(2-alkyl-2-oxazoline)s. In this context, small model molecules such as dimers, trimers or tetramers of sarcosine, *N*-ethylglycine, 2-methyl-2-oxazoline and 2-ethyl-2-oxazoline could be gradually oxidized and degraded by hydrogen peroxide. The obtained degradation products can be identified via ^{1}H-, ^{13}C- and ^{15}N-NMR spectroscopy as well as GC/MS measurement and should enable conclusions to be drawn on the mechanism of oxidation and potential toxic effects of oxidative pseudo-polypeptide degradation *in vivo*.

Hydrolysis

Like blood, most tissues of the human body benefit from a slightly alkaline pH value. Nevertheless, specific areas like the human stomach or tumor tissues possess acidic conditions potentially capable to cleave amide bonds comprised by poly(2-alkyl-2-oxazoline)s and polypeptoids.
Earlier results on the acidic hydrolysis of poly(2-alkyl-2-oxazoline)s conducted by Hoogenboom and coworkers[225, 228, 230] rejecting side chain cleavage yielding toxic PEI during passage of the stomach to a critical extent are confirmed via closely related investigations. Subsequently, the developed experimental set up is applied to investigate the hydrolysis of polysarcosine by 6 M HCl at 37, 55, 75, 90 and 99 °C as well as by simulated gastric fluid (SGF) (pH 1.1 - 1.3) and simulated intestinal fluid (SIF) (pH 6.50 - 6.60) at 37 °C.

Unlike the hydrolysis of poly(2-alkyl-2-oxazoline)s resulting in side chain cleavage, the hydrolysis of polypeptoids induces backbone scission decreasing the polymer chain length tremendously and releasing, if performed exhaustively, the respective amino acids. Hydrolysis of polysarcosine is monitored by quantification of the released sarcosine via ^{1}H-NMR spectroscopy and determination of the residual M_w via GPC. Its cyclic dimer sarcosine anhydride is formed as an intermediate product in this process via cyclization of unstable linear dimers of sarcosine.

Hydrolysis by 6 M HCl confirms the expected strong temperature-dependency of polysarcosine cleavage (*cf.* Figure 5.3). Reducing the applied temperature to 37 °C results in

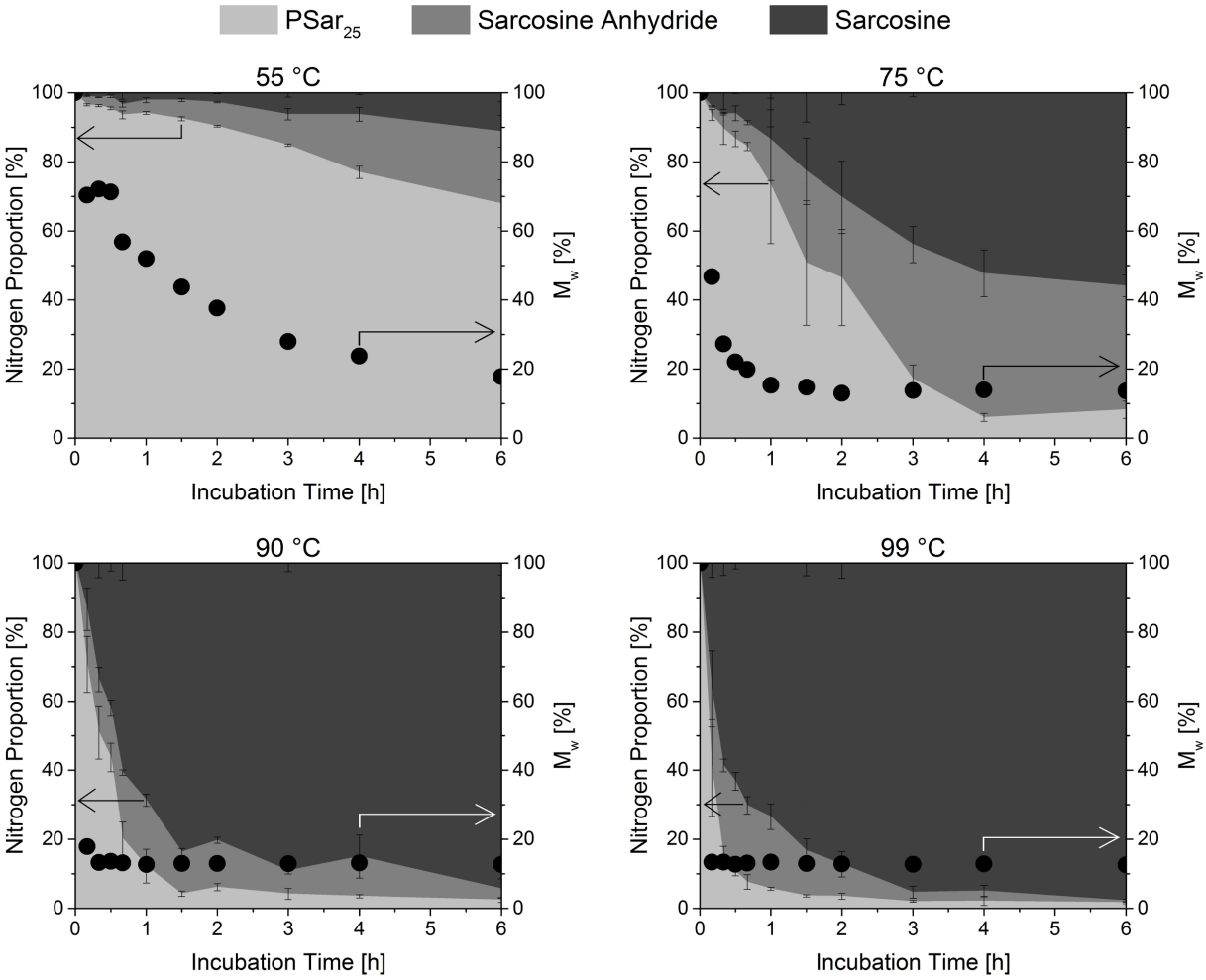

Figure 5.3: Kinetic plots showing the proportions of nitrogen bound within polysarcosine (light grey), sarcosine anhydride (grey) and sarcosine (dark grey) as determined via ^{1}H-NMR spectroscopy as well as the residual M_w as determined via GPC for the acidic hydrolysis of $PSar_{25}$ by 6 M HCl at 55 to 99 °C. Data are presented as mean ± SD (n = 3).

a marked deceleration of sarcosine and sarcosine anhydride release which is even more

apparent in SGF and SIF where only negligible amounts of sarcosine are released over a course of 14 d. It has to be noted that addition of polysarcosine to SGF resulted in an instant increase of the pH-value from ≈ 1.1 to ≈ 6.5. Thus, further pronounced hydrolysis could not be reasonably expected. However, both the generation of sarcosine anhydride and a molecular weight decrease of about 15 % within 4 h confirm the partial degradation of polysarcosine under the applied conditions.

In view of the foregoing, fragmentation of polysarcosine during passage of the human stomach with a maximum retention time of 4 h is quite conceivable. In contrast to poly(2-alkyl-2-oxazoline) hydrolysis, in which case cleavage of amide bonds does not results in shortening of the polymer chains but the generation of toxic PEI, cleavage of polysarcosine amide bonds proceeds via backbone scission yielding shorter polymer chains underlying faster elimination from the human body.

In order to evaluate the potential degradation of polysarcosine and other polypeptoids during passage of the human stomach, experiments with SGF should be repeated applying a large excess of the acid. Furthermore, influences of the side chains remain to be elucidated as longer side chains bear the potential to decelerate the hydrolysis rate by sterical effects.

Enzymatic Degradation

Modification and degradation of bio(macro)molecules is an essential part of human metabolism. Polymers bearing amide bonds and showing a great similarity to natural occurring and widely distributed polypeptides, like poly(2-alkyl-2-oxazoline)s and polypeptoids, bear the potential of an enzymatic biodegradability by (more or less specific) peptidases. Just like the acidic hydrolysis described previously, peptidase activity would result in the cleavage of polymer amide bonds.

The aim of the present thesis was to evaluate the stability of poly(2-alkyl-2-oxazoline)s and polypeptoids as well as poly(ethylene glycol) for the sake of reference under circumstances resembling *in vivo* conditions as closely as possible. Initial experiments focused on the degradation of dye-labeled upon incubation with homogenates of freshly harvested rat liver and kidney. However, although the obtained results are promising for the most part, they are considered rather unreliable and non-reproducible for various reasons.

More conclusive data are attained from the incubation of non-labeled polymers in freshly laid chicken eggs. Elugrams of poly(ethylene glycol), poly(2-methyl-2-oxazoline) and polysarcosine (Figure 5.4) comprising different chain ends incubated for up to 40 d reveal

distinct patterns depending on the chemical structure of the respective polymer. While

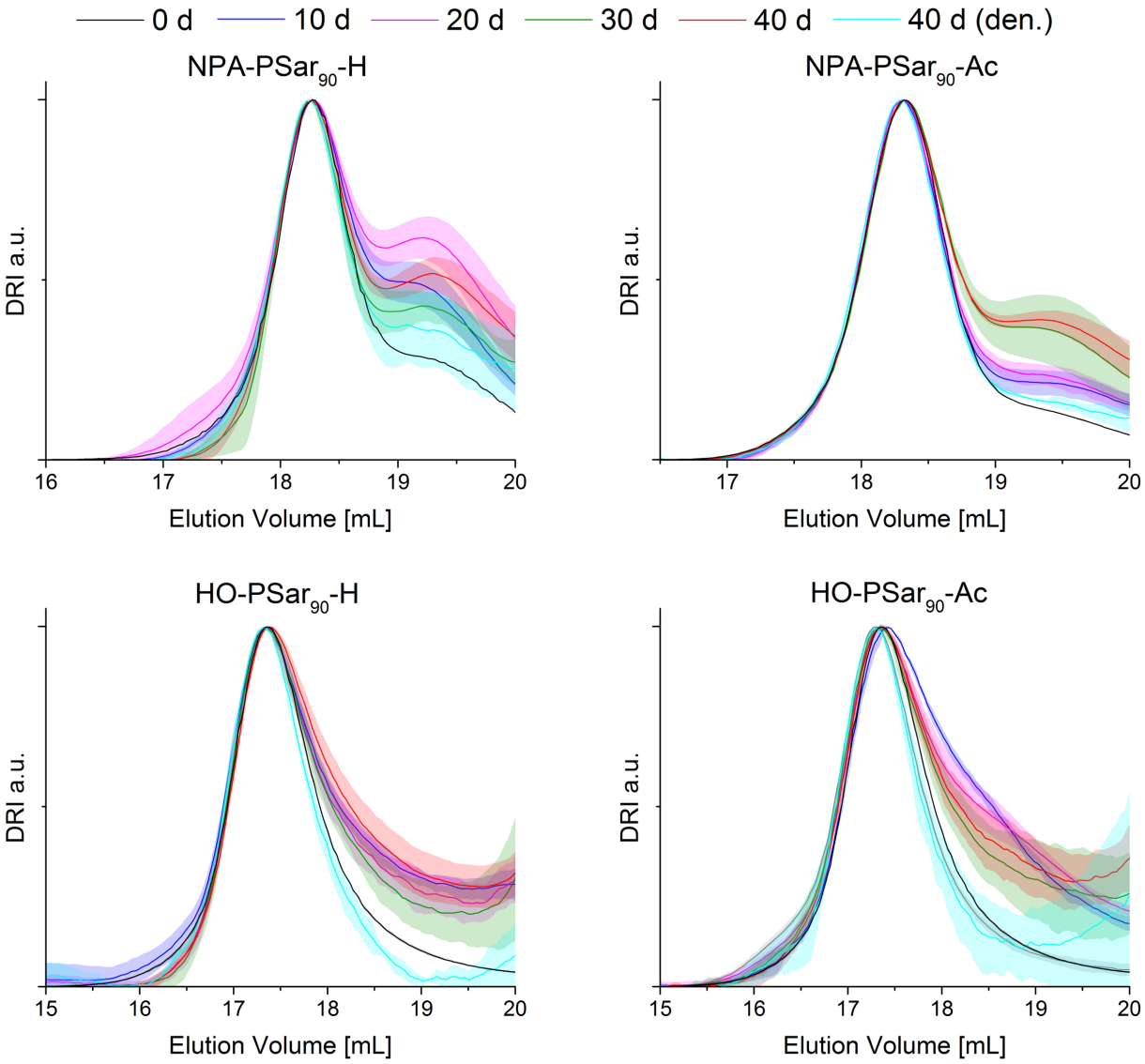

Figure 5.4: Normalized GPC elugrams of eggs injected with polysarcosine comprising different chain ends and incubated at 37 °C. Data are presented as mean ± SD (n = 6).

no evidence for an enzymatic digestion of poly(ethylene glycol) in chicken egg white is found and deterioration of poly(2-methyl-2-oxazoline) upon incubation apparently derives from non-enzymatic hydrolysis, incubated polysarcosine samples reveal distinct elugram patterns depending on the respective C- and N-terminal end groups indicating both exopeptidase and endopeptidase activity. It has to be kept in mind though, that an enzymatic digestibility of polysarcosine does not necessarily imply the digestion of polypeptoids bearing longer side chains by peptidases as well, which should be investigated in further studies.

Since *in ovo* experiments proved promising, animal studies should be initiated to investigate the long term stability of pseudo-polypeptides *in vivo*. For this purpose, studies should involve polymers radioactively labeled on the C- or N-terminus as well as the side chain, respectively. As it has to be expected that the vast majority of the polymer is excreted rapidly, multiple injections over a longer period of time or long-term release of the polymer through an implanted capsule can be used to simulate long-term intake of the polymers. After several months, organs like liver, kidney and spleen can be harvested, potential polymer residuals extracted and analyzed regarding their size via GPC applying a radiation detector. Subsequently, it should be possible to isolate individual enzymes from the respective organs or work with characteristic enzyme mixes (e.g. S9-mix) to narrow down the number of eligible enzymes and identify the ones that are capable to digest polypeptoids or poly(2-alkyl-2-oxazoline)s.

The present thesis provides an overview on the most important possibilities of polymer degradation *in vivo*. Poly(2-alkyl-2-oxazoline)s and polypeptoids proved to be prone to oxidation by reactive oxygen species and hydrolysis under acidic conditions. Furthermore, the obtained results indicate the susceptibility of polysarcosine to enzymatic digestion *in ovo*.

Apart from their various beneficial properties described in detail elsewhere, the likely slow but steady biodegradability of poly(2-alkyl-2-oxazoline)s and especially polypeptoids highlights both polymer species as ideal candidates for *in vivo* applications.

It remains to be elucidated whether or not the obtained results are transferable to *in vivo* conditions and, if so, which enzymes are involved in the digestion of pseudo-polypeptides.

6 Zusammenfassung und Ausblick

Die vorgestellte Arbeit befasst sich mit der Untersuchung des Abbauverhaltens von Polymeren unter biologisch relevanten Bedingungen. Vertreter der Poly(2-alkyl-2-oxazolin)e und Polypeptoide sowie Polyethylenglycol und Poly(*N*-vinylpyrrolidon) als Referenzpolymere (vgl. Abbildung 6.1) werden im Hinblick auf ihre Stabilität unter oxidativen und hydrolytischen Bedingungen sowie gegen enzymatische Verdauung untersucht, um Rückschlüsse auf ihren potentiellen Abbau *in vivo* ziehen und die damit verbundenen Auswirkungen auf lebendes Gewebe abschätzen zu können.

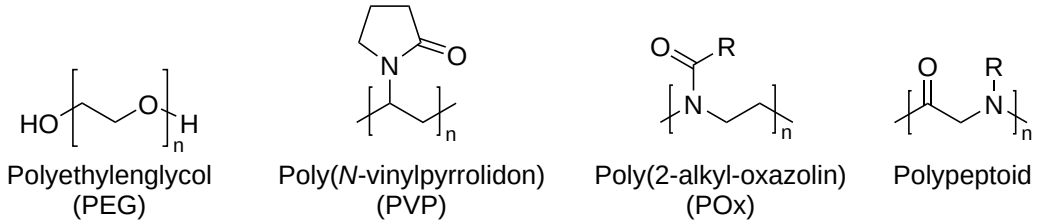

Abbildung 6.1: Strukturformeln der im Rahmen dieser Arbeit untersuchten Polymere.

Die im Rahmen dieser Arbeit untersuchten Polymere sind von großem Interesse für biomedizinische Anwendungen, werden in der Literatur in der Regel jedoch als nicht bioabbaubar eingestuft. Sowohl Polyethylenglycol als auch Poly(*N*-vinylpyrrolidon) werden bzw. wurden intensiv *in vivo* angewendet, zum Teil mit erhebliche Nebenwirkungen wie tödliche Blutvergiftungen durch Oxidation von Polyethylenglycol-Kettenenden oder die sogenannte Poly(*N*-vinylpyrrolidon)-Speicherkrankheit. Poly(2-alkyl-2-oxazolin)e und Polypeptoide, zwei vielversprechende, jedoch noch wenig untersuchte Polymerklassen, sind als Biomaterialien für eine Vielzahl von *in vivo* Anwendungen interessant, werden aber bisher nicht kommerziell eingesetzt. Wie auch Polyethylenglycol und Poly(*N*-vinylpyrrolidon) werden Poly(2-alkyl-2-oxazolin)e und Polypeptoide als nicht bioabbaubar angesehen, was in Anbetracht der im Polymerrückgrat bzw. der davon abgehenden Seitenkette enthaltenen Amidbindungen kritisch zu hinterfragen ist. Die vorliegende Arbeit befasst sich mit dem biologisch relevanten Abbau der vorgenannten Polymere durch drei bedeutungsvolle Initiatoren des Abbaus von (Bio-)Makromolekülen: oxidative und saure Bedingungen sowie den Einfluss von Enzymen.

Oxidation

Reaktive Sauerstoff- und Stickstoffspezies werden *in vivo* in einer Vielzahl von Prozessen gezielt oder auch als unerwünschtes Nebenprodukt gebildet. Superoxid entsteht häufig als Nebenprodukt der Zellatmung in den Mitochondrien, während gewebespezifische NADPH Oxidasen sowohl Superoxid als auch Wasserstoffperoxid für eine Reihe wichtiger Funktionen und Prozesse generieren. Diese relativ harmlosen Spezies unterliegen dem Metabolismus und werden, spontan oder katalysiert durch Enzyme, in schädlichere reaktive Sauerstoff- und Stickstoffspezies wie Hydroxylradikale, Hypochlorige Säure oder Stickstoffmonoxid umgewandelt.

Vorangegangene Untersuchungen konnten bereits die Anfälligkeit von Polyethylenglycol, Poly(*N*-vinylpyrrolidon), Poly(2-alkyl-2-oxazolin)en und Polypeptoiden für Modifikationen durch *in situ* durch Reaktion von Wasserstoffperoxid und Kupferionen gebildete Hydroxylradikale zeigen.[169, 218, 219] Desweiteren wiesen die Resultate auf eine starke Abhängigkeit der scheinbaren Abbaurate von der Polymerkettenlänge hin. Die vorliegende Arbeit soll die bereits erlangten Kenntnisse nicht nur bestätigen, sondern durch Untersuchung weiterer Polymer- sowie reaktiver Sauerstoffspezies auch grundlegend erweitern.

Basierend auf dem bereits etablierten Protokoll werden mittels Fenton-artiger Reaktion von Wasserstoffperoxid und Kupferionen *in situ* hochreaktive Hydroxylradikale erzeugt:

$$H_2O_2 \; + \; Cu^{+} \; \longrightarrow \; OH\cdot \; + OH^{-} \; + \; Cu^{2+}$$

Die *in vivo* Verfügbarkeit von Kupferionen ist mit etwa 80 mg deutlich geringer als die Verfügbarkeit von Eisenionen ($\approx$ 4 g), welche ebenfalls die Bildung von Hydroxylradikalen mittels Fenton-Reaktion initiieren können. Im direkten Vergleich der beiden Metallionen zeigt sich eine signifikant niedrigere scheinbare Abbaurate bei Verwendung von Eisen anstatt Kupferionen, was höchstwahrscheinlich auf die geringere Reaktionskonstante der Fenton-Reaktion von 76 $mol^{-1}sec^{-1}$[367] für Eisen im Vergleich zu $4.7 \cdot 10^3$ $mol^{-1}sec^{-1}$[366] für Kupfer und der damit verbundenen langsameren Erzeugung von Hydroxylradikalen zurückzuführen ist.

Desweiteren werden in vorangegangenen Arbeiten erfasste Daten zum oxidativen Abbau von Polyethylenglycol, Poly(*N*-vinylpyrrolidon) und Poly(2-ethyl-2-oxazolin) durch Hydroxylradikale vervollständigt um somit einen Überblick über einen Molmassenbereich von 2 bis 500 kg/mol zu ermöglichen. Die erhaltenen Daten bestätigen die früheren Ergebnisse

zum Anstieg der scheinbaren Abbaurate mit steigender Kettenlänge durch selbstinhibitorische Endgruppeneffekte für alle drei Polymerspezies (vgl. Abbildung 6.2). Die Oxidation

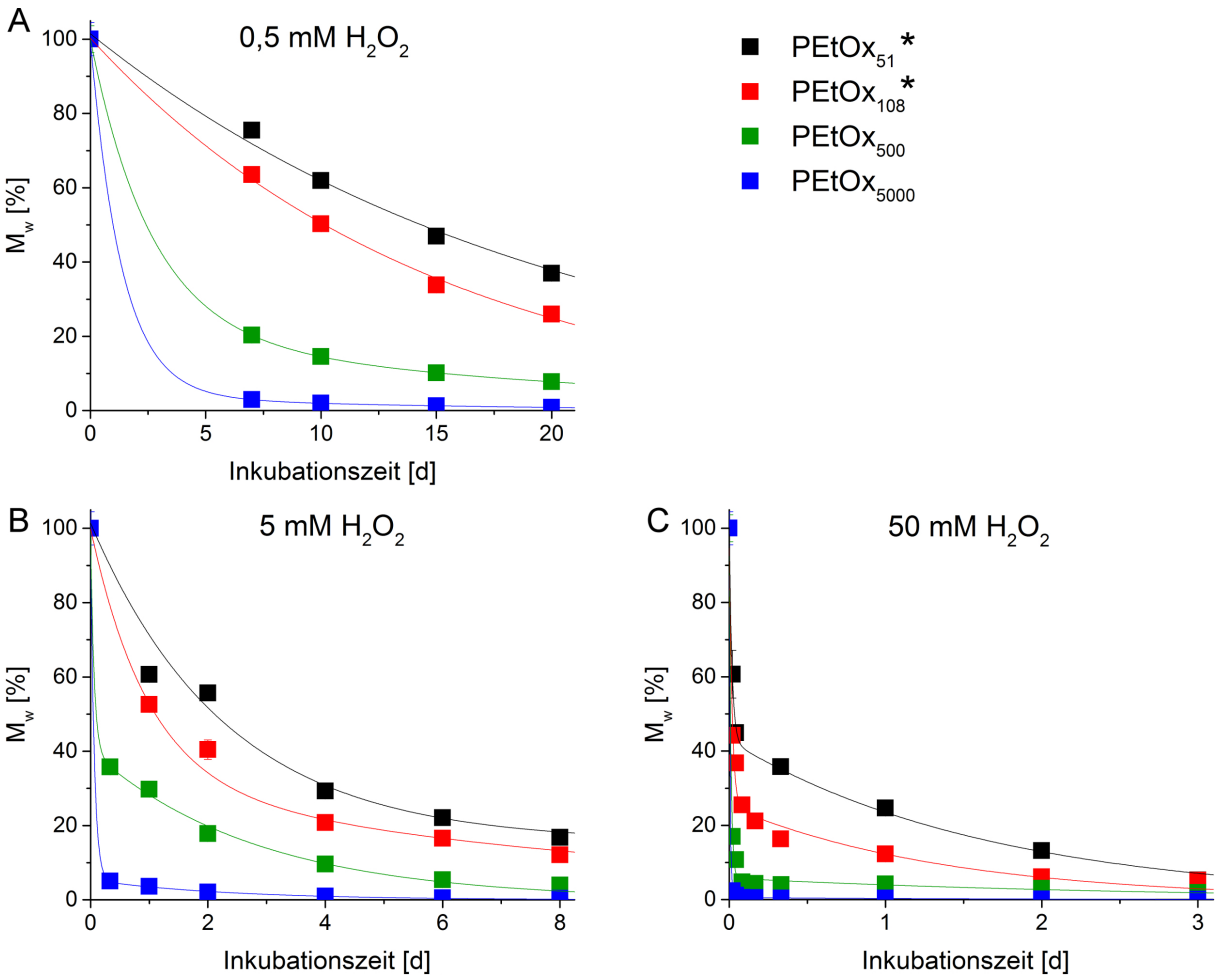

Abbildung 6.2: Entwicklung der molaren Masse von Polymeren in Abhängigkeit von ihrer ursprünglichen molaren Masse während des oxidativen Abbaus durch Hydroxylradikale, die *in situ* durch Fenton-artige Reaktion von 0.5 bis 50 mM H_2O_2 und 50 μM $CuSO_4$ erzeugt werden am Beispiel von PEtOx. Daten sind als Mittelwert ± Standardfehler (n = 3) dargestellt, Linien dienen der Orientierung. *Daten übernommen aus Quelle [169].

von Endgruppen statt des Polymerrückgrates verbraucht reaktive Sauerstoffspezies und verlangsamt dadurch die Kettenspaltung, was besonders bei Polymeren mit geringem Polymerisationsgrad und entsprechend großem Anteil terminaler Gruppen deutlich ins Gewicht fällt. Da jede Spaltung des Polymerrückgrates zwei zusätzliche Kettenenden erzeugt, erhöht sich deren Anteil währen der Oxidation erheblich, was mit entsprechender Abnahme der scheinbaren Abbaurate einhergeht.

Schließlich sollte durch Einbeziehung weiterer oxidativer Spezies das Ausmaß des oxidativen

Abbaus durch schwächere Oxidationsmittel eingeschätzt werden. Im direkten Vergleich von Wasserstoffperoxid mit und ohne zusätzlicher Zugabe von Kupfersulfat werden sowohl für Polyethylenglycol als auch für Polysarkosin siginifikant geringere scheinbare Abbauraten deutlich wenn ausschließlich Wasserstoffperoxid eingesetzt wird, was angesichts des höheren oxidativen Potentials von Hydroxylradikalen im Vergleich zu Wasserstoffperoxid leicht nachvollziehbar ist. Desweiteren zeigte sich, dass durch 0.5 mM Hypoxanthin und 20 U/L Xanthinoxidase gebildetes Superoxid innerhalb von 24 h Inkubation keinen signifikanten Effekt auf die Molmassenverteilung von Polyethylenglycol und Polysarkosin hat, während die Inkubation mit Hypochloriger Säure die partielle Zersetzung der Polymere initiiert. Interessanterweise zeigen die Elugramme von Polyethylenglycol nach Inkubation mit 50 mM Hypochlorige Säure eine ausgeprägte hochmolekulare Schulter, die vermutlich auf Kettenrekombination zurückzuführen ist. Hypochlorige Säure reagiert in wässriger Lösung auf vielfältige Weise, wobei unter anderem Hydroxylradikale und Singulett-Sauerstoff aber auch Hydroxidionen entstehen und somit eine Vielzahl von Polymermodifikations- und Abbaureaktionen möglich machen.
Die Untersuchung vollständig oxidativ abgebauter Polyethylenglycol, Poly(2-alkyl-2-oxazolin), Polypeptoid und Poly(*N*-vinylpyrrolidon) Spezies mittels GC/MS erzielte im Falle von Polyethylenglycol und den Polypeptoiden keine bzw. kaum aussagekräftige Ergebnisse, während die für Poly(*N*-vinylpyrrolidon) erhaltenen Daten gut mit in der Literatur beschriebenen Mechanismen des oxidativen Poly(*N*-vinylpyrrolidon)-Abbaus korrelieren. Im Falle der Poly(2-alkyl-2-oxazolin)e sind die erhaltenen GC/MS Daten weniger deutlich, legen aber sowohl die Abspaltung der Seitenketten als auch die Spaltung des Polymerrückgrates unter Bildung von Acetaldehyd, Acetamid und Kohlenstoffdioxid nahe.

Die tatsächlichen Konzentrationen reaktiver Sauerstoffspezies *in vivo* werden kontrovers diskutiert, hinsichtlich ihrer großen Vielfalt und breiten Verteilung im Körper ist es jedoch durchaus wahrscheinlich, dass die untersuchten Polymere *in vivo* in unterschiedlichem Maße dem oxidativen Abbau unterliegen. Dabei sind nicht nur die Abbauraten, sondern auch der Mechanismus und die entsprechend gebildeten Abbauprodukte von der Art der reaktiven Spezies, der Polymerstruktur und der entsprechenden Kettenlänge abhängig.
Weiterführende Studien sollten sich insbesondere mit der Aufklärung des Mechanismus des oxidativen Abbaus von Polypeptoiden und Poly(2-alkyl-2-oxazolin)en befassen. Dafür können kleinere Modelmoleküle wie z.B. Dimere, Trimere und Tetramere von Sarkosin,

N-ethylglycin, 2-Methyl-2-oxazolin und 2-Ethyl-2-oxazolin sukzessiv durch Wasserstoffperoxid oxidiert und abgebaut werden. Die dabei frei werdenden Abbauprodukte können mittels ^{1}H-, ^{13}C- and ^{15}N-NMR Spektroskopie sowie GC/MS Messungen identifiziert werden und Rückschlüsse auf ablaufende Mechanismen und eventuelle toxische Nebeneffekte des oxidativen *in vivo* Abbaus von Pseudo-Polypeptiden ermöglichen.

Hydrolyse

Blut und die meisten Gewebe des menschlichen Körpers sind auf einen leicht alkalischen pH-Wert angewiesen. Dennoch weisen spezifische Regionen wie den Magen oder Tumorgewebe ein saures Milieu auf, welches eventuell in der Lage ist, Amidbindungen, wie sie in Poly(2-alkyl-2-oxazolin)en und Polypeptoiden enthalten sind, zu spalten.

Frühere Ergebnisse zur sauren Hydrolyse von Poly(2-alkyl-2-oxazolin)en, welche die Seitenkettenabspaltung unter Bildung von toxischem Polyethylenimin (PEI) während der Magenpassage als unbedenklich einstufen, können im Rahmen dieser Arbeit bestätigt werden. Im Anschluss wird das in diesem Zusammenhang entwickelte experimentelle Verfahren zur Untersuchung der Hydrolyse von Polysarkosin durch 6 M HCl bei 37, 55, 75, 90 und 99 °C sowie durch simulierte Magenflüssigkeit (SGF) und simulierte Darmflüssigeit (SIF) bei 37 °C genutzt. Im Gegensatz zur Hydrolyse von Poly(2-alkyl-2-oxazolin)en, welche in Abspaltung der Seitenkette resultiert, kommt es bei der Hydrolyse von Polypeptoiden zur Spaltung des Polymerrückgrates, welche mit einer drastischen Verringerung der Kettenlänge und, mit fortschreitender Hydrolyse, mit der Freisetzung der entsprechenden Aminosäure einhergeht. Die Hydrolyse von Polysarkosin wird durch Quantifizierung des freigesetzten Sarkosins via ^{1}H-NMR Spektroskopie sowie durch Bestimmung des M_w via GPC verfolgt. Dabei zeigt sich, dass sich das zyklische Dimer Sarkosinanhydrid als Zwischenprodukt der Hydrolyse durch Zyklisierung instabiler linearer Dimere bildet.

Die Hydrolyse von Polysarkosin durch 6 M HCl bestätigt die vermutete starke Temperaturabhängigkeit der Polysarkosinspaltung (vgl. Abbildung 6.3). Durch Reduzierung der Inkubationstemperatur auf 37 °C kommt es zu einer erheblichen Verringerung der Freisetzung von Sarkosin und Sarkosinanhydrid. Dies wird noch deutlicher bei Verwendung von SGF und SIF statt 6 M HCl, wodurch trotz einer Inkubationszeit von 14 d nur vernachlässigbare Mengen Sarkosin gebildet werden. In diesem Zusammenhang ist zu beachten, dass sich bereits durch Zugabe von Polysarkosin zu SGF der pH-Wert der Lösung von ca. 1.1 auf 6.5 erhöhte und somit keine weitere ausgeprägte Hydrolyse zu erwarten war.

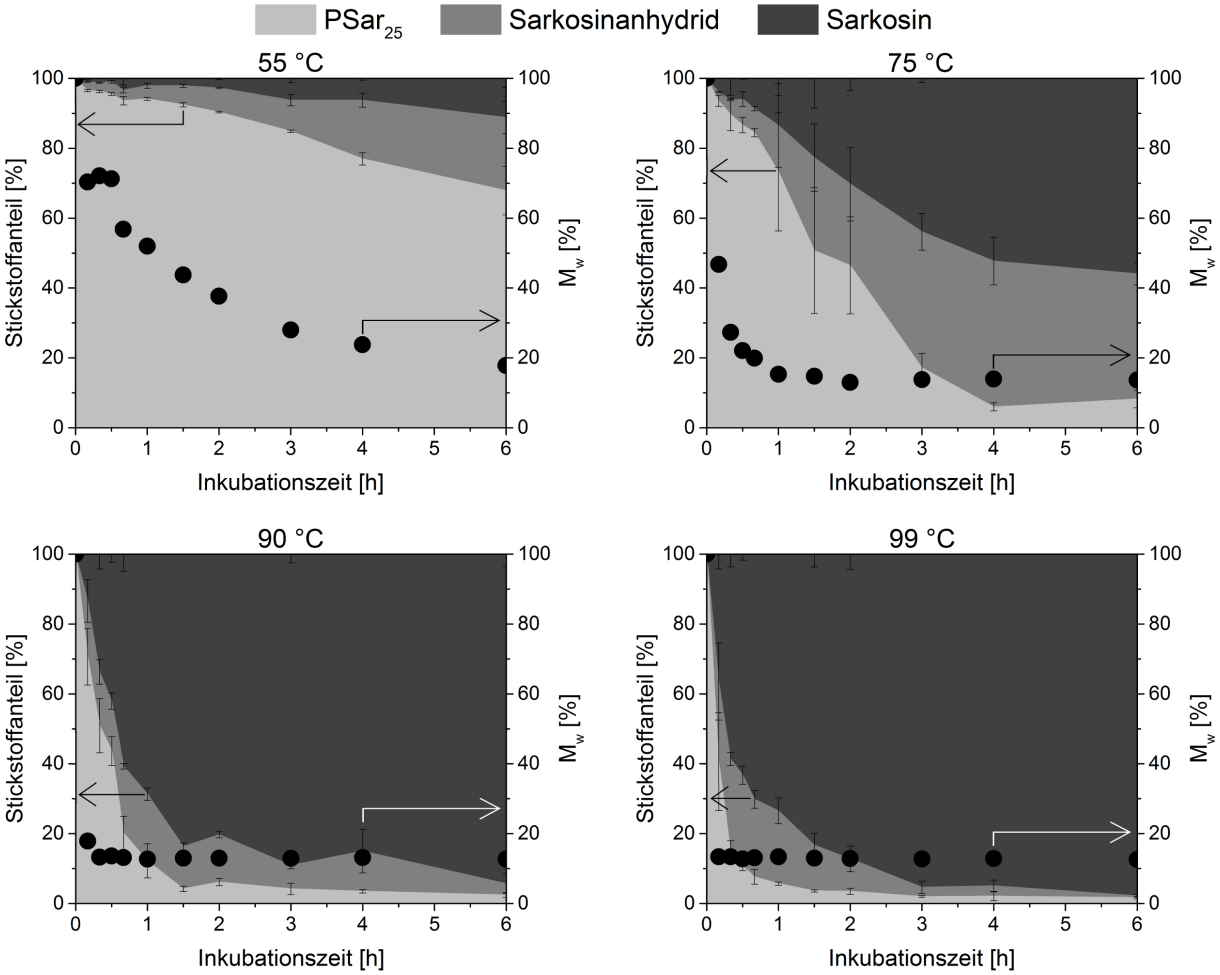

Abbildung 6.3: Kinetische Plots der durch ^{1}H-NMR Spektroskopie bestimmten Anteile des in Polysarkosin (hellgrau), Sarkosinanhydrid (grau) und Sarkosin (dunkelgrau) gebundenen Stickstoffs sowie das zugehörige via GPC ermittelte M_w während der Hydrolyse von Polysarkosin durch 6 M HCl bei 55 bis 99 °C. Daten sind als Mittelwert ± Standardfehler (n = 3) dargestellt.

Dennoch bestätigen die Freisetzung von Sarkosinanhydrid und die Abnahme des M_w um 15 % innerhalb der ersten 4 h der Inkubation den partiellen Abbau von Polysarkosin unter den gewählten Bedingungen.

In Anbetracht der vorstehenden Ergebnisse kann vermutet werden, dass es während der Passage des menschlichen Magens mit einer maximalen Verweilzeit von 4 h zur Fragmentierung von Polysarkosin durch saure Hydrolyse kommt. Im Gegensatz zur Hydrolyse von Poly(2-alkyl-2-oxazolin)en, in deren Fall die Spaltung von Amidbindungen nicht in einer Verkürzung der Polymerketten sondern in der Bildung von toxischem PEI resultiert,

erfolgt die Hydrolyse von Amidbindungen des Polysarkosins durch Spaltung des Polymerrückgrates unter Bildung kürzerer Polysarkosinketten, welche schneller aus dem Körper ausgeschieden und daher als unbedenklich eingestuft werden können.
Um das Ausmaß der Hydrolyse von Polysarkosin während der Magenpassage genauer abschätzen zu können sollten die Experimente mit SGF unter deutlichem Überschuss der Säure wiederholt werden.

Enzymatischer Abbau

Die Modifikation und der Abbau von Bio(makro)molekülen sind essentieller Bestandteil des menschlichen Metabolismus. Polymere, die wie die Poly(2-alkyl-2-oxazolin)e und Polypeptoide Amidbindungen und damit große Ähnlichkeit zu den natürlich vorkommenden und weit verbreiteten Polypeptiden aufweisen, bergen das Potential einer möglichen Bioabbaubarkeit durch (mehr oder weniger spezifische) Peptidasen. Wie die im Vorangegangenen beschriebende saure Hydrolyse resultiert auch die Einwirkung von Peptidasen in der Spaltung von Amidbindungen.
Ziel der vorliegenden Arbeit war die Evaluierung der Stabilität von Poly(2-alkyl-2-oxazolin)en und Polypeptoiden sowie Polyethylenglycol als Referenzpolymer ohne Amidbindungen unter Bedingungen, welche den *in vivo* vorliegenden Verhältnisse möglichst ähnlich sind. In ersten Experimenten liegt der Schwerpunkt auf der Inkubation Farbstoff-markierter Polymere in Homogenaten von frisch entnommenen Rattenlebern und -nieren. Obwohl die erhaltenen Ergebnisse zum Großteil vielversprechend sind, bestehen aus einer Vielzahl von Gründen Zweifel an ihrer Zuverlässigkeit und Reproduzierbarkeit.
Die Inkubation von nicht marktierten Polymeren in frisch gelegten Hühnereiern liefert aussagekräftigere Ergebnisse.
Nach Inkubation für 40 d weisen die Elugramme von Polyethylenglycol, Poly(2-methyl-2-oxazolin) und Polysarkosin (Abbildung 6.4) mit verschiedenen terminalen Gruppen klar unterscheidbare und in Abhängigkeit von der Polymerstruktur stehende Muster auf. Es sind keine Hinweise auf einen enzymatischen Abbau von Polyethylenglycol in Hühnereiweiß ersichtlich. Abweichungen der Elugramme des Poly(2-methyl-2-oxazolin)s deuten auf eine Modifikation während der Inkubation hin, die jedoch vermutlich nicht enzymatischen Ursprungs ist. Im Gegensatz dazu zeigen die Polysarkosin-Proben in Abhängigkeit der entsprechenden C- und N-terminalen Gruppen charakteristische Elugrammmodifikationen, welche auf die Aktivität von Exo- und Endopeptidasen hindeuten. Dennoch muss erwähnt

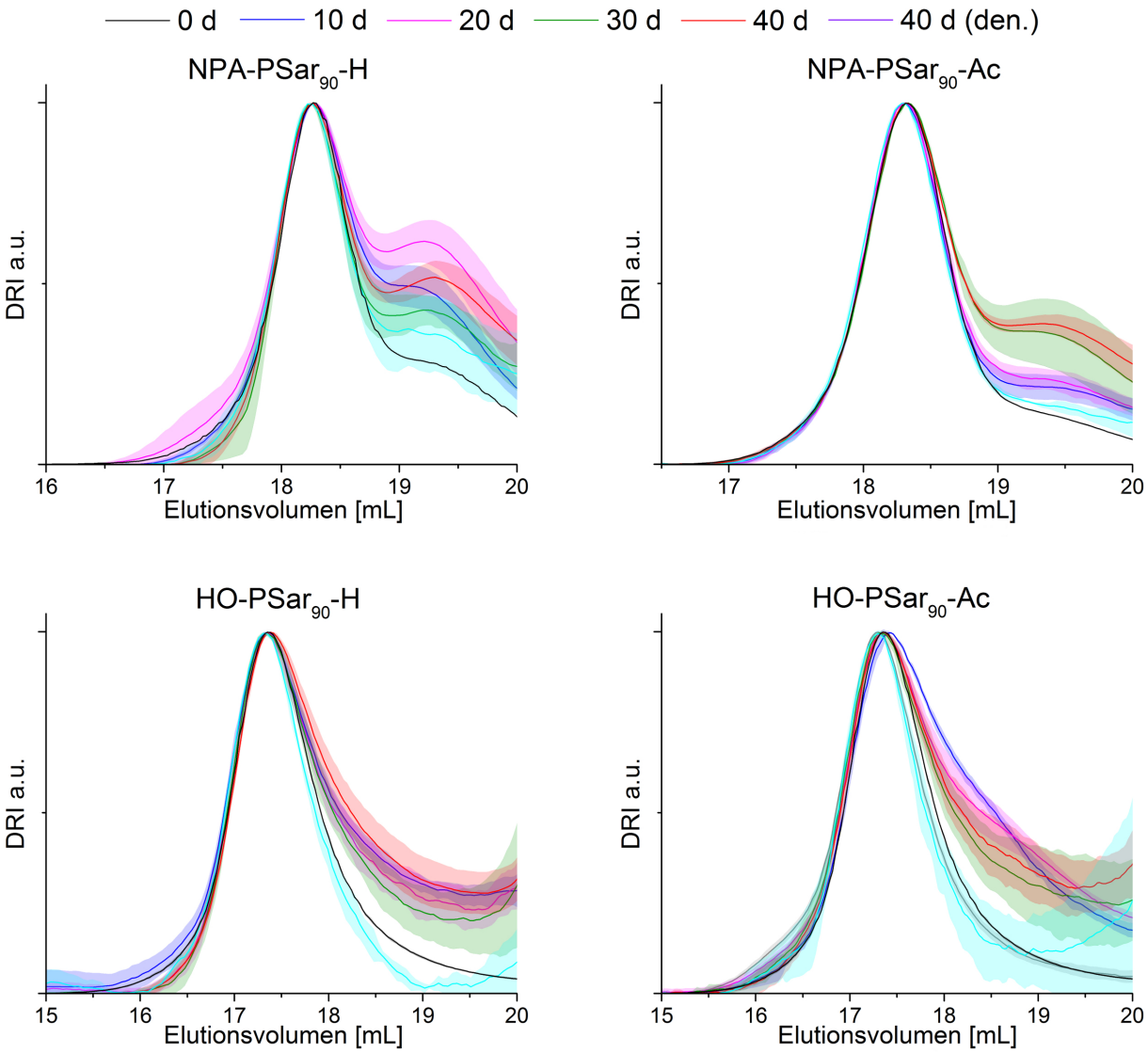

Abbildung 6.4: Normalisierte GPC Elugramme der in Hühnereier injizierten Polysarkosin-Proben mit verschiedenen Endgruppen nach Inkubation bei 37 °C. Daten sind als Mittelwert ± Standardabweichung (n = 6) dargestellt.

werden, dass die enzymatische Abbaubarkeit von Polysarkosin nicht zwingend den Abbau von Polypeptoiden mit längeren Seitenketten impliziert, was Gegenstand weiterer Untersuchungen sein sollte.

Da die durchgeführten *in ovo* Experimente sehr vielversprechende Ergebnisse hervorgebracht haben, sollten sich weiterführende Studien mit der Langzeitstabilität von Pseudo-Polypetiden in Versuchstieren befassen. Zu diesem Zweck können unterschiedlich radioaktiv markierte Polymere (C- bzw. N-terminal und Markierung der Seitenketten) eingesetzt werden. Es ist zu erwarten, dass der überwiegende Anteil der injizierten Polymerspezies

innerhalb kurzer Zeit ausgeschieden wird. Um die Anreicherung und den Abbau der Polymere *in vivo* zu untersuchen, sollte die Gabe daher über einen längeren Zeitraum erfolgen, was durch multiple Injektionen oder durch kontrollierte Langzeitabgabe durch eine implantierte Kapsel erfolgen kann. Nach einigen Monaten können verschiedene Organe wie Leber, Niere und Milz entnommen, Polymerbestandteile extrahiert und im Hinblick auf ihre Größe via GPC mit angeschlossenem Radioaktivitätsdetektor untersucht werden. Darauf aufbauend ist es möglich, einzelne Enzyme aus den entsprechenden Organen zu isolieren oder mit spezifischen Enzymmixen (z.B. S9-Mix) den Abbau der Polymerspezies *in vitro* zu untersuchen, um dadurch die Anzahl in Frage kommender Enzyme einzuschränken und schließlich diejenigen zu identifizieren, die in der Lage sind Polypeptoide bzw. Poly(2-alkyl-2-oxazoline) abzubauen.

Die vorliegende Arbeit bietet einen Überblick über die wichtigsten Möglichkeiten des Polymerabbaus *in vivo*. Poly(2-alkyl-2-oxazolin)e und Polypeptoide unterliegen nicht nur dem Abbau unter oxidativen Bedingungen, sondern auch der Modifikation bzw. Kettenspaltung unter sauren Bedingungen. Zudem weisen die erhaltenen Ergebnisse auf die enzymatische Abbaubarkeit von Polysarkosin durch in Hühnereiweiß enthaltene Enzyme hin.
Neben den an anderer Stelle umfangreich beschriebenen positiven Eigenschaften der Poly(2-alkyl-2-oxazolin)e und Polypeptoide unterstreicht ihre wahrscheinliche langsame, aber stetige Bioabbaubarkeit die Rolle beider Polymerklassen als vielversprechende zukünftige Biopolymere.

7 Experimental

7.1 Equipment

Glovebox

Polymerizations were intiated under the dry conditions of a *LabMaster 130* glovebox (*MBraun*, Garching, Germany) comprising nitrogen atmosphere (5.0).

Melting Point Determination

Melting points were measured using a *KSP1N* instrument (*KRÜSS*, Hamburg, Germany) with a heating rate of 1 K/min.

Infrared Spectroscopy

IR spectra were recorded on a *FT/IR-4100* spectrometer (*JASCO*, Groß-Umstadt, Germany) with *PIKE MIRacle* single reflection attenuated total reflection sampling accessory (ZnSe crystal, *PIKE Technologies*, Madison, Wisconsin, USA) and a deuterated triglycine sulfate (DTGS) detector. Evaluation of the obtained spectra was performed using the corresponding *JASCO spectra manager* software.

Nuclear Magnetic Resonance Spectroscopy

NMR spectra were recorded on a *Fourier 300* spectrometer (^{1}H; 300 MHz and ^{13}C{^{1}H}; 75 MHz; *Bruker Biospin*, Rheinstetten, Germany) at a temperature of 25 °C and evaluated using *MestReNova* software (*Mestrelab Research*, Santiago de Compostela, Spain). Spectra were calibrated using residual solvent signals ($CHCl_3$ 7.26 ppm, D_2O 4.67 ppm, DMSO-d_6 2.50 ppm, MeOD 3.31 ppm) or the internal standard trimethylsilylpropanoic acid (TMSP) (0.00 ppm). Multiplicities of signals are categorized as follows: singlet (s), doublet (d), triplet (t), quartet (q), quintet (quin), doublet of triplets (dt), multiplet (m), broad (b).

UV/Vis Spectroscopy

UV/Vis spectra were recorded using a *Varian Cary 50 UV-Vis* spectrophotometer (*Agilent Technologies*, Santa Clara, USA).

Fluorescence Spectroscopy

Fluorescence spectroscopy was performed using a *FP-8300* spectrometer (*JASCO*, Groß-Umstadt, Germany). Samples were tempered at 20 °C with a thermo-electrical Peltier cuvette holder. Obtained spectra were evaluated using *JASCO spectra manager* software.

Gel Permeation Chromatography

Depending on the solvent, GPC measurement was performed on one of the following systems:

HFIP GPC was carried out on a *Polymer Standard Service SECurity* (*PSS*, Mainz, Germany) system with a MDS RI detector (*Agilent Technologies*, Santa Clara, USA) using a 50 mm PFG precolumn and three 300 mm PFG columns (pore size 7 μm). HFIP was supplemented with 5 mmol/L ammonium trifluoroacetate. Columns were heated to 40 °C and the flow rate was set to 1 mL/min. Prior to each measurement, samples were filtered through 0.2 μm PTFE syringe filters (*A-Z Analytik-Zubehör*, Langen, Germany). Calibration was performed using poly(methyl methacrylate) standards (PSS) with molar masses from 800 g/mol to 1600 kg/mol. Data were processed using WinGPC software.

DMF GPC was performed on the same *Polymer Standard Service SECurity* (*PSS*, Mainz, Germany) system with a MDS RI detector (*Agilent Technologies*, Santa Clara, USA) using a 50 mm GRAM precolumn (pore size 30 Å) and a 300 mm GRAM column (pore size 1000 Å). DMF was supplemented with 1 g/L LiBr, columns were heated to 40 °C and the flow rate was adjusted to 1 mL/min. The system was calibrated using PEG standards with molar masses ranging from 106 g/mol to 1015 kg/mol. Sample preparation and evaluation was performed as described for the HFIP GPC.

Water GPC was conducted on a *Viscotek GPCmax* (*Malvern*, Herrenberg, Germany) with a *Viscotek* RI detector using two 300 mm *Viscotek* A-Columns A6000M (porous poly(hydroxyethylmethacrylate) with a particle size of 13 µm) at 35 °C. Calibration was performed using PEG standards with molar masses ranging from 106 g/mol to 1015 kg/mol. Sample preparation was conducted as described for the HFIP GPC. Evaluation was performed using *OmniSEC* software (*Malvern*, Herrenberg, Germany).

Gas Chromatography - Mass Spectrometry

GC/MS was performed by Dr. Oliver Tröppner and Carina Süßmeier at the Süddeutsches Kunststoff-Zentrum (SKZ) using the thermal desorber TurboMatrix 650 ATD (*Perkin Elmer*, Rodgau, Germany), the Clarus 500 GC gas chromatograph (*Perkin Elmer*) and the Clarus 560 MS mass spectrometer (*Perkin Elmer*) with helium as carrier gas and an Elite-5MS capillary column (*Perkin Elmer*). The following temperature program was used: isothermal at 50 °C for 2 min, with 25 K/min to 160 °C, with 10 K/min to 280 °C, isothermal for 30 min at 280 °C. Transfer line temperature was maintained at 280 °C and mass spectra were recorded from 29 to 450 amu with > 2 scans/s.

Water Determination according to Karl Fischer

Water content of the applied solvents was determined by coulometric titration using a *TitroLine 7500 KF trace* (*SI analytics*, Mainz, Germany).

Homogenization

Fresh, iced rat organs were reduced to small pieces with a scalpel and homogenized using either a *T25 Ultra-Turrax* dispersing instrument (*IKA*, Staufen, Germany) or a *BeadBug* homogenizer (*Süd-Laborbedarf GmbH SLG*, Gauting, Germany) and stainless steel beads (ø = 1.0 mm, *Kugel-Rollen UG*, Röthlein, Germany).

Incubation

Samples were incubated at 37 °C in a *FD 53* oven (*Binder*, Tuttlingen, Germany).

7.2 Reagents and Solvents

All chemicals and solvents were purchased from Sigma-Aldrich, Acros or Roth and used as received unless otherwise stated. Benzonitrile (PhCN) was dried by refluxing over P_2O_5, benzylamine over BaO, and methyl trifluoromethanesulfonate (MeOTf) as well as 2-ethyl-2-oxazoline (EtOx) over CaH_2 under dry argon atmosphere and subsequent distillation prior to use. Acetonitrile (ACN) and chloroform were dried by storage over 3 Å and 4 Å molecular sieve, respectively.

7.3 Methods

7.3.1 Synthesis of Sarcosine *N*-carboxyanhydride

Large proportions of the applied Sar-NCA were kindly provided by Fabian Wieghardt and synthesized repeatedly over the course of this studies following a modified procedure of Fetsch and coworkers.[55] For short, dry sarcosine and toluene were stirred to yield a fine suspension. Diphosgene was added and the reaction mixture was heated to 65 °C and stirred for 2 h to obtain a clear solution. The solvent was evaporated under reduced pressure and the residual was dried at 75 °C under reduced pressure yielding a brown solid, which was purified by sublimation (p < 0,05 mbar, 85 °C) to obtain Sar-NCA as a colorless solid.

Yield: 60 - 80 %

Melting point: 102 - 105 °C (literature: 103 - 105 °C)[417]

^{1}H-NMR (300 MHz, DMSO-d_6): δ = 2.85 (3 H, s, H^1), 4.21 (2 H, s, H^2)

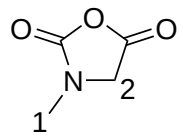

7.3.2 Polymer Synthesis

7.3.2.1 Poly(2-alkyl-2-oxazoline)s

General Procedure

Monomers (2-methyl-2-oxazoline (MeOx) or EtOx) and MeOTf were dissolved in dry solvent. The solution was heated to 85 °C and stirred for several days. After allowing the solution to cool down to RT, piperazine or piperidine were added to terminate the polymerization and the mixture was stirred over night. Sodium carbonate (1.5 eq) was added and the turbid solution was stirred over night again. The solvent was evaporated under reduced pressure and the residual solid was dissolved in a 2:1 (v/v) mixture of MeOH/$CHCl_3$, filtered and precipitated from cold diethyl ether. After precipitation, the mixture was centrifuged, decanted and the procedure repeated twice. Finally, the residual was collected in millipore water and freeze dried to obtain a colorless solid.

As an alternative approach, purification was performed via dialysis against millipore water using a Spectra/POR® dialysis membrane (1kD) and subsequent freeze-drying.

$PEtOx_{51}$

The synthesis of $PEtOx_{51}$ was conducted during the preceding master thesis and was described before.[169, 218]

Label: UBJ039

EtOx: 1.99 g (20.0 mmol)

MeOTf: 65 mg (0.40 mmol)

Solvent: acetonitrile (ACN), 13 mL

Monomer-to-initiator ratio: 50:1

Polymerization time: 3 d

Termination: piperazine (750 mg, 8.71 mmol, 22 eq)

Purification: precipitation

Yield: 1.77 g (88.1 %)

GPC (HFIP): M_n = 15.4 kg/mol, Đ = 1.09

^{1}H-NMR (300 MHz, D_2O): δ = 0.94 (152 H, br, H^5), 2.25 (102 H, br, H^4), 2.56 (6 H, br, H^3), 2.83 (3 H, br, H^1), 3.41 ppm (184 H, br, H^2)

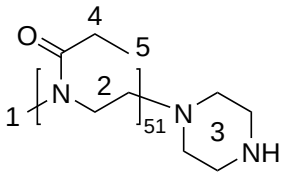

$PEtOx_{108}$

The synthesis of $PEtOx_{108}$ was conducted during the preceding master thesis and was described before.[169, 218]

Label: UBJ040

EtOx: 1.91 g (19.30 mmol)

MeOTf: 21 mg (0.13 mmol)

Solvent: ACN, 13 mL

Monomer-to-initiator ratio: 150:1

Polymerization time: 7 d

Termination: piperazine (375 mg, 4.35 mmol, 34 eq)

Purification: precipitation

Yield: 1.48 g (77.1 %)

GPC (HFIP): M_n = 20.9 kg/mol, Đ = 1.08

^{1}H-NMR (300 MHz, D_2O): δ = 0.94 (324 H, br, H^5), 2.25 (216 H, br, H^4), 2.56 (8 H, br, H^3), 2.96 (3 H, br, H^1), 3.41 ppm (432 H, br, H^2)

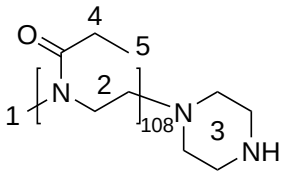

PMeOx$_{90}$

Label: UBJ073

MeOx: 6.36 g (74.7 mmol)

MeOTf: 135 mg (0.82 mmol)

Solvent: benzonitrile, 20 mL

Monomer-to-initiator ratio: 90:1

Polymerization time: 1 d

Termination: piperidine (210 mg, 2.47 mmol, 3 eq)

Purification: dialysis

Yield: 5.86 g (91.6 %)

GPC (DMF): M_n = 5300 g/mol, Đ = 1.24

GPC (H_2O): M_n = 2350 g/mol, Đ = 1.09

^{1}H-NMR (300 MHz, D_2O): δ = 2.02 (264 H, br, H^4), 2.60 (6 H, br, H^3), 2.94 (3 H, br, H^1), 3.47 ppm (351 H, br, H^2)

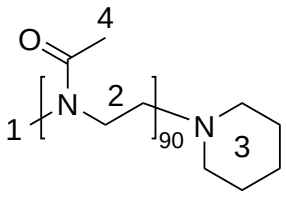

7.3.2.2 Polypeptoids

General Procedure

Sar-NCA was dissolved in dry solvent and the initiator was added to initiate the polymerization. The reaction mixture was stirred over night in the dark at RT under a constant

pressure of 50 mbar. Subsequently, the solvent was evaporated under reduced pressure and the residual dissolved in a 2:1 (v/v) mixture of MeOH/$CHCl_3$. The clear solution was precipitated from cold diethyl ether and centrifuged. The solid was decanted, dried, dissolved in a 2:1 (v/v) mixture of MeOH and $CHCl_3$ and the procedure was repeated twice. Finally, the product was dissolved in millipore water and freeze-dried to obtain a colorless solid.

As an alternative approach, purification was performed via dialysis against millipore water using a Spectra/POR® dialysis membrane (1kD) and subsequent freeze-drying.

$PSar_{138}$

The synthesis of $PSar_{138}$ was conducted by Julian Schreck and described previously.[379]

Label: SEJ004

Sar-NCA: 2.69 g* (23.4 mmol*)

Initiator: benzylamine, 16.7 mg (0.16 mmol)

Solvent: benzonitrile, 23 mL

Monomer-to-initiator ratio: 150:1

Polymerization time: 4 d

Purification: precipitation

Yield: 1.09 g (64.9 %*)

GPC (DMF): M_n = 7000 g/mol, Đ = 1.06

^{1}H-NMR (300 MHz, D_2O): δ = 3.00 (413 H, br, H^3), 4.32 (272 H, br, H^2), 7.39 ppm (5 H, br, H^1)

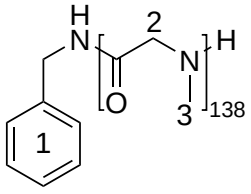

**Calculated based on the quantity of benzylamine and the monomer-to-initiator ratio, as the exact weighing of Sar-NCA was not documented.*

$PSar_{25}$

Label: UBJ083

Sar-NCA: 4.09 g (35.6 mmol)

Initiator: benzylamine, 158 mg (1.48 mmol)

Solvent: benzonitrile, 35 mL

Monomer-to-initiator ratio: 24:1

Polymerization time: 4 d under glovebox atmosphere

Purification: precipitation

Yield: 2.44 g (90.3 %)

GPC (DMF): M_n = 1950 g/mol, Đ = 1.12

^{1}H-NMR (300 MHz, D_2O): δ = 3.00 (87 H, br, H^3), 4.32 (65 H, br, H^2), 7.39 ppm (5 H, br, H^1)

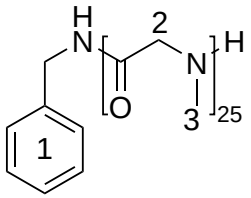

PSar$_{333}$

The synthesis of PSar$_{333}$ was conducted by Fabian Wieghardt and described previously.[385]

Label: WEF015

Sar-NCA: 408 mg (3.5 mmol)

Initiator: benzylamine, 1.1 mg (0.01 mmol)

Solvent: benzonitrile, 3.5 mL

Monomer-to-initiator ratio: 350:1

Polymerization time: 1 d

Purification: precipitation

Yield: 229 mg (91.8 %)

GPC (HFIP): M_n = 62 kg/mol, Đ = 1.07

^{1}H-NMR (300 MHz, D_2O): δ = 3.00 (1002 H, br, H^3), 4.30 (665 H, br, H^2), 7.35 ppm (5 H, br, H^1)

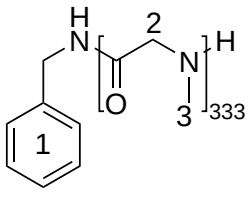

$PSar_{333}$-FITC

Label: WEF018

Fluorescence labeling of $PSar_{333}$ with FITC was conducted by Fabian Wieghardt and described previously.[385]

Labeling of $PSar_{333}$ with a fluorescent dye enables the detection of lower amounts of polymer due to the high sensitivity of fluorescence measurement. For this purpose, $PSar_{333}$ (52 mg, 0.002 mmol, 1 eq), FITC (8.2 mg, 0.021 mmol, 10 eq) and potassium carbonate (2.0 mg, 0.014 mmol, 7 eq) were dissolved in 1 mL DMF and shaken vigorously over night. Subsequently, the solvent was evaporated under reduced pressure, the residual solid was collected in millipore water and freeze-dried. Purification and removal of non-bound FITC was ensured by separation of the mixture using a Sephadex® LH-20 column (*GE Healthcare Life Sciences*, Freiburg, Germany) comprising 1 g Sephadex® LH-20 in millipore water. Labeling efficiency was determined using UV/Vis spectroscopy amounting to only 3.0 %. Fluorescence intensity at 518 nm was measured using an excitation wavelength of 494 nm.

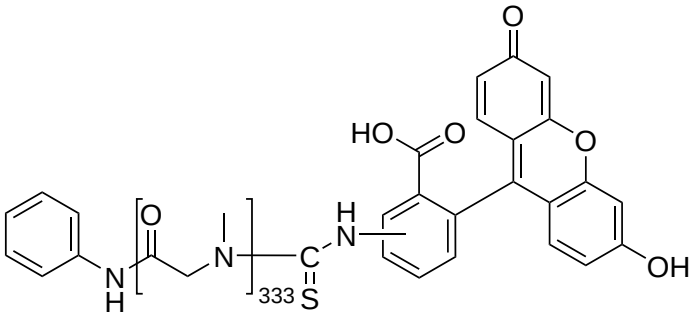

SulfoPBI-$PSar_{185}$

The synthesis of SulfoPBI-$PSar_{185}$ was conducted by Maria Krebs and described in detail previously.[388]

Label: KEM008

Sar-NCA: 257 mg (2.23 mmol)

Initiator: SulfoPBI, 28.6 mg (0.022 mmol)

Solvent: DMF, 4 mL

Monomer-to-initiator ratio: 100:1

Polymerization time: 5 d under glovebox atmosphere

After 5 d of polymerization under glovebox atmosphere, the IR spectrum recorded to control the status of the polymerization still revealed peaks corresponding to the monomer.

In order to enhance the polymerization rate, 4-dimethylaminopyridine (DMAP) (10.9 mg, 0,089 mmol, 4 eq) was dissolved in 0.3 mL DMF and added to the reaction mixture. The IR spectrum recorded after further 3 d of continuously stirring revealed no more monomer peaks and the reaction was considered to be complete.

Purification: precipitation and subsequent dialysis

Yield: 133 mg (71.0 %)

GPC (DMF): M_n = 6400 g/mol, Đ = 1.31

^{1}H-NMR (300 MHz, MeOD): δ = 3.00 (555 H, br, H^1), 4.6 (370 H, br, H^2), 6.90 (2 H, d, $^3J_{H,H}$ = 7.6 Hz, H^3), 7.39 (8 H, br, H^4), 7.29 (1 H, br, H^5), 7.71 (8 H, br, H^6), 8.01 (2 H, d, $^3J_{H,H}$ = 7.6 Hz, H^3), 8.16 ppm (4 H, br, H^7)

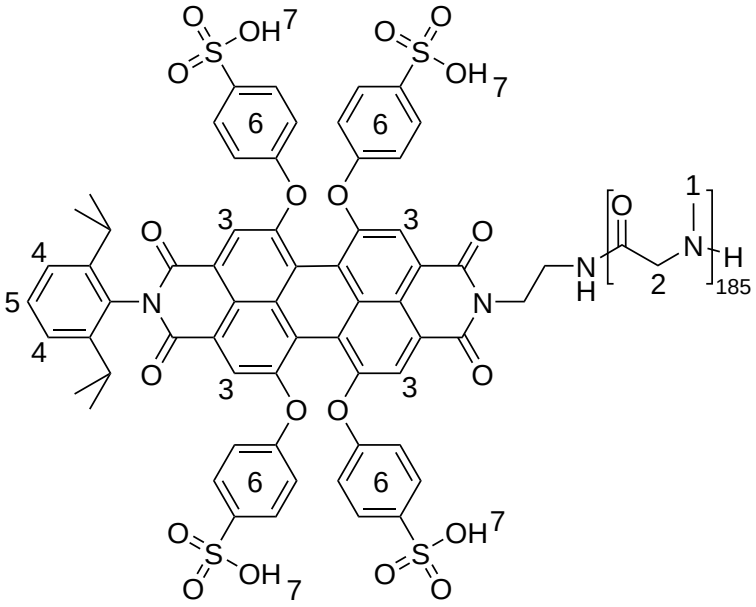

PSar$_{68}$

The synthesis of PSar$_{68}$ was conducted by Maria Krebs and described in detail previously.[388]

Label: KEM009

Sar-NCA: 4.32 g (37.5 mmol)

Initiator: benzylamine, 79.6 mg (0.74 mmol)

Solvent: benzonitrile, 18 mL

Monomer-to-initiator ratio: 51:1

Polymerization time: 3 d under glovebox atmosphere

Purification: precipitation

Yield: 2.0 g (80.9 %)

GPC (DMF): M_n = 4200 g/mol, Đ = 1.07

^{1}H-NMR (300 MHz, D_2O): δ = 2.95 (204 H, br, H^3), 4.20 (138 H, br, H^2), 7.25 ppm (5 H, br, H^1)

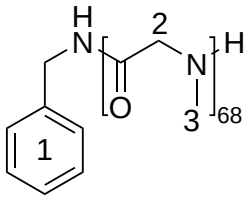

NPA-PSar$_{90}$-H

Label: UBJ074

Sar-NCA: 4.38 g (38.0 mmol)

Initiator: NPA, 37.3 mg (0.43 mmol)

Solvent: benzonitrile, 35 mL

Monomer-to-initiator ratio: 89:1

Polymerization time: 3 d

Subsequently, the mixture was divided into two approximately equal parts, one of which was further modified (see NPA-PSar$_{90}$-Ac).

Purification: precipitation and dialysis

Yield: 0.63 g (55.3 %*)

GPC (DMF): M_n = 5000 g/mol, Đ = 1.14

^{1}H-NMR (300 MHz, D_2O): δ = 0.91 (9 H, br, H^3), 3.02 (252 H, br, H^3), 4.33 ppm (167 H, br, H^2)

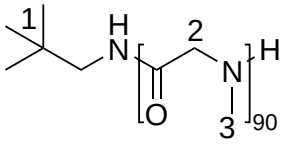

* *Calculated based on the assumption that the reaction mixture was divided exactly by half.*

NPA-PSar$_{90}$-Ac

Label: UBJ075

Approximately half of aforementioned reaction mixture was further modified by addition of TEA (296 μL, 2.14 mmol, 10 eq) and acetic anhydride (202 μL, 2.14 mmol, 10 eq) and stirring at RT over night.

Purification: precipitation and dialysis

Yield: 1.45 g (103.0 %*)

GPC (DMF): M_n = 5400 g/mol, Đ = 1.10

^{1}H-NMR (300 MHz, D_2O): δ = 0.91 (9 H, br, H^3), 2.10 (3 H, br, H^4), 3.02 (293 H, br, H^3), 4.33 ppm (194 H, br, H^2)

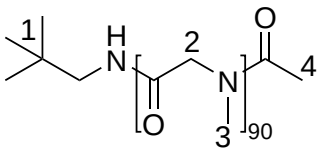

Calculated based on the assumption that the reaction mixture was divided exactly by half.

HO-PSar$_{90}$-H

Label: UBJ076

Sar-NCA: 4.06 g (35.3 mmol)

Initiator: water, 7.1 mg (0.39 mmol) and TEA, 98.0 mg (0.98 mmol, 2.5 eq)

Solvent: nitromethane, 40 mL

Monomer-to-initiator ratio: 89:1

Polymerization time: 3 d

Subsequently, the mixture was divided into two approximately equal parts, one of which was further modified (see HO-PSar$_{90}$-Ac).

Purification: precipitation and dialysis

Yield: 1.37 g (103.2 %*)

GPC (DMF): M_n = 6800 g/mol, Đ = 1.39

^{1}H-NMR (300 MHz, D_2O): δ = 3.02 (3 H, br, H^2), 4.35 ppm (2 H, br, H^1)

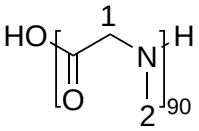

Calculated based on the assumption that the reaction mixture was divided exactly by half.

HO-PSar$_{90}$-Ac

Label: UBJ077

Approximately half of aforementioned reaction mixture was further modified by addition

of acetic anhydride (1.85 mL, 19.6 mmol, 25 eq) and stirring at RT over night.
Purification: precipitation and dialysis
Yield: 0.93 g (73.9 %*)
GPC (DMF): M_n = 7900 g/mol, Đ = 1.34
^{1}H-NMR (300 MHz, D_2O): δ = 2.13 (3 H, br, H^3), 3.02 (601 H, br, H^2), 4.33 ppm (401 H, br, H^1)

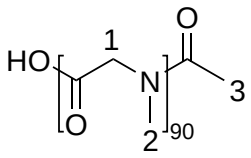

** Calculated based on the assumption that the reaction mixture was divided exactly by half.*

7.3.3 Incubation Experiments

7.3.3.1 Oxidative Degradation

Unless otherwise stated, experiments on the oxidative degradation of polymers were conducted in PBS comprising sodium chloride (8.00 g/L, 136.9 mmol/L), potassium chloride (0.20 g/L, 2.68 mmol/L), disodium hydrogen phosphate (1.42 g/L, 10.0 mmol/L) and potassium dihydrogen phosphate (0.27 g/L, 1.98 mmol/L), resulting in a pH value of 7.40 ± 0.01.

Polymers
In order to investigate the kinetics of oxidative degradation, different polymer species as well as polymers comprising similar structures but different chain lengths were investigated regarding their susceptibility towards oxidative deterioration. An overview about the applied polymers is given in Table 7.1.

Table 7.1: DP, molecular weight and source of polymers applied for experiments on oxidative degradation.

Polymer	**Label**	**DP**	**M_n [g/mol]**	**Source**
PEG	PEG_{45}	45[a]	2000	Roth #0154.1

Continued on next page

Continued from previous page

Table 7.1: DP, molecular weight and source of polymers used for degradation experiments.

Polymer	**Label**	**DP**	**M_n [g/mol]**	**Source**
	PEG_{136}	136[a]	6000	Acros #192280010
	PEG_{230}	230[a]	10000	Roth #2634.1
	PEG_{800}	800[a]	35000	Sigma Aldrich #81310
	PEG_{9100}	9100[a]	400000	Sigma Aldrich #372773[d]
polypeptoids	$PSar_{138}$	138[b]	10000[c]	synthesis (SEJ004)
POx	$PEtOx_{51}$	51[b]	5000[c]	synthesis (UBJ039)
	$PEtOx_{108}$	108[b]	11000[c]	synthesis (UBJ040)
	$PEtOx_{500}$	500[b]	50000[c]	Sigma Aldrich #372846
	$PEtOx_{5000}$	5000[b]	500000[c]	Kremer Pigmente #63905
PVP	PVP_{30}	30[b]	3500[c]	Acros #276142500
	PVP_{90}	90[b]	10000[c]	Sigma Aldrich #PVP10
	PVP_{360}	360[b]	40000[c]	Roth #4607.1
	PVP_{3250}	3250[b]	360000[c]	Roth #CP15.1

[a] *according to M_n*

[b] *determined by ^{1}H-NMR*

[c] *according to DP*

[d] *contained butylhydroxytoluene (BHT) as inhibitor which was removed via dialysis*

Incubation with H_2O_2

Incubation of the investigated polymers with H_2O_2 was investigated in presence of either 50 μM $CuSO_4$ or 50 μM $FeSO_4$ in order to generate hydroxyl radicals via a Fenton-like reaction or without further addition of metal ions.

In any case, polymers were dissolved to a concentration of 1 g/L in PBS and stored at 37 °C over night. Depending upon the experimental requirements, $CuSO_4$ or $FeSO_4$ or no further supplements and H_2O_2 (0.5, 5 or 50 mM) were added and samples shaken at 37 °C. Provided that the samples contained metal ions, addition of H_2O_2 was repeated every 24 h to replenish degraded H_2O_2. After defined periods of time, aliquots of 5 mL were

withdrawn and subsequently freeze-dried. The obtained salt-like residuals were dissolved in HFIP and analyzed via GPC.
Unless otherwise stated, all experiments were performed in triplicate.

Incubation with ClO^-

Experiments on the ClO^- induced oxidative degradation of PEG and PSar were conducted by Julian Schreck following the procedure previously described for H_2O_2.[379]
Polymers were dissolved to a final concentration of 1 g/L in PBS and incubated at 37 °C over night. Different concentrations of 0.5, 5 or 50 mM HClO were added and mixtures were shaken at 37 °C. Withdrawn aliquots of each 5 mL were freeze-dried and analyzed via GPC (HFIP).

Incubation with $\cdot O_2^-$

For incubation experiments with $\cdot O_2^-$ conducted by Julian Schreck, the reactive species was generated *in situ* by a system comprising HX and XO.[379]
Solutions of the respective polymer in PBS (1 g/L) were supplemented with 0.5 mM HX and 20 U/L XO. In order to prevent contaminations of the samples, addition of HX and XO as well as withdrawal of the samples were performed under the sterile conditions of a laminar flow hood. Subsequently, samples were freeze-dried and analyzed as described previously.

Sample Preparation for GC/MS

Polymers were dissolved in PBS to a final concentration of 1 g/L and incubated at 37 °C over night. $CuSO_4$ (50 μM) and H_2O_2 (50 mM, replenished daily) were added and samples were shaken for 14 d and subsequently stored at -18 °C until analysis via GC/MS.

7.3.3.2 Acidic Hydrolysis

Hydrolysis of $PMeOx_{90}$

The acidic hydrolysis of PMeOx was investigated based on earlier studies conducted by Hoogenboom and coworkers.[225, 228]
A stock solution of $PMeOx_{90}$ in millipore water with a concentration of 100 g/L was prepared and aliquoted (100 μL) in Eppendorf Tubes®. Addition of each 100 μL of concentrated HCl ($\approx$ 37 w-%, 12 M) yielded a solution of 50 g/L $PMeOx_{90}$ in 6 M HCl,

which was incubated and vigorously shaken at 90 °C. After predefined periods of time of up to 6 h, hydrolysis was terminated by immediate cooling in iced water and subsequent neutralization by addition of 800 μL of 1.5 M NaOH to ensure full protonation of the released acetic acid. The solvent was removed at 100 °C and the residual was dissolved in deuterated methanol and analyzed via ^{1}H-NMR spectroscopy and GPC in DMF.

Hydrolysis of PSar$_{25}$

The acidic hydrolysis of PSar was investigated following the procedure described for PMeOx.

PSar$_{25}$ was dissolved in millipore water to a concentration of 100 g/L and aliquoted to 100 μL in Eppendorf Tubes®. Concentrated HCl (each 100 μL) was added yielding a concentration of 50 g/L PSar$_{25}$ in 6 M HCl. Samples were vigorously shaken at four different reaction temperatures (55, 75, 90 and 99 °C) for up to 6 h and subsequently cooled in ice water and neutralized by addition of ≈ 800 μL of 1.5 M NaOH as controlled using pH test stripes. Finally, the solvent was evaporated at 100 °C and the residuals collected in deuterated methanol at 70 °C and analyzed via ^{1}H-NMR spectroscopy and GPC in DMF.

Long-time experiments were performed at 37 °C for up to 14 d using not only 6 M HCl but also SGF (2.0 g/L NaCl and 2.9 g/L HCl, pH 1.38) and SIF (0.62 g/L NaOH and 6.8 g/L KH_2PO_4, pH 6.49) and handled in a similar manner.

7.3.3.3 *In vitro* Investigations on the enzymatic Digestion of Polymers

PSar$_{333}$-FITC in Rat Liver and Kidney Homogenates as well as Chicken Egg White

Experiments on the stability of PSar$_{333}$-FITC in organ homogenates were conducted by Johanna Eisenreich (Liver)[386] and Fabian Wieghardt (Kidney and Egg White)[385]. Shortly, PSar$_{333}$-FITC was dissolved in Tris/HCl comprising 242.4 mg Tris, 372.5 mg KCl, 102.3 mg $MgCl_2 \cdot 6\ H_2O$ in 200 mL of millipore water (polymer concentration 40 μg/mL) and added to freshly harvested organs (0.5 mL per gram of organ). Denaturation of control samples was achieved by storing organs or egg white at 42 °C for 24 h prior to addition of the polymer. Subsequently, the mixture was homogenized using an *T25 Ultra Turrax*® dispersing instrument (*IKA*, Staufen, Germany) and incubated at 37 °C for 24 h. Samples

were centrifuged and 100 μL of the supernatant were withdrawn and fractionated using a Sephadex® LH-20 column (*GE Healthcare Life Sciences*, Freiburg, Germany) comprising 1 g Sephadex® LH-20 swollen in millipore water. For fluorescence measurement, 100 μL of each fraction were diluted with 1400 μL of millipore water. Fluorescence intensity was determined in triplicate at 518 nm using an excitation wavelength of 494 nm.

SulfoPBI-PSar$_{185}$ in Rat Liver Homogenate

Based on the investigations of Johanna Eisenreich and Fabian Wieghart, Maria Krebs investigated the enzymatic digestion of SulfoPBI-PSar$_{185}$ by rat kidney and liver.[388] The polymer was dissolved to a final concentration of 50 μg/mL in PBS supplemented by 0.5 mM $MnCl_2$ and each 500 μL of the obtained solution were added to 0.5 g of freshly harvested organ. Prior to incubation at 37 °C for up to 48 h, mixtures were homogenized using a *BeadBug* microtube homogenizer (*Benchmark Scientific*, Edison, USA) and stainless steel beads purchased from *Kugel Rollen OnlineShop* (#1.4034). For control experiments, organs were heated to 100 °C for 1 h prior to addition of the polymer. After incubation, samples were heated to 100 °C for 10 min to inactivate enzymes. Subsequently, mixtures were centrifuged and 100 μL of the supernatant was fractionated using a Sephadex® LH-20 column (*GE Healthcare Life Sciences*, Freiburg, Germany) comprising 1 g Sephadex® LH-20 swollen in millipore water. For fluorescence measurement, 100 μL of each collected fraction was diluted with 1 mL of millipore water. Fluorescence intensity was determined in quintuplicate at 615 nm using a excitation wavelength of 566 nm.

PSar$_{333}$ in Chicken Egg White

Using higher amounts of unlabeled PSar$_{333}$ for the incubation in egg white enabled analysis via GPC in an experiment conducted by Fabian Wieghardt.[385] For this purpose, 5 mg of PSar$_{333}$ were dissolved in Tris/HCl, blended with 1 g of egg white and incubated at 37 °C for 24 h. Subsequently, samples were freeze-dried, extracted with HFIP and analyzed via GPC. For control experiments, egg white was denatured by incubation at 100 °C for 2 h prior to addition of the polymer. All experiments were performed in triplicate.

7.3.3.4 *In ovo* Investigations on the enzymatic Digestion of Poly(ethylene glycol), Polyproline, Polysarcosine and Poly(2-methyl-2-oxazoline)

Preliminary Studies

Preliminary studies conducted by Maria Krebs focused on the degradation of PEG, PSar and PPro in freshly laid whole chicken eggs. PEG_{45}, $PSar_{68}$ and $PPro_{80}$ were dissolved in PBS supplemented by 0.5 mM $MnCl_2$ to a final concentration of 50 g/L ($PPro_{80}$: 22 g/L in 44 % PBS) and sterilized by filtration prior to use. The surface of the eggs was cleaned with ethanol and a cannula was used to drill a hole in the upper quarter of the egg. Subsequently, 0.2 mL of the PEG or PSar solutions or 0.46 mL of the PPro solution, respectively, were injected into the egg white and the hole was sealed with instant adhesive. Sealed eggs were either denatured by cooking at 100 °C for 1 h or left untreated and incubated at 37 °C for up to 20 d. Eggs were chilled within the refrigerator for at least 4 h and egg white and yolk were separated. While the latter one was discarded without further analysis, egg whites were freeze-dried, crushed and extracted with a 2:1 (v/v) mixture of MeOH and $CHCl_3$. The solvent was evaporated and the residual solid was dispersed in DMF and filtered to enable analysis via GPC. All experiments were performed in quintuplicate.

***In ovo* Degradation of Poly(ethylene glycol), Polysarcosine and Poly(2-methyl-2-oxazoline)**

More detailed investigations on the *in ovo* degradation of polymers were conducted in essentially the same manner as described previously with some modifications. All polymers (PEG_{90}, $PMeOx_{90}$, NPA-$PSar_{90}$-H, NPA-$PSar_{90}$-Ac, HO-$PSar_{90}$-H and HO-$PSar_{90}$-Ac) were purified via dialysis using a Spectra/POR® dialysis membrane (1kD) and dissolved in millipore water without further supplementation of $MnCl_2$. Solutions were further purified by sterile filtration prior to use and injection was performed under the sterile conditions of a laminar flow hood to prevent contaminations by external agents. Finally, incubation times were prolonged to a maximum of 40 d reflecting approximately twice the length of the breeding time of chicken eggs. Unless otherwhise stated, all experiments were performed in sextuplicate.

Bibliography

[1] Slow Food terminology, http://www.slowfood.com/about-us/slow-food-terminology/ (June 9th, 2016).

[2] D. G. Rudmann, J. T. Alston, J. C. Hanson, S. Heidel, *Toxicol. Pathol.* **2013**, *41*, 970–983.

[3] A. J. Teo, A. Mishra, I. Park, Y.-J. Kim, W.-T. Park, Y.-J. Yoon, *ACS Biomater. Sci. Eng.* **2016**, *2*, 454–472.

[4] D. S. Kohane, R. Langer, *Nature* **2008**, *63*, 487–491.

[5] W. B. Liechty, D. R. Kryscio, B. V. Slaughter, N. A. Peppas, *Annu. Rev. Chem. Biomol. Eng.* **2010**, *1*, 149–173.

[6] N. A. Peppas, K. B. Keys, M. Torres-Lugo, A. M. Lowman, *J. Control. Release* **1999**, *62*, 81–87.

[7] J. Zhu, *J. Biomed. Mater. Res.* **2010**, *31*, 4639–4656.

[8] J. H. Lee, H. B. Lee, J. D. Andrade, *Prog. Polym. Sci.* **1995**, *20*, 1043–1079.

[9] N. A. Alcantar, E. S. Aydil, J. N. Israelachvili, *J. Biomed. Mater. Res.* **2000**, *51*, 343–351.

[10] F. M. Veronese, G. Pasut, *Drug Discov. Today* **2005**, *10*, 1451–1458.

[11] J. S. Kang, P. P. DeLuca, K. C. Lee, *Expert Opin. Emerging Drugs* **2009**, *14*, 363–380.

[12] R. W. Payne, B. M. Murphy, M. C. Manning, *Pharm. Dev. Technol.* **2011**, *16*, 423–440.

[13] R. Webster, E. Didier, P. Harris, N. Siegel, J. Stadler, L. Tilbury, D. Smith, *Drug Metab. Dispos.* **2007**, *35*, 9–16.

[14] K. Knop, R. Hoogenboom, D. Fischer, U. S. Schubert, *Angew. Chem. Int. Ed.* **2010**, *49*, 6288–6308.

[15] M. Barz, R. Luxenhofer, R. Zentel, M. J. Vicent, *Polym. Chem.* **2011**, *2*, 1900–1918.

[16] R. P. Garay, R. El-Gewely, J. K. Armstrong, G. Garratty, P. Richette, *Expert Opin. Drug Deliv.* **2012**, *9*, 1319–1323.

[17] J. J. F. Verhoef, T. J. Anchordoquy, *Drug Deliv. Transl. Res.* **2013**, *3*, 499–503.

[18] H. Hatakeyama, H. Akita, H. Harashima, *Biol. Pharm. Bull.* **2013**, *36*, 892–899.

[19] C. Conover, L. Lejeune, R. Linberg, K. Shum, R. G. L. Shorr, *Artif. Cells Blood Substit. Immobil. Biotechnol.* **1996**, *24*, 599–611.

[20] A. Bendele, J. Seely, C. Richey, G. Sennello, G. Shopp, *Toxicol. Sci.* **1997**, *42*, 152–157.

[21] R. Webster, V. Elliott, B. K. Park, D. Walker, M. Hankin, P. Taupin in *PEGylated Protein Drugs: Basic Science and Clinical Applications*, (Ed.: F. M. Veronese), Birkhäuser Basel, Basel, **2009**, pp. 127–146.

[22] A. Baumann, D. Tuerck, S. Prabhu, L. Dickmann, J. Sims, *Drug Discov. Today* **2014**, *19*, 1623–1631.

[23] A. W. Richter, E. Åkerblom, *Biochemical Pharmacology* **1984**, *74*, 36–39.

[24] Y. Liu, H. Reidler, J. Pan, D. Milunic, D. Qin, D. Chen, Y. R. Vallejo, R. Yin, *J. Pharmacol. Toxicol. Methods* **2011**, *64*, 238–245.

[25] G. Garratty, *Transfus. Med. Rev.* **2004**, *18*, 245–256.

[26] G. Garratty, *Vox Sang.* **2008**, *94*, 87–95.

[27] J. K. Armstrong in *PEGylated Protein Drugs: Basic Science and Clinical Applications*, (Ed.: F. M. Veronese), Birkhäuser Basel, Basel, **2009**, pp. 147–168.

[28] H. Schellekens, W. E. Hennink, V. Brinks, *Pharm. Res.* **2013**, *30*, 1729–1734.

[29] T. Shimizu, M. Ichihara, Y. Yoshioka, T. Ishida, S. Nakagawa, H. Kiwada, *Biol. Pharm. Bull.* **2012**, *35*, 1336–1342.

[30] D. A. Herold, K. Keil, D. E. Bruns, *Biochem. Pharmacol.* **1989**, *38*, 73–76.

[31] R. Pietruszko in *Biochemical Pharmacology of Ethanol*, (Ed.: E. Majchrowicz), Springer US, Boston, MA, **1975**, pp. 1–31.

[32] D. A. Tomalia, D. P. Sheetz, *J. Polym. Sci. A Polym. Chem.* **1966**, *4*, 2253–2265.

[33] W. Seeliger, E. Aufderhaar, W. Diepers, R. Feinauer, R. Nehring, W. Thier, H. Hellmann, *Angew. Chem. Int. Ed.* **1966**, *5*, 875–888.

[34] T. Kagiya, S. Narisawa, T. Maeda, K. Fukui, *J. Polym. Sci. B Polym. Lett.* **1966**, *4*, 441–445.

[35] T. G. Bassiri, A. Levy, M. Litt, *J. Polym. Sci. B Polym. Lett.* **1967**, *5*, 871–879.

[36] K. Aoi, M. Okada, English, *Prog. Polym. Sci.* **1996**, *21*, 151–208.

[37] R. Hoogenboom, *Angew. Chem. Int. Ed.* **2009**, *48*, 7978–7994.

[38] H. Schlaad, C. Diehl, A. Gress, M. Meyer, A. L. Demirel, Y. Nur, A. Bertin, *Macromol. Rapid Commun.* **2010**, *31*, 511–525.

[39] R. Luxenhofer, Y. Han, A. Schulz, J. Tong, Z. He, A. V. Kabanov, R. Jordan, *Macromol. Rapid Commun.* **2012**, *33*, 1613–1631.

[40] B. Verbraeken, B. D. Monnery, K. Lava, R. Hoogenboom, *Eur. Polym. J.* **2017**, *88*, 451–469.

[41] S. Zalipsky, C. B. Hansen, J. M. Oaks, T. M. Allen, *J. Pharm. Sci.* **1996**, *85*, 133–137.

[42] A. Mero, G. Pasut, L. D. Via, M. W. Fijten, U. S. Schubert, R. Hoogenboom, F. M. Veronese, *J. Control. Release* **2008**, *125*, 87–95.

[43] B. Pidhatika, M. Rodenstein, Y. Chen, E. Rakhmatullina, A. Mühlebach, C. Acikgöz, M. Textor, R. Konradi, *Biointerphases* **2012**, *7*, 1–15.

[44] N. Zhang, T. Pompe, I. Amin, R. Luxenhofer, C. Werner, R. Jordan, *Macromol. Biosci.* **2012**, *12*, 926–936.

[45] Z. He, L. Miao, R. Jordan, D. S-Manickam, R. Luxenhofer, A. V. Kabanov, *Macromol. Biosci.* **2015**, *15*, 1004–1020.

[46] R. Luxenhofer, A. Schulz, C. Roques, S. Lia, T. K. Bronich, E. V. Batrakova, R. Jordan, A. V. Kabanov, *Biomaterials* **2010**, *31*, 4972–4979.

[47] R. Hoogenboom, H. Schlaad, *Polym. Chem.* **2017**, *8*, 24–40.

[48] R. Luxenhofer, G. Sahay, A. Schulz, D. Alakhova, T. K. Bronich, R. Jordan, A. V. Kabanov, *J. Control. Release* **2011**, *153*, 73–82.

[49] M. Bauer, S. Schröder, L. Tauhardt, K. Kempe, U. S. Schubert, D. Fischer, *J. Polym. Sci. A Polym. Chem.* **2013**, *51*, 1816–1821.

[50] J. Kronek, Z. Kroneková, J. Lustoň, E. Paulovičová, L. Paulovičová, B. Mendrek, *J. Mater. Sci. Mater. Med.* **2011**, *22*, 1724–1734.

[51] R. W. Moreadith, T. X. Viegas, M. D. Bentley, J. M. Harris, Z. Fang, K. Yoon, B. Dizman, R. Weimer, B. P. Rae, X. Li, C. Rader, D. Standaert, W. Olanow, *Eur. Polym. J.* **2017**, *88*, 524–552.

[52] clinicaltrials.gov: A Study of Weekly Subcutaneous Injections of SER-214 in Subjects With Parkinson's Disease (PD), to Determine the Safety, Tolerability and Pharmacokinetic (PK) Profile of SER-214, https://clinicaltrials.gov/ct2/show/study/NCT02579473 (july 11, 2017).

[53] R. J. Simon, R. S. Kania, R. N. Zuckermann, V. D. Huebner, D. A. Jewell, S. Banville, S. Ng, L. Wang, S. Rosenberg, C. K. Marlowe, D. C. Spellmeyer, R. Tans, A. D. Frankel, D. V. Santi, F. E. Cohen, P. A. Bartlett, *Proc. Natl. Acad. Sci. USA* **1992**, *89*, 9367–9371.

[54] E. K. Bradley, J. M. Kerr, L. S. Richter, G. M. Figliozzi, D. A. Goff, R. N. Zuckermann, D. C. Spellmeyer, J. M. Blaney, *Mol. Diversity* **1997**, *3*, 1–15.

[55] C. Fetsch, A. Grossmann, L. Holz, J. Nawroth, R. Luxenhofer, *Macromolecules* **2011**, *44*, 6746–6758.

[56] S. H. Lahasky, X. Hu, D. Zhang, *ACS Macro Lett.* **2012**, *1*, 580–584.

[57] C. Fetsch, S. Flecks, D. Gieseler, C. Marschelke, J. Ulbricht, K.-H. van Pée, R. Luxenhofer, *Macromol. Chem. Phys.* **2015**, *216*, 547–560.

[58] P. H. Maurer, D. Subrahmanyam, E. Katchalski, E. R. Blout, *J. Immunol.* **1959**, *83*, 193–197.

[59] M. Sela, *Adv. Immunol.* **1966**, *5*, 29–129.

[60] E. Hara, A. Makino, K. Kurihara, F. Yamamoto, E. Ozeki, S. Kimura, *Int. Immunopharmacol.* **2012**, *14*, 261–266.

[61] M. A. Dechantsreiter, E. Planker, B. Mathä, E. Lohof, G. Hölzemann, A. Jonczyk, S. L. Goodman, H. Kessler, *J. Med. Chem.* **1999**, *42*, 3033–3040.

[62] D. J. Gordon, K. L. Sciarretta, S. C. Meredith, *Biochemistry* **2001**, *40*, 8237–8245.

[63] A. Janecka, R. Kruszynski, J. Fichna, P. Kosson, T. Janecki, *Peptides* **2006**, *27*, 131–135.

[64] X. Tao, C. Deng, J. Ling, *Macromol. Rapid Commun.* **2014**, *35*, 875–881.

[65] X. Tao, Y. Deng, Z. Shen, J. Ling, *Macromolecules* **2014**, *47*, 6173–6180.

[66] X. Tao, J. Du, Y. Wang, J. Ling, *Polym. Chem.* **2015**, *6*, 3164–3174.

[67] L. Guo, D. Zhang, *J. Am. Chem. Soc.* **2009**, *131*, 18072–18074.

[68] L. Guo, S. H. Lahasky, K. Ghale, D. Zhang, *J. Am. Chem. Soc* **2012**, *134*, 9163–9171.

[69] L. Guo, J. Li, Z. Brown, K. Ghale, D. Zhang, *Pept. Sci.* **2011**, *96*, 596–603.

[70] R. B. Merrifield, *J. Am. Chem. Soc.* **1963**, *85*, 2149–2154.

[71] R. N. Zuckermann, *Pept. Sci.* **2011**, *96*, 545–555.

[72] J. Sun, R. N. Zuckermann, *ACS Nano* **2013**, *7*, 4715–4732.

[73] J. Seo, B.-C. Lee, R. N. Zuckermann in *Comprehensive Biomaterials*, (Ed.: P. Ducheyne), Elsevier, Oxford, **2011**, pp. 53–76.

[74] D. Zhang, S. H. Lahasky, L. Guo, C.-U. Lee, M. Lavan, *Macromolecules* **2012**, *45*, 5833–5841.

[75] A. S. Knight, E. Y. Zhou, M. B. Francis, R. N. Zuckermann, *Adv. Mater.* **2015**, *27*, 5665–5691.

[76] C. Secker, S. M. Brosnan, R. Luxenhofer, H. Schlaad, *Macromol. Biosci.* **2015**, *15*, 881–891.

[77] N. Gangloff, J. Ulbricht, T. Lorson, H. Schlaad, R. Luxenhofer, *Chem. Rev.* **2016**, *116*, 1753–1802.

[78] B. A. Chan, S. Xuan, A. Li, J. M. Simpson, G. L. Sternhagen, D. Zhang in *Polymers for Biomedicine*, John Wiley & Sons, Inc., **2017**, pp. 77–119.

[79] M. H. Hart, *Icarus* **1978**, *33*, 23–39.

[80] I. I. Borzenkova, I. Y. Turchinovich, *Environmental Structure and Function: Cilimate System, Vol. II*, (Ed.: G. V. Gruza), Encyclopedia of Life Support Systems (EOLSS), Chapter History of the Atmospheric Composition.

[81] G. Toole, S. Toole, *Advanced Human and Social Biology*, (Ed.: N. Thornes), **1997**.

[82] M. C. Brahimi-Horn, J. Pouysségur, *FEBS Letters* **2007**, *581*, 3582–3591.

[83] O. D. Saugstad, *J. Perinatol.* **2006**, *26*, 46–50.

[84] T. P. Devasagayam, J. C. Tilak, K. K. Boloor, K. S. Sane, S. S. Ghaskadbi, R. D. Lele, *J. Assoc. Physicians India* **2004**, *52*, 794–804.

[85] V. Lobo, A. Patil, A. Phatak, N. Chandra, *Pharmacogn. Rev.* **2010**, *4*, 118–126.

[86] K. H. Cheeseman, T. F. Slater, *Br. Med. Bull.* **1993**, *49*, 481–493.

[87] F. C. Fang, *mBio* **2011**, *2*, e00141–11.

[88] K. Brieger, S. Schiavone, F. J. Miller, K.-H. Krause, *Swiss Med. Wkly.* **2012**, *142*, w13659.

[89] P. G. Heyworth, A. R. Cross, J. T. Curnutte, *Curr. Opin. Immunol.* **2003**, *15*, 578–584.

[90] M. G. Schäppi, V. Jaquet, D. C. Belli, K.-H. Krause, *Semin. in Immunopathol.* **2008**, *30*, 255–271.

[91] R. P. Magnusson, A. Taurog, M. L. Dorris, *J. Biol. Chem.* **1984**, *259*, 197–205.

[92] C. C. Winterbourn, M. B. Hampton, *Free Radical Biol. Med.* **2008**, *45*, 549–561.

[93] M. Schieber, N. Chandel, *Curr. Biol.* **2014**, *24*, R453–R462.

[94] J. Zhang, X. Wang, V. Vikash, Q. Ye, D. Wu, Y. Liu, W. Dong, *Oxid. Med. Cell. Longev.* **2016**, *2016*, article ID 4350965.

[95] H. Shi, N. Noguchi, E. Niki, *Free Radical Biol. Med.* **1999**, *27*, 334–346.

[96] M. Levine, S. C. Rumsey, R. Daruwala, J. B. Park, Y. Wang, *JAMA* **1999**, *281*, 1415–1423.

[97] J.-M. Lü, P. H. Lin, Q. Yao, C. Chen, *J. Cell. Mol. Med.* **2010**, *14*, 840–860.

[98] M. S. Cooke, M. D. Evans, M. Dizdaroglu, J. Lunec, *FASEB J.* **2003**, *17*, 1195–1214.

[99] L. Lyras, R. H. Perry, E. K. Perry, P. G. Ince, A. Jenner, P. Jenner, B. Halliwell, *J. Neurochem.* **1998**, *71*, 302–312.

[100] D. Harman, *J. Gerontol.* **1956**, *11*, 298–300.

[101] S. Hekimi, J. Lapointe, Y. Wen, *Trends Cell Biol.* **2011**, *21*, 569–576.

[102] S. C. Gupta, D. Hevia, S. Patchva, B. Park, W. Koh, B. B. Aggarwal, *Antioxid. Redox Signal.* **2012**, *16*, 1295–1322.

[103] M. López-Lázaro, *Anticancer Agents Med. Chem.* **2009**, *9*, 517–525.

[104] R. Franco, O. Schoneveld, A. G. Georgakilas, M. I. Panayiotidis, *Cancer Lett.* **2008**, *266*, 6–11.

[105] U. Z. Paracha, K. Fatima, M. Alqahtani, A. Chaudhary, A. Abuzenadah, G. Damanhouri, I. Qadri, *Virol. J.* **2013**, *10*, 1–9.

[106] K. B. Schwarz, *Free Radical Biol. Med.* **1996**, *21*, 641–649.

[107] G. W. Pace, C. D. Leaf, *Free Radical Biol. Med.* **1995**, *19*, 523–528.

[108] G. Kennedy, V. A. Spence, M. McLaren, A. Hill, C. Underwood, J. J. F. Belch, *Free Radical Biol. Med.* **2005**, *39*, 584–589.

[109] M. Keith, A. Geranmayegan, M. J. Sole, R. Kurian, A. Robinson, A. S. Omran, K. N. Jeejeebhoy, *J. Am. Coll. Cardiol.* **1998**, *31*, 1352–1356.

[110] P. Jenner, *Ann. Neurol.* **2003**, *53*, 26–38.

[111] J. L. Fleming, C. J. Phiel, A. E. Toland, *Curr. Alzheimer Res.* **2012**, *9*, 1077–1096.

[112] D. Liu, J. Wen, J. Liu, L. Li, *FASEB J.* **1999**, *13*, 2318–2328.

[113] S. E. Browne, R. J. Ferrante, M. F. Beal, *Brain Pathol.* **1999**, *9*, 147–163.

[114] M. Bošković, T. Vovk, B. Kores Plesničar, I. Grabnar, *Curr. Neuropharmacol.* **2011**, *9*, 301–312.

[115] E. Niki, *BioFactors* **2008**, *34*, 171–180.

[116] F. Cai, Y. M. Dupertuis, C. Pichard, *Curr. Opin. Clin. Nutr. Metab. Care* **2012**, *15*, 99–106.

[117] M. S. Cooke, M. D. Evans, M. Dizdaroglu, J. Lunec, *FASEB J.* **2003**, *17*, 1195–1214.

[118] R. A. Floyd, *Carcinogenesis* **1990**, *11*, 1447–1450.

[119] R. C. Cattley, S. E. Glover, *Carcinogenesis* **1993**, *14*, 2495–2499.

[120] K. Bagchi, S. Puri, *East Mediterranean Health Jr.* **1998**, *4*, 350–360.

[121] M. W. Calhoun, J. W. Thomas, R. B. Gennis, *Trends Biochem. Sci.* **1994**, *19*, 325–330.

[122] E. Cadenas, K. J. A. Davies, *Free Radical Biol. Med.* **2000**, *29*, 222–230.

[123] M. P. Murphy, *Biochem J.* **2009**, *417*, 1–13.

[124] A. Y. Andreyev, Y. E. Kushnareva, A. A. Starkov, *Biochemistry (Mosc.)* **2005**, *70*, 200–214.

[125] D. E. Edmondson, *Curr. Pharm. Des.* **2014**, *20*, 155–160.

[126] H. Imai, Y. Nakagawa, *Free Radical Biol. Med.* **2003**, *34*, 145–169.

[127] S. G. Rhee, S. W. Kang, T.-S. Chang, W. Jeong, K. Kim, *IUBMB Life* **2001**, *52*, 35–41.

[128] M. Salvi, V. Battaglia, A. M. Brunati, N. La Rocca, E. Tibaldi, P. Pietrangeli, L. Marcocci, B. Mondovì, C. A. Rossi, A. Toninello, *J. Biol. Chem.* **2007**, *282*, 24407–24415.

[129] S. G. Rhee, K.-S.Yang, S. W. Kang, H. A. Woo, T.-S. Chang, *Antioxid. Redox Signal.* **2005**, *7*, 619–626.

[130] R. A. Weisiger, I. Fridovich, *J. Biol. Chem.* **1973**, *248*, 3582–3592.

[131] M. Erecińska, I. A. Silver, *Respir. Physiol.* **2001**, *128*, 263–276.

[132] J. A. Imlay, I. Fridovich, *J. Biol. Chem.* **1991**, *266*, 6957–65.

[133] K. Bedard, K.-H. Krause, *Physiol. Rev.* **2007**, *87*, 245–313.

[134] K. Bedard, B. Lardy, K.-H. Krause, *Biochimie* **2007**, *89*, 1107–1112.

[135] T. Kawahara, M. T. Quinn, J. D. Lambeth, *BMC Evolutionary Biology* **2007**, *7*, 109.

[136] B. M. Babior, J. D. Lambeth, W. Nauseef, *Arch. Biochem. Biophys.* **2002**, *397*, 342–344.

[137] J. M. Robinson, T. Ohira, J. A. Badwey, *Histochem. Cell Biol.* **2004**, *122*, 293–304.

[138] A. R. Cross, A. W. Segal, *Biochim. Biophys. Acta* **2004**, *1657*, 1–22.

[139] J. A. Winkelstein, M. C. Marino, R. B. Johnston Jr, J. Boyle, J. Curnutte, J. I. Gallin, H. L. Malech, S. M. Holland, H. Ochs, P. Quie, R. H. Buckley, C. B. Foster, S. J. Chanock, H. Dickler, *Medicine* **2000**, *79*, 155–169.

[140] Y.-A. Suh, R. S. Arnold, B. Lassegue, J. Shi, X. Xu, D. Sorescu, A. B. Chung, K. K. Griendling, J. D. Lambeth, *Nature* **1999**, *401*, 79–82.

[141] B. Bánfi, A. Maturana, S. Jaconi, S. Arnaudeau, T. Laforge, B. Sinha, E. Ligeti, N. Demaurex, K. H. Krause, *Science* **2000**, *287*, 138–142.

[142] B. Bánfi, R. A. Clark, K. Steger, K.-H. Krause, *J. Biol. Chem.* **2003**, *278*, 3510–3513.

[143] B. Bánfi, R. A. Clark, K. Streger, K.-H. Krause, *J. Biol. Chem.* **2003**, *278*, 3510–3513.

[144] A. Perner, L. Andresen, G. Pedersen, J. Rask-Madsen, *Gut* **2003**, *52*, 231–236.

[145] N. Salles, I. Szanto, F. Herrmann, B. Armenian, M. Stumm, E. Stauffer, J.-P. Michel, K.-H. Krause, *Exp. Gerontol.* **2005**, *40*, 353–357.

[146] S. Teshima, H. Kutsumi, T. Kawahara, K. Kishi, K. Rokutan, *Am. J. Physiol.* **2000**, *279*, 1169–1176.

[147] K.-H. Krause, *Jpn. J. Infect. Dis.* **2004**, *57*, 28–29.

[148] H. Kikuchi, M. Hikage, H. Miyashita, M. Fukumoto, *Gene* **2000**, *254*, 237–243.

[149] B. Bánfi, B. Malgrange, J. Knisz, K. Steger, M. Dubois-Dauphin, K.-H. Krause, *J. Biol. Chem.* **2004**, *279*, 46065–46072.

[150] R. Paffenholz, R. A. Bergstrom, F. Pasutto, P. Wabnitz, R. J. Munroe, W. Jagla, U. Heinzmann, A. Marquardt, A. Bareiss, J. Laufs, A. Russ, G. Stumm, J. C. Schimenti, D. E. Bergstrom, *Genes Dev.* **2004**, *18*, 486–491.

[151] A. Shiose, J. Kuroda, K. Tsuruya, M. Hirai, H. Hirakata, S. Naito, M. Hattori, Y. Sakaki, H. Sumimoto, *J. Biol. Chem.* **2001**, *276*, 1417–1423.

[152] M. Geiszt, J. B. Kopp, P. Várnai, T. L. Leto, *Proc. Natl. Acad. Sci. USA* **2000**, *97*, 8010–8014.

[153] F. Chen, S. Haigh, S. A. Barman, D. Fulton, *Front. Physiol.* **2012**, *3*, 412.

[154] B. Bánfi, G. Molnár, A. Maturana, K. Steger, B. Hegedûs, N. Demaurex, K.-H. Krause, *J. Biol. Chem.* **2001**, *276*, 37594–37601.

[155] G. Cheng, Z. Cao, X. Xu, E. G. Meir, J. Lambeth, *Gene* **2001**, *269*, 131–140.

[156] D. J. Fulton, *Antioxid. Redox. Signal.* **2009**, *11*, 2443–2452.

[157] X. De Deken, D. Wang, M.-C. Many, S. Costagliola, F. Libert, G. Vassart, J. E. Dumont, F. Miot, *J. Biol. Chem.* **2000**, *275*, 23227–23233.

[158] R. Ameziane-El-Hassani, S. Morand, J.-L. Boucher, Y.-M. Frapart, D. Apostolou, D. Agnandji, S. Gnidehou, R. Ohayon, M.-S. Noël-Hudson, J. Francon, K. Lalaoui, A. Virion, C. Dupuy, *J. Biol. Chem.* **2005**, *280*, 30046–30054.

[159] S. Rigutto, C. Hoste, H. Grasberger, M. Milenkovic, D. Communi, J. E. Dumont, B. Corvilain, F. Miot, X. De Deken, *J. Biol. Chem.* **2009**, *284*, 6725–6734.

[160] S. Dupré-Crochet, M. Erard, O. Nüße, *J. Leukoc. Biol.* **2013**, *94*, 657–670.

[161] M. Rabinovitch, *Trends Cell Biol.* **1995**, *5*, 85–87.

[162] P. Elsbach, J. Weiss, *Immunol. Lett.* **1985**, *11*, 159–163.

[163] B. M. Babior, J. T. Curnutte, B. J. McMurrich, *J. Clin. Invest.* **1976**, *58*, 989–996.

[164] B. M. Babior, *J. Clin. Invest.* **Mar. 1984**, *73*, 599–601.

[165] I. Fridovich, *J. Biol. Chem.* **1997**, *272*, 18515–18517.

[166] C. C. Winterbourn, M. B. Hampton, J. H. Livesey, A. J. Kettle, *J. Biol. Chem.* **2006**, *281*, 39860–39869.

[167] J. A. Imlay, S. Linn, *J. Bacteriol.* **1986**, *166*, 519–527.

[168] T. Huahua, J. Rudy, C. M. Kunin, *J. Clin. Microbiol.* **1991**, *29*, 328–332.

[169] J. Ulbricht, Master Thesis, Oxidative Degradation of Poly(ethylen glycol), Poly(2-oxazoline)s and Poly(peptoid)s, **2013**.

[170] D. Harrison, K. K. Griendling, U. Landmesser, B. Hornig, H. Drexler, *Am. J. Cardiol.* **2003**, *91*, 7–11.

[171] A. Puppo, B. Halliwell, *Biochem J.* **1988**, *249*, 185–190.

[172] B. Lipinski, *Oxid. Med. Cell. Longevity* **2011**, *2011*, 1–9.

[173] B. Babior, *Blood* **1984**, *64*, 959–966.

[174] G. M. Rosen, S. Pou, C. L. Ramos, M. S. Cohen, B. E. Britigan, *FASEB J.* **1995**, *9*, 200–209.

[175] S. J. Klebanoff, *J. Leukoc. Biol.* **2005**, *77*, 598–625.

[176] A. L. P. Chapman, M. B. Hampton, R. Senthilmohan, C. C. Winterbourn, A. J. Kettle, *J. Biol. Chem.* **2002**, *277*, 9757–9762.

[177] C. Nathan, M. U. Shiloh, *Proc. Natl. Acad. Sci. USA* **2000**, *97*, 8841–8848.

[178] M. T. Silva, M. Correia-Neves, *Front. Immunol.* **2012**, *3*, article 174.

[179] A. Savina, S. Amigorena, *Immunol. Rev.* **2007**, *219*, 143–156.

[180] O. Levy, *J. Leukoc. Biol.* **2004**, *76*, 909–925.

[181] A. W. Segal, *Annu. Rev. Immunol.* **2005**, *23*, 197–223.

[182] L. Sherwood, *Human Physiology: From Cells to Systems*, **2014**.

[183] B. Alberts, A. Johnson, J. Lewis, M. Raff, K. Roberts, P. Walter, *Molecular Biology of the Cell, 4th edition*, Garland Science, New York, **2002**.

[184] C. Summers, S. M. Rankin, A. M. Condliffe, N. Singh, A. M. Peters, E. R. Chilvers, *Trends Immunol.* **2010**, *31*, 318–324.

[185] R. van Furth, Z. A. Cohn, *J. Exp. Med.* **1968**, *128*, 415–435.

[186] C. Shi, E. G. Pamer, *Nat. Rev. Immunol.* **2011**, *11*, 762–774.

[187] H. Kosaka, J. S. Wishnok, M. Miwa, C. D. Leaf, S. R. Tannenbaum, *Carcinogenesis* **1989**, *10*, 563–566.

[188] D. A. Wink, H. B. Hines, R. Y. S. Cheng, C. H. Switzer, W. Flores-Santana, M. P. Vitek, L. A. Ridnour, C. A. Colton, *J. Leukoc. Biol.* **2011**, *89*, 873–891.

[189] J. S. Beckman, T. W. Beckman, J. Chen, P. A. Marshall, B. A. Freeman, *Proc. Natl. Acad. Sci. USA* **1990**, *87*, 1620–1624.

[190] R. E. Huie, S. Padmaja, *Free Radic. Res. Commun.* **1993**, *18*, 195–199.

[191] T. Yamaoka, Y. Tabata, Y. Ikada, *J. Pharm. Sci.* **1994**, *83*, 601–606.

[192] P. B. Danielson, *Curr. Drug Metab.* **2002**, *3*, 561–597.

[193] D. R. Nelson, T. Kamataki, D. J. Waxman, F. Guengerich, R. W. Estabrook, R. Feyereisen, F. J. Gonzalez, M. J. Coon, I. C. Gunsalus, O. Gotoh, K. Okuda, D. W. Nebert, *DNA Cell Biol.* **1993**, *12*, 1–51.

[194] A. R. Goeptar, H. Scheerens, N. P. E. Vermeulen, *Crit. Rev. Toxicol.* **1995**, *25*, 25–65.

[195] R. M. Isham, C. E. Vail, *J. Am. Chem. Soc.* **1915**, *37*, 902–906.

[196] A. M. Clover, *J. Am. Chem. Soc.* **1922**, *44*, 1107–1118.

[197] S. Di Tommaso, P. Rotureau, O. Crescenzi, C. Adamo, *Phys. Chem. Chem. Phys.* **2011**, *13*, 14636–14645.

[198] M. N. Schuchmann, C. von Sonntag, *J. Phys. Chem.* **1982**, *86*, 1995–2000.

[199] X.-R. Xu, Z.-Y. Zhao, X.-Y. Li, J.-D. Gu, *Chemosphere* **2004**, *55*, 73–79.

[200] C. W. McGary Jr., *J. Polym. Sci.* **1960**, *46*, 51–57.

[201] S. Han, C. Kim, D. Kwon, *Polymer* **1997**, *38*, 317–323.

[202] O. A. Mkhatresh, F. Heatley, *Polym. Int.* **2004**, *53*, 1336–1342.

[203] B. Chen, J. R. G. Evans, S. Holding, *J. Appl. Polym. Sci.* **2004**, *94*, 548–552.

[204] S. P. Vijayalakshmi, J. Chakraborty, G. Madras, *J. Appl. Polym. Sci.* **2005**, *96*, 2090–2096.

[205] E. Fischer, A. Speier, *Ber. Dtsch. Chem. Ges.* **1895**, *28*, 3252–3258.

[206] E. R. Stadtman, *Science* **1992**, *257*, 1220–1224.

[207] B. S. Berlett, E. R. Stadtman, *J. Biol. Chem.* **1997**, *272*, 20313–20316.

[208] E. R. Stadtman, *Free Radical Res.* **2006**, *40*, 1250–1258.

[209] Y. Kato, K. Uchida, S. Kawakishi, *J. Agric. Food Chem.* **1992**, *40*, 373–379.

[210] Y. Kato, K. Uchida, S. Kawakishi, *J. Biol. Chem.* **1992**, *267*, 23646–23651.

[211] H. W. Schüßler, K. Schilling, *Int. J. Radiat. Biol.* **1984**, *45*, 267–281.

[212] S. S. Yu, R. L. Koblin, A. L. Zachman, D. S. Perrien, L. H. Hofmeister, T. D. Giorgio, H.-J. Sung, *Biomacromolecules* **2011**, *12*, 4357–4366.

[213] K. Uchida, Y. Kato, S. Kawakishi, *Biochem. Biophys. Res. Commun.* **1990**, *169*, 265–271.

[214] B. Åkesson, B. A. Jönsson, *Drug Metab. Dispos.* **1997**, *25*, 267–269.

[215] P. Kestell, M. Gill, M. Threadgill, A. Gescher, O. Howarth, E. Curzon, *Life Sci.* **1986**, *38*, 719–724.

[216] L. Constantino, E. Rosa, J. Iley, *Biochem. Pharmacol.* **1992**, *44*, 651–658.

[217] J. Iley, R. Tolando, L. Constantino, *J. Chem. Soc. Perkin Trans. 2* **2001**, 1299–1305.

[218] J. Ulbricht, R. Jordan, R. Luxenhofer, *Biomaterials* **2014**, *35*, 4848–4861.

[219] M. Faust, Master Thesis, Oxidative degradation of poly(N,N-dimethylacrylamide), poly(N-vinylpyrrolidone)s and poly(glycidol)s, **2014**.

[220] G. D. Fasman, E. R. Blout, *Biopolymers* **1963**, *1*, 99–109.

[221] A. Tsugita, J.-J. Scheffler, *Eur. J. Biochem.* **1982**, *124*, 585–588.

[222] T. Saegusa, H. Ikeda, H. Fujii, *Macromolecules* **1972**, *5*, 108–108.

[223] R. Tanaka, I. Ueoka, Y. Takaki, K. Kataoka, S. Saito, *Macromolecules* **1983**, *16*, 849–853.

[224] J. H. Jeong, S. H. Song, D. W. Lim, H. Lee, T. G. Park, *J. Control. Release* **2001**, *73*, 391–399.

[225] H. M. L. Lambermont-Thijs, F. S. van der Woerdt, A. Baumgärtel, L. Bonami, F. E. D. Prez, U. S. Schubert, R. Hoogenboom, *Macromolecules* **2010**, *43*, 927–933.

[226] S. K. T. Saegusa, A. Yamada, *Macromolecules* **1975**, *8*, 390–396.

[227] G. H. Hsiue, H. Z. Chiang, C. H Wang, T. M. Juang, *Bioconjugate Chem.* **2006**, *17*, 781–786.

[228] H. P. C. Van Kuringen, J. Lenoir, E. Adriaens, J. Bender, B. G. De Geest, R. Hoogenboom, *Macromol. Biosci.* **2012**, *12*, 1114–1123.

[229] H. P. C. van Kuringen, V. R. de la Rosa, M. W. M. Fijten, J. P. A. Heuts, R. Hoogenboom, *Macromol. Rapid Commun.* **2012**, *33*, 827–832.

[230] M. Mees, E. Haladjova, D. Momekova, G. Momekov, P. S. Shestakova, C. B. Tsvetanov, R. Hoogenboom, S. Rangelov, *Biomacromolecules* **2016**, *17*, 3580–3590.

[231] A. Yaron, F. Naider, S. Scharpe, *Crit. Rev. Biochem. Mol. Biol.* **1993**, *28*, 31–81.

[232] D. F. Cunningham, B. O'Connor, *Biochim. Biophys. Acta* **1997**, *1343*, 160–186.

[233] A. Yaron, *Biopolymers* **1987**, *26*, 215–222.

[234] M. D. Shoulders, R. T. Raines, *Annu. Rev. Biochem.* **2009**, *78*, 929–958.

[235] P. Szpak, *J. Archaeolog. Sci.* **2011**, *38*, 3358–3372.

[236] J. Chatterjee, C. Gilon, A. Hoffman, H. Kessler, *Acc. Chem. Res.* **2008**, *41*, 1331–1342.

[237] S. M. Miller, R. J. Simon, S. Ng, R. N. Zuckermann, J. M. Kerr, W. H. Moos, *Bioorg. Med. Chem. Lett.* **1994**, *4*, 2657–2662.

[238] N. D. Rawlings, M. Waller, A. J. Barrett, A. Bateman, *Nucleic Acids Res.* **2014**, *42*, D503–D509.

[239] R. Walter, W. H. Simmons, T. Yoshimoto, *Mol. Cell. Biochem.* **1980**, *30*, 111–127.

[240] J. Gass, C. Khosla, *Cell. Mol. Life Sci.* **2006**, *64*, 345–355.

[241] R. Walter, H. Shlank, J. D. Glass, I. L. Schwartz, T. D. Kerenyi, *Science* **1971**, *173*, 827–829.

[242] J. I. Venäläinen, R. O. Juvonen, P. T. Männistö, *Eur. J. Biochem.* **2004**, *271*, 2705–2715.

[243] T. Yoshimoto, K. Ogita, R. Walter, M. Koida, D. Tsuru, *Biochim. Biophys. Acta* **1979**, *569*, 184–192.

[244] F. Goossens, I. De Meester, G. Vanhoof, S. Scharpé, *Eur. J. Clin. Chem. Clin. Biochem.* **1996**, *34*, 17–22.

[245] T. Kabashima, M. Fujii, Y. Meng, K. Ito, T. Yoshimoto, *Arch. Biochem. Biophys.* **1998**, *358*, 141–148.

[246] A. Moriyama, M. Nakanishi, M. Sasaki, *J. Biochem. (Tokyo)* **1988**, *104*, 112–117.

[247] L. Shan, Ø. Molberg, I. Parrot, F. Hausch, F. Filiz, G. M. Gray, L. M. Sollid, C. Khosla, *Science* **2002**, *297*, 2275–2279.

[248] T. Yoshimoto, M. Fischl, R. C. Orlowski, R. Walter, *J. Biol. Chem.* **1978**, *253*, 3708–3716.

[249] F. Bordusa, H.-D. Jakubke, *Bioorg. Med. Chem.* **1998**, *6*, 1775–1780.

[250] Y. Ikehara, S. Ogata, Y. Misumi, *Methods Enzymol.* **1994**, *244*, 215–227.

[251] L. Polgar, *Cell. Mol. Life Sci.* **2002**, *59*, 349–362.

[252] V. K. Hopsu-Havu, G. G. Glenner, *Histochemie* **1966**, *7*, 197–201.

[253] A. J. Kenny, A. G. Booth, S. G. George, J. Ingram, D. Kershaw, A. R. Wood, E. J .and Young, *Biochem. J.* **1976**, *157*, 169–182.

[254] V. K. Hopsu-Havu, S. R. Sarimo, *Hoppe-Seyler's Z. Physiol. Chem.* **1967**, *348*, 1540–1550.

[255] J. Elovson, *J. Biol. Chem.* **1980**, *255*, 5807–5815.

[256] K. M. Fukasawa, K. Fukasawa, B. Y. Hiraoka, M. Harada, *Biochim. Biophys. Acta* **1981**, *657*, 179–189.

[257] H. C. Krutzsch, J. J. Pisano, *Biochim. Biophys. Acta* **1979**, *576*, 280–289.

[258] A. Barth, H. Schulz, K. Neubert, *Acta Biol. Med. Ger.* **1974**, *32*, 157–174.

[259] T. Yoshimoto, R. Walter, *Biochim. Biophys. Acta* **1977**, *485*, 391–401.

[260] B. Svensson, M. Danielsen, M. Staun, L. Jeppsen, O. Norén, H. Sjöström, *Eur. J. Biochem.* **1978**, *90*, 489–498.

[261] H. Öya, I. Nagatsu, T. Nagatsu, *Biochimica et Biophysica Acta (BBA) - Enzymology* **1972**, *258*, 591–599.

[262] R. Mentlein, G. Struckhoff, *J. Neurochem.* **1989**, *52*, 1284–1293.

[263] H. Duve, A. Johnsen, A. Scott, A. Thorpe, *Regul. Pept.* **1995**, *57*, 237–245.

[264] B. R. Stevens, A. Fernandez, C. Sumners, L. Hearing, *Neurosci. Lett.* **1988**, *89*, 319–322.

[265] D. A. Eisenhauer, J. K. McDonald, *J. Biol. Chem.* **1986**, *261*, 8859–8865.

[266] G. A. Bezerra, E. Dobrovetsky, A. Dong, A. Seitova, L. Crombett, L. M. Shewchuk, A. M. Hassell, S. M. Sweitzer, T. D. Sweitzer, P. J. McDevitt, K. O. Johanson, K. M. Kennedy-Wilson, D. Cossar, A. Bochkarev, K. Gruber, S. Dhe-Paganon, *PLoS ONE* **Aug. 2012**, *7*, 1–13.

[267] S. Lampelo, K. Lalu, T. Vanha-Perttula, *Placenta* **1987**, *8*, 389–398.

[268] B. R. Stevens, M. Raizada, C. Sumners, A. Fernandez, *Brain Res.* **1987**, *406*, 113–117.

[269] K. Lynn, *Int. J. Biochem.* **1991**, *23*, 47–50.

[270] J. K. McDonald, F. H. Leibach, R. E. Grindeland, S. Ellis, *J. Biol. Chem.* **1968**, *243*, 4143–4150.

[271] K. Imai, T. Hama, T. Kato, *J. Biochem. (Tokyo)* **1983**, *93*, 431–437.

[272] J. D. Kramer, B. J. Bogitsh, *Exp. Parasitol.* **1985**, *60*, 163–170.

[273] S. Sarid, A. Berger, E. Katchalski, *J. Biol. Chem.* **1959**, *234*, 1740–1746.

[274] S. Sarid, A. Berger, E. Katchalski, *J. Biol. Chem.* **1962**, *237*, 2207–2212.

[275] F. Medrano, J. Alonso, J. García, A. Romero, W. Bode, F. Gomis-Ruth, *EMBO J.* **1998**, *17*, 1–9.

[276] H. Neumann, M. Sela, *B. Res. Counc. Israel* **1960**, *9A*, 103–104.

[277] H. Kirschke, H. Hanson, *Hoppe-Seyler´s Z. physiol. Chem.* **1969**, *350*, 1437–1448.

[278] G. D. Fasman, E. R. Blout, *Biopolymers* **1963**, *1*, 3–14.

[279] A. Yaron, A. Berger, *Methods Enzymol.* **1970**, *19*, 521–534.

[280] Çağatay Erşahin, A. M. Szpaderska, A. T. Orawski, W. H. Simmons, *Arch. Biochem. Biophys.* **2005**, *435*, 303–310.

[281] A. Yaron, D. Mlynar, *Biochem. Biophys. Res. Commun.* **1968**, *32*, 658–663.

[282] X. Li, Z. Lou, X. Li, W. Zhou, M. Ma, Y. Cao, Y. Geng, M. Bartlam, X. C. Zhang, Z. Rao, *J. Biol. Chem.* **2008**, *283*, 22858–22866.

[283] I. Mars, V. Monnet, *Biochim. Biophys. Acta* **1995**, *1243*, 209–215.

[284] M. J. Butler, A. Bergeron, G. Soostmeyer, T. Zimny, L. T. Malek, *Gene* **1993**, *123*, 115–119.

[285] P. Dehm, A. Nordwig, *Eur. J. Biochem.* **1970**, *17*, 364–371.

[286] A. J. Kenny, A. G. Booth, R. D. C. Macnair, *Acta Biol. Med. Ger.* **1977**, *36*, 1575–1585.

[287] A. T. Orawski, J. P. Susz, W. H. Simmons, *Mol. Cell. Biochem.* **1987**, *75*, 123–132.

[288] H.-T. Harbeck, R. Mentlein, *Eur. J. Biochem.* **1991**, *198*, 451–458.

[289] A. T. Orawski, W. H. Simmons, *Biochemistry* **1995**, *34*, 11227–11236.

[290] W. Sidorowicz, P. C. Canizaro, F. J. Běhal, *Am. J. Hematol.* **1984**, *17*, 383–391.

[291] R. J. Hyde, N. M. Hooper, A. J. Turner, *Biochem. J.* **1996**, *319*, 197–201.

[292] N. M. Hooper, A. J. Turner, *FEBS Lett.* **1988**, *229*, 340–344.

[293] W. Sidorowicz, J. Szechinski, P. C. Canizaro, F. J. Behal, *Proc. Soc. Exp. Biol. Med.* **1984**, *175*, 503–509.

[294] I. Rusu, A. Yaron, *Eur. J. Biochem.* **1992**, *210*, 93–100.

[295] H. Y. T. Yang, E. G. Erdös, T. S. Chiang, *Nature* **1968**, *218*, 1224–1226.

[296] H. Y. T. Yang, E. G. Erdös, T. S. Chiang, T. A. Jenssen, J. G. Rodgers, *Biochem. Pharmacol.* **1970**, *19*, 1201–1211.

[297] C. E. Odya, D. V. Marinkovic, K. J. Hammon, T. A. Stewart, E. G. Erdös, *J. Biol. Chem.* **1978**, *253*, 5927–5931.

[298] P. Dehm, A. Nordwig, *Eur. J. Biochem.* **1970**, *17*, 372–377.

[299] L. R. Zieske, K.-L. Hsi, L. Chen, P.-M. Yuan, *Arch. Biochem. Biophys.* **1992**, *295*, 76–83.

[300] B. J. Freij, H. L. Levy, G. Dudin, D. Mutasim, M. Deeb, V. M. Der Kaloustian, *Am. J. Med. Genet.* **1984**, *19*, 561–571.

[301] E. L. Smith, *Methods Enzymol.* **1955**, *2*, 93–109.

[302] N. C. Davis, E. Adams, *Arch. Biochem. Biophys.* **1955**, *57*, 301–305.

[303] N. C. Davis, E. L. Smith, *J. Biol. Chem.* **1953**, *200*, 373–384.

[304] W. Grassmann, O. von Schoenebeck, G. Auerbach, *Hoppe-Seyler's Z. Physiol. Chem.* **1932**, *210*, 1–14.

[305] R. E. Neuman, E. L. Smith, *J. Biol. Chem.* **1951**, *193*, 97–111.

[306] A. F. Akrawi, G. S. Bailey, *Biochim. Biophys. Acta* **1976**, *422*, 170–178.

[307] W. Grassmann, H. Dyckerhoff, O. v. Schoenebeck, *Ber. Dtsch. Chem. Ges.* **1929**, *62*, 1307–1310.

[308] D. A. Priestman, J Butterworth, *Biochem. J.* **1985**, *231*, 689–694.

[309] A. J. Barrett, N. D. Rawlings, J. F. Woessner, *Handbook of Proteolytic Enzymes*, *Vol. 3*, Elsevier Science Publishing Co. Inc., **2012**.

[310] A. Bennick, R. Wong, M. Cannon, *Calcium Binding Proteins and Calcium Function*, (Eds.: R. H. Wasserman, R. A. Corradino, E. Carafoli, R. H. Kretsinger, D. H. MacLennan, F. L. Siegel), Elsevier, **1977**.

[311] D. H. Schlesinger, D. I. Hay in Pept., Struct. Biol. Funct., Proc. Am. Pept. Symp., 6th, (Eds.: E. Gross, J. Meienhofer), Dep. Physiol. Biophys. Univ. Illinois Med. Cent. Chicago IL, USA, Pierce Chem. Co. Rockford, Ill, **1979**, pp. 133–136.

[312] M. Manea, G. Mező, F. Hudecz, M. Przybylski, *J. Pept. Sci.* **2007**, *13*, 227–236.

[313] P. R. Carnegie, *Nature* **1969**, *223*, 958–959.

[314] W. G. Lewis, J. M. Basford, P. L. Walton, *Biochim. Biophys. Acta* **1978**, *522*, 551–560.

[315] M. Wingard, G. Matsueda, R. S. Wolfe, *J. Bacteriol.* **1972**, *112*, 940–949.

[316] V. Juillard, H. Laan, E. R. Kunji, C. M. Jeronimus-Stratingh, A. P. Bruins, W. N. Konings, *J. Bacteriol.* **1995**, *177*, 3472–3478.

[317] J. R. Reid, T. Coolbear, C. J. Pillidge, G. G. Pritchard, *Appl. Environ. Microbiol.* **1994**, *60*, 801–806.

[318] C. Becker-Pauly, O. Barré, O. Schilling, U. auf dem Keller, A. Ohler, C. Broder, A. Schütte, R. Kappelhoff, W. Stöcker, C. M. Overall, *Mol. & Cell. Proteomics* **2011**, *10*, M111.009233.

[319] D. R. Thatcher, *Biochem. J.* **1980**, *187*, 875–883.

[320] K. K. Rao, H. Matsubara, *Biochem. Biophys. Res. Commun.* **1970**, *38*, 500–506.

[321] S. Glerup, H. B. Boldt, M. T. Overgaard, L. Sottrup-Jensen, L. C. Giudice, C. Oxvig, *J. Biol. Chem.* **2005**, *280*, 9823–9832.

[322] M. L. Biniossek, D. K. Nägler, C. Becker-Pauly, O. Schilling, *J. Proteome Res.* **2011**, *10*, 5363–5373.

[323] N. S. Gee, A. J. Kenny, *Biochem. J.* **1987**, *246*, 97–102.

[324] J. K. McDonald, C. Schwabe, *Proteinase of Mammalian Cells and Tissues*, (Ed.: A. J. Barrett), North-Holland, Amsterdam, **1977**, pp. 311–391.

[325] K. K. Sharma, B. J. Ortwerth, *J. Biol. Chem.* **1986**, *261*, 4295–4301.

[326] R. Hayashi, *Methods Enzymol.* **1976**, *45*, 568–587.

[327] F. Dal Degan, B. Ribadeau-Dumas, K. Breddam, *Appl. Environ. Microbiol.* **1992**, *58*, 2144–2152.

[328] A. Yaron, *Methods Enzymol.* **1976**, *45*, 599–610.

[329] R. L. Soffer, *Annu. Rev. Biochem.* **1976**, *45*, 73–94.

[330] http://www.historyworld.co.uk (June 8th, 2016).

[331] *Proc. Roy. Soc. London* **1875**, *24*, XXVII–XXXVII.

[332] J. Liebig, *Justus Liebigs Ann. Chem.* **1847**, *62*, 257–369.

[333] J. Volhard, *Justus Liebigs Ann. Chem.* **1862**, *123*, 261–265.

[334] A. J. Rocke, *The Quiet Revolution: Hermann Kolbe and the Science of Organic Chemistry*, University of California, Berkeley, **1993**, Chapter 10: The Theory of Chemical Structure and the Structure of Chemical Theory, pp. 239–264.

[335] R. H. Allen, S. P. Stabler, J. Lindenbaum, *Metabolism.* **1993**, *42*, 1448–1460.

[336] T. Gerritsen, H. A. Waisman, *N. Engl. J. Med.* **1966**, *275*, 66–69.

[337] E. S. Kang, J. Seyer, T. A. Todd, C. Herrera, *Hum. Genet.* **1983**, *64*, 80–85.

[338] S. Mudd, M. H. Ebert, C. R. Scriver, *Metabolism* **1980**, *29*, 707–720.

[339] T. Meissner, E. Mayatepek, *J. Inherit. Metab. Dis.* **1997**, *20*, 717–718.

[340] C. R. S. Scott, *The Metabolic and Molecular Bases of Inherited Disease, Vol II, Chapter: Sarcosinemia*, 8th ed., (Eds.: C. R. Scriver, A. L. Beaudet, W. S. Sly, D. Valle), McGraw-Hill Professional, New York, **2001**.

[341] N. Cernei, Z. Heger, J. Gumulec, O. Zitka, M. Masarik, P. Babula, T. Eckschlager, M. Stiborova, R. Kizek, V. Adam, *Int. J. Mol. Sci.* **2013**, *14*, 13893–13908.

[342] S. Stabler, T. Koyama, Z. Zhao, M. Martinez-Ferrer, R. H. Allen, Z. Luka, L. V. Loukachevitch, P. E. Clark, C. Wagner, N. A. Bhowmick, *PLoS ONE* **2011**, *6*, 1–9.

[343] C. M. Metallo, *Cancer Prev. Res.* **2012**, *5*, 1337–1340.

[344] D. C. Montrose, X. K. Zhou, L. Kopelovich, R. K. Yantiss, E. D. Karoly, K. Subbaramaiah, A. J. Dannenberg, *Cancer Prev. Res.* **2012**, *5*, 1358–1367.

[345] A. D. Mitchell, N. J. Benevenga, *J. Nutr.* **1976**, *106*, 1702–1713.

[346] Z. Luka, S. Pakhomova, L. V. Loukachevitch, M. E. Newcomer, C. Wagner, *Biochim. Biophys. Acta* **2012**, *1824*, 286–291.

[347] S. J. Kerr, *J. Biol. Chem.* **1972**, *247*, 4248–4252.

[348] E. J. Yeo, C. Wagner, *Proc. Natl. Acad. Sci. U.S.A.* **1994**, *91*, 210–214.

[349] C. Beyer, I. H. Alting, E. T. Backer, *Clin. Chem.* **1993**, *39*, 1743–1744.

[350] A. Sreekumar, L. M. Poisson, T. M. Rajendiran, A. P. Khan, Q. Cao, J. Yu, B. Laxman, R. Mehra, R. J. Lonigro, Y. Li, M. K. Nyati, A. Ahsan, S. Kalyana-Sundaram, B. Han, X. Cao, J. Byun, G. S. Omenn, D. Ghosh, S. Pennathur, D. C. Alexander, A. Berger, J. R. Shuster, J. T. Wei, S. Varambally, C. Beecher, A. M. Chinnaiyan, *Nature* **2009**, *457*, 910–914.

[351] X. Chen, R. Overcash, T. Green, D. Hoffman, A. S. Asch, M. J. Ruiz-Echevarría, *J. Biol. Chem.* **2011**, *286*, 16091–16100.

[352] M. Ianni, E. Porcellini, I. Carbone, M. Potenzoni, A. M. Pieri, C. D. Pastizzaro, L. Benecchi, F. Licastro, *Prostate Cancer Prostatic Dis.* **2013**, *16*, 56–61.

[353] A. P. Khan, T. M. Rajendiran, A. Bushra, I. A. Asangani, J. N. Athanikar, A. K. Yocum, R. Mehra, J. Siddiqui, G. Palapattu, J. T. Wei, G. Michailidis, A. Sreekumar, A. M. Chinnaiyan, *Neoplasia* **2013**, *15*, 491–IN13.

[354] B. Cavaliere, B. Macchione, M. Monteleone, A. Naccarato, G. Sindona, A. Tagarelli, *Anal. Bioanal.Chem.* **2011**, *400*, 2903–2912.

[355] C.-C. Huang, I.-H. Wei, C.-L. Huang, K.-T. Chen, M.-H. Tsai, P. Tsai, R. Tun, K.-H. Huang, Y.-C. Chang, H.-Y. Lane, G. E. Tsai, *Biol. Psychiatry* **2013**, *74*, Novel Therapeutics for Depression, 734–741.

[356] D. Strzelecki, J. Szyburska, J. Rabe-Jabłońska, *Neuropsychiatr. Dis. Treat.* **2014**, *10*, 263–266.

[357] D. Strzelecki, J. Szyburska, M. Kotlicka-Antczak, O. Kałużyńska, *Neuropsychiatr. Dis. Treat.* **2015**, *11*, 533–536.

[358] D. E. Owends 3rd, N. A. Peppas, *Int. J. Pharm.* **2006**, *307*, 93–102.

[359] M. E. Fox, F. C. Szoka, J. M. J. Fréchet, *Acc. Chem. Res.* **2009**, *42*, 1141–1151.

[360] L. Illum, I. M. Hunneyball, S. S. Davis, *Int. J. Pharm.* **1986**, *29*, 53–65.

[361] M. T. Peracchia, E. Fattal, D. Desmaële, M. Besnard, J. P. Noël, J. M. Gomis, M. Appel, J. d'Angelo, P. Couvreur, *J. Control. Release* **1999**, *60*, 121–128.

[362] J.-P. Plard, D. Bazile, *Colloid. and Surf. B.* **1999**, *16*, 173–183.

[363] I. F. Tannock, D. Rotin, *Cancer Res.* **1989**, *49*, 4373–4384.

[364] J. A. Simpson, K. H. Cheeseman, S. E. Smith, R. T. Dean, *Biochem J.* **1988**, *254*, 519–523.

[365] H. Fischer, S. S. Ghosh, P. A. Heiney, N. C. Maliszewskyj, T. Plesnivy, H. Ringsdorf, M. Seitz, *Angew. Chem.* **1995**, *107*, 879–881.

[366] B. Halliwell, J. M. Gutteridge in *Oxygen Radicals in Biological Systems Part B: Oxygen Radicals and Antioxidants*, Methods in Enzymology, Academic Press, **1990**, pp. 1 –85.

[367] C. Walling, *Acc. Chem. Res.* **1975**, *8*, 125–131.

[368] B. Halliwell, J. M. C. Gutteridge, *Biochem J.* **1984**, *219*, 1–14.

[369] A. I. Cederbaum, E. Dicker, *Biochem J.* **1983**, *210*, 107–113.

[370] R. Fang, H. Xu, W. Cao, L. Yang, X. Zhang, *Polym. Chem.* **2015**, *6*, 2817–2821.

[371] C. de Gracia Lux, S. Joshi-Barr, T. Nguyen, E. Mahmoud, E. Schopf, N. Fomina, A. Almutairi, *J. Am. Chem. Soc.* **2012**, *134*, 15758–15764.

[372] B. Halliwell, M. V. Clement, L. H. Long, *FEBS Lett.* **2000**, *486*, 10–13.

[373] Y. Fujita, K. Wakabayashi, M. Nagao, T. Sugimura, *Mutat. Res. Lett.* **1985**, *144*, 227–230.

[374] K. Hiramoto, X. Li, M. Makimoto, T. Kato, K. Kikugawa, *Mutat. Res.* **1998**, *419*, 43–51.

[375] L. H. Long, A. N. B. Lan, F. T. Y. Hsuan, B. Halliwell, *Free Radical Res.* **1999**, *31*, 67–71.

[376] N. Kuge, M. Kohzuki, T. Sato, *Free Radical Res.* **1999**, *30*, 119–123.

[377] L. H. Long, P. J. Evans, B. Halliwell, *Biochem. Biophys. Res. Commun.* **1999**, *262*, 605–609.

[378] S. Laborie, J.-C. Lavoie, P. Chessex, *J. Pediatr.* **2000**, *136*, 628–632.

[379] J. Schreck, Bachelor Thesis, Oxidativer Abbau von Polysarkosin durch verschiedene reaktive Sauerstoffspezies, **2016**.

[380] J. Chen, S. C. Rogers, M. Kavdia, *Ann. Biomed. Eng.* **2013**, *41*, 327–337.

[381] I. M. Wienk, E. E. B. Meuleman, Z. Borneman, T. van den Boomgaard, C. A. Smolders, *J. Polym. Sci. Part A: Polym. Chem.* **1995**, *33*, 49–54.

[382] H. Kaczmarek, A. Kamińska, M. Światek, J. F. Rabek, *Angew. Makromol. Chem.* **1998**, *261-262*, 109–121.

[383] E. Y. Davydov, V. P. Pustoshnyi, G. B. Pariyskii, G. E. Zaikov, *Int. J. Polym. Mater.* **2000**, *46*, 107–120.

[384] K. M. Kem, *J. Polym. Sci. Part A: Polym. Chem.* **1979**, *17*, 1977–1990.

[385] F. Wieghardt, Bachelor Thesis, Untersuchungen zum Metabolismus von Polysarkosin, **2014**.

[386] J. Eisenreich, Bachelor Thesis, Studien zu Bioabbaubarkeit von Polysarkosin, **2014**.

[387] Thermo Fisher Scientific, Labels & Labeling Kits, product catalog, `https://www.thermofisher.com/order/catalog/product/46410(05.10.2016)`.

[388] M. Krebs, Master Thesis, In Vitro Investigation of the Biodegradation of Polysarcosine and Polyproline, **2015**.

[389] A. Eisfeld, J. S. Briggs, *Chem. Phys.* **2006**, *324*, 376–384.

[390] U. Rösch, S. Yao, R. Wortmann, F. Würthner, *Angew. Chem.* **2006**, *118*, 7184–7188.

[391] M. Roe, H. Pinchen, S. Church, P. Finglas, Nutrient analysis of eggs, Institute of Food Research, Norwich Research Park, **2013**.

[392] P. F. Sharp, C. K. Powell, *Ind. Eng. Chem.* **1931**, *23*, 196–199.

[393] J. L. Heath, *Poultr. Sci.* **1977**, *56*, 822–828.

[394] P. Banerjee, K. M. Keener, V. D. Lukito, *Poult. Sci.* **2011**, *90*, 889–895.

[395] V. L. Hughey, P. A. Wilger, E. A. Johnson, *Appl. Environ. Microbiol.* **1989**, *55*, 631–638.

[396] A. N. Yousif, L. J. Albright, T. P. T. Evelyn, *Di. aquat. Org.* **1994**, *19*, 15–19.

[397] R. Cegielska-Radziejewska, G. Lesnierowski, J. Kijowski, *Eur. Food Res. Technol.* **2009**, *228*, 841–845.

[398] J. M. Tiedje, M. Alexander, *J. Agric. Food Chem.* **1969**, *17*, 1080–1084.

[399] E. Schramm, B. Schink, *Biodegradation* **1991**, *2*, 71–79.

[400] J. R. Haines, M. Alexander, *Appl. Microbiol.* **1975**, *29*, 621–625.

[401] D. P. Cox, *Adv. Appl. Microbiol.* **1978**, *23*, (Ed.: D. Perlman), 173–194.

[402] F. Kawai, B. Schink, *Crit. Rev. Biotechnol.* **1987**, *6*, 273–307.

[403] D. E. Bruns, D. A. Herold, G. T. Rodeheaver, R. F. Edlich, *Burns* **1982**, *9*, 49–52.

[404] C.-H. Wang, K.-R. Fan, G.-H. Hsiue, *Biomaterials* **2005**, *26*, 2803–2811.

[405] Y. Mine, *Trends Food Sci. Technol.* **1995**, *6*, 225–232.

[406] Y. Mine, F. Shahidi, *Nutraceutical proteins and peptides in health and disease*, CRC Press Inc., **2005**.

[407] A. Hoppe, PhD thesis, University of Nebraska at Lincoln, **2010**.

[408] K. Mann, M. Mann, *Proteome Sci.* **2011**, *9*, 7.

[409] A. E. Henderson, D. S. Robinson, *J. Sci. Food Agric.* **1969**, *20*, 755–760.

[410] F. Makki, T. Durance, *Food Res. Int.* **1996**, *29*, 635–645.

[411] G. F. White, N. J. Russell, E. C. Tidswell, *Microbiol. Rev.* **1996**, *60*, 216–232.

[412] J. Frings, E. Schramm, B. Schink, *Appl. Environ. Microbiol.* **1992**, *58*, 2164–2167.

[413] M. Sugimoto, M. Tanabe, M. Hataya, S. Enokibara, J. A. Duine, F. Kawai, *J. Bacteriol.* **2001**, *183*, 6694–6698.

[414] J. L. Spier, *Chemistry* **1964**, *37*, 6–11.

[415] I. I. Marochkin, O. V. Dorofeeva, *Comput. Theor. Chem.* **2012**, *991*, 182–191.

[416] R. G. Board, *J. Appl. Bacteriol.* **1965**, *28*, 437–453.

[417] H. R. Kricheldorf, *Chem. Ber.* **1971**, *104*, 87–91.